EVALUATION OF DUCTILE BEAM-COLUMN CONNECTIONS FOR USE IN SEISMIC-RESISTANT PRECAST FRAMES

by

ELIAS ISSA SAQAN, B.S.C.E, M.S.E

DISSERTATION

Presented to the Faculty of the Graduate School of
The University of Texas at Austin
in Partial Fulfillment
of the Requirements
for the Degree of

DOCTOR OF PHILOSOPHY

THE UNIVERSITY OF TEXAS AT AUSTIN
December, 1995

EVALUATION OF DUCTILE BEAM-COLUMN CONNECTIONS FOR USE IN SEISMIC-RESISTANT PRECAST FRAMES

APPROVED BY

DISSERTATION COMMITTEE:

Supervisor: _____

_____

_____

_____

_____

To the loving memory of my father

and

to my mother, sisters, and brothers

ACKNOWLEDGMENT

The research described here was conducted at Ferguson Structural Engineering Laboratory as part of the US-PRESSS program by support from the National Science Foundation under grant number BCS-9122950.

My sincere thanks and appreciation to Dr. Michael Kreger for supervising this research. His suggestions and comments to improve this dissertation were invaluable. His support to me throughout the course of this research is deeply appreciated. Also, his devotion to ensure that I would not leave The University without knowing the basics of Golf will always be remembered. My deep thanks are to all the committee members of this dissertation, Dr. Ned Burns, Dr. Michael Engelhardt, Dr. James Jirsa, and Dr. Morris Stern for their invaluable suggestions and constructive criticisms. Many thanks also to all the Professors who taught me at The University especially Dr. John Breen and Dr. Joseph Yura.

Many companies donated materials that were needed for building the specimens. ERICO donated the couplers used in the first and second specimens. Nikon Fibers donated the plastic fibers used in the grout mixes. Shinko Wire America, Inc. donated the prestressing strands for the fourth specimen. Precision Screw Products Company, Inc. donated the strand wedges for the fourth specimen. The generous donations of all these companies is gratefully acknowledged.

The help of Dr. Lin Fa, who was a visiting scholar from Shanghai University, in building the first specimen and the testing frame is deeply appreciated. The help of undergraduate assistant Mohammed El-mrabet in building and testing the specimens and the help of Yong-Mook Kim in testing the first and fourth specimens is appreciated. Many fellow students were generous in their help during concrete casting and other difficult times during construction of the specimens especially Brad Wood and Robert Frosch. Their help and assistance is gratefully appreciated. The assistance of the technical and administrative staff of Ferguson Structural Engineering Laboratory is acknowledged. The assistance of the

administrative staff of the Department of Civil Engineering is appreciated especially that of Carole Reese, who was the administrative assistant in the structures division.

My parents were always supporting and encouraging me throughout my years in college. I cannot thank enough my mother and my late father for devoting their lives to their children's education. Dedicating this dissertation to my father's memory is the least I can do to show my appreciation. I would also like to thank my sisters Eliana, Aida, and Mona, and my brothers Joseph, Bashir, and Johnny not only for their encouragement and for their financial support, but also for being the best sisters and brothers anybody can have.

Many thanks to all the friends I met during my stay in Austin for making this place a second home away from home.

Finally, I thank God for He always directs my path and always answers my prayers.

Elias Issa Saqan

Austin, Texas
December, 1995

EVALUATION OF DUCTILE BEAM-COLUMN CONNECTIONS FOR USE IN SEISMIC-RESISTANT PRECAST FRAMES

Publication No._____

Elias Issa Saqan, Ph.D.
The University of Texas at Austin, 1995

Supervisor: Michael E. Kreger

Precast frame systems represent an economic alternative for building construction in regions of high seismicity. Advantages of precast concrete over cast-in-place concrete include superior quality control, speed of erection, and aesthetic architectural form. However, this system is not widely used in the US because framing methods and connections between precast elements suitable to US construction practices have not been adequately tested, and as a result, there is a lack of comprehensive design recommendations. The primary objective of the research program described herein is to develop precast beam-column connections for use in seismic-resistant structural frame systems which (1) require minimal or no cast-in-place concrete, and (2) are economical and ductile. The different types of connections considered in this program are (1) tension/compression yielding, in which energy is dissipated through inelastic behavior of the connecting elements, (2) friction connections in which energy is dissipated through friction when slip occurs between connecting elements, and (3) nonlinear-elastic in which energy dissipation is minimal but the advantage is the small residual drift following ground movement. Four half-scale models of prototype precast beam-column connections subjected to reversed cyclic loads have been constructed and tested. Load-deformation responses for complete connections and connecting elements, load-strain response for select connecting elements, as well as comparison of energy

dissipation, residual drifts, and stiffness will be presented. Based on the behavioral information collected during connection tests, analytical models were developed to investigate the behavior of complete precast frame systems.

TABLE OF CONTENTS

LIST OF TABLES

LIST OF FIGURES

CHAPTER 1

INTRODUCTION

1.1 ADVANTAGES OF PRECAST CONCRETE

Precast concrete is experiencing increased use in the United States. Heavier use is attributed to increasing interest by both researchers and contractors to find competitive alternatives for other commonly used construction materials, such as cast-in-place concrete. The Prestressed Concrete Institute (PCI) was established in 1954 for the purpose of advancing the design, manufacture, and use of prestressed and precast concrete. Since then many buildings and structures have been designed and built using precast/prestressed concrete. Examples of such structures are parking garages, office buildings, and bridges.

The reason for increased interest in precast concrete is its many and obvious advantages over cast-in-place concrete. Some of the advantages are:

1. *Speed of construction*. One can think of cast-in-place construction as essentially building the structure twice. First, a wood or steel structure is built (formwork), then concrete is cast. Finally, formwork is removed to reveal the reinforced concrete structure. This extra field procedure is eliminated in precast concrete. However, it should be noted that some special erection and support procedures are needed for precast concrete. Moreover, there will be no need to wait for concrete to cure and gain strength since this phase has already taken place in the precast manufacturing plant.

2. *Economy*. In general, in buildings where dead load is the predominant load, precast concrete is more economical than cast-in-place concrete because simple connections can be used instead of the more complicated moment-resisting connections. Formwork, which is usually a substantial percentage of the total construction cost, is substantially less for precast concrete construction. However,

some of the savings can be lost due to the use of some special erection and support procedures needed for this type of construction.

3. *Quality control*. Structural concrete members fabricated in a plant under controlled factory conditions are typically of higher quality than cast-in-place concrete. This additional quality control is recognized by relaxed cover requirements of building codes [1]. In addition, plant conditions afford more control over the concrete design mix and its constituents, placement, curing, and specified cover.

4. *Aesthetics*. Precast concrete offers more freedom to the designer to specify irregular member shapes due to the improved casting facilities in a precast plant. The end result is aesthetically better buildings.

Despite the many advantages of precast concrete, it is not widely used throughout the United States. This is especially true in regions of high seismic risk. The reason behind the very limited use of precast concrete in seismic zones is the lack of design recommendations. For this reason the US-PRESSS program (**PRE**cast **S**eismic **S**tructural **S**ystems) was initiated. The objectives of the PRESSS program are discussed in the next section.

1.2 US-PRESSS PROGRAM

1.2.1 Objectives

Precast concrete buildings are not widely used in seismic regions of the United States. Framing methods and seismic resistant connections between precast concrete elements suitable to US construction practices have not been adequately tested. As a result, there is a lack of adequately proven design recommendations.

The US-PRESSS program was initiated to address these needs. The ultimate objective of the program is to develop precast concrete systems for seismic regions and corresponding design recommendations.

1.2.2 Description of US-PRESSS Program

The US-PRESSS program was divided into two major phases. Phase I, which was completed in 1993, concentrated on analytical and design studies to investigate feasible design concepts. It was also intended to provide the framework for design recommendations and future analytical parametric studies needed to calibrate and quantify the design recommendations.

Phase II, which was initiated prior to completion of phase I, is to investigate experimentally and analytically the behavior of "ductile-joint frames". The definition of "ductile-joint frames" will be discussed in detail in Chapter 2. Phase II was further divided into three major parts:

1. *Development of Ductile Connection Details*. In this part of the project a variety of connection concepts were developed in close cooperation with other institutions and industry representatives involved in the PRESSS program. Modification of connection concepts and feedback from precasters and contractors was considered essential since this will eventually lead to the implementation of the program results.

2. *Experimental Investigation of Beam-Column Subassemblages*. In this part of phase II, beam-column subassemblages incorporating connections deemed to have the most promise were designed, built, and tested in the laboratory in an effort to characterize the behavior of the connections. Detailed discussion of the development of the connections as well as the experimental investigation are included in Chapters 2 and 3.

3. *Analytical Modeling of Precast Systems*. The experimental investigation provided detailed information about the behavior of individual connections, particularly in the form of load-deformation hysteretic response. This information was then used to determine whether a frame built with such details will perform well during an earthquake. The observed experimental behavior was incorporated

in nonlinear dynamic analyses of five- and fifteen-story frame systems subjected to a variety of ground motions. The objective of the analyses was to determine the suitability of frame systems incorporating various connection details using gross measures of response, such as story drifts, and local ductility demands.

1.3 LITERATURE REVIEW

Precast concrete has been in use in the United States since the 1950's. However, there have been only a limited number of studies on the performance of precast concrete moment-resisting frames for use in seismic zones, that do not emulate cast-in-place concrete. Due to the limited data available, only general provisions for the design of precast structures have been included in building codes such as the Uniform Building Code (UBC) [22]. As a result, precast concrete construction is not prevalent in seismically active regions of the United States.

Considerable research has been performed in Japan and New Zealand on precast concrete connections [7,25,31]. In these studies, precast beams and columns are typically tied together by cast-in-place concrete in the joints. Although reinforcement details that are substantially different from those used in monolithic construction are used to accommodate connections between the precast members, the final product has been shown to behave very similar to cast-in-place construction. Because of this, the Japanese precast design approach is often referred to as "emulation design". This type of construction is not favored in the United States, and the specimens discussed here were designed with a different objective in mind, as will be discussed in Chapter 2.

In 1981 the Applied Technology Council (ATC) [4] held a workshop on the design of precast concrete buildings for earthquake loads. The objective was to determine current knowledge of precast structures and to identify research needs. The topic receiving the highest priority was the development of design recommendations for moment-resisting beam-column connections.

In response to these needs, several studies were initiated at universities and research institutions in the United States. A multi-year multi-phase program was initiated at the National Institute for Standards and Technology (NIST) in 1987. The work at NIST investigated a number of precast moment-resisting connection details that fall into the following categories:

1. Fully bonded post-tensioning (PT) bars, no mild steel
2. Fully bonded PT strand, no mild steel
3. Partially bonded PT strand, no mild steel
4. Fully bonded PT strand, bonded mild steel
5. Unbonded PT bars, bonded mild steel
6. Unbonded PT bars, unbonded mild steel

The precast subassemblages tested were models of planar interior beam-column connections and consisted of one precast column and two precast beams connected in a cruciform shape. The NIST program was divided into four phases, and included monolithic connections for control purposes. For phases I through III, only (PT) strands or bars in precast connections crossed the interface between precast beams and the column. The cross-sections of the beams used in these phases are shown in Fig. 1.1.

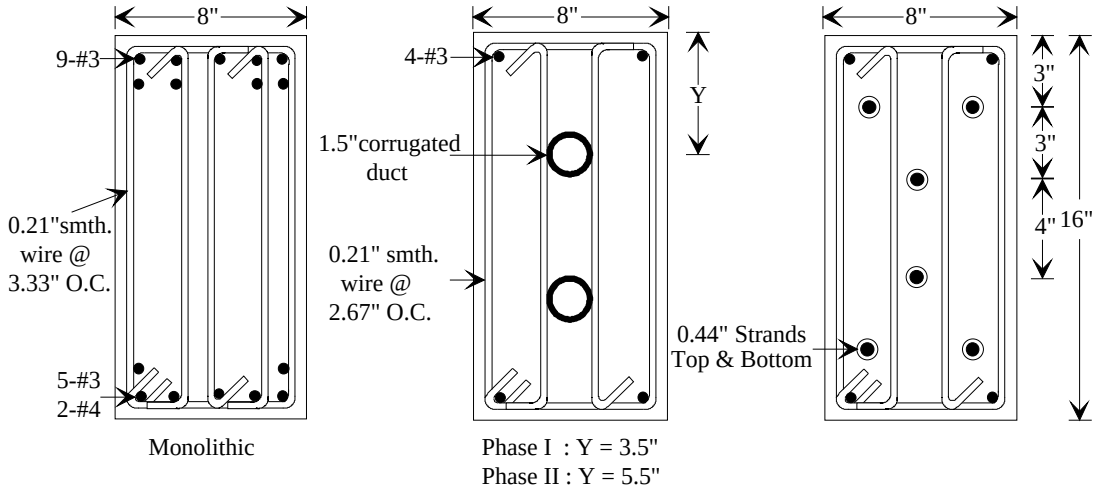

Figure 1.1 Beam Cross-Sections for Connections Tested at NIST

In phase I, four 1/3-scale model monolithic specimens and two precast post-tensioned concrete specimens with fully bonded PT bars were tested. The monolithic specimens served as a benchmark for the precast specimens. In phase II, six precast specimens were tested. The main variables investigated in this phase were the location of the PT steel and the use of prestressing strands vs. PT bars. Researchers at NIST reported in phase I [8,11] that the precast specimens demonstrated the post-tensioning concept is a viable method. The strength of the precast specimens was comparable to the monolithic specimens. However, energy dissipation was not as great because of the narrow hysteresis loops demonstrated by the precast specimens. To improve energy dissipation, the PT steel was moved closer to the beam centroid. By doing this, the PT steel would experience less strain and would therefore retain its post-tensioning force through larger connection distortions. It was reported [12] that the effect of moving the post-tensioning force closer to the beam centroid improved the energy dissipation characteristics of the connection with little effect on strength of the connection. Also, the use of prestressing strands as opposed to PT bars seemed to improve the energy dissipation characteristics and increased the

Figure 1.2 Hysteretic Response of a Specimen Tested in Phase II at NIST

reserve strength of the connections. It was also reported that the hysteresis loops were still severely pinched and stiffness quickly degraded during later stages of tests. The load-deflection response for one of the NIST specimens with fully-grouted PT strands is shown in Fig. 1.2.

Because of a lack of stiffness in the precast specimens in the later stages of the tests, two specimens were tested in phase III with partially debonded tendons. The tendons were debonded in the joint and to a predetermined length in the beams on both sides of the column. If this length is carefully chosen, tendon strains will not exceed the limit of proportionality and the post-tensioning force will be maintained further into the test program. It was reported that the partially debonded tendons improved the stiffness of the specimens up to large deformations. However, the energy dissipated by these specimens was less than that for any of the other specimens due to the expected bilinear elastic behavior. One thing to note though is that the residual drift for these specimens was minimal because the strands remained

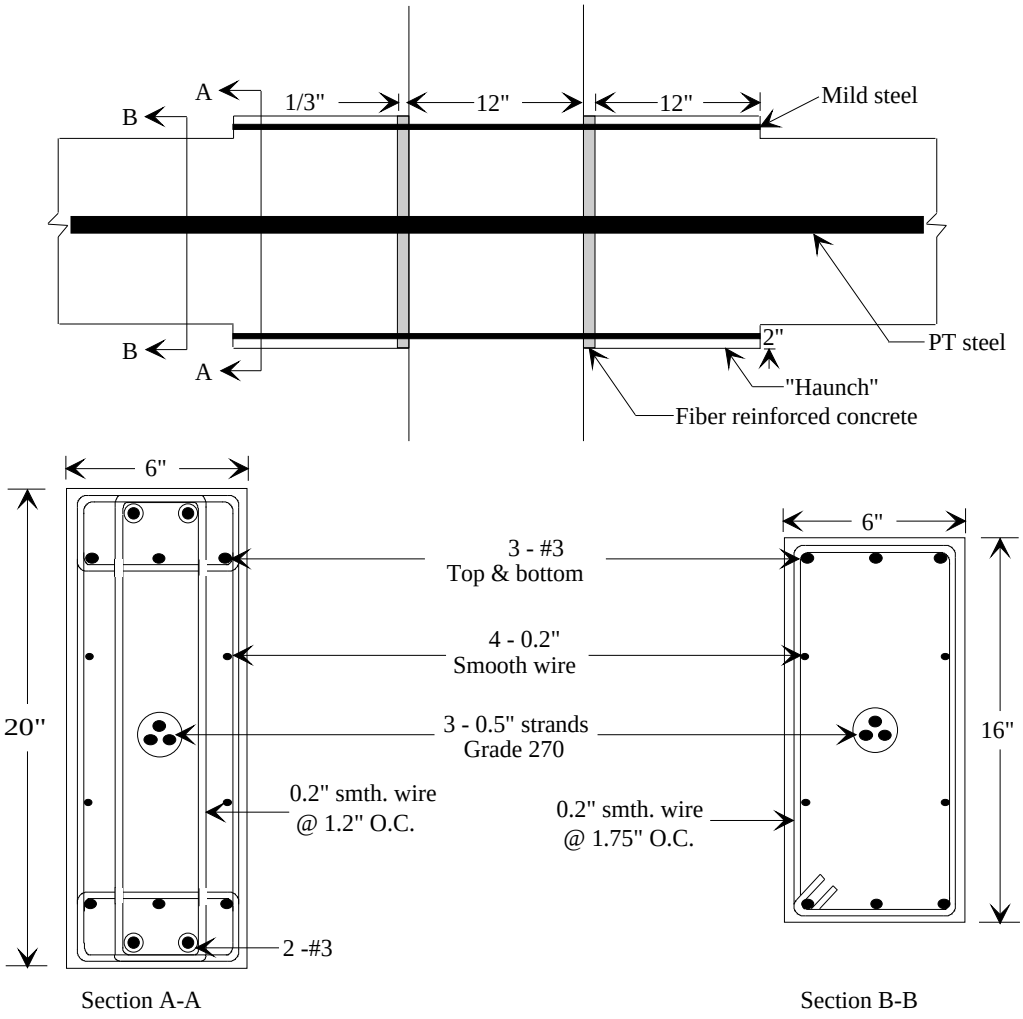

Figure 1.3 Schematic of Connections Tested in Phase IV at NIST

virtually elastic.

Phase IV of the NIST program examined the use of non-prestressed steel in conjunction with PT steel as a means of improving the energy dissipation characteristics of the specimens. The premise for this concept was that conventional reinforcement would be used as an energy dissipater while the friction force developed between the beam and column by the post-tensioning force would be used to provide the necessary shear resistance. Figure 1.3 shows the structural

concept tested in this phase.

The NIST program has concluded that post-tensioned precast concrete beam-column connections can perform as well as or better than equivalent monolithic specimens in terms of connection strength and drift capacity. Improved energy dissipation per cycle can be achieved by:

a) including conventional reinforcement through the joint region near the top and bottom of the beams;

b) locating the PT steel closer to the beam centroid; and

c) having fully bonded PT steel (if no conventional steel is included). However, the last arrangement risks a loss of shear resistance if the PT steel yields.

Priestley and Tao at the University of California, San Diego studied interior connections [34] using analytical models. They subjected a number of single degree of freedom oscillators of different initial natural periods and hysteretic characteristics to a range of different accelerograms. In all cases the accelerograms were scaled to give a peak ground acceleration of 0.4g. The models had periods of vibration ranging from 0.4 to 2 seconds. The hysteretic characteristics considered are shown in Fig. 1.4 and included:

a) linear elastic with unlimited strength;

b) bilinear elastic response (like an idealized debonded PT connection);

c) bilinear elasto-plastic response; and

d) response similar to a bonded prestressed connection with severe stiffness degradation.

Priestley and Tao concluded that the concept of connecting precast beam and column elements using beam prestressing tendons debonded through the joint and for a distance on each side of the joint should result in maintenance of prestress

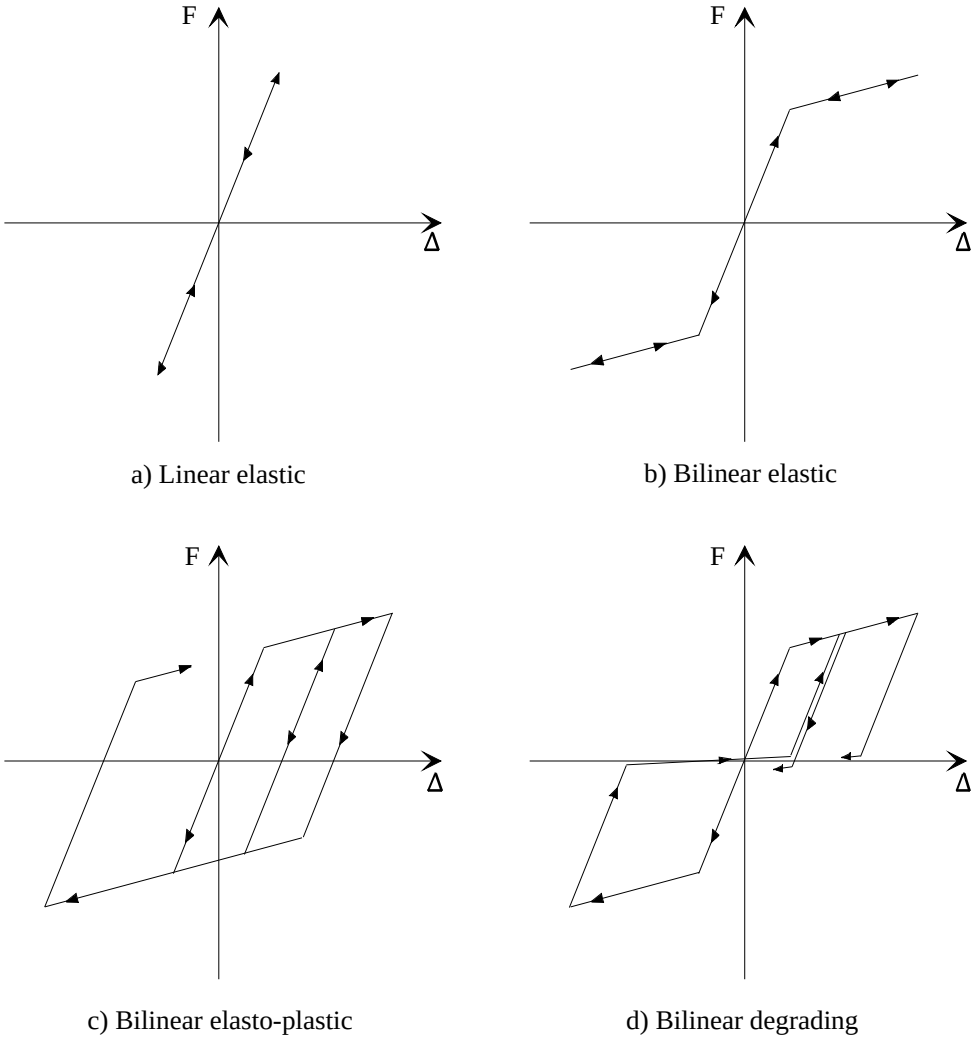

a) Linear elastic b) Bilinear elastic

c) Bilinear elasto-plastic d) Bilinear degrading

Figure 1.4 Hystertic Characteristics Consisdered by Priestley and Tao

compression across the connection even after large seismic displacements occur. They also reported that residual displacements should be negligible after a design level earthquake, and residual stiffness at low displacements should remain close to the initial value. The dynamic inelastic analyses demonstrated that ductility demands for structures with partially debonded tendons would be no greater than for fully bonded tendons where prestress degrades as a consequence of inelastic behavior of

Figure 1.5 Hysteretic Response of Interior Specimen Tested by MacRae and Priestley

the prestressing tendon. Finally, they suggested that the concept of partially debonded tendons is most appropriate for structures higher than six stories. This is so because low period structures generally experience higher ductility demands.

MacRae and Priestley at University of California, San Diego have recently tested, as part of the US-PRESSS program, one interior and one exterior 2/3-scale fully-unbonded post-tensioned precast concrete beam-column connections [26]. They reported that both specimens behaved well, attaining interstory drifts of close to 3 percent without significant strength degradation. The response reported was essentially elastic, though nonlinear. The story shear-story drift response for the interior connection is shown in Fig. 1.5. Energy dissipation was minimal and the residual drift was 2.2 percent of the maximum drift. They concluded that if the length of tendon over which elongation may occur is sufficient to prevent yield, and the compression zone and the anchorage details are satisfactory, then ungrouted post-tensioned precast concrete beam-column joint subassemblages can be expected to function well as earthquake-resisting structural systems.

Six exterior and one interior precast beam-column connections were tested at the University of Minnesota by French et al [18,19] in 1989. The connections were quite varied and contained the following attributes: post-tensioning bars; a composite connection consisting of cast-in-place topping and a precast beam connected with post-tensioning bar; welded connecting elements; bolted connecting elements; threaded rebars which were threaded into couplers anchored in the column; and a connection with tapered-threaded splices. Details of the connections can be found in references [18,19]. Four of the exterior specimens were designed so that the plastic hinge was relocated away from the connection region. The other two exterior connections and the interior connection were designed so that the plastic hinge occurred in the connection region. Beams were partially prestressed. Specimens with the plastic hinge occurring in the joint region showed better energy dissipation characteristics than those with the plastic hinge located in the prestressed beams. In general, it was concluded that the threaded rebar connection with tapered splices and composite connection appeared to be the most likely candidates for use in seismic regions.

As part of the US-PRESSS program, Palmieri and French at the University of Minnesota recently tested four 1/2-scale interior precast beam-column connections [30]. The first two subassemblages represented the nonlinear-elastic post-tensioning concept proposed by Priestley and Tao, and described above. The precast beams and columns were connected with unbonded post-tensioning steel which passed through the joint and was anchored in horizontal “dogbones” located at the beam ends, as shown in Fig. 1.6. Substantial quantities of confining steel were provided in those zones. The difference between the two specimens was the post-tensioning types. One specimen was post-tensioned with strands and the other with high-strength bars.

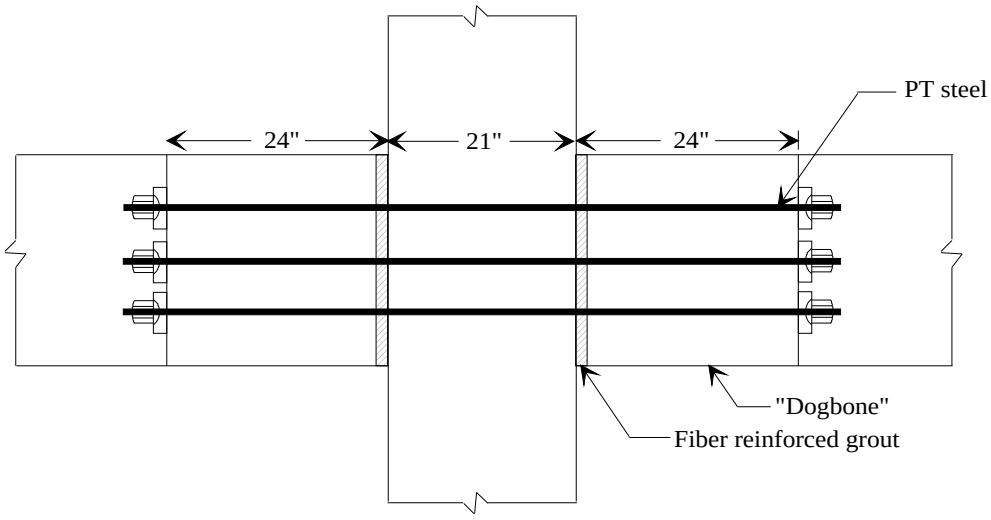

Figure 1.6 First and Second Connections Tested at the University of Minnesota

It was suggested that the strand system offers more economical use of post-tensioning steel, while the bars are more easily installed and exhibit lower seating losses than the former. Both specimens reached the design strength and drift without any significant damage. The story shear-story drift response of the specimen with post-tensioning strands is shown in Fig. 1.7. In that specimen, fracture of the strands was observed at 3 percent drift, which left a residual opening of 1 inch between the beam and column at the end of the test. In the specimen where bars were used, the specimen did not show any residual opening after test completion. Some inelastic behavior was observed, which the researchers suggested could enhance the performance of the system by providing some energy dissipation.

The third and fourth specimens tested at the University of Minnesota represented a different concept, namely tension/compression yielding. This system, as well as other systems studied here are described in detail in Chapter 2. The general concept for the third specimen is shown in Fig. 1.8a. The bottom connection was made using a lightly post-tensioned rod. A gap exists over most of the interface

Figure 1.7 Hysteretic Response of Specimen with PT Strands Tested at the University of Minnesota

between the beam and the column. The ends of three No. 9 reinforcing bars were threaded to mate with couplers that were embedded in the column. The top of the beam was then cast. The bottom connection of the beam was intended to permit rotation only while concentrating nearly all of the nonlinear material activity at the top of the beam. It was reported that the specimen behaved satisfactorily up to a story drift of 1.5 percent. During a subsequent load cycle some of the threaded bars were fractured at the coupler face leading to the failure of the specimen. The story shear-story drift response is shown in Fig. 1.9.

The connection concept utilized in the fourth specimen tested at the University of Minnesota is shown in Fig. 1.8b. This connection incorporated block-outs through the beams, and embedded corrugated pipes in the column to accommodate placement of reinforcement. No couplers were used, but instead, continuous reinforcement was placed in the beam block-outs and through the column, then grout was pumped into the column ducts and the beam block-outs.

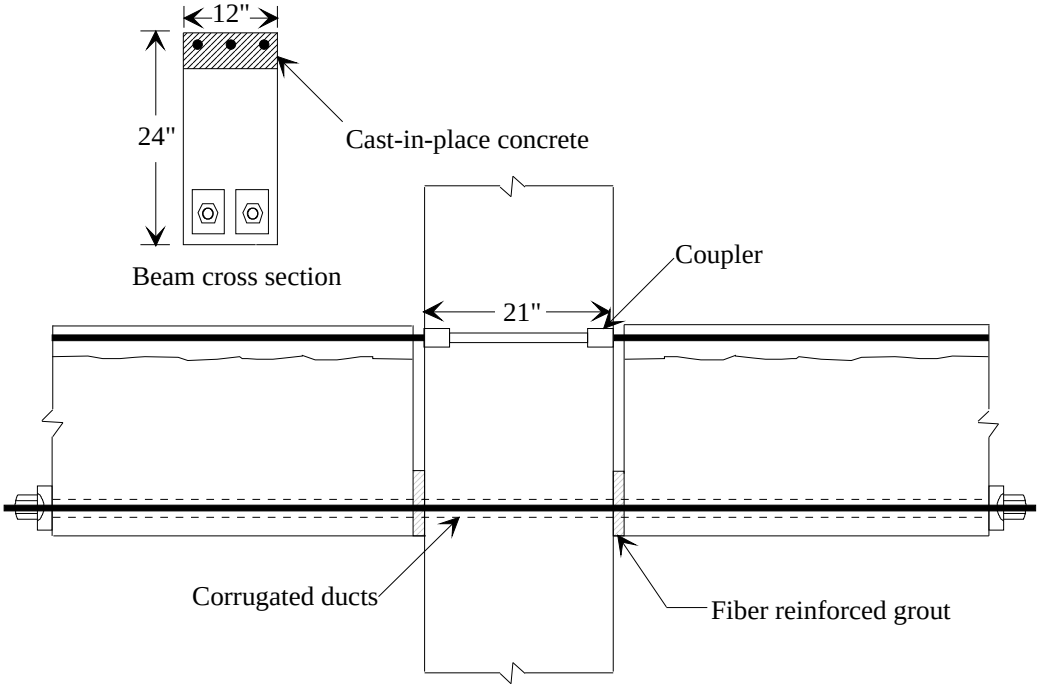

a) Third Connection

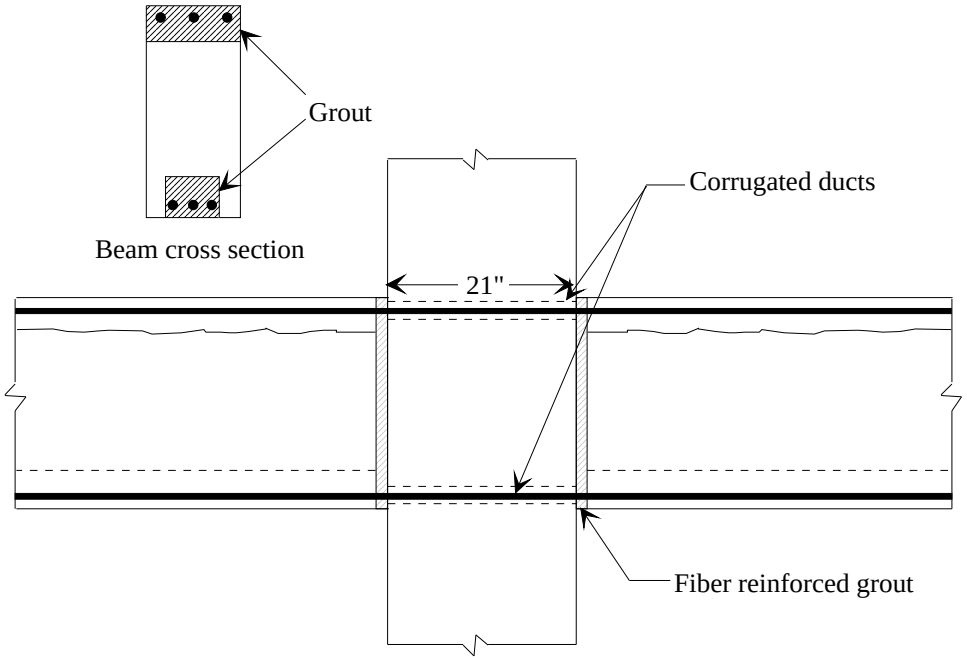

b) Fourth Connection

Figure 1.8 Third and Fourth Connections Tested at the University of Minnesota

Figure 1.9 Hysteretic Response of Third Specimen Tested at the University of Minnesota

The connection reinforcement was intended to yield both in tension and compression at the beam-column interface. It was reported that this specimen behaved quite well up to drifts exceeding 4 percent. The story shear-story drift response is shown in Fig. 1.10. Even at drifts up to 6 percent, the strength decreased by only 9 percent of the load attained at 4 percent. Significant pinching occurred in the latter parts of the test due to buckling of the longitudinal beam reinforcement in the connection region accompanied with concrete spalling. Also, pinching was attributed to the relative vertical movement between the beam and column due to yielding and bending of longitudinal reinforcement, and due to slip between the corrugated pipes housing the beam longitudinal reinforcement and the column concrete.

At the University of Canterbury, New Zealand, Blakely and Park tested four full-scale exterior post-tensioned precast connections [6]. Typical details of the connections are shown in Fig 1.11. The columns were prestressed and the beams were partially prestressed. The construction joint between the beam and column

was

Figure 1.10 Hysteretic Response of Fourth Specimen Tested at the University of Minnesota

filled with mortar. Units 1 and 2 were designed so that plastic hinging occurred in the beams at the joint while units 3 and 4 were designed so that plastic hinging occurred in the column immediately above and below the beams. The transverse reinforcement for units 1 and 2 was designed to satisfy the requirements of prestressed concrete, while that of units 3 and 4 was increased to study the effect of confinement on ductility. The precast elements were connected with prestressing strands. Prior to crushing of concrete, energy dissipation was minimal. A substantial increase in energy dissipation was observed once concrete crushing occurred. Blakely and Park also reported that the increase in transverse reinforcement did not result in significant improvement in performance.

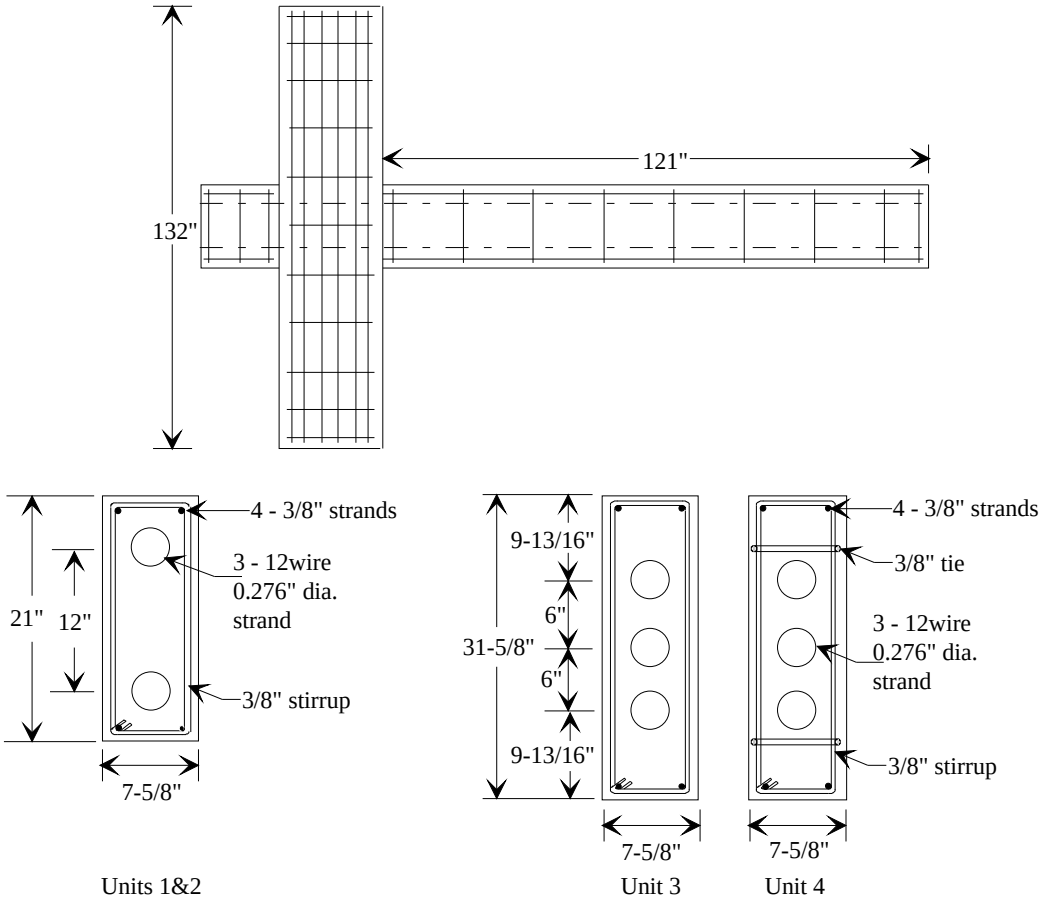

Figure 1.11 Connections Tested at the University of Canterbury, New Zealand

1.4 OBJECTIVES OF CURRENT WORK

Until now few buildings have been built with precast concrete frames as the main lateral force resisting system in high seismic regions in the United States. Designers of this system have faced the dilemma of designing such structures without clear guidelines or recommendations.

An experimental project which is part of the US-PRESSS program, was undertaken at The University of Texas at Austin to help in this regard. Four half-

scale precast beam-column connections were built and tested. The subassemblages represented an interior connection in the lower stories of a fifteen-story building. The connections were tested to large deformation levels applying a prescribed cyclic deformation history.

The objectives of this study were two-fold:

1. *Experimental phase*. In this phase very different types of connections were considered for testing. The connections that appeared to hold the most promise, in terms of ease of construction, strength, ductility, and energy dissipation were tested. However, it should be reiterated here that this study was part of the US-PRESSS program. Coordination between The University of Texas at Austin and NIST, the University of Minnesota, and University of California, San Diego, who were partners in the US-PRESSS program, was required in order to avoid duplication of tests.

2. *Analytical phase*. In this phase of the study, using the data collected from the experimental phase, the behavior of five- and fifteen-story precast moment-resisting frames subjected to a number of strong-motion earthquakes was investigated. Results of the analyses were used to examine both gross response of the frames and local demands on the connections to determine the suitability of the frame systems and different connection types for use in zones of high seismic risk.

1.5 ORGANIZATION

This study is divided into seven chapters. Chapter 2 describes the different types of connections considered and the design objectives. It also describes the prototype building, and the design of prototype connections. In Chapter 3 the details of the test specimens as well as their fabrication and instrumentation are presented. The test setup, loading history, and test procedure are also presented in Chapter 3. In Chapter 4 the general behavior of the connections is presented, as well as the crack patterns and the modes of failure. In Chapter 5 the specimens

stiffness, response envelopes, residual drift, and energy dissipation are compared. Also, in Chapter 5 the internal behavior of the connections is assessed through examination of strain gauge data. Chapter 6 is devoted to the analytical modeling of connections and frame behavior. Chapter 7 contains a summary of test results and conclusions.

CHAPTER 2

DEVELOPMENT OF DUCTILE CONNECTIONS

2.1 INTRODUCTION

The definition of a ductile connection is presented, and comparisons with other connection types are discussed in this chapter. The different ductile connections considered in this program are presented, and characteristics of each type are described. The prototype structure modeled in this study is also presented. Finally, the design criteria used for designing the prototype structure as well as the test specimens are discussed.

2.2 TYPES OF PRECAST CONNECTIONS

The US-PRESSS program defined two types of precast connections:

1. *Rigid connections*. Connections which force the plastic hinge to form in the precast member outside the connection region are termed "rigid connections". The design of this type of connection is such that the connecting elements between beams and columns are proportioned to have more strength than the precast beams. Consequently, plastic hinges form in the precast beams away from the column face, and energy is dissipated in a fashion similar to that in monolithic concrete frames. There is a substantial amount of information available from Japanese, New Zealand, and US researchers on behavior of rigid connections[7,25,31]. Therefore, the current research effort did not focus on behavior of such connections.

2. *Ductile connections*. Connections which force nonlinear behavior to occur in the connection region or elements, while the precast members remain relatively undamaged, are termed "ductile connections". Therefore, in contrast to rigid connections, the precast beams and columns are designed with strengths higher

than the strength of the connecting elements. The current research effort at the University of Texas at Austin is focused on this type of connection.

2.3 TYPES OF DUCTILE CONNECTIONS

Four types of ductile connections were considered in this study. The connections are classified according to their behavior and method of dissipating energy during seismic excitation. The four classifications are:

1. *Tension/Compression Yielding*. Energy is dissipated through yielding of the connecting elements, and connecting elements are allowed to yield in both tension and compression, hence the name tension/compression yielding. For some connections, tension/compression yielding takes place on one side of the beam (top or bottom) while the other side behaves primarily as a pivot point to permit only rotation. To achieve yielding in both tension and compression at that location, a gap was left between the beam and column. This type of connection has also been called a "gap-joint" connection. Examples of tension/compression yielding connections are shown in Fig. 2.1.

2. *Friction*. In this connection type, energy is dissipated through friction when slip occurs between connecting elements. Special material can be used to enhance the slip behavior. The advantage of this connection type is reinforcing steel does not yield, resulting in cracking in the precast members that is relatively small even at large displacement levels. The same concept can be used as in the tension/compression connections where slip occurs on one side of the beam while the other side permits only rotation. A gap also must be provided to allow the slip to occur in both directions. An example of this connection type is shown in Fig. 2.2.

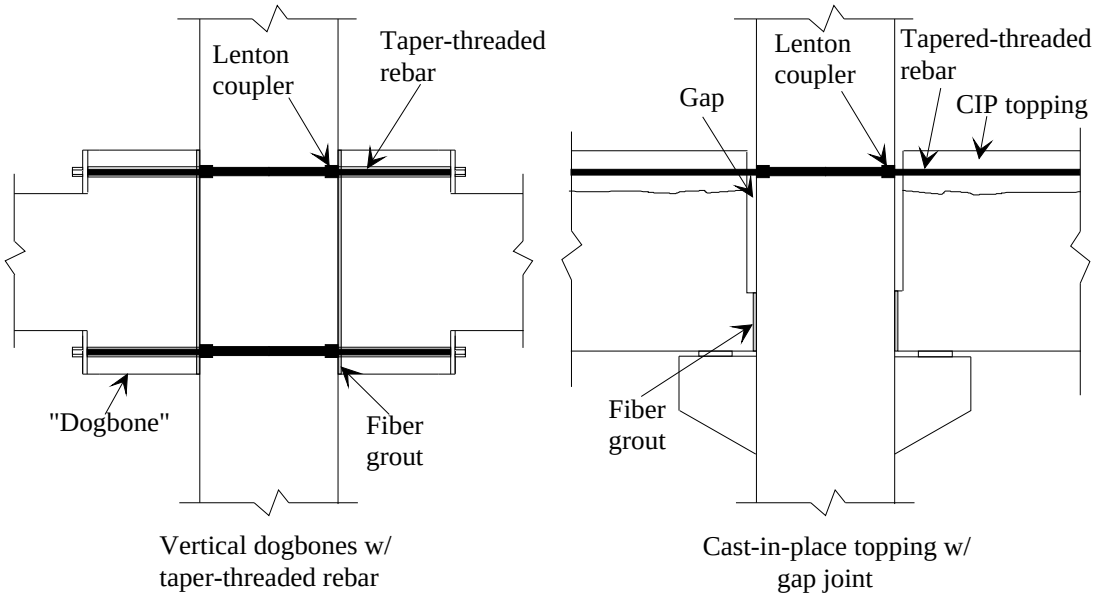

Figure 2.1 Examples of Tension/Compression Yielding Connections

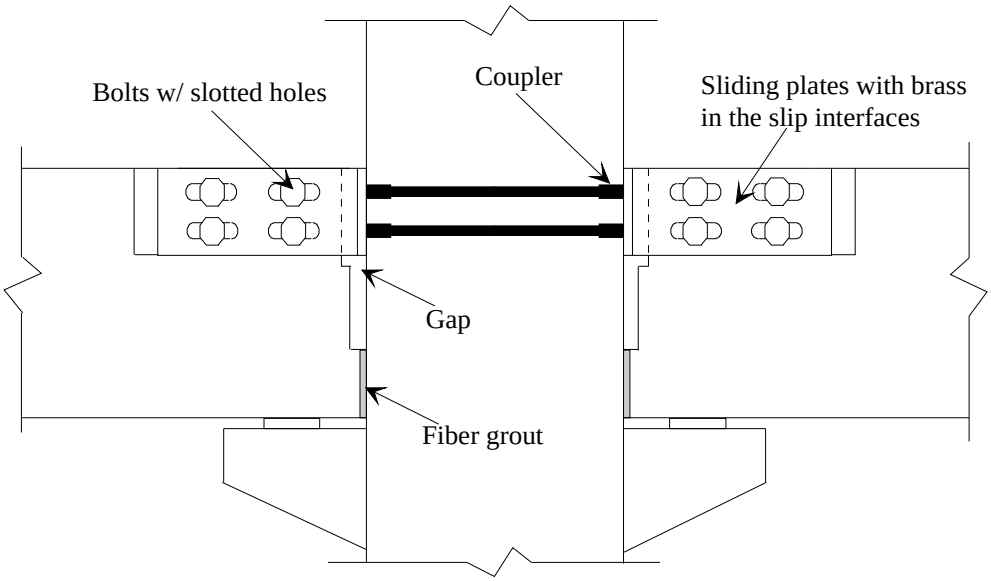

Figure 2.2 Example of a Friction Connection

3. *Nonlinear Elastic*. For this connection type, nonlinear behavior is achieved through crack opening and closing at the interface between each beam and column. This nonlinearity is related to geometric nonlinearity rather than material nonlinearity. Beams used in this connection type were prestressed, with tendons unbonded through the joint and for some length on each side of the column. Cracks or joints at the column face open when bending moments produce flexural stresses large enough to exceed the precompression stresses at the face of the column. Prestressing steel does not yield if it is unbonded over an adequate length. The behavior of this connection type is completely different from the first two types. In this connection type, energy dissipation is minimal. However, because of the prestressed beam, only small residual drifts are expected following strong ground movement. As a result, this connection also is described as "self-righting". Examples of this connection type are shown in Fig. 2.3.

4. *Shear Yielding*. This concept was previously investigated [32] in steel frames employing eccentric bracing. The rigidity of a concrete frame may promote development of shear yielding in a structural steel element similar to that used in an eccentrically braced steel frame. Consequently, energy is dissipated when yielding occurs in the steel element. An example of this connection type is shown in Fig. 2.4 in its original and deformed configuration.

2.4 DESIGN OBJECTIVES

In the process of developing ductile connection details, guidelines were first established to promote practical details. A number of meetings between US-PRESSS researchers and industry representatives occurred to establish the guidelines and review proposed connection details. This interaction was considered vital to future implementation of the research program results.

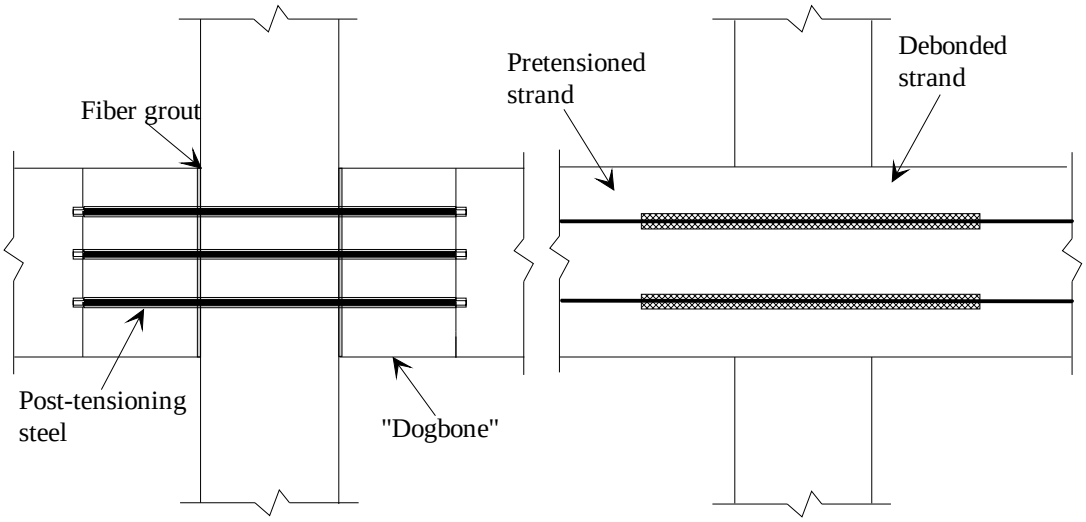

Figure 2.3 Examples of Elastic Nonlinear Connections

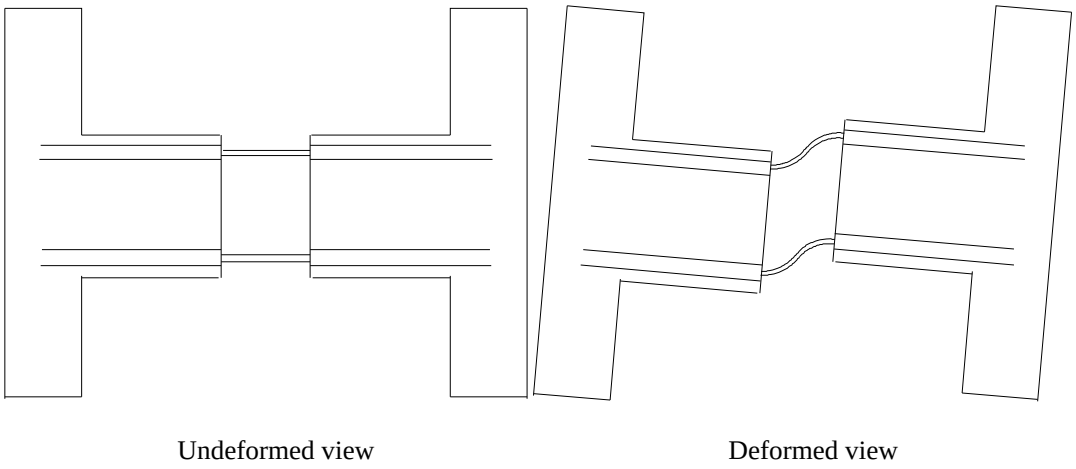

Figure 2.4 Example of Shear Yielding Connection

The following objectives were considered in developing ductile connection

details for precast frame systems:

1. *Ductility and Energy Dissipation.* Ductility and energy dissipation are understood to be important characteristics of a structure built to withstand earthquake loads. The definition of these terms will be discussed in Chapter 5.

2. *Dry Construction*. Connections that use minimal or no cast-in-place concrete are referred to as “dry connections”. In countries like Japan and New Zealand, precast concrete structural systems are widely used in seismic areas. The connections used in these systems utilize cast-in-place concrete to join precast elements. The resulting system emulates cast-in-place construction. In fact, in some cases the amount of cast-in-place concrete is so large that it is reasonable to describe the structure as a cast-in-place structure formed by precast concrete shells. These connections are referred to as “wet connections”. An example of “wet construction” is shown in Fig. 2.5. This approach is permitted by the UBC [22] in the United States. However, it is seldom used because the mixing of precast concrete and cast-in-place concrete can result in scheduling conflicts between construction trades when the cast-in-place concrete is required for structural stability of the system. The preferred method of construction in the US utilizes dry connections.

3. *Constructibility*. One objective of the program is to produce details that will be implemented in the future. This is less likely to happen if precasters and other industry representatives are not involved during the development of precast frame systems and details. However, consensus was not always achieved because materials and construction methods tend to vary from one region to another, and from one precast producer to another.

4. *Economy*. The aim of the program is to seek innovation, taking advantage of the unique characteristics of precast construction to provide economical building systems. This point must be considered in terms of both the initial cost of the

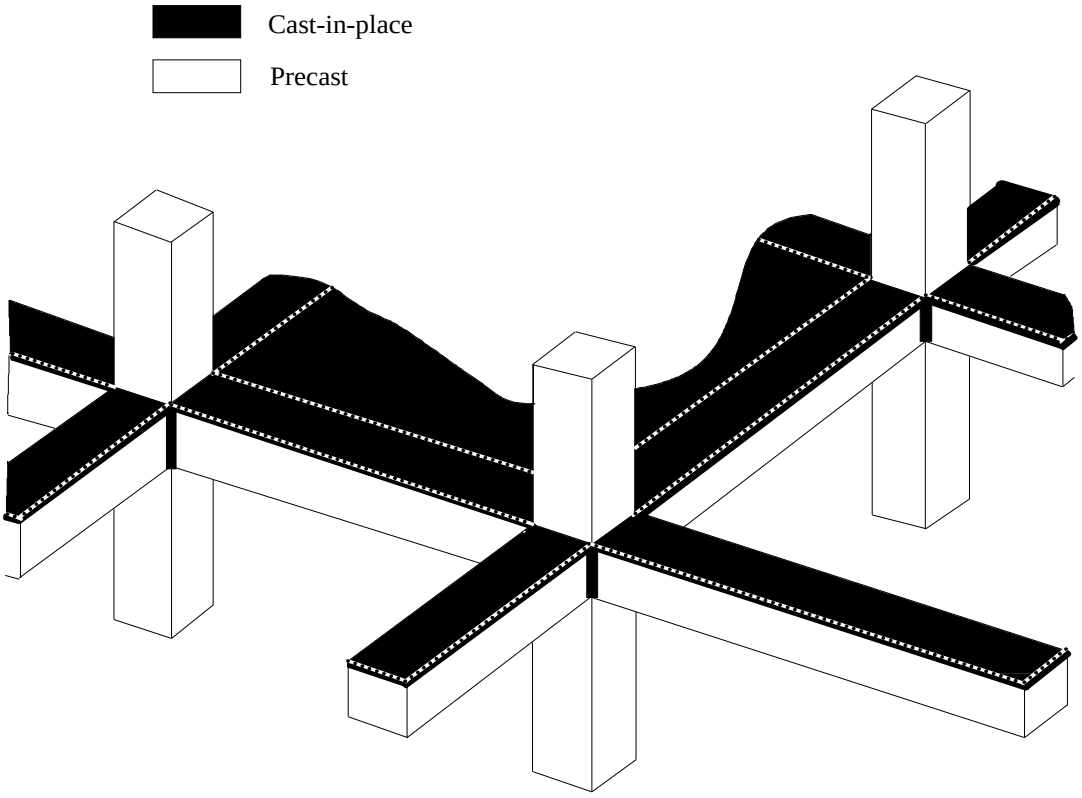

Figure 2.5 Wet Construction Concept

structure and the cost of repairs after an earthquake event. The initial cost of the structure can be divided into the cost of the precast members and the cost of labor. Precast frame systems eliminate most of the formwork, field assembly of reinforcing cages, and concrete placement.

On the other hand, the precast system typically requires transportation and on-site assembly of members, which are not necessary for conventional construction methods. In addition, some economy is lost if architectural demands result in a number of variations in formwork in the precast plant. However, even if the cost of manufacturing members is higher than that for conventional cast-in-place concrete, the precast frame system will still be attractive provided the time and labor required for erection make up the difference in cost associated with manufacture of the

members.

5. *Replacement.* This objective was given the lowest priority because it was not considered equitable to place a requirement on precast connections that is not also a requirement of conventional cast-in-place connections.

2.5 DESCRIPTION OF PROTOTYPE STRUCTURE

The structure used as a prototype in this study is a fifteen-story building. The elevation and plan views of the building, which is intended to be an office building are shown in Fig. 2.6 and Fig. 2.7, respectively. Design of the prototype was carried out by PRESSS phase I researchers at Englekirk and Sabol Consulting Engineers, Inc.

As shown in Fig. 2.7, the lateral-force-resisting elements of this building are concentrated along the perimeter. Notice also that the two perpendicular frames are not connected to each other with moment-resisting connections. All other frames in the building were intended to carry gravity loads only. In a frame designed for earthquake loading, moment connections, or ductile connections as they are called in this study, are designed to undergo significant deformation while dissipating energy through hysteresis. Connections in the gravity-load-carrying frames must be able to deform with the lateral-force-resisting system without attracting significant lateral force, and without compromising gravity load resistance. These connections are referred to as “extensible connections”.

As mentioned earlier, speed of erection is one of the most important elements in this system. Moment connections are, in general, complicated (and as a result, expensive) and time-consuming in terms of construction time. For this reason, PRESSS Phase I researchers minimized the number of such connections in a building

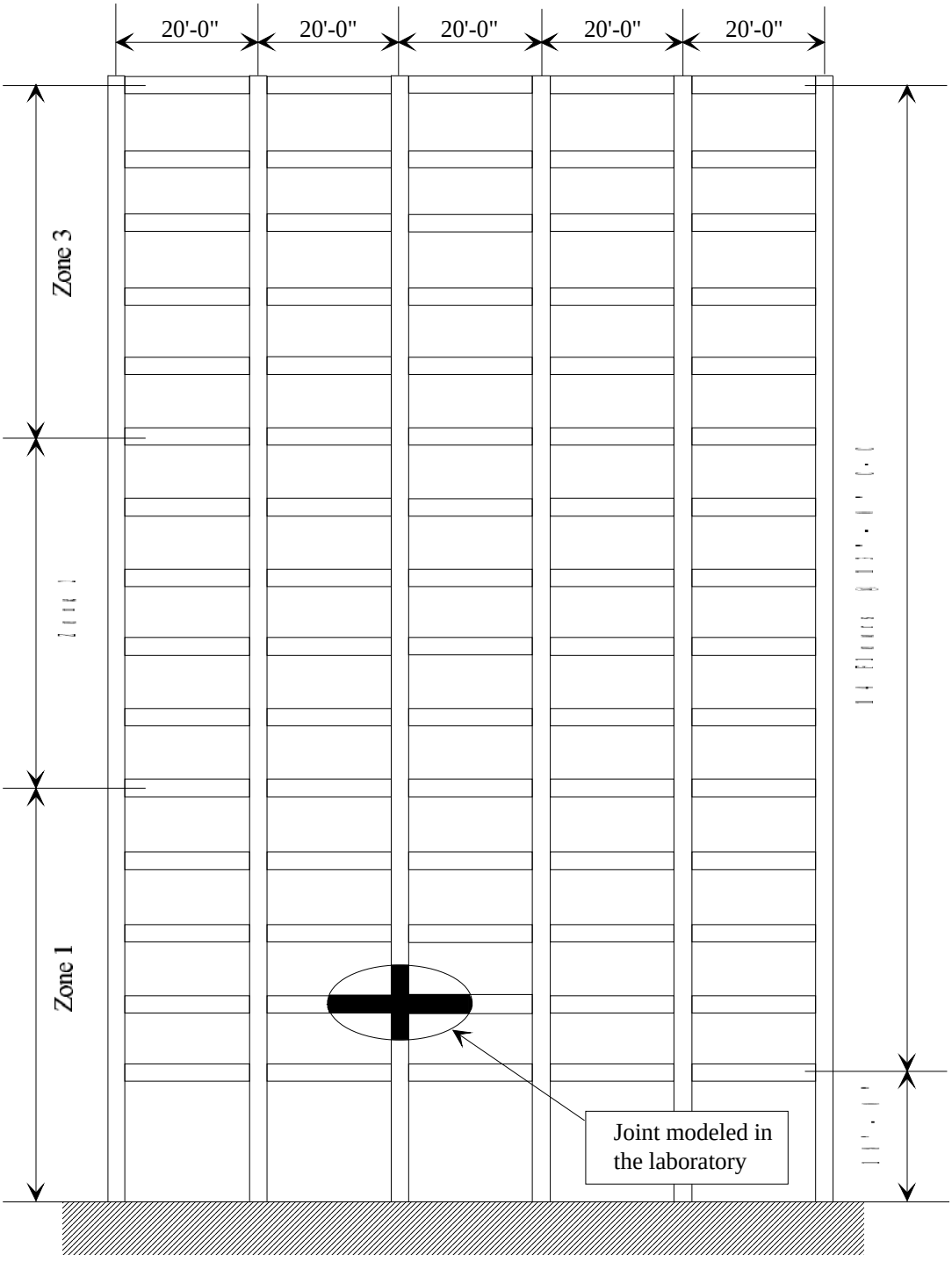

Figure 2.6 Elevation of Prototype Structure

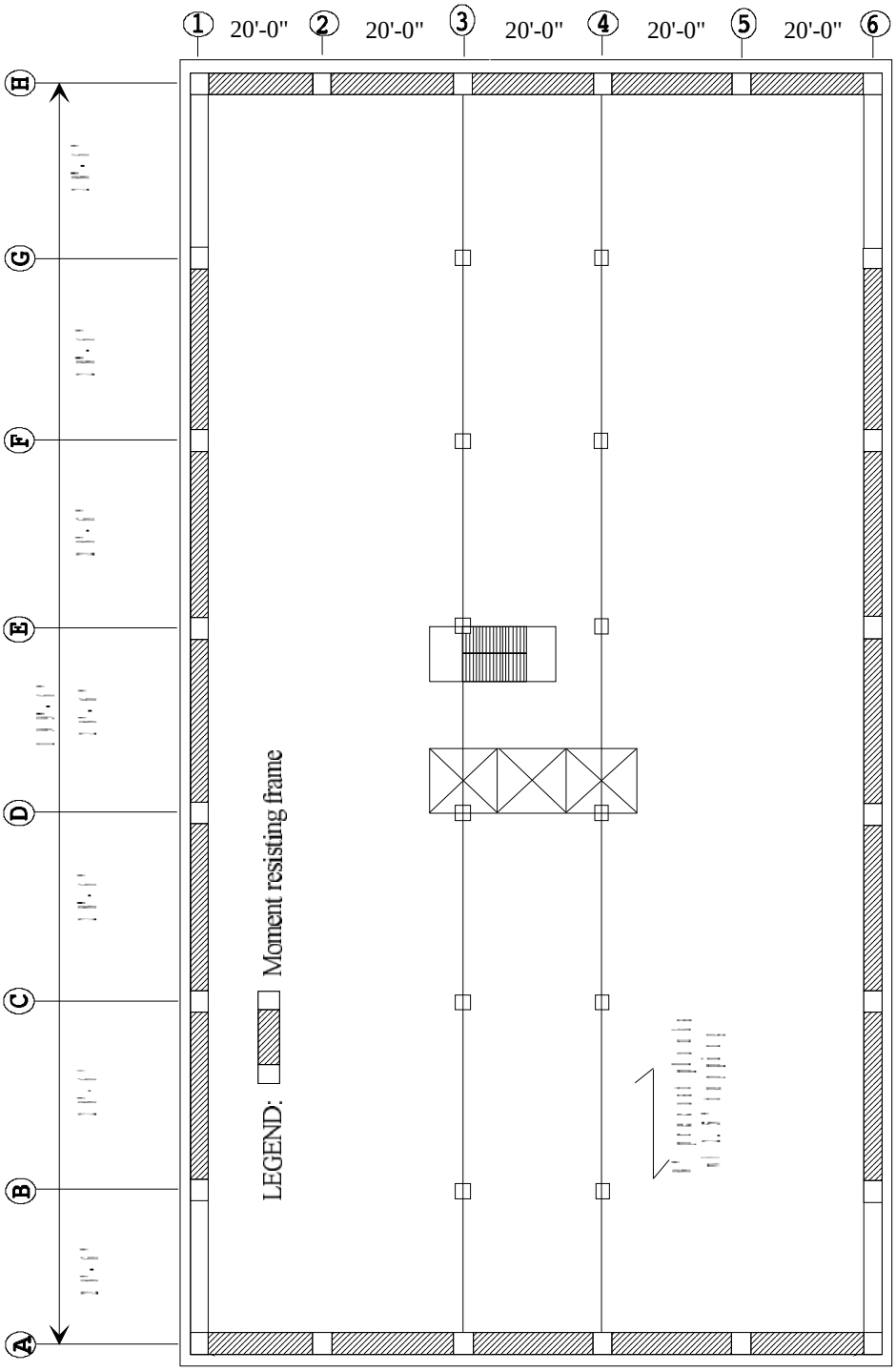

Figure 2.7 Typical Floor Plan for Prototype Structure

to speed the erection process and reduce cost. Consequently, the decision was made to make the perimeter frames the primary lateral-load-resisting system and make all interior elements the gravity-load-resisting system.

However, this framing scheme has its drawbacks. First, the system becomes less redundant which may jeopardize the stability of the entire building should a frame fail during an earthquake. Second, it puts extra demand on the elements in the lateral-load-resisting frames resulting in huge member sizes and substantial amounts of reinforcement. It is worth mentioning here that the second observation made it very difficult to fabricate the test specimens; connections were very congested with reinforcement to resist the required scaled forces. Figure 2.8 shows the reinforcement cage for the beams in one of the specimens.

Connections tested in the laboratory were models of a typical interior connection in Zone 1 of the frame elevation shown in Fig. 2.6. Also, to test the most critical connections in the building, specimens represented connections from the frames in the short direction of the building, because shorter beam spans result in higher shears.

2.6 DESIGN OF PROTOTYPE STRUCTURE AND SUBASSEMBLAGES

The UBC presents seismic design requirements in terms of elastic design loads combined with prescriptive detailing requirements. These requirements have evolved over time through investigation of several standard building systems. Specifically, concrete systems approved for use in high seismic zones are limited to ductile frames, often called special-moment-resisting frames, and shear walls that meet the prescriptive detailing requirements of the code. Alternative systems can be used only if they are shown to behave similar to emulate approved systems.

Due to the limited data available, it has been presumed that precast concrete

Figure 2.8 Congestion of Reinforcement

connections are less ductile and tend to have less stable inelastic response than conventional cast-in-place concrete connections. As a result, only general provisions for the design of precast concrete structures have been included in the US building codes. The UBC requires that the design of connections for precast structures should be as required for cast-in-place structures. Because of this, design recommendations for monolithic construction were often used as a guide for designing the prototype structure and for proportioning connection specimens.

2.6.1 Design of Prototype Structure

The 15-story building described in the previous section was designed using the criteria presented in UBC-1991[22]. According to the UBC method, the frame under consideration must be designed for a total base shear given by:

$$V = \frac{ZIC}{R_w} W \tag{2.1}$$

where V = the total lateral force or shear at the base.

Z = seismic zone factor.

I = importance factor depending on the function of the building and equal to 1 for regular use buildings such as offices and apartments.

R_w = numerical coefficient depending on the type of structural system used and reflects the ductility of the structure.

W = total weight of the structure.

C = numerical coefficient defined as:

$$C = \frac{1.25S}{T^{2/3}} \leq 2.75 \tag{2.2}$$

where S = site coefficient for soil characteristics.

T = fundamental period of the structure, in seconds.

Beam moment demands were based on an R_w factor of 12, which is the highest allowed by the UBC; zone factor equal to 0.4, which corresponds to ground acceleration of 0.4g; a site factor equal to 1.2; and an assumed building period of 1.5 seconds. Consequently, the design moment, M_u, for the prototype beam-column connection was 2160 ft-k. A strength reduction factor of 0.9 was used to obtain the nominal moment capacity, M_n, of 2400 ft-k. Vertical acceleration was not considered in the design.

2.6.2 Design of Subassemblages

Subassemblage specimens were detailed in accordance with the provisions of the ACI-318 Building Code and the latest design recommendations of ACI-ASCE Committee 352 [2]. The 352 report, which contains recommendations for joint shear stresses, and the amount of transverse reinforcement in the joint, was intended for monolithic connections. Because no specific design recommendations exist for ductile precast connections, the recommendations for monolithic connections were used as a conservative guide for detailing the joint region of connections.

The beam design moment for the test specimens was 300 k-ft. This moment was determined by scaling down the moment capacity for the prototype connection using a scale factor of 1/2. A capacity design approach was used in the design of the connections so that the connecting elements between each beam and column was the weak link in the subassemblage. In addition, the column flexural strength was increased by at least 40 percent to satisfy the strong column - weak beam design criterion in the 352 design recommendations. Also, to ensure a flexural failure rather than shear failure, the shear strength of the beams was increased by at least 30 percent.

In this study the following assumptions were incorporated in the design:

- No axial force was imposed on the column. In reality, the column is subjected to axial force due to the dead and live loads and also due to the lateral seismic forces. In general, the axial force helps improve the behavior of the joint and joint shear strength. Since this study concentrated on the behavior of the connecting elements rather than the joint, it was believed that the application of the axial force was irrelevant here.

- There were no transverse beams framing into the joint. The prototype building was considered to consist of precast one-way peripheral-moment frames with interior gravity-load-carrying frames as explained in the previous section.

- The floor system was not modeled in these tests. In the prototype building the flooring system was considered to be precast hollow-core planks spanning between interior frames and the perimeter frames.

CHAPTER 4

EXPERIMENTAL RESULTS

4.1 INTRODUCTION

Overall behavior of the specimens is discussed in this chapter with the aid of story shear versus story drift ratio curves and observations of cracking. To better understand the behavior of the specimens, beam rotation response and other relevant measurements for particular specimens also are presented. Comparison of specimen behavior is presented in Chapter 5.

4.2 OVERALL SPECIMEN BEHAVIOR

4.2.1 Story Shear- Drift Ratio Relationships

As discussed in Section 3.5, it was more practical to impose specimen deformations through the beam tips rather than either column end (see Fig. 3.37). Using statics, the story shear, *V*, can be obtained by:

$$V = (P_{bE} + P_{bW})\frac{L}{2H} \tag{4.1}$$

where P_{bE}, P_{bw} = east and west beam tip loads, respectively

L = beam length = 120 in.

H = column height = 78 in.

Similarly, the story drift ratio, *R*, can be obtained by:

$$R = \frac{\Delta_{bE} + \Delta_{bW}}{L} \tag{4.2}$$

where Δ_{bE}, Δ_{bW} = east and west beam tip displacements, respectively.

4.2.1.1 Specimen DB-TC

Figure 4.1 shows the story shear-drift ratio response for Specimen DB-TC. The specimen exhibited little damage during displacement cycles through 1 percent drift ratio. The high-strength bars were estimated to have yielded at a drift ratio between 0.75 and 1 percent. This was based on changes in stiffness observed in the envelope of story shear-drift response. Measured strain data from the high strength bars were not available to confirm this observation. Strain gages were intentionally not attached to the high-strength bars to avoid altering the bond characteristics between the grout and bars.

During the first excursion to 1.5 percent drift ratio, concrete between the 90 degree hooks on the reinforcing bars and the ends of the high strength thread bars on the tension side of each beam crushed (see Fig. 4.2). Consequently, the load dropped as indicated by the arrow in Fig. 4.1. The same concrete crushed on the opposite side of each beam when forces on the connection were reversed. The nuts were then removed from each group of four high-strength thread bars and another displacement cycle was applied to attempt to identify the ultimate bond strength between the high-strength bars and the grout. Unfortunately, too little concrete compressive strength remained in the connection regions to facilitate pullout of the bars.

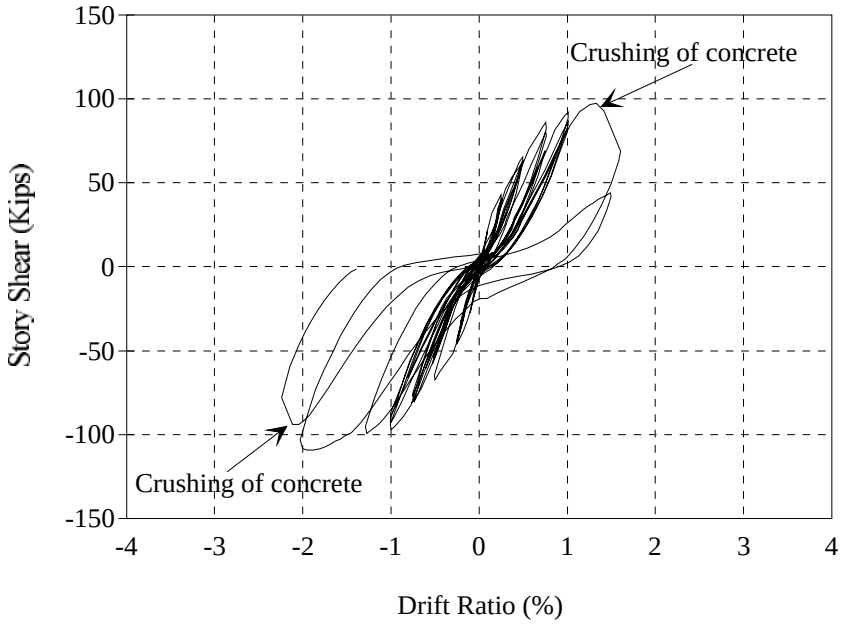

Figure 4.1 Story Shear vs. Story Drift Ratio Response for Specimen DB-TC

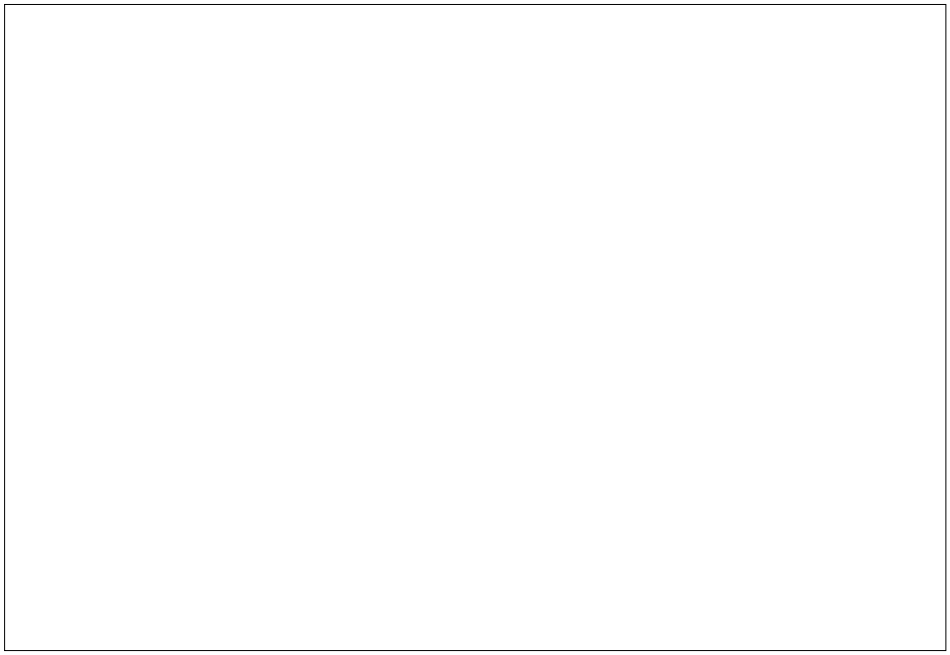

Figure 4.2 Crushing of Concrete in Beams of Specimen DB-TC

Cycles up to 1 percent drift ratio did not show any significant pinching in the hysteresis loops. The hysteresis loops became significantly pinched after crushing of the concrete at 1.5 percent drift ratio. Although no corbel or bracket was used, no significant slip across the beam-column interface was detected by linear potentiometers.

4.2.1.2 Specimen GJ-TC

Figure 4.3 illustrates the story shear-drift ratio response for Specimen GJ-TC. Yielding of reinforcement in the beams was evident at approximately 0.75 percent drift ratio. Unlike Specimen DB-TC this connection achieved its full design strength at slightly more than 0.75 percent drift ratio. At higher drifts, the connection continued to harden at approximately 2 percent of its initial stiffness. This hardening is mainly attributed to the stress-strain properties of the beam top reinforcement. Coupon tests showed that strain hardening in this steel began at a strain of approximately 0.006, or 2.6 times the yield strain, which is unlike what is typically measured during tensile tests of reinforcement.

Up to 0.75 percent drift ratio this specimen showed little pinching. The hysteresis loops became pinched at higher drifts. This pinching is attributed primarily to relative horizontal displacements (in the plane of the beam-column connection) at what was assumed during design to be a “pin” connection between the beams and the corbel. This relative movement was most pronounced when beams were subjected to positive bending. The maximum relative displacement at the beam-corbel interface for each displacement cycle is illustrated in Fig. 4.4. Notice that the trend is not linearly related to increases in drift, and that the stiffness of the pin connection appears to deteriorate, especially at large drifts, during successive cycles to the same drift. Relative displacements between the beams and corbels were aggravated by the

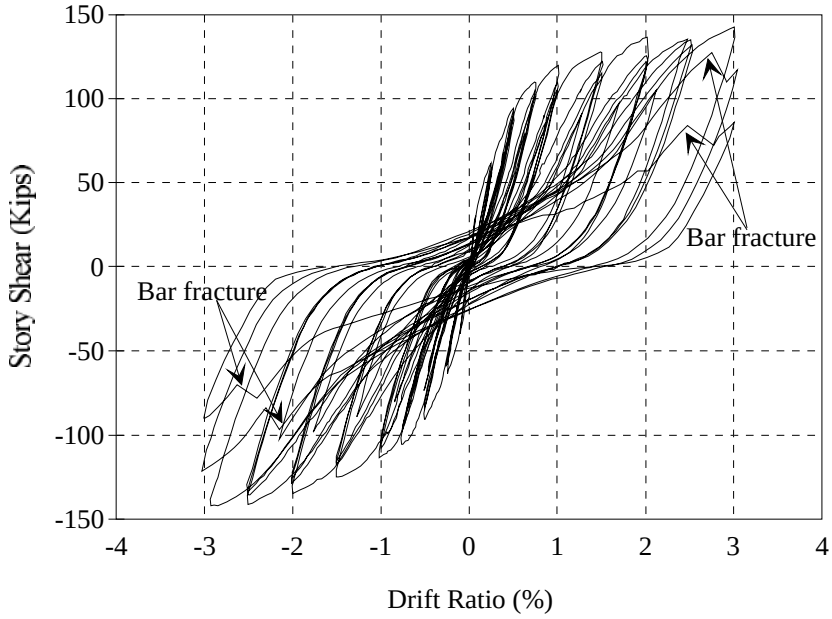

Figure 4.3 Story Shear vs. Story Drift Ratio Response for Specimen GJ-TC

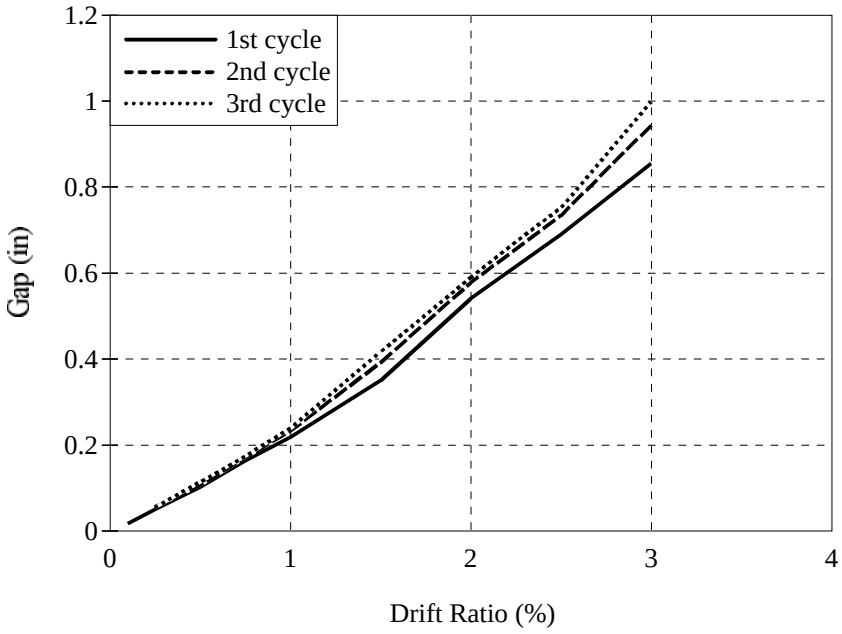

Figure 4.4 Maximum Relative Displacement Between Beam and Corbel

stress-strain properties of the beam top reinforcement as explained above.

As a result, the strength demand on the pin connections was increased substantially at lower drift levels. Crushing of the grout surrounding the vertical high-strength dowels contributed to deterioration of the pin connections and increased flexibility of the specimen. During the second cycle to 3 percent drift ratio, a loud noise was emitted from each beam when it was subjected to positive bending. This was followed by a substantial decrease in load. In the third cycle further reduction in strength occurred. Fracture of the dowel bars was the cause of the specimen failure. This was verified when the specimen was autopsied at the end of

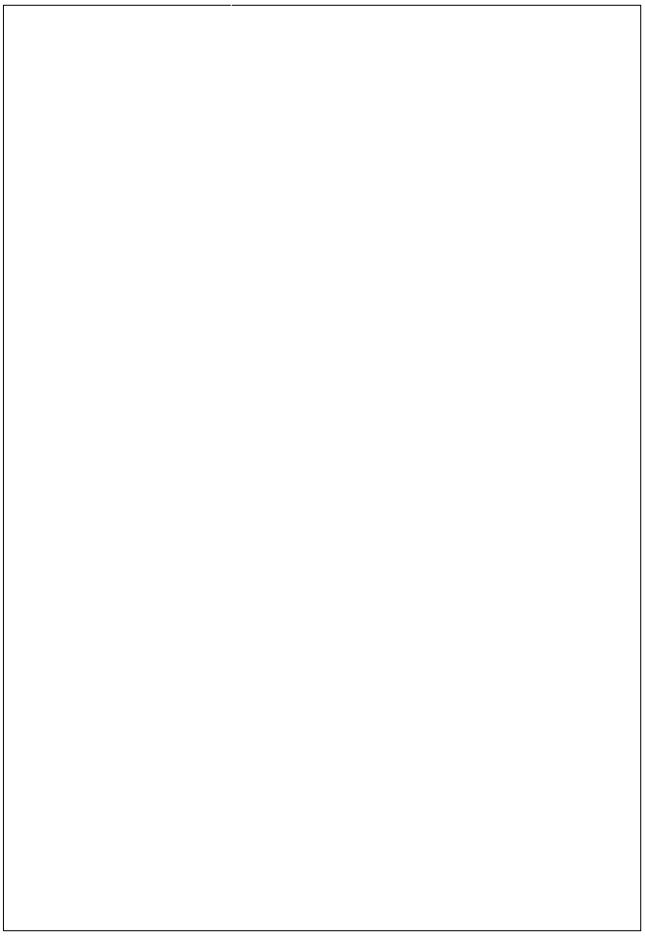

Figure 4.5 Fractured Dowels after Removal of Beams

Figure 4.6 Deterioration of Grout Around Dowels

the test. Figure 4.5 shows the corbel and the fractured dowels after removal of the beams. Figure 4.5 shows the deterioration of the grout around the dowels at the bottom of the beams.

4.2.1.3 Specimen GJ-FR

The story shear-drift ratio response for Specimen GJ-FR is shown in Fig. 4.7. Cycles up to 1 percent drift ratio demonstrated practically elastic response. As explained before, this specimen was intended to dissipate energy through friction when slip occurred between the beams and the column in both tension and compression. During the 1.5 percent drift ratio, slip occurred in both beams. Slip of the beam connections continued after that throughout the test. In general, slip was not perfectly smooth. Friction built up to a critical load and then slip occurred.

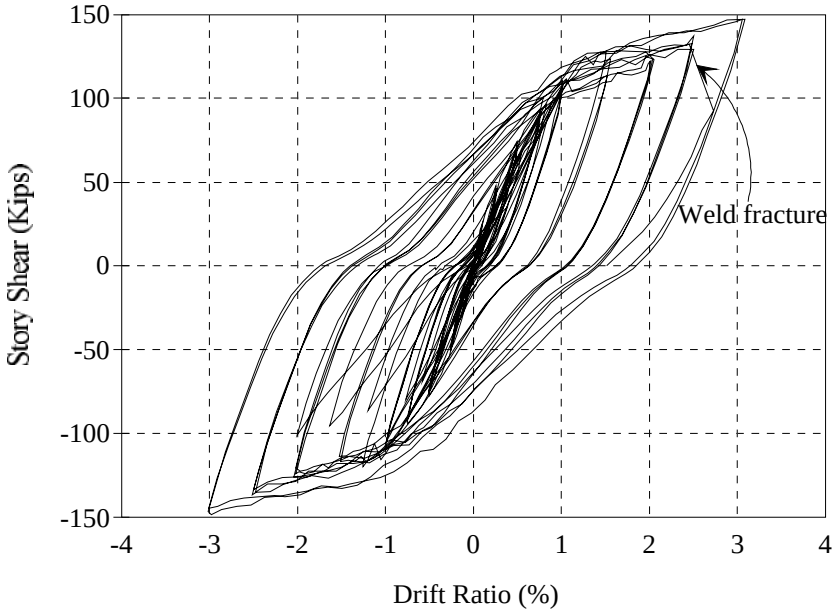

Figure 4.7 Story Shear vs. Story Drift Ratio Response for Specimen GJ-FR

When slip occurred the load dropped just slightly and then increased again as loading continued. Sound was usually emitted when slip occurred. Figure 4.8 illustrates the load at the tip of one of the beams vs. actual slip of the beam relative to the plates connected to the column. Notice that during unloading no slip occurred (the lines are nearly vertical), and when the slip load was reached while loading in the opposite direction, slip occurred again.

This specimen exhibited very little damage during testing. Through the first two cycles to 3 percent drift ratio, the hysteretic behavior was stable. Unlike Specimen GJ-TC where the hysteresis loops were pinched, hysteresis loops exhibited only slight pinching. The pinching is mainly attributed to the flexibility and bending of the connecting plates and flexibility of the bolts connecting the plates to the couplers in the column.

The specimen reached its design strength at slightly greater than 1 percent drift ratio. Following slip of the friction connections, ideally, the strength attained

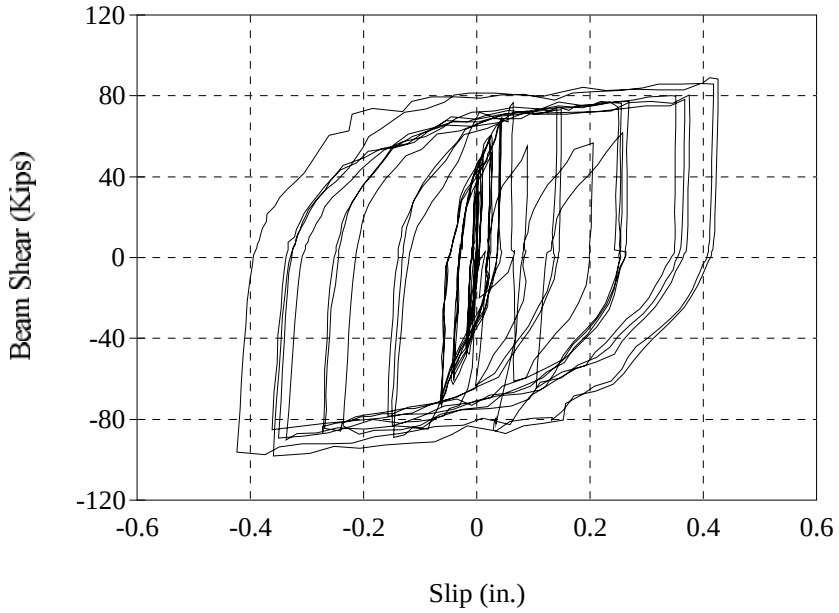

Figure 4.8 Beam Shear vs. Slip for Specimen GJ-FR

should remain virtually constant. As demonstrated in Fig. 4.7, the resistance of the specimen continued to increase with increases in drift level. Slip in the friction connections was not the same as slip of the isolated plates tested by Grigorian et al. [20] and described in Section 3.3.3. In that setup, plates are expected to slip along a straight line. In the connection described here, as the connections slip they also rotate (due to rotation about the bottom connection). Therefore, the bolts in the slotted holes could not slide along the slotted holes without bearing against the sides of the holes. Inspection of the specimen showed that the bolts did bear against the top and bottom edges of the slotted holes. The unexpected bearing against the bolts resulted in increased resistance to slip.

As mentioned above, the specimen behaved quite well through the first two cycles to 3 percent drift ratio. However, the continued increase in specimen resistance imposed extra demand on other connection components that were intended to remain elastic. In general, all other connection components were designed to have 30 percent more strength than needed for design slip of the friction

connections. During the third cycle to 3 percent drift ratio, the weld between one of the plates containing the slotted holes and the plate connected to the column fractured.

4.2.1.4 Specimen GJ-FR-R

The decision was made to retest the specimen after repairing the connecting plates. By doing so, the feasibility of repairing such a connection could be assessed. The plates connecting the beams to the column were removed. The beams were then repositioned in their initial horizontal position. New plates were designed and manufactured. To reduce bending of the plates bolted to the column, a finite element program was used to design the plate in an attempt to avoid yielding and excessive bending under the design loads. The thickness of the plates used this time was 1.5 in (instead of 13/16 in.). The thickness of the weld was also increased from 3/8 in. to 1/2 in. This was done to prevent failure at the same location. Considering that the specimen already contained a significant amount of cracking, it was decided to reduce the strength of the connection in order to avoid excessive resistance and potential failure of the specimen before assessing its new hysteretic behavior. As a result, bolts were tensioned to 58 kips each instead of the 64 kips used in the original specimen. The corresponding design moment became 3387 k-in. (versus 3635 k-in. for the original connection).

The loading history applied varied from the history described in Section 3.5. Because the specimen was already cracked, small drift level cycles were considered unnecessary. The main reason for carrying out the test was to investigate the stiffness of the repaired/rehabilitated connection and the influence of the friction connections that were expected to slip at reduced loads. The loading history applied

Figure 4.9 Story Shear vs. Story Drift Ratio Response for Specimen GJ-FR-R

consisted of the following cycles: 2 cycles each at 0.25 percent drift ratio, 1 cycle at 0.5 percent drift ratio, followed by 2 cycles each at 1, 1.5, 2, 2.5, and 3 percent drift ratio. After each set of two cycles another cycle to 75 percent of the maximum load applied in the previous two cycles was applied. At the time it was intended to also load the specimen with 2 cycles to 4 percent drift ratio and then monotonically load it to failure.

Figure 4.9 shows the story shear-drift ratio response. No slip took place during cycles up to 1 percent drift ratio. During these cycles the response was primarily elastic. Pinching of the hysteresis loops was obvious in these cycles unlike in the original test. This pinching is mainly attributed to the fact that the specimen was already cracked. A crack which existed at the bottom corner of the column and the corbel opened and closed a significant amount (1/32 in.) leading to some of the observed pinching. Like the original specimen, some pinching was observed in the hysteresis loops at large drifts. This pinching was not as great due to reduced bending of the plates bolted to the column. However, the flexibility of

the bolts connecting the plates to the couplers in the column still existed. No significant tension was applied in these bolts because they were not easily accessible. Significant tensioning of these bolts would have eliminated a significant amount of flexibility and reduced the pinching.

During cycles to 1.5 percent drift ratio, slip of the beams was initiated. Slip in these cycles was very smooth, and the slip load remained almost constant. At this drift level the load was lower than expected. The expected resistance is a function of the bolt tension and the coefficient of friction between the steel and brass plates. As higher drift was imposed on the specimen, the resistance of the specimen increased in a fashion similar to that observed during the original test. During the second excursion to 3 percent drift ratio, one of the bolts used in the bottom beam connection pulled out (as evidenced in Fig. 4.9). At this stage the specimen was considered to have failed.

When the specimen was later autopsied, the bolt appeared as shown in Fig. 4.10. The threads on the bolt had been stripped. The autopsy also revealed that one of the #7 bottom reinforcing bars welded to the plate in the same beam had fractured. In general, the rehabilitated/retested specimen behaved well considering that it was subjected to drifts well beyond the design drift in the previous test. At the conclusion of testing, no large cracks or concrete spalling was observed.

4.2.1.5 Specimen PT-NE

Figure 4.11 shows the story shear-drift ratio response for Specimen PT-NE. As was explained in Chapter 3, this specimen was intended to exhibit nonlinear behavior yet remain elastic throughout the test. The connection was designed to remain elastic by proportioning the length of the debonded strands and their initial

Figure 4.10 Bottom Connection Bolt for Specimen GJ-FR-R After Pull Out

stress so that yielding would not take place even at high drift levels. The nonlinear action occurred when a crack on each side of the column opened at the beam-column interface. The story shear-drift ratio response shown in the inset of Fig. 4.11 through 2 percent drift ratio illustrates the nonlinear-elastic behavior. The specimen tends to return to its original undeformed position when it is unloaded. An ideal nonlinear-elastic specimen would unload along the same load-deformation path for loading. In reality, some energy is dissipated while unloading due to closing of cracks.

This specimen was taken to drift ratios exceeding 3 percent while exhibiting stable hysteretic behavior. Pinching, however, was evident from the very beginning of the test. This pinching was mainly attributed to slip in the couplers used to connect the bottom column with the top column. The couplers used here are typically used for coupling post-tensioning bars. The threads in the couplers are coarse, leaving space for the bars to slip. When the bars experienced tensile forces,

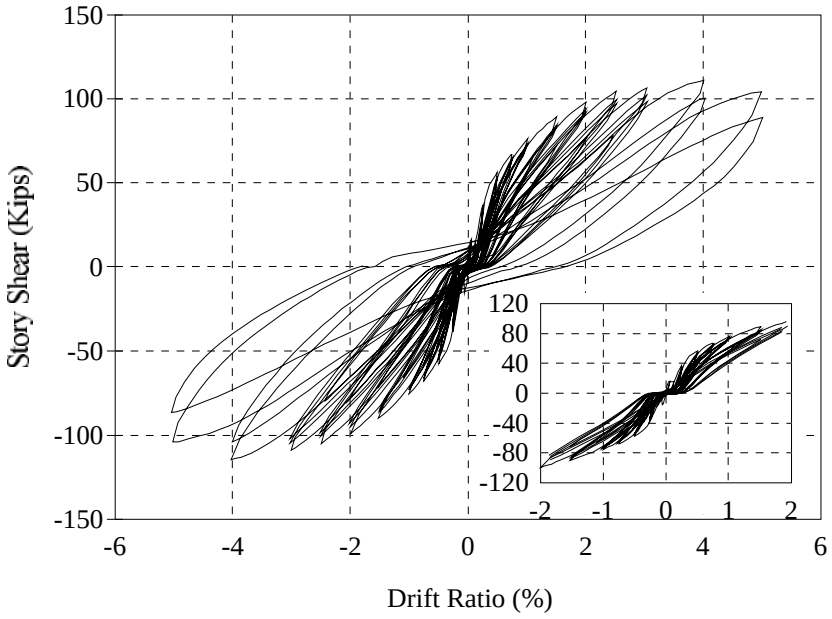

Figure 4.11 Story Shear vs. Story Drift Ratio Response for Specimen PT-NE

they slipped until the threads in the coupler were engaged. Once a crack formed in the column, a very small load was needed to produce slip in the couplers.

The process reversed itself when the load was reversed, leading to the pinching observed in the hysteresis loops. Notice, however, that the amount of pinching remained fairly constant throughout the test. Therefore, pinching can be eliminated by using a commercial coupler more suitable for bar splicing. As was stated in Section 3.3.4, this type of coupler was used because commercial couplers that would fit in this 1/2 scale specimen were not available. An effort was made here to remove the effect of the coupler slip from the story shear-drift ratio response. Data gathered using two linear potentiometers located across the crack where the couplers were located were used to geometrically subtract the additional drift caused by this crack opening. Figure 4.12 is a reproduction of Fig. 4.11 after the estimated additional drift was removed. As can be seen, this crack at the bar couplers appears to account for a significant amount of the pinching.

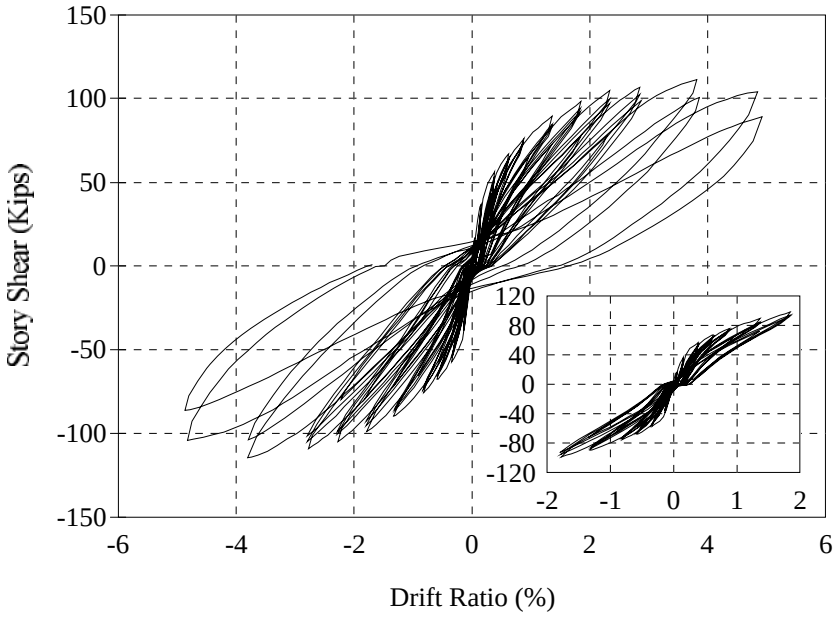

Figure 4.12 Modified Story Shear vs. Story Drift Ratio Response for Specimen PT-NE

This specimen was designed to achieve its full design strength at a drift ratio of approximately 2 percent. Figure 4.12 indicates that the strength of the specimen at 2 percent drift ratio was approximately 88% of the design strength. The lower strength was attributed to concrete spalling at the extreme fibers of the beam. Although the outer regions of the beam were confined with spirals, extensive crushing and spalling of the concrete took place at those locations. During design, (cover was assumed to have spalled) calculations were based on the confined concrete in the beams only. However, inspection of the beams indicated that spalling penetrated more than the depth of the cover concrete. As a result, the resultant of the compression force in the beams was closer to the resultant of the tensile force.

As mentioned above, the specimen sustained little damage through drifts to 3 percent. Even during excursions to 4 percent drift ratio, the strength of the specimen did not reduce. Excursions to 5 percent drift ratio resulted in wide

diagonal cracks in the joint and spalling of concrete. The rapid deterioration of the joint strength at excessively large drifts was the cause of specimen failure.

4.2.2 Observation of Cracking

Crack patterns were used to visually assess damage during a given loading cycle and for the total loading history. Cracks were typically marked at the end of the first cycle in each set of cycles. Different pen colors were used for each loading direction. During other cycles at the same drift level, in general, no new cracks opened because load was usually lower than for the first cycle due to stiffness degradation in the connection.

4.2.2.1 Specimen DB-TC

The interface between the beam and column opened during the 0.1 percent drift ratio cycle. During that cycle the story shear was 27 kips. Distributed flexural cracks were observed in the beams and column during cycles to 0.25 percent drift ratio. An inclined crack at the corner of the dogbone became visible during the next set of cycles at 0.5 percent drift ratio. At that time strain gauges on the beam stirrups at that location indicated yielding of the reinforcement. During load reversal cracks on the opposite sides were observed. This crack, which assumed the shape of the letter “C”, followed closely the hooks on the main beam reinforcement, and became nearly 0.04 in. wide at 1 percent drift ratio. Figure 4.13 shows the specimen at 1 percent drift ratio. At this level the specimen achieved 85% of its design strength.

Cracks in the column remained small for the entire loading history and closed after removal of the load. Joint diagonal cracks were also very small (less than 0.005

Figure 4.13 Crack Patterns at 1% Drift Ratio for Specimen DB-TC

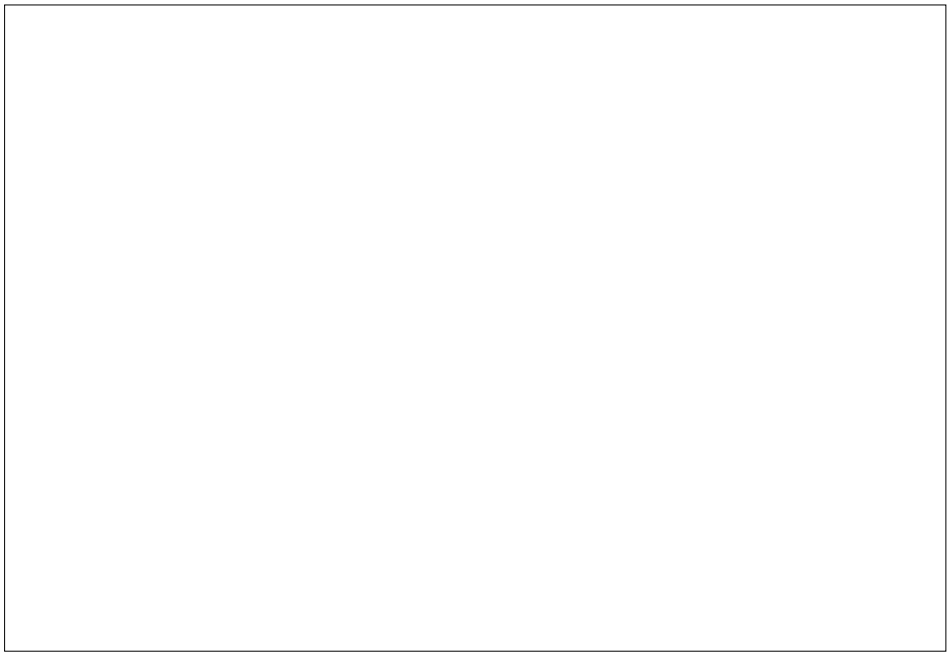

Figure 4.14 Specimen DB-TC at End of Test

in.) and virtually invisible upon load removal. The maximum joint opening between the beams and column at loading was 0.15 in. Figure 4.14 shows the crack patterns and the damage sustained at the end of the test.

4.2.2.2 Specimen GJ-TC

During the 0.25 percent drift ratio cycles hairline cracks opened in both the beams and column. These cracks were mainly flexural cracks. At this stage these cracks were not visible on the bottom of the beams since the stiffness of the beams under positive bending was lower than that under negative bending. Consequently, the load needed to achieve the same displacement in the upward direction was smaller than that needed in the downward direction. During the first excursion to 0.5 percent drift ratio, cracks were observed on the bottom of the beams. Cracks in the top of the beams and in the column continued to grow and to become inclined due to interaction of flexure and shear. Also during this cycle, cracks opened at the lower corner of each corbel when the corresponding beam was subjected to positive bending. This crack indicated that the vertical high-strength bars were resisting the uplift force imposed on the beams. Fine diagonal cracks (less than 0.005 in.) in the joint area were also observed during these cycles.

During the 0.75 percent and 1 percent drift ratio cycles the fiber-grout-filled joint between the beam and the column opened. The opening of the joint was approximately 0.15 in. and was constant during cycles to the same drift level. Up through 1 percent drift ratio all cracks, except the joint between the beam and the column, closed upon removal of load. No crushing or spalling of concrete was observed through this stage. Figure 4.15 shows a general view of the specimen at 1 percent drift ratio.

During the 1.5 percent drift ratio cycles, only a few new cracks opened.

Figure 4.15 Crack Patterns at 1% Drift Ratio for Specimen GJ-TC

However, the joint opening between the beam and column continued to grow rapidly. During the 2 percent drift ratio cycles this opening became as wide as 0.6 in. Yielding in the top reinforcement of the beams became very pronounced at this stage as splitting cracks in the top of the beams near the column became wide, (approximately 1/16 in.). Some concrete crushing at the bottom of the beams took place during this set of cycles. Figure 4.16 shows the specimen at 2 percent drift ratio, and Fig. 4.17 illustrates the joint opening and concrete crushing.

During cycles to 2.5 and 3 percent drift ratio, some spalling of concrete around the couplers in the column was observed. Cracks at the top of the beams became as wide as 1/8 in. due to yielding of reinforcement. Crushing of concrete at the corner of the corbel and column also occurred. Although a fine crack was observed at the interface between the precast and cast-in-place concretes, no relative movement was detected at that construction joint for the entire test. Figure 4.18 shows the specimen at the end of the test.

Figure 4.16 Crack Patterns at 2% Drift Ratio for Specimen GJ-TC

Figure 4.17 Joint Opening at 2% Drift Ratio for Specimen GJ-TC

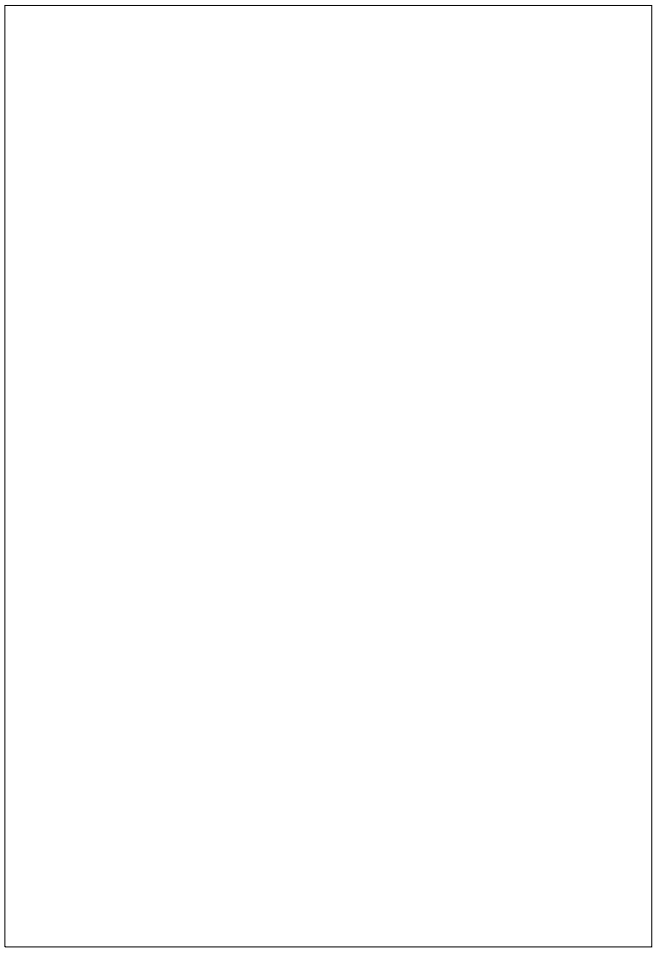

Figure 4.18 Specimen GJ-TC at End of Test

4.2.2.3 Specimen GJ-FR

This specimen was designed to minimize structural damage and to achieve energy dissipation and good hysteretic response with the aid of friction devices used in the connecting elements. During the 0.25 percent drift ratio cycles, flexural cracks were observed in the column. Also at this level, diagonal cracks in the joint region started to appear. Beams cracks appeared during the 0.5 percent drift ratio cycles. These cracks, which continued to develop during later cycles to 0.75 and 1

percent drift ratio, were very well distributed and spaced at approximately 4 in. apart. The crack widths were invisible upon load removal. Crack distribution at 1 percent drift ratio is shown in Fig. 4.19.

As loading continued through the next set of cycles, no new cracks appeared but existing flexural cracks observed in the beams and column grew deeper in the members and some became inclined. During the 1.5 percent drift ratio the beams started to slip. Figure 4.20 shows the specimen at 2 percent drift ratio, and Fig. 4.21 shows a close-up of the slip of one of the beams at 2 percent drift ratio. The white line indicates the original position of the beam before it slipped.

Joint cracks remained very small during the entire test and, in general, joint behavior was satisfactory. The corbels also showed no significant distress during the test. Fine cracks developed at the corners of the corbels but generally closed after removal of load. At the end of the test the only location where some spalling of concrete occurred was in the beam dap at the location of the beam support. This spalling can be attributed to the high concentrated stress at that location as the beams rotate. Figure 4.22 shows the specimen at the end of the test. As can be seen, the specimen sustained no significant damage after cycles through 3 percent drift ratio. Most of the cracks closed after removal of load.

4.2.2.4 Specimen PT-NE

During the 0.1 percent cycle, the grout around the couplers cracked due to sloppiness in the couplers, as explained earlier. This crack was approximately horizontal and continuous on all four sides of the column. The crack was about 0.075 in. wide. It continued to open and close throughout the test and was the primary reason for pinching in the hysteresis loops.

Hairline flexural cracks were observed in the lower column element during

Figure 4.19 Crack Patterns at 1% Drift Ratio for Specimen GJ-FR

Figure 4.20 Crack Patterns at 2% Drift Ratio for Specimen GJ-FR

Figure 4.21 Slip of Beams at 2% Drift Ratio for Specimen GJ-FR

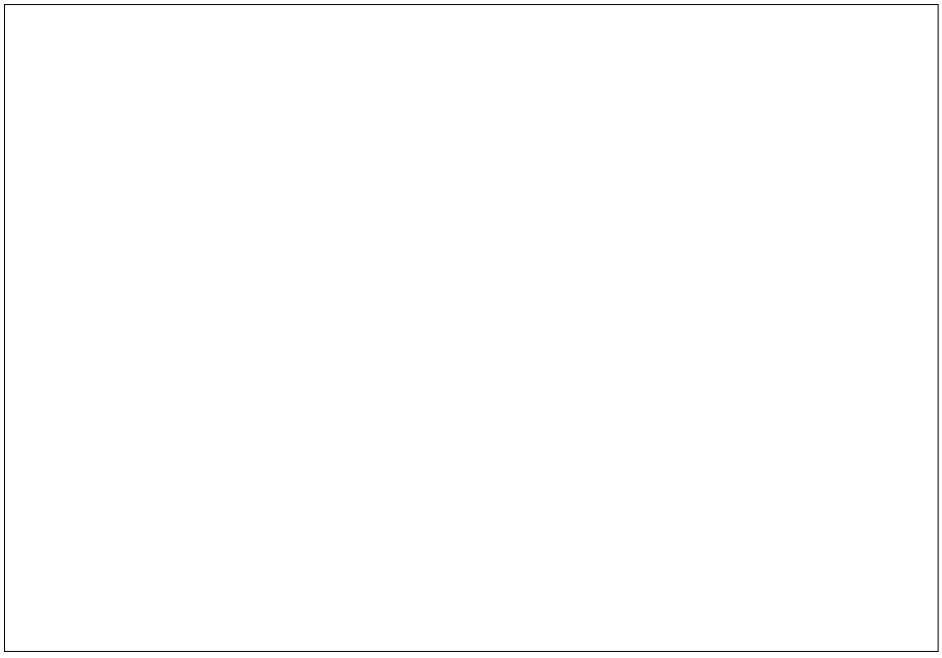

Figure 4.22 Specimen GJ-FR at End of Test

cycles to 0.25 percent drift ratio. During the first excursion to 0.5 percent drift ratio the beams cracked. As anticipated, the crack was at the beam-column interface where the tensile stress was maximum (and where non-pretensioned steel was discontinuous). When the beam cracks were observed, the drift was approximately 0.4 percent. The corresponding load at the tip of the beams was approximately 32 kips. At this level also, cracks started to develop in the upper column element and in the joint. During cycles through 1 percent drift ratio these same cracks continued to grow with a few more opening in the column and joint. However, only the single crack at the beam-column interface was observed in each beam. The width of the crack at the extreme fibers at 1 percent drift ratio was 0.13 in. Figure 4.23 shows the specimen and the crack patterns at 1 percent drift ratio.

Crushing of concrete in the beam compression zones started during the 1.5 percent drift ratio cycles. A few more cracks appeared in the column and in the joint. The crack at the beam-column interface became approximately 0.25 in. wide. Crushing of concrete in the compression zones continued during the 2 percent drift ratio cycles. At this time, spalling of the concrete cover occurred. Inspection of the joint also indicated that cracks in the direction of the compression strut became wider (approximately 0.015 in.). The width of the crack at the beam-column interface became 0.4 in. wide. Figure 4.24 shows the joint and the crushing and spalling of concrete at 2 percent drift ratio.

Crushing and spalling at the beam-column interface continued and became substantial during the 2.5 and 3 percent drift ratios. The rapid crushing and spalling can be attributed to the large rotation, and consequently, large curvature at the end of the beams near the column. The width of the crack at the beam-column interface approached 0.6 in. at 3 percent drift ratio. Also, spalling of concrete at the upper corners of the lower column element took place during the first cycle to 3 percent drift ratio. As mentioned earlier, cracks in the joint region became more visible after

Figure 4.23 Crack Patterns at 1% Drift Ratio for Specimen PT-NE

Figure 4.24 Crushing of Concrete at 2% Drift Ratio for Specimen PT-NE

the 2 percent drift ratio cycles. Strain gauges indicated yielding of the central joint hoops and cross ties during the 1.5 percent drift ratio cycles. When the specimen was subjected to 4 percent drift ratio, diagonal cracks in the joint region opened substantially (0.03-0.04 in.) and permanently. Also, concrete in the joint region started to bulge out orthogonal to the plane of the specimen. During the 5 percent drift ratio cycles, joint cracks became very wide (1/16-1/8 in.) and extensive spalling of the joint cover occurred. At this stage the specimen was considered to have failed. Figure 4.25 shows a close up of the beam and the joint opening at 5 percent drift ratio, and Fig. 4.26 shows the specimen at the end of the test.

4.3 BEAM ROTATION

Typically, most beam deformations occurred in the region adjacent to the column. For all specimens, linear potentiometers were located at the top and bottom of the beams at approximately 6 in. from the face of the column. Data collected from these potentiometers was used to calculate beam-end rotations. This was done by adding the displacements of the top and bottom potentiometers and dividing by the distance between them. Beam tip deflection angle, on the other hand, was calculated by dividing the beam tip deflection by the length of the beam. Both calculations include both elastic and inelastic deformations. The beam-tip deflection angle is always larger than the beam-end rotation. By comparing the two terms (i.e. the ratio of beam-end rotation to beam tip deflection angle), an assessment of the inelastic activity or hinging in the beam can be made.

Table 4.1 lists the ratio (expressed as a percentage) of the beam-end rotation to the beam tip deflection angle for the various specimens. Beam tip deflection consists mainly of three components: beam deflection, column deflection, and joint shear deformations. As beam yielding initiates and a plastic hinge forms, the beam-

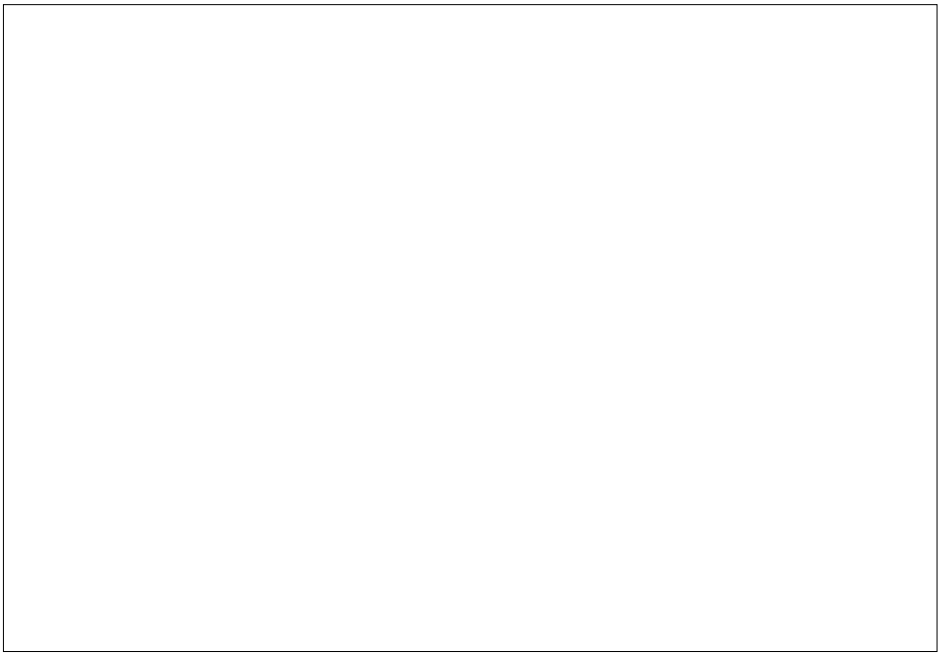

Figure 4.25 Joint Opening at 5% Drift Ratio for Specimen PT-NE

Figure 4.26 Specimen PT-NE at End of Test (Drift Ratio=5%)

end rotation constitutes an increasing portion of the beam deflection component.

Table 4.1 Ratio of Beam-End Rotation to Beam Tip Deflection Angle (in %)

Drift Ratio %	Specimen DB-TC		Specimen GJ-TC		Specimen GJ-FR		Specimen PT-NE	
	+ Rot.	- Rot.	+ Rot.	- Rot.	+ Rot.	- Rot.	+ Rot.	- Rot.
0.25	50.2	54.7	95.6	51.3	55.2	75.9	17.3	23.6
0.50	44.4	51.6	92.6	51.9	50.9	71.8	30.0	44.4
0.75	41.9	46.2	90.3	61.4	55.4	72.3	42.9	57.7
1.00	40.8	46.6	85.1	64.6	58.6	76.4	52.7	62.7
1.50	36.0	39.0	86.4	63.2	72.4	92.9	61.4	71.2
2.00	35.1	-	87.5	69.4	91.0	94.0	67.0	76.5
2.50	-	-	88.9	73.2	94.0	95.0	73.2	78.4
3.00	-	-	91.6	72.1	95.0	97.0	76.0	77.8
4.00	-	-	-	-	-	-	73.5	74.3
5.00	-	-	-	-	-	-	67.5	66.4

It was discussed earlier that Specimen DB-TC failed prematurely due to crushing of concrete located between the 90 degree hooks on the longitudinal beam reinforcement and the anchor plates at the ends of the dogbones. In addition, yielding of the high-strength threaded bars connecting the beams to the column was estimated to have occurred at approximately 1.0 percent drift ratio. The data presented in Table 4.1 for Specimen DB-TC illustrate a downward trend in the value of the ratio of the beam-end rotation to the beam tip deflection angle. This is in agreement with premature deterioration of the dogbone region rather than yielding of the threaded bars.

It was also discussed previously that a gap opened in Specimen GJ-TC as

beams were loaded in the upward (positive moment) direction. This gap later dominated the response of the entire specimen and led to failure of the connection. To better understand the general response of the specimen, the behavior of the beams must be examined. Figure 4.27 shows the beam moment vs. beam tip deflection angle for one of the beams. Note that stiffness was considerably less for loading in the upward direction. This low stiffness corresponds with opening of the gap at the bottom of the beam. When the beam was loaded to produce negative moment, the stiffness of the beam was much higher after the gap closed. The ratio of the positive bending stiffness to the negative bending stiffness was approximately one half. The data presented in Table 4.1 for Specimen GJ-TC indicates that the flexibility of the beam bottom connection and corresponding gap opening dominated the response of the beams from the early stages of loading when they were subjected to positive

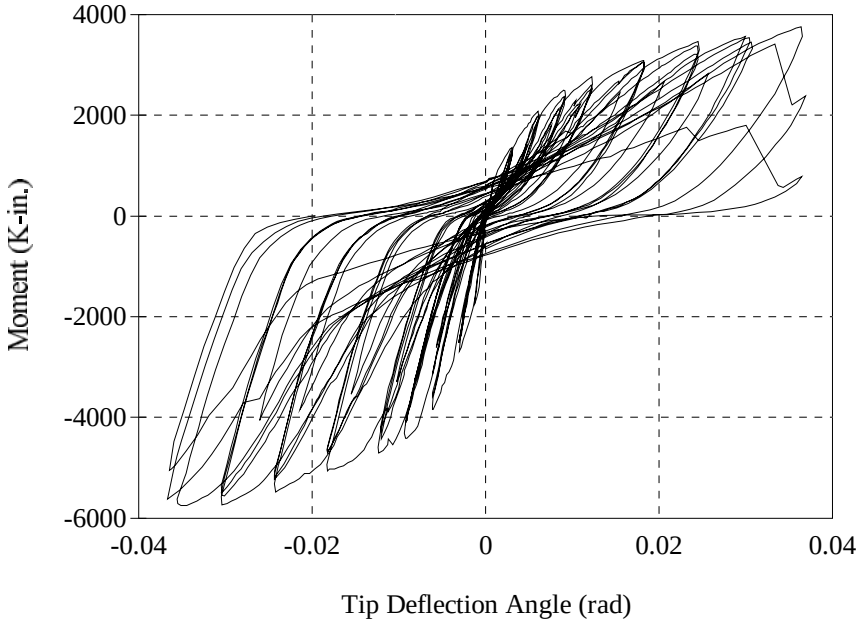

Figure 4.27 Beam Moment vs. Beam Tip Deflection Angle for Specimen GJ-TC

bending. The high percentage of the ratio of the beam-end rotation to the beam tip deflection angle (approximately 90%) indicates that the beam was behaving much

like a rigid body. Data corresponding to the negative beam rotation supports the previous conclusion that yielding of beam top reinforcement started between 0.5 and 0.75 percent drift ratio (the ratio jumped from 52 percent to 61 percent). This ratio continued to increase as loading of the specimen continued to larger drifts.

Two observations can be made from the data corresponding to Specimen GJ-FR. First, the rapid jump in the ratio of beam-end rotation to the beam tip deflection angle at 1.5 percent drift ratio confirms that the first significant slip in the friction connections took place at 1.5 percent drift ratio. It also confirms that beam slip was the main source of beam tip deflection which was also the main source of energy dissipation in this specimen. Second, the percentage corresponding to the beam negative rotation was always higher, especially before slip in the connections occurred. When a beam was subjected to negative bending, the bolts threaded to the couplers in the column were under tension. It was noted before that these bolts were only snug tightened. The flexibility of these bolts along with deflection of the plate bolted to the column made the beam-end rotation consistently higher when the beam was subjected to negative bending. When the beam connections started to slip, this flexibility became less significant.

For Specimen PT-NE, the trend of the percentages shown in Table 4.1 is increasing until cycles to 4 percent drift were experienced. This was expected since only one crack opened at the beam-column interface. The reductions that occurred for 4 and 5 percent drifts are attributed to deterioration in the joint which appeared to accelerate during these cycles. Large diagonal cracks in the joint reflected the severe joint shear distortions that contributed to beam tip deflections.

CHAPTER 3

EXPERIMENTAL PROGRAM

3.1 INTRODUCTION

Design details of the test specimens, material properties, and a description of construction of each specimen are presented in this chapter. The test setup used to load the specimens is shown, and locations of both internal (strain gauges) and external (displacement transducers) instrumentation for each specimen is also described. The displacement history used to load the specimens is presented and discussed. Finally, the test procedure is described.

3.2 DESIGNATION OF SPECIMENS

Four half-scale specimens representing interior precast beam-column connections with strengths consistent with connections in the prototype building discussed in Section 2.5 were designed, built, and subjected to a severe cyclic load history. All specimens had a cruciform shape with the column extending from midheight of the column below the connection to midheight of the column above the connection, and the beam extending between midspan of the beams on each side of the connection as shown in Fig. 2.6. The resulting column height was 6.5 ft and the beam span was 10 ft.

Each specimen is designated by a name that describes a particular characteristic of the precast elements, such as **d**og-**b**one shaped beams, or a **g**ap **j**oint between the beam elements and column, or **p**re**t**ensioned beam. In addition, a two letter suffix is added to describe the type of energy dissipation that is associated with the connecting elements in each specimen such as, **t**ension-**c**ompression yielding, energy dissipation by **fr**iction, or **n**onlinear-**e**lastic behavior. These connection concepts were discussed in Chapter 2. Specimen designations are summarized in Table 3.1.

Table 3.1 Names of Test Specimens

Characteristics of Precast Elements	Type of Energy Dissipation	Specimen Designation
Dog **B**one	**T**ension/**C**ompression	DB-TC
Gap **J**oint	**T**ension/**C**ompression	GJ-TC
Gap **J**oint	**Fr**iction	GJ-FR
Gap **J**oint/**R**etest	**Fr**iction	GJ-FR-R
Pre**t**ensioned Beam	**N**onlinear **E**lastic	PT-NE

3.3 DESCRIPTION OF SPECIMENS

A detailed description of each specimen along with material properties is presented. The design concept for each specimen will be discussed followed by a presentation of the actual design and specimen dimensions and reinforcement details. Because each specimen represents a unique system different from the other specimens, each specimen is presented separately. Design concepts and requirements that are common to all four specimens will be discussed for the first specimen only.

3.3.1 Specimen DB-TC

This specimen is referred to as the Dogbone Connection with tension/compression yielding. It corresponds to the first connection type discussed

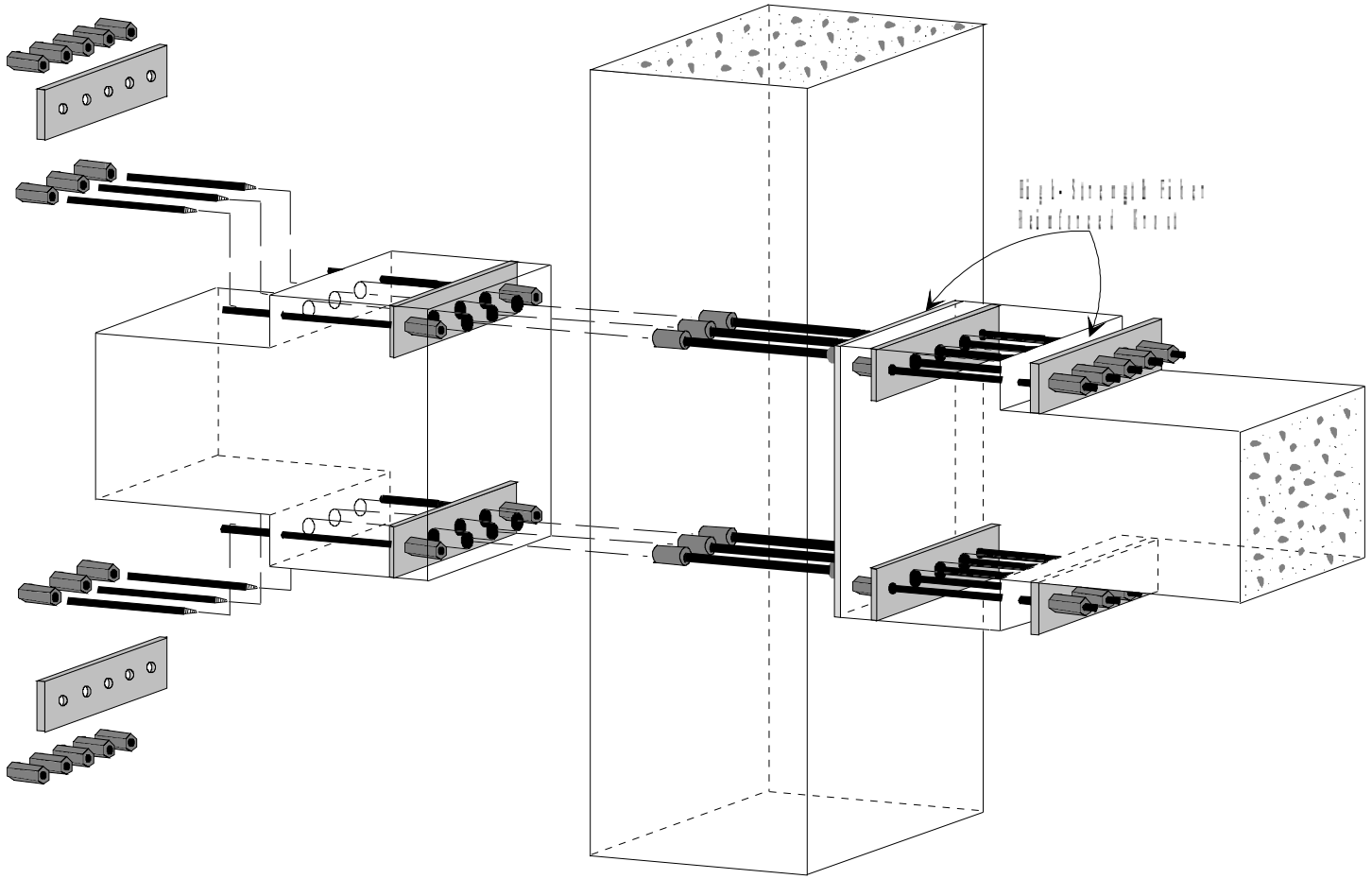

Figure 3.1 Schematic of Connection Concept and Connecting Elements for Specimen UB-1C

Figure 3.2 ERICO Lenton Coupler

in Chapter 2 which relies on tension/compression yielding of the connecting elements. The basic concept and connecting elements are shown in Fig. 3.1. A combination of 5/8 in. diameter Dywidag high-strength threaded bars and plates were used in the dogbone region (i.e. the haunches above and below the beams adjacent to the column) to connect the beam elements to the column.

The bars at each connection location were placed through ducts and were joined with oversized bars that were cast in the column using specially manufactured ERICO Lenton couplers. A photograph illustrating a coupler is shown in Fig. 3.2. Ducts in the dogbone region were later grouted with non-shrink cement grout. Energy was intended to be dissipated in this connection through tension and compression yielding of the high-strength connecting bars. The primary reason for using high-strength bars rather than conventional reinforcement was to reduce the number of bars needed to achieve the design moment, and therefore, reduce the reinforcement congestion. In general, high-strength steel is typically less ductile than regular reinforcing bars. The influence of the high-strength bars on the behavior of the connection will be discussed in the next chapter.

During design of this connection there was a concern that after initiation of tensile yielding of the threaded bars a gap would open at the interface between each precast

beam and the column. Upon load reversal, the compressive force would be primarily resisted by the bars until the gap between the beam end and column face closes. Deterioration of bond that would result in slip of the high-strength bars was expected due to the short grouted length of the bars (18 in.) which was only 40 percent of the development length computed by ACI 318-89. For this reason the embedded plates and bars in the dogbone region were added, as shown in Fig. 3.1, to provide a path for force to be transferred through the dogbone in the event slip occurs in the bars. Consequently, special attention was focused on the design of the interface between the beam and haunches at the ends of the beams.

3.3.1.1 Specimen Design and Reinforcement Details

External specimen dimensions are shown in Fig. 3.3, and reinforcement details are show in Fig. 3.4. Because of symmetry, only half of the specimen is shown . Detailing of reinforcement was performed according to Chapter 21 of ACI 318-89.

Figure 3.5 shows the reinforcement details at select cross sections. The beam section at the end of the haunches, Fig. 3.5b, was designed for a moment 30 percent greater than that required by statics when the design moment at the interface of the column was achieved. This was done in order to satisfy the ductile design concept which is intended to force nonlinear behavior in the connecting elements at the interface between the beam and the column. The column, which was intended to

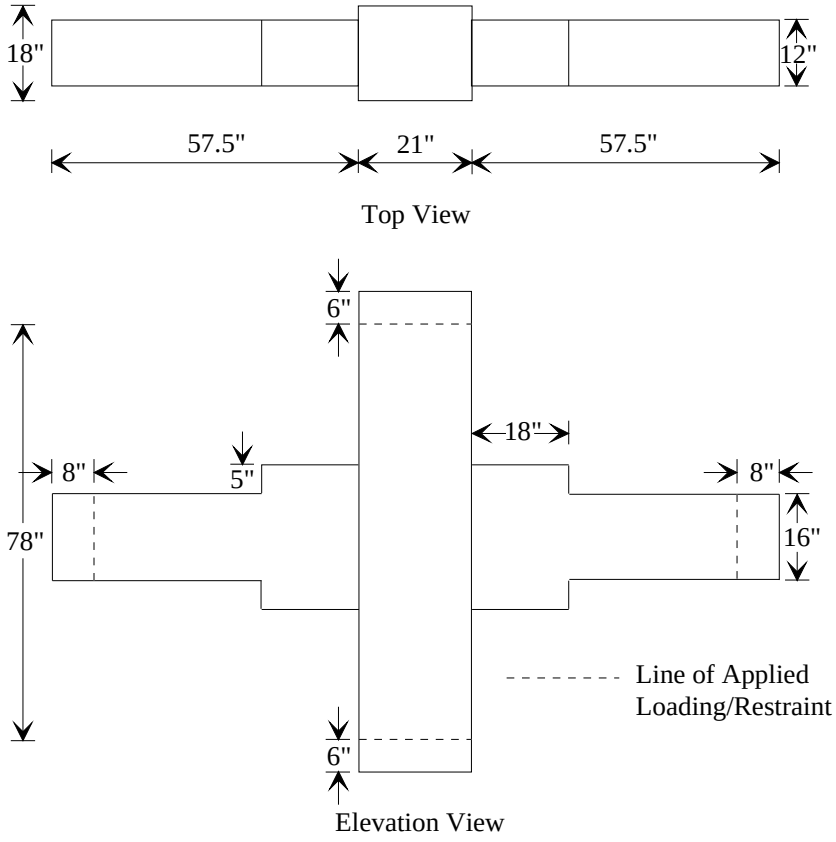

Figure 3.3 Dimensions of Specimen DB-TC

rema

in elastic during the test, was designed to have approximately 40 percent more flexural strength than the beam. This was done to satisfy both the strong column-weak beam concept and the ductile design approach, and was done in the design of all four specimens. The column cross section is shown in Fig. 3.5c.

The requirements of ACI 318-89 for shear specify that the contribution of concrete to the shear strength of a member must be ignored if the earthquake-induced shear force is more than 50 percent of the total shear force and the axial force on the member, including earthquake effects, is less than $A_g f'_c/20$, where A_g is the gross area of the member, and f'_c is the concrete compressive strength. Therefore, in determining the required transverse reinforcement for both the beams

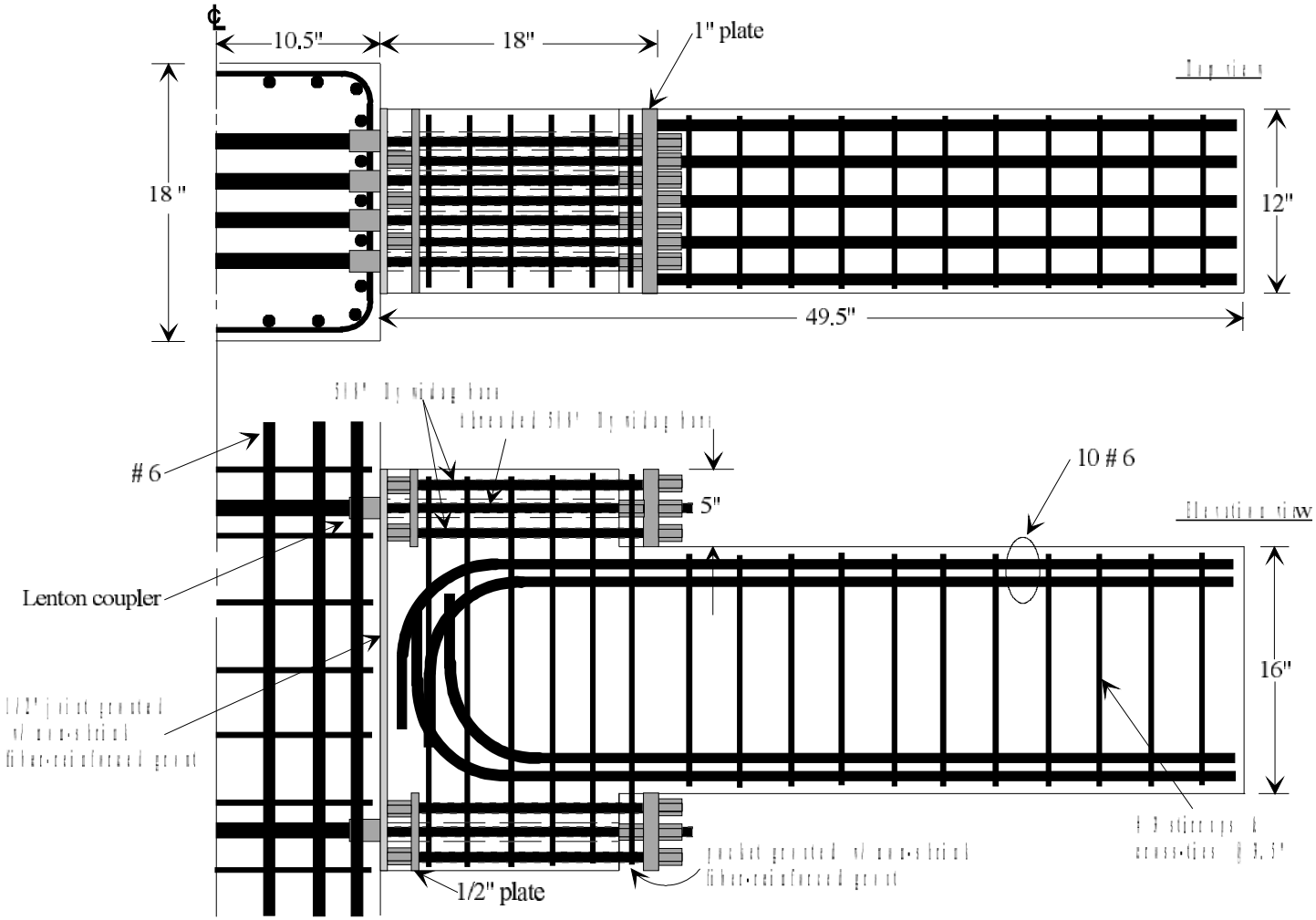

Figure 3.4 Reinforcement Details for Specimen DB-11

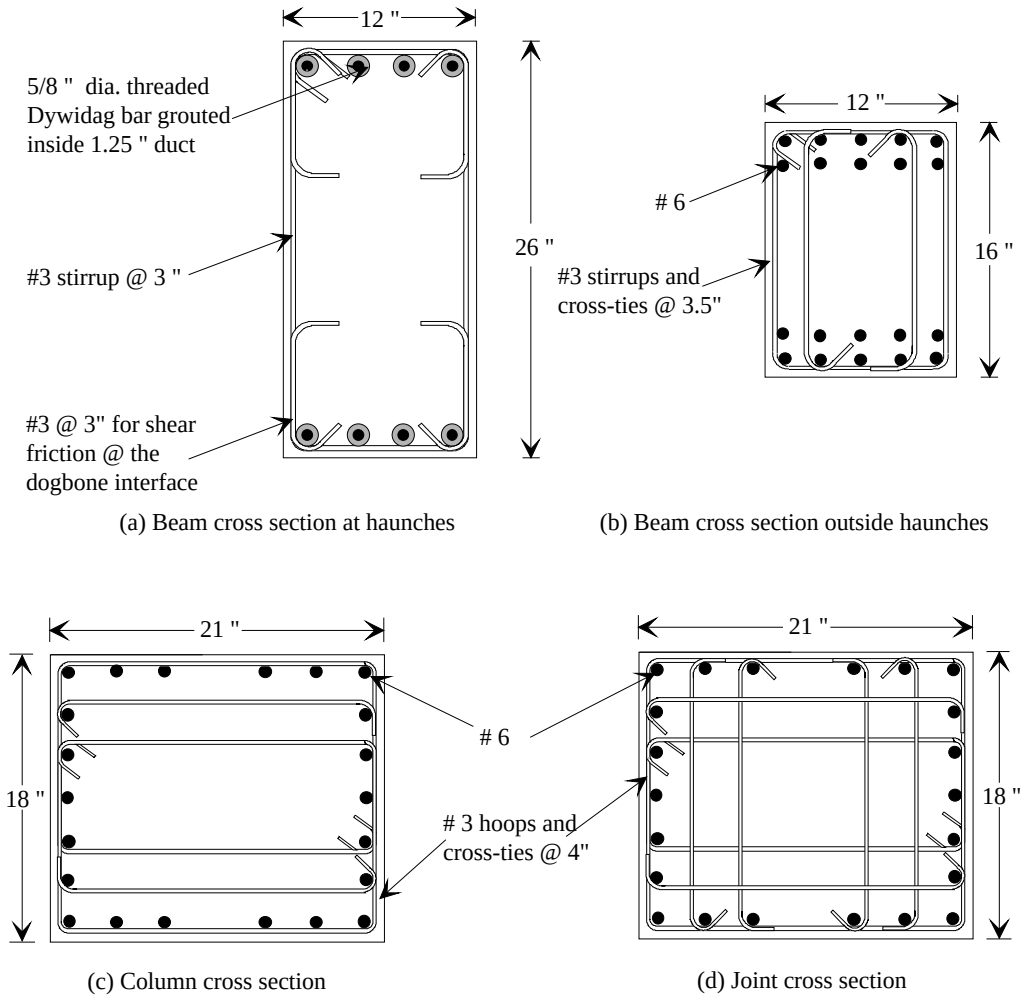

Figure 3.5 Cross Section Details for Specimen DB-TC

and the column, the concrete contribution was taken as zero. Also, to ensure that shear failure did not occur, all members were designed for 30 percent more shear than is required by statics. This was done for all specimens.

The joint shear mechanism in this specimen is similar to that for monolithic concrete connections. The joint shear design and confinement was performed according to the ACI 318-89 requirements which are based on the recommendations of ACI-ASCE Committee 352. These requirements specify allowable shear stresses on the joint cross section. The amount of transverse reinforcement in the joint is not directly related to shear resistance, but instead, is based on confinement requirements. Perimeter hoops and cross-ties were provided in the joint in both directions at a spacing of 4 in., which is the

maximum allowed by the code. The maximum allowed spacing outside the joint region for shear requirements is 4.75 in. (d/4). Because the remaining length of the column on both sides of the joint was relatively short, the same spacing of 4 in. was used over the entire column length.

The interface between the haunches and beam at the end of the beams was designed according to the ACI 318-89 shear friction provisions. The interface must be able to resist at least a force equal to that required to develop the full strength of the bars connecting each side of the beam to the column. In designing the shear friction reinforcement, stirrups provided for shear were utilized. Because the shear reinforcement was not sufficient by itself, additional reinforcement in the form of short supplemental ties was added as shown in Fig. 3.5a.

3.3.1.2 Material Properties

All conventional reinforcing bars used in the specimens were ASTM A615 Grade 60 steel. In addition to the mild steel, high-strength steel in the form of Dywidag bars were also used in this specimen and other specimens. The tensile properties of the reinforcing bars used in Specimen DB-TC are summarized in Table 3.2. Bar strengths were based on the average results of two tests.

The same concrete design was used for all specimens. The design compressive strength of the normal weight concrete was 6000 psi. A maximum coarse aggregate size of 3/8 in. was used due to the congestion of reinforcement. The concrete slump was adjusted to between 7 and 9 in. by adding superplasticizer to the mix in the laboratory. The grout used in the construction joints between the beams and column and other pockets was Euclid non-shrink grout. One-half inch long nylon fibers were added to the grout. Grout used for the ducts did not have fibers. The specimens and concrete cylinders and grout cubes were cured in the laboratory under wet burlap and plastic for 3 days. The age of the concrete and grout at 28 days and at the last day of testing are listed in Table 3.3. Concrete cylinder and grout cube strengths were based on the average results of three tests.

Table 3.2 Reinforcing Steel Properties for Specimen DB-TC

Bar Size	f_y (ksi)	ε_y (%)	f_u (ksi)
#3	61.9	0.213	100.7
#6	59.8	0.206	99.6
5/8 in. Dywidag[+]	141.8[*]	0.489	157.6

[+] Test performed with the bar threaded into a Lenton coupler.

[*] Based on $0.9f_u$ as per PCI Design Handbook [33].

Table 3.3 Compressive Strength of Concrete and Grout for Specimen DB-TC

Concrete & Grout	28-day Strength (psi)	Strength at Last Day of Testing (psi)	Age at Last Day of Testing (days)
Beams and Column	5530	7990	167
Grout in Joints	6680	7680	76
Grout in Ducts	6090	8170	67

3.3.1.3 Fabrication and Erection

To avoid repetition, the following discussion applies to all the specimens. More discussion unique to each specimen is presented in separate sections corresponding with the remaining specimens.

Each specimen consisted of three units; either two beams and a column or one beam and two columns. The units were fabricated in position which was convenient for fabrication but not necessarily in the same position as in the erected specimen. Some strain gauges were attached to reinforcing bars prior to assembling the reinforcing cages, while others were attached after the cages were assembled. Prior to moving the reinforcing cages to the platforms that were used as the base forms, the wooden forms

were coated with form oil. Ready-mix normal weight concrete with 3/8 in. maximum size coarse aggregate was used for all the specimens. Concrete was placed with an overhead crane and a bucket. Consolidation of concrete was achieved with electric pencil vibrators.

In the erection process the column was moved into the test setup first. The ends of the beams adjacent to the column and the column sides that were adjacent to the grout joint were roughened to a 1/4 in. amplitude using a chisel and hammer, as shown in Fig. 3.6, to improve the shear transfer between the two faces. As mentioned earlier, no corbels were used in this specimen. To facilitate erection of the beams, temporary supports were used as shown in Fig. 3.7. A 1/2 in. joint was left between the beams and the column. The threaded bars were inserted through the ducts in the haunches of the beams and tightened to the couplers. The joints were then grouted with fiber-reinforced grout. Next, the nuts at the other end of the threaded bars were tightened and the ducts were grouted. Each duct had two ports. Grout was injected into the ducts using a manual hand pump. When the grout started flowing from the other port, as shown in Figure 3.8, the ports were sealed.

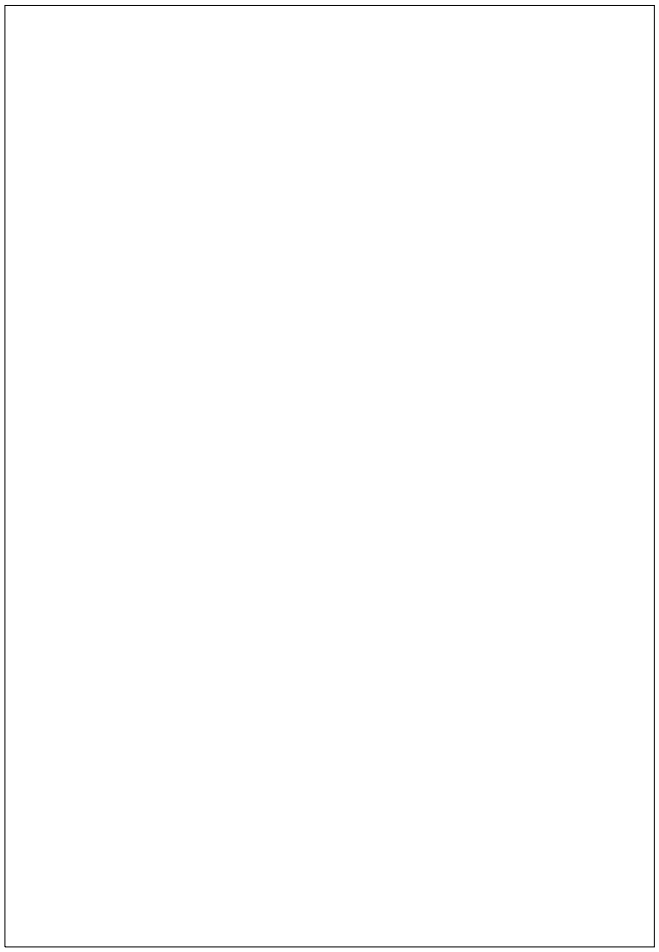

Figure 3.6 Roughening of Column Faces of Specimen DB-TC

3.3.2 Specimen GJ-TC

This specimen is referred to as the Gap-Joint connection with tension/compression yielding. It corresponds to the first connection type discussed in Chapter 2, which relies on tension/compression yielding of the connecting elements. The basic concept and connecting elements are shown in Fig. 3.9. In this specimen the bottom connection between each beam and the column was intended to act as a pin connection (restraining horizontal and vertical movement). The top

Figure 3.7 Erection of Beams of Specimen DB-TC

Figure 3.8 Grouting Ducts of Specimen DB-TC

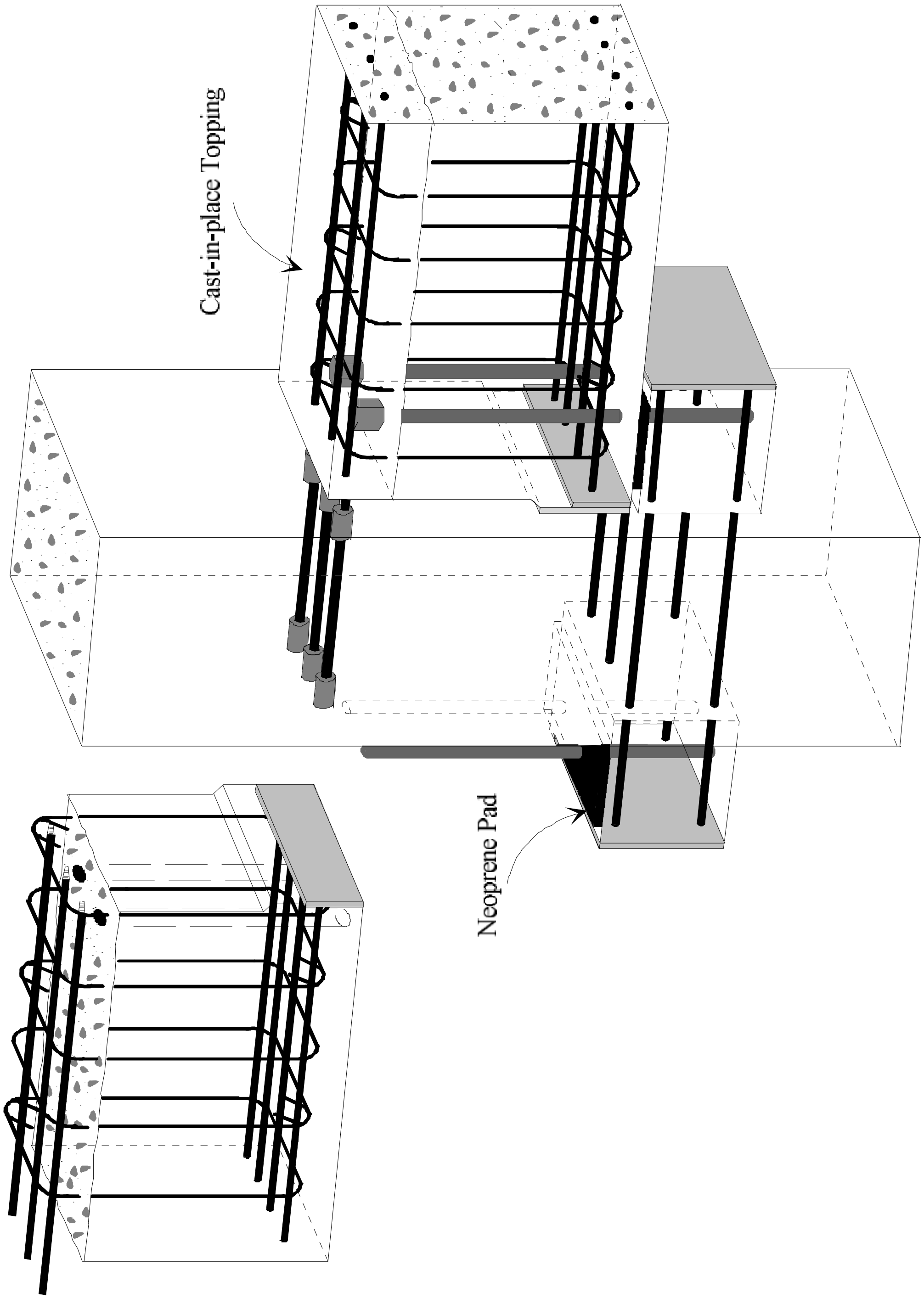

Figure 3.[illegible] Schematic of Connection Concept and Connecting Elements for Specimen [illegible]J-1C

conn

ection was intended to facilitate movement between the beams and column, and as a result, concentrate most of the nonlinear behavior in the specimen at that location. A gap

over 75 percent of the depth of the interface between each beam and column was provided to force compressive as well as tensile yielding in the top connection at the face of the column. For this specimen, conventional longitudinal reinforcing bars in the beams were connected using Lenton couplers to bars embedded in the column. The top longitudinal beam bars were intended to be the yielding connecting elements.

In contrast to Specimen DB-TC, a corbel on each side of the column was provided to assist in erection and, more importantly, to act as part of the pin connections mentioned above. Four vertical high-strength thread bars were embedded through each corbel. Vertical ducts were cast in the precast beams to accommodate the high-strength bars. Each beam was placed over the vertical bars, and ducts were later grouted with non-shrink grout. Tensile force in the bottom of each beam was transmitted to the corbel through direct shear in the high-strength bars, and from corbel to column through high-strength horizontal bars in the corbel. Conventional reinforcement in the top of the beams was connected to the column with Lenton couplers, then the top portion of each beam was cast. Cast-in-place concrete could be used to tie precast slab panels to beam elements. It should also be noted that no attempt was made to conceal connection hardware, although the author is confident that precast producers would be able to make the connection more aesthetically appealing.

3.3.2.1 Specimen Design and Reinforcement Details

The external dimensions of the specimen are shown in Fig. 3.10. This specimen consisted of a precast column and two precast beams. A corbel was

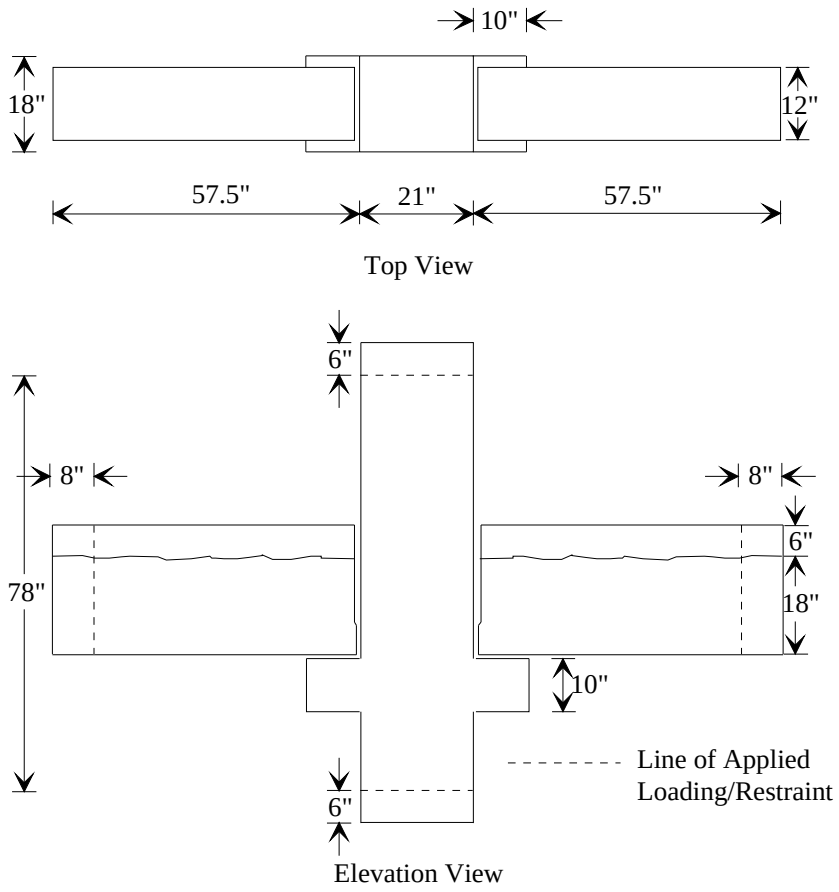

Figure 3.10 Dimensions of Specimen GJ-TC

prov

ided on each side of the column. Reinforcement details for half of the specimen are shown in Fig. 3.11, and reinforcement details at select cross sections are shown in Fig. 3.12. Detailing of the reinforcement was performed according to Chapter 21 of ACI 318-89.

Beam flexural reinforcement was designed so bottom steel remained elastic through design drift ratio of approximately 2 percent. This was done in order to ensure that damage resulting from nonlinear material behavior was concentrated at the top of the beam for both loading directions. Beam bottom bars were anchored by welding their ends to a 1 in. thick plate. The top bars were threaded into Lenton

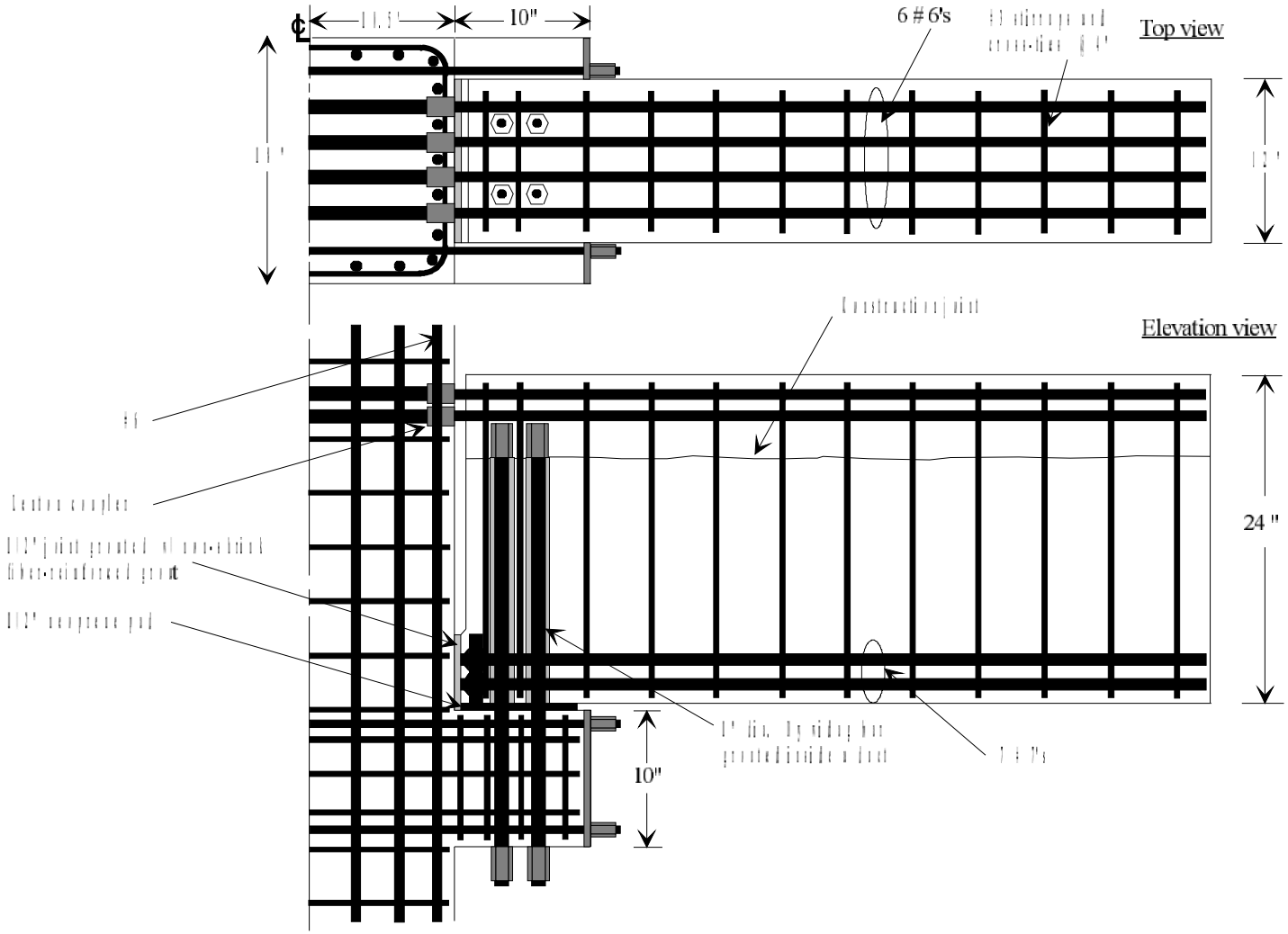

Figure 3.11 Reinforcement Details for Specimen GJ-2.0

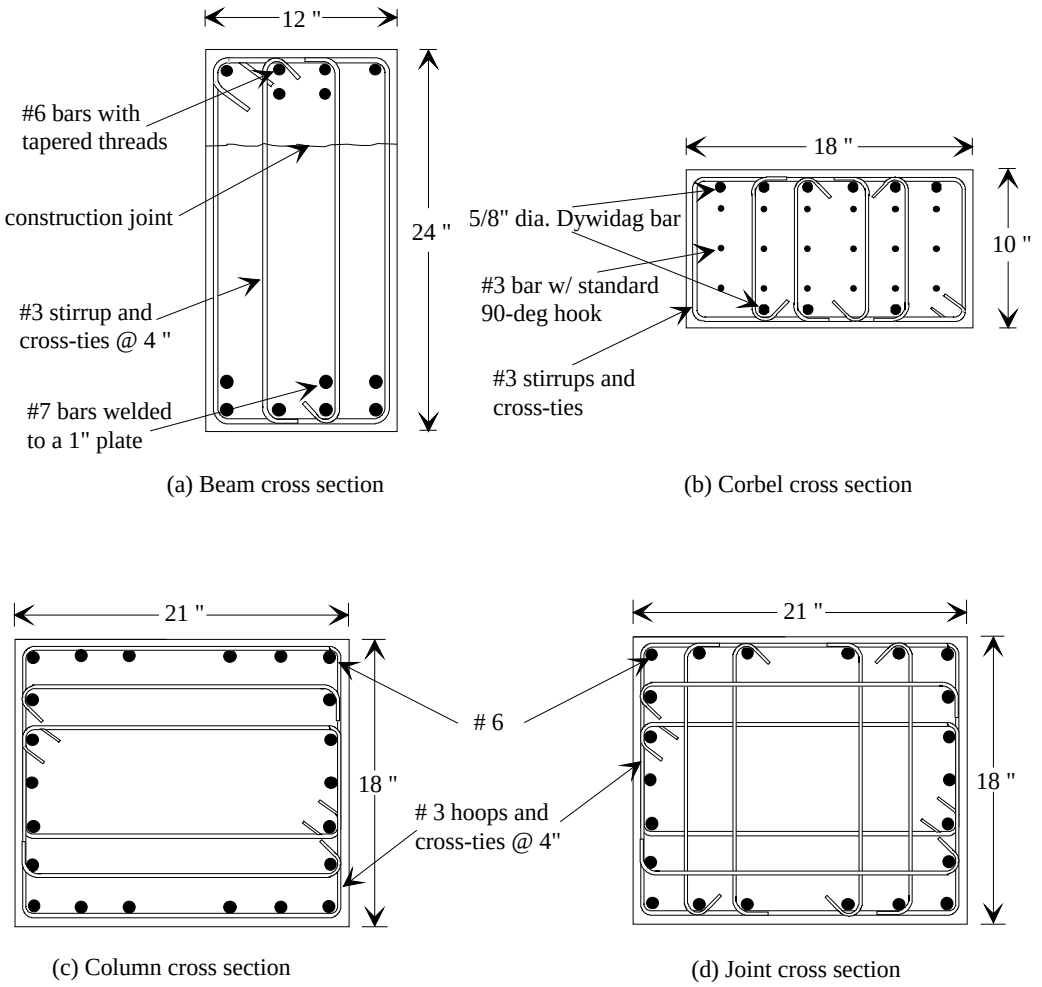

Figure 3.12 Cross Section Details for Specimen GJ-TC

coup

lers that were embedded in the column. The cross section of the beam is shown in Fig. 3.12a. Vertical bars that connected each beam to its corbel were designed to resist upward loading of the beam. This loading condition imposed both tension as well as shear on the bars. As for the first specimen, flexural strength of the column was more than 1.4 times the flexural strength of the beams. The column cross section is shown in Fig. 3.12c.

The joint shear transfer mechanism in this specimen is not the same as that discussed for the previous specimen. The first difference is in the force transfer at the bottom of the beam. Tensile force in the bottom of either beam is not directly transferred to the joint through bond stresses. Tensile forces are transferred into the column via a

circuitous route through the high-strength vertical bars in the corbel and horizontal reinforcement through the corbels. The transfer mechanism through the column is somewhat dubious. Moreover, the gap that exists over most of the beam depth, results in a very different introduction of beam compression forces at the top and bottom of the beams.

No recommendations for design of such joints exist in current codes. Therefore, a different method was initially considered for the joint design. The first approach was to consider the joint as a deep beam and to design the reinforcement based on the applied shear. This approach was very conservative, leading to an amount of transverse reinforcement that would not fit in the joint. The second approach was to follow the basic recommendations of ACI-ASCE Committee 352 for monolithic joints. The limiting joint shear stresses specified by these recommendations are related to the degree of joint confinement by beams framing into the joint. Because a substantial gap exists between the beams and column, the joint was treated as a "corner joint" (without beams framing into opposite sides of the connection). In fact, the resulting design did not differ from Specimen DB-TC because that joint was also treated as a "corner joint" due to the fact that the beams did not mask at least 75 percent of the column face as required by the 352 recommendations. Therefore, the same joint reinforcement as in specimen DB-TC was used.

Design of the corbels was performed using a strut-and-tie procedure. Forces applied on the corbel were different from those encountered in applications where beams are simply supported. For the case of a simply supported beam, the primary force is the downward force. A secondary force, which is usually taken as a percentage of the primary force, is assumed to act horizontally applying tension on the corbel. Corbels for this specimen were designed for an upward force equal to the design shear force in the beam plus a horizontal force equal to the maximum tension force in the bottom of the beam applied at the top of the corbel. Notice for this case that the horizontal force was substantially greater than the vertical force. The vertical force was resisted by a steel cage consisting of horizontal and vertical reinforcement, and by horizontal high-strength bars at the bottom of the corbel, as shown in Fig. 3.12b. The horizontal component of the steel cage also contributed to resistance of the horizontal force applied at the top of the

corbel. The remainder of the horizontal force was resisted by horizontal high-strength bars at the top of the corbel. To ensure that corbel failures did not occur, forces used to proportion reinforcement were computed using the design moment amplified by 30 percent.

3.3.2.2 Material Properties

The tensile properties of the reinforcing bars for both conventional and high-strength steel used in this specimen are summarized in Table 3.4.

The concrete used for the precast beams, column, and topping had a design compressive strength of 6000 psi. The actual compressive strengths for the different concrete casts and grouts are shown in Table 3.5.

3.3.2.3 Fabrication and Erection

The beams for this specimen were partially precast. The beams were cast in the same orientation as in their final position. Concrete was cast to within 18 in. of the top of the beams, and the top surface of the beams were intentionally left rough to provide good bond between the precast concrete and the topping concrete. The column was cast in a horizontal position. Figure 3.13 shows the reinforcing cages

Table 3.4 Reinforcing Steel Properties for Specimen GJ-TC

Bar Size	f_y (ksi)	ε_y (%)	f_u (ksi)
#3	61.3	0.211	101.3
#6 Beams[+]	66.7	0.230	107.6
#6 Column	61.6	0.212	101.9
#7	57.0	0.197	87.8
5/8 in. Dywidag	148.8*	0.513	165.4
1 in. Dywidag	142.6*	0.492	158.4

[+] Test performed with the bar threaded into a Lenton coupler.

* Based on $0.9f_u$ as per PCI Design Handbook [33].

Table 3.5 Compressive Strength of Concrete and Grout for Specimen GJ-TC

Concrete	28-day (psi)	Day of test (psi)	Age at day of test (days)
Beams and Column	7244	7276	57
Topping	7013	7013	28
Joints Grout	8087	Not available	-
Ducts Grout	6063	Not available	-

for the column and beams in the wooden forms before casting. After erecting the column, the beams were lifted in place. Neoprene pads were placed on the corbels prior to seating the beams (see Fig. 3.14). The pad was intended to permit the beam to rotate without coming in contact with the edge of the corbel. The bottom portion

Figure 3.13 Reinforcing Cages for Specimen GJ-TC

Figure 3.14 Erection of Specimen GJ-TC Beams

Figure 3.15 Installation of Threaded Bars for Specimen GJ-TC

of the joint between each beam and the column was grouted with fiber-reinforced grout, then the ducts containing the vertical high-strength bars were grouted and a nut was tightened on the top of each bar. The top longitudinal beam reinforcement was threaded

into the couplers embedded in the column, as shown in Fig. 3.15. Wooden forms were then placed around the beams and the top portion of the beams was cast. In actual construction, less formwork for this operation would likely be required. This is because precast concrete panels would be placed on the edges of the beams spanning between parallel frames. Concrete would then be cast on top of the panels and between panels on top of the precast beams to tie the floor diaphragm together.

3.3.3 Specimen GJ-FR

This specimen is referred to as the Gap-Joint Connection with Friction. It corresponds to the second connection type discussed in Chapter 2, which utilizes friction devices to dissipate energy. The basic concept and connecting elements are shown in Fig. 3.16. The concept of utilizing friction in seismic applications as a means to dissipate energy has been investigated by several researchers [3,14,29]. Various types of devices have been developed to achieve this goal. A common problem with most of those devices is their cost and installation requires special training. Consequently, additional expense in using such devices has prevented their wide acceptance in engineering practice. Grigorian et al. [20] at the University of California at Berkeley tested slotted bolted connections (SBC) to investigate friction as a means of energy dissipation. A schematic view of a SBC is shown in Fig. 3.17. Two types of SBC's were tested; one with brass insert plates and one without. The main plate had elongated or slotted holes. Belleville washers were placed under the nuts. These washers are conical in shape, and thus, they perform the job of an elastic spring, maintaining the tension force in the bolts. Upon tightening the bolts, the main plate is sandwiched directly between either brass insert plates or outer steel plates. The holes in the brass insert plates and in the outer steel plates were of standard size. When the tensile or compressive force applied exceeds the frictional forces developed between the plate surfaces, the main plate slips relative to the brass insert plates or outer steel plates. Upon reversal of the load, slip occurs in the opposite direction. Energy is dissipated by means of friction between the sliding

surfaces.

The force-displacement curves for the cases with and without brass plates are shown in Fig. 3.18. It was shown that such a scheme is not only capable of dissipating significant quantities of energy (as demonstrated by the areas enclosed by

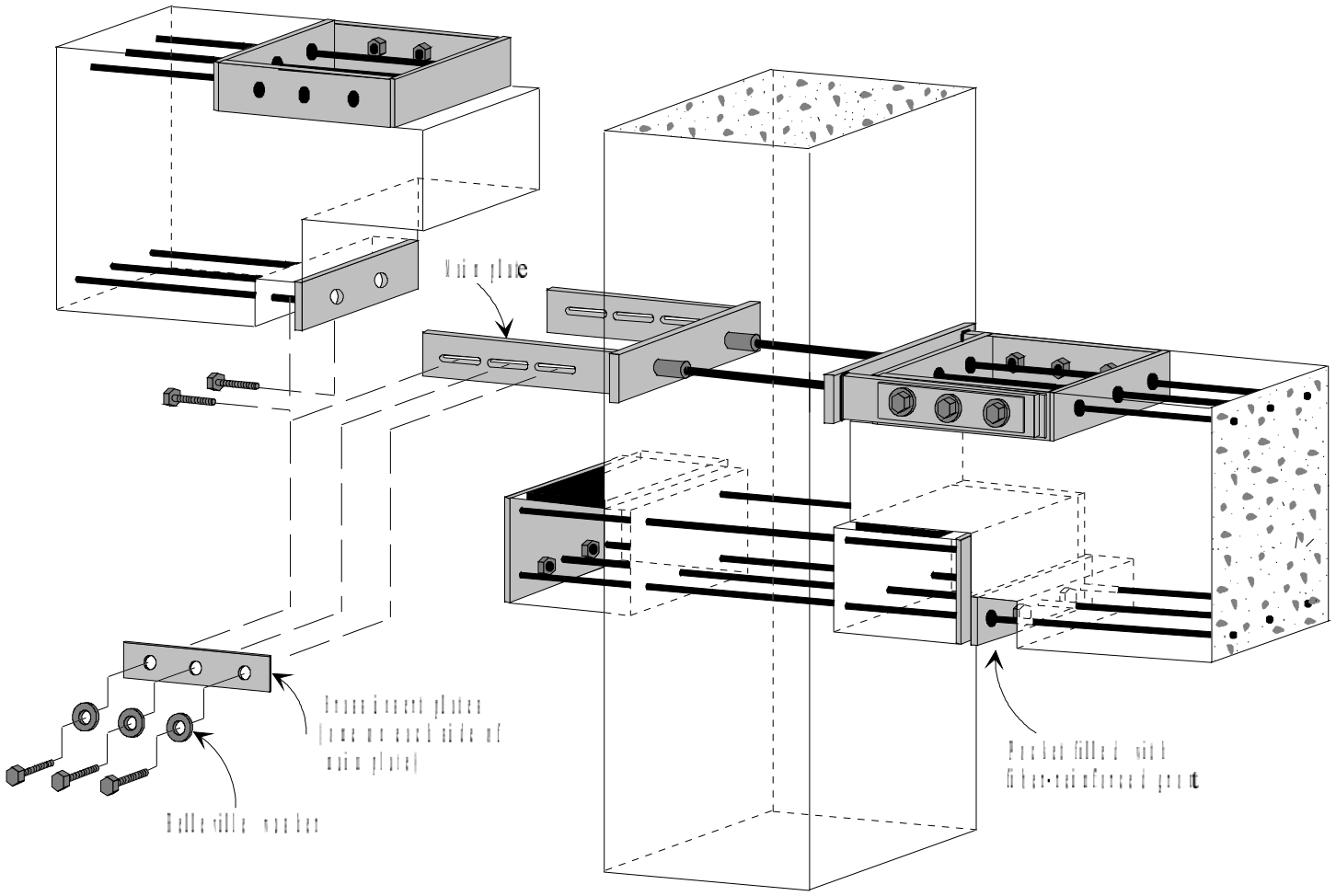

Figure 3.16 Schematic of Connection Concept and Connecting Elements for Specimen CJ-ER

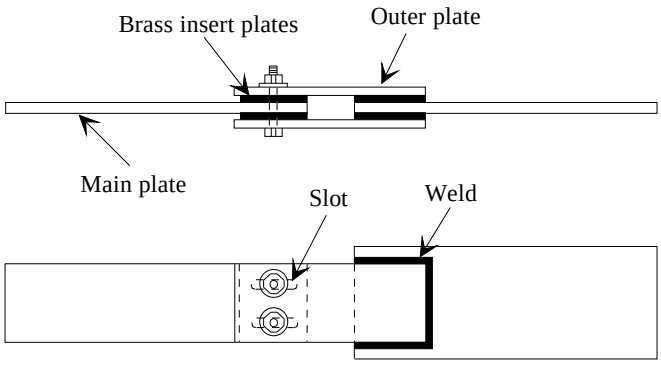

Figure 3.17 Schematic of a Slotted Bolted Connection

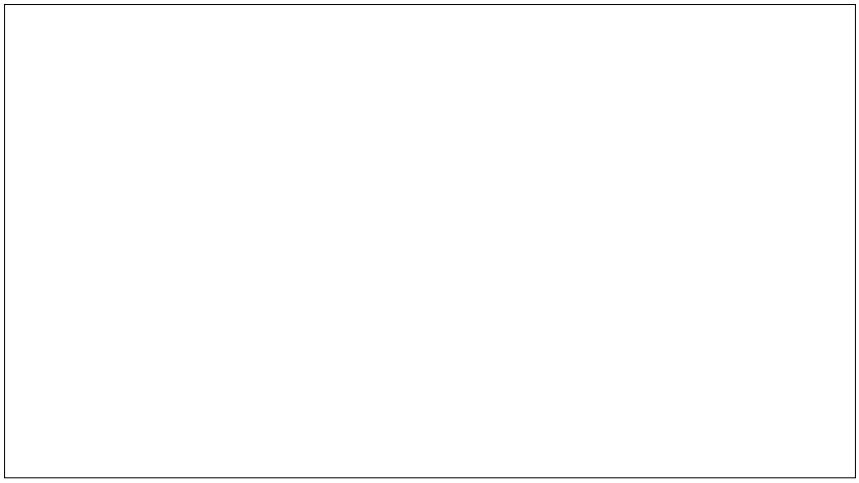

a) Steel on Steel b) Steel on Brass

Figure 3.18 Hysteresis Diagram for Steel on Steel and Steel on Brass

the hysteresis loops) but also that the use of brass shims between the steel plates results in the slip force remaining relatively constant over the range of interest. Furthermore, this device does not require special training to install and utilizes materials that are widely available.

As for Specimen GJ-TC, the bottom connection between each beam and corbel was intended to act as a "pin connection". A pocket was left in the precast beam to allow for the placement of bolts that thread into nuts welded to the inside of the steel plate on the face of the corbel. The pocket was later filled with high-strength fiber-reinforced grout. The top connection consisted of steel plates on the sides of the precast beam (with

nuts welded to the inside face of the plates) and steel plates connected to the precast column (with bolts that thread to couplers cast in the column). The plates that are attached to the column had 4 in. long slotted holes, that were parallel to the beams. The beams were then connected to the plates on the column by eight 1 in. dia. A490 bolts that were each tensioned to a force of 64 kips.

The level of clamping force needed depended on the design moment and the friction coefficient assumed between the steel and brass plates. A 1/8 in. brass shim was sandwiched between the steel plates and the Belleville washers to enhance the slip behavior. Slotted holes were made in the plates connected to the column to allow the beams to slip without the bolts coming into bearing. The gap between the beams and the column was provided in order to permit slip to occur in both directions. Therefore, the length of the slot and the width of the gap had to be chosen carefully to accommodate the expected slip displacement.

3.3.3.1 Specimen Design and Reinforcement Details

This connection consisted of a precast column and two precast beams. The external dimensions of the specimen are shown in Fig. 3.19. Two corbels were provided, one on each side of the column. However, the corbel locations are different from those in Specimen GJ-TC. For aesthetic reasons, the beam ends were dapped to conceal the corbel. In addition, it was desirable to test a different detail for the pin that permitted rotation at the base of each beam. In this design, the transfer of tensile force from the bottom of each beam to the column was achieved through a direct tension path rather than through shear or dowel action.

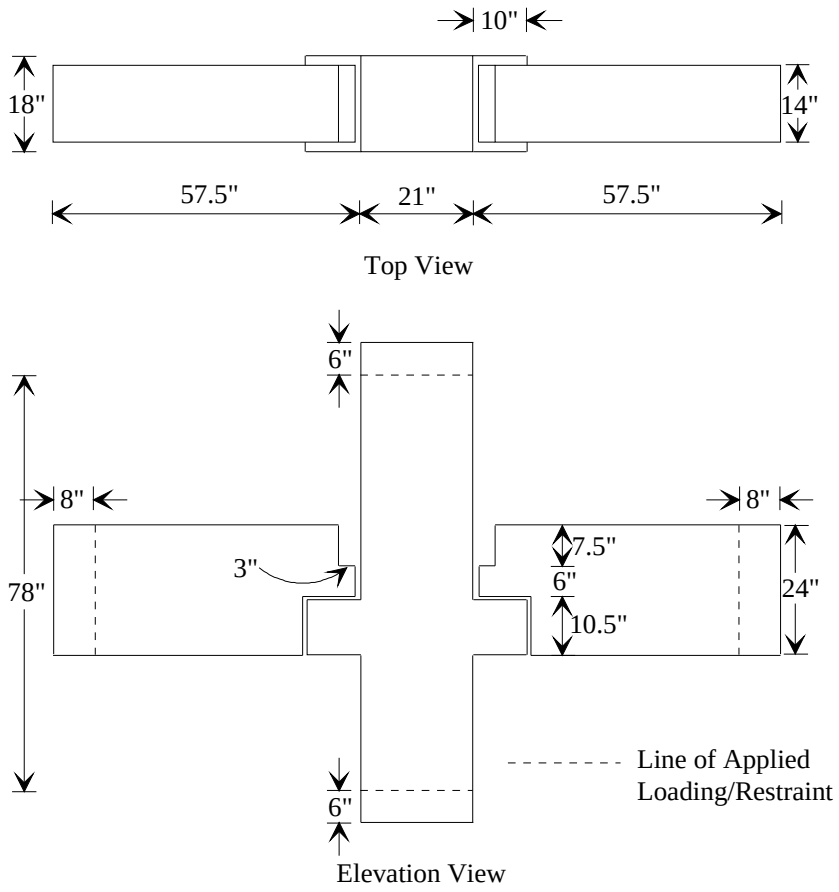

Figure 3.19 Dimensions of Specimen GJ-FR

Rein

forcement details of half of the specimen are shown in Fig. 3.20, and reinforcement details at select cross sections are shown in Fig. 3.21. Whenever applicable, the provisions of Chapter 21 of ACI 318-89 were used to detail the reinforcement.

As for Specimen GJ-TC, the beam was designed so that the bottom steel remained elastic throughout the design drift of the connection (approximately 2 percent drift). The bottom reinforcing bars, which consisted of 8#7 bars, were anchored by welding them to a 13/16 in. thick plate. Holes were drilled in the plate and a pocket was left in the beam, as shown in Fig. 3.16, to allow for placement of

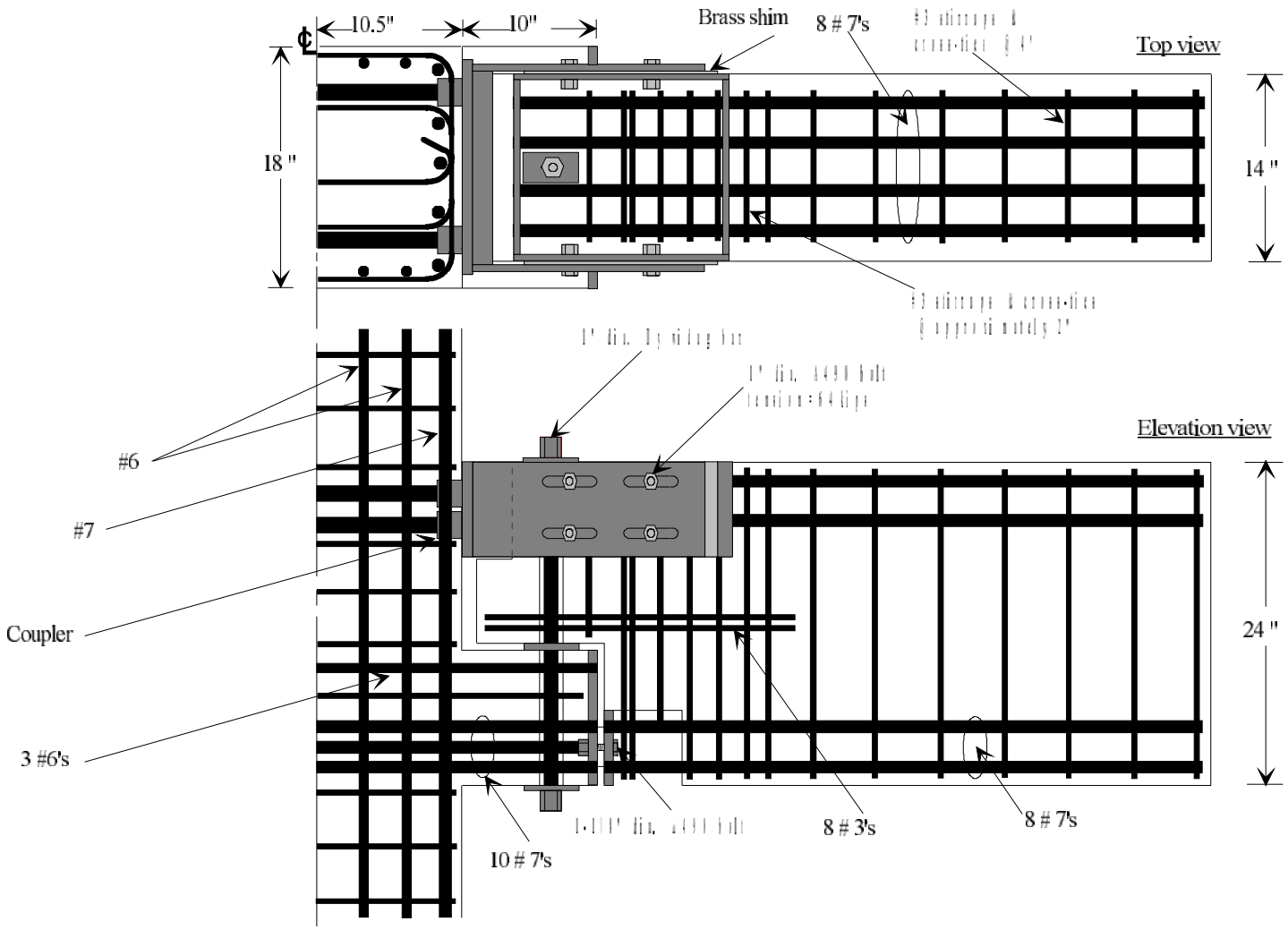

Figure 3.11 Reinforcement Details for Specimen UJ-ER

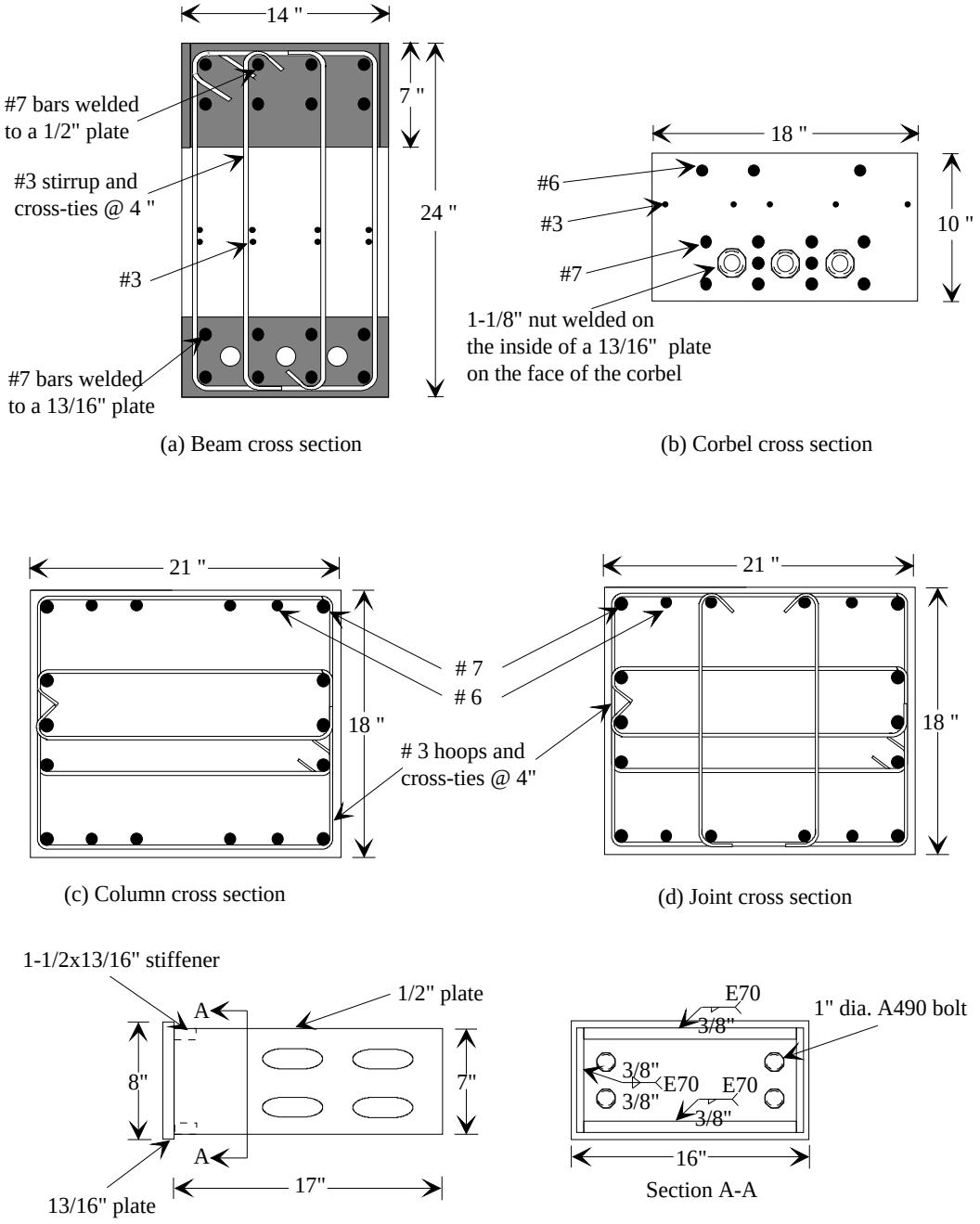

Figure 3.21 Cross Section Details for Specimen GJ-FR

three 1-1/8 in. dia. A490 bolts that connected to nuts welded on the inside of a 13/16 in. thick plate on the end face of the corbel. These bolts transferred force from the beam to the column through direct tension when the force applied on the tip of the beam was upward.

Therefore, the plate that anchored the bottom beam bars was subjected to large forces and had to be designed to avoid yielding and extreme bending. The method used to design the plate was to treat it as a base plate of a structural steel column. Reinforcing bars in the corbels were anchored on both ends by welding them to the steel plates at the ends of the corbels.

As explained above, energy in this specimen was dissipated when slip occurred in the friction devices. Therefore, contrary to Specimen GJ-TC, the top beam reinforcement was intended to remain elastic. Four 1/2 in. thick plates were welded in the form of a box as shown in Fig. 3.16. The same amount of reinforcement as in the bottom of each beam was provided and was anchored by welding it to the side of the box that was nearest the column face. On the inside of the box, four 1 in. dia. nuts were welded to each of the plates parallel to the beam longitudinal axis. The nut locations match the holes in the friction plates.

A duct was embedded in the dapped end of the beam and in the corbel. A 1 in. dia. ungrouted Dywidag bar was used to tie the beam to the corbel to resist uplift of the beam. As a result, the corbels had to be designed for an upward force equal to the design shear force in the beam applied at the bottom of the corbel plus a horizontal force equal to the tension force in the bottom of the beam applied at the face of the corbel (the location of the 1-1/8 in. dia. bolts). When the load at the tip of a beam was downward, the shear was assumed to be resisted completely by the corbel.

As a consequence, special horizontal and vertical reinforcement was provided at the dapped end of the beam to resist the stresses induced by the beam reaction. Figure 3.22 shows a possible strut and tie model for the beam when the applied load

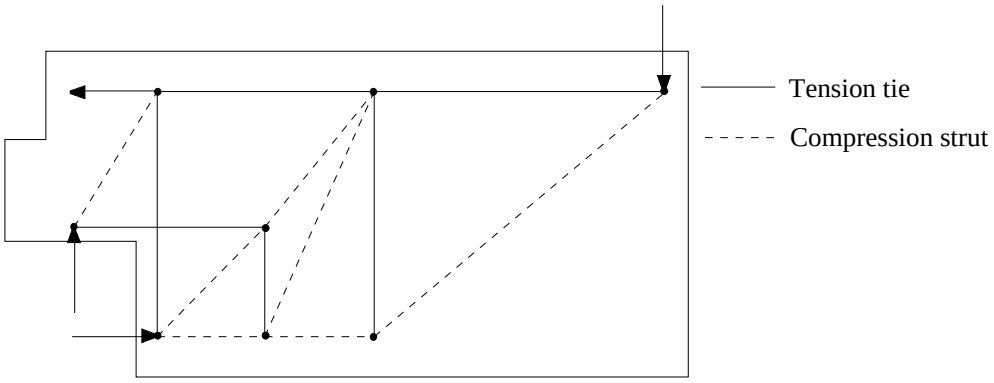

Figure 3.22 Strut-and-Tie Model for Beam of Specimen GJ-FR

is downward. Accordingly, the amount of reinforcement for the dapped end and for shear can be designed. The top reinforcement in the corbel must be designed for a downward force equal to the shear force in the beam. The horizontal force applied on the corbel by the bottom of the beam is assumed to be taken by direct compression. The cross section of the corbel is shown in Fig. 3.21b. To ensure that failures in the corbel or in the beam did not occur, forces used to proportion reinforcement were based on forces resulting from application of the design moment amplified by 30 percent.

The friction plates, shown in Fig. 3.21e, were designed to satisfy the following criteria at the design drift:

* The plates parallel to the beams must remain elastic under both tension and compression.

* The plates must not buckle when they are in compression.

* The stiffness of the plate bolted on the face of the column must be adequate to avoid excessive deformations when the friction plates are in tension.

As for the two specimens described previously, column flexural strength was at least 1.4 times the beam flexural strength. The column cross section is shown in Fig. 3.21c. The joint shear mechanism was not the same as for Specimen DB-TC or Specimen GJ-TC. Tension and compression forces from the bottom of the beams were introduced to the joint in a similar fashion but at a slightly higher location than in Specimen GJ-TC. The introduction of forces to the top of the joint are quite similar to Specimen DB-TC. In addition, the gap that exists over most of the depth of the interface

between the beams and column are somewhat similar to Specimen GJ-TC.

The amount of transverse joint reinforcement was proportioned as discussed for Specimen GJ-TC but was reduced by 16 percent for two reasons. First, in this specimen only five longitudinal bars were provided on the column faces adjacent to the beams making it difficult to provide the sixth cross-tie used in Specimen GJ-TC. Second, and more important, because the design according to the ACI-ASCE Committee 352 report for the previous two specimens proved to be conservative during testing, it was believed that less joint reinforcement could be used. *3.3.3.2 Material Properties*

The tensile properties for the reinforcing bars and structural steel plates used in this specimen are summarized in Table 3.6. The design compressive strength of the concrete used for the precast beams and column was 6000 psi. The actual compressive strengths for the concrete and fiber grout are shown in Table 3.7.

3.3.3.3 Fabrication and Erection

As for Specimen GJ-TC the column was cast horizontally. The beams, however, were cast on their sides. The pocket in the bottom of the beams needed for installation of the bolts between the beams and corbels was blocked out using Styrofoam. After casting, the Styrofoam was removed. Figure 3.23 shows the reinforcing cages for the column and beams in the wooden forms before casting.

The column was erected first. The beams were then seated on a 1/2 in. thick steel plate which was placed on the corbel to provide a pivot point for the dapped end of each beam. Next, 1/2 in. shims with 1-1/4 in. dia. holes were placed between the beam and the face of the corbel. Figure 3.24 shows the erection process for the beams. The 1-1/8 in. dia. bolts were then threaded into the nuts embedded in the corbels, as shown in Fig. 3.25, and then the pockets in the beams were filled with fiber-reinforced grout.

Table 3.6 Reinforcing Steel Properties for Specimen GJ-FR

Bar Size & Plates	f_y (ksi)	ε_y (%)	f_u (ksi)

#3	64.5	0.223	105.2
#6	59.3	0.205	100.8
#7	59.6	0.205	96.2
1 in. dia. Dywidag	142.6*	0.492	158.4
Friction Plates	53.8	0.186	77.7

* Based on $0.9f_u$ as per PCI Design Handbook [33].

Table 3.7 Compressive Strength of Concrete and Grout for Specimen GJ-FR

Concrete & Grout	28-day Strength (psi)	Strength at Last Day of Testing (psi)	Age at Last Day of Testing (days)
Beams and Column	7800	7970	91
Grout in Pockets	8010	8080	80

[Data missing]

connection concept and connecting elements used in this specimen is shown in Fig. 3.26. For this connection, threaded bar couplers were used to connect the "lower story" column to the "upper story" column. The column longitudinal reinforcement consisted of 5/8 in. dia. Dywidag bars. High-strength bars were used instead of conventional reinforcing bars to reduce reinforcement congestion in the joint region.

It should be noted that couplers for conventional reinforcing bars are commercially available. These were not used here because the coupler size and number of conventional bars could not be accommodated by the half-scale column. The beam was pretensioned with seven-wire 3/8 in. dia. low-relaxation strands. Each strand was tensioned to $0.4f_{pu}$ after losses. The strands were debonded through the column and 24 inches on each side of the column. The debonded length was chosen to maintain elastic

behavior in the connection up to 2 percent story drift, which was the design drift.

A crack was expected to form at the interface between the beam and the column, and geometric nonlinear behavior was anticipated as the crack width increased. Strain in the strands was not expected to change significantly because the crack opening was averaged over the entire debonded length of the strands. By tensioning the strands to a small fraction of their ultimate strength, yielding of the strands was intended to be delayed until considerable deformations were attained in the beams. Therefore, energy dissipation was expected to be very minimal. However, an important advantage to this system is that the frame system should have minimal residual drift after an earthquake. For this reason this type of connections is also called “self-righting”.

In contrast to Specimens GJ-TC and GJ-FR, this specimen did not require corbels. For Specimens GJ-TC and GJ-FR the corbels served as a support for erection in addition to serving as part of the pin connection described earlier. Also, unlike Specimen DB-TC, this specimen did not require temporary corbels for

erection since the beam is directly supported by the column. Because neither corbels nor haunches were used in this connection, it was also more aesthetically appealing.

3.3.4.1 Specimen Design and Reinforcement Details

This connection was different from the three connections described previously in both design and expected behavior. It consisted of a precast prestressed beam and two column elements representing the lower and upper-story columns in the prototype building. Specimen external dimensions are shown in Fig. 3.27. Reinforcement details for half of the specimen are shown in Fig. 3.28, and details at select cross sections are shown in Fig. 3.29. Design of the reinforcement did not entirely follow ACI 318-89 for two reasons. First, the expected specimen behavior as well as force transfer in the joint are different from monolithic construction behavior. Second, the design of the previous specimens (especially the joint) according to the ACI 318-89 provisions proved to be conservative.

Details of the beam cross section are shown in Fig. 3.29a. The beam flexural strength was designed so that strands would reach the limit of proportionality when the design moment was achieved. Another design goal was to achieve the design story drift when the design moment was reached. There were two variables available in the design that permitted these goals to be reached simultaneously. The first was the initial strand stress (after losses), and the second was the debonded length of the strands. By choosing a relatively low initial stress, it was possible to shorten the unbonded strand length because the difference between the strain at the limit of proportionality and the strain at initial stress became large.

Due to the short beam span for the scaled connection, the goal was to choose a reasonable unbonded length in order to leave sufficient length for force transfer between the prestressing strand and concrete. Spirals with a 7 in. diameter and 1-

1/2

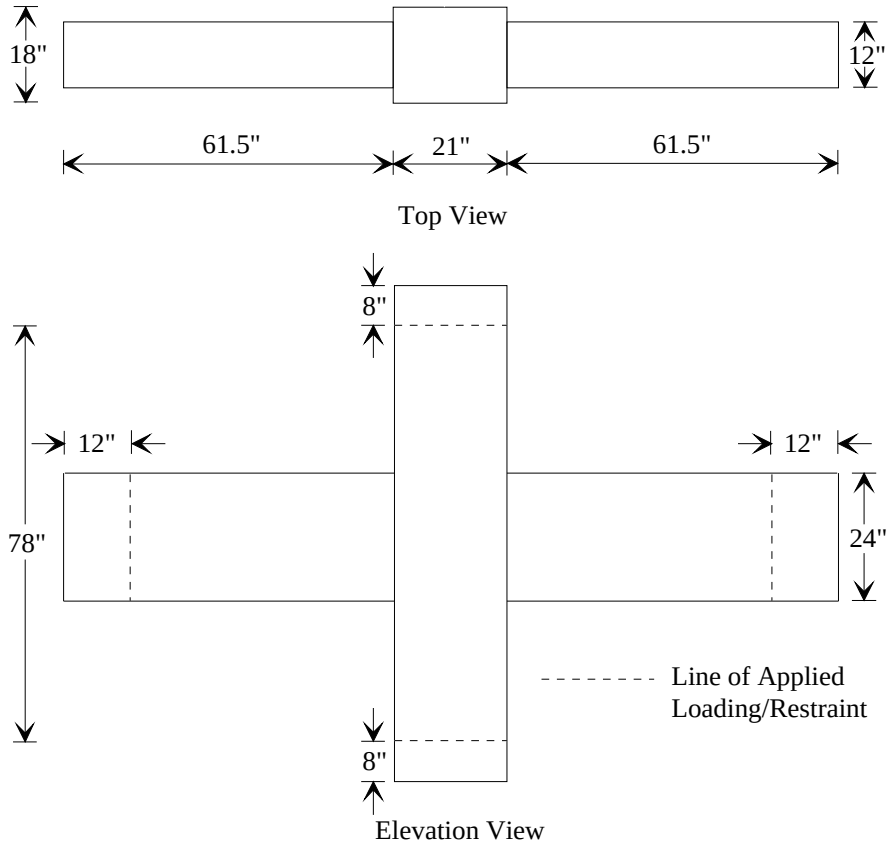

Figure 3.27 Dimensions of Specimen PT-NE

in. pitch, and fabricated from 1/4 in. dia. wire, were placed at the top and bottom of the beams near the column interface. These spirals were used to provide additional concrete confinement in regions where large concrete compression strains were expected. The confined strength of the concrete was calculated according to recommendations by Mander et al. [27]. Because beam flexural strengths were anticipated to occur at large drifts, the concrete cover was ignored in the flexural calculations. As for all the other specimens, the column was designed to have at least 40 percent more flexural strength than the beams. The cross section for the column is shown in Fig. 3.29b.

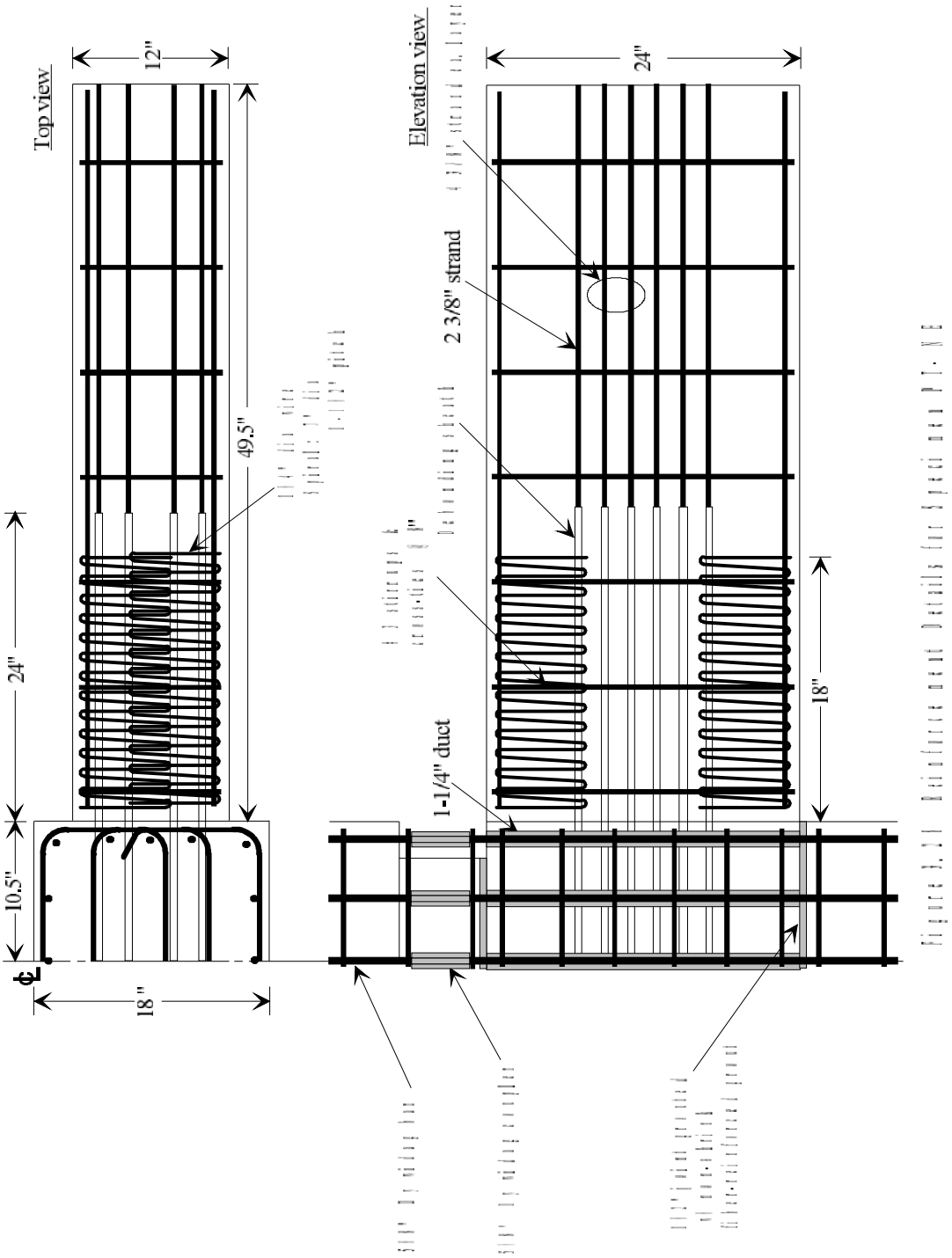
Top view
12"
49.5"
24"
10.5"
18"
Elevation view
24"
2 3/8" strand
1-1/4" duct
18"

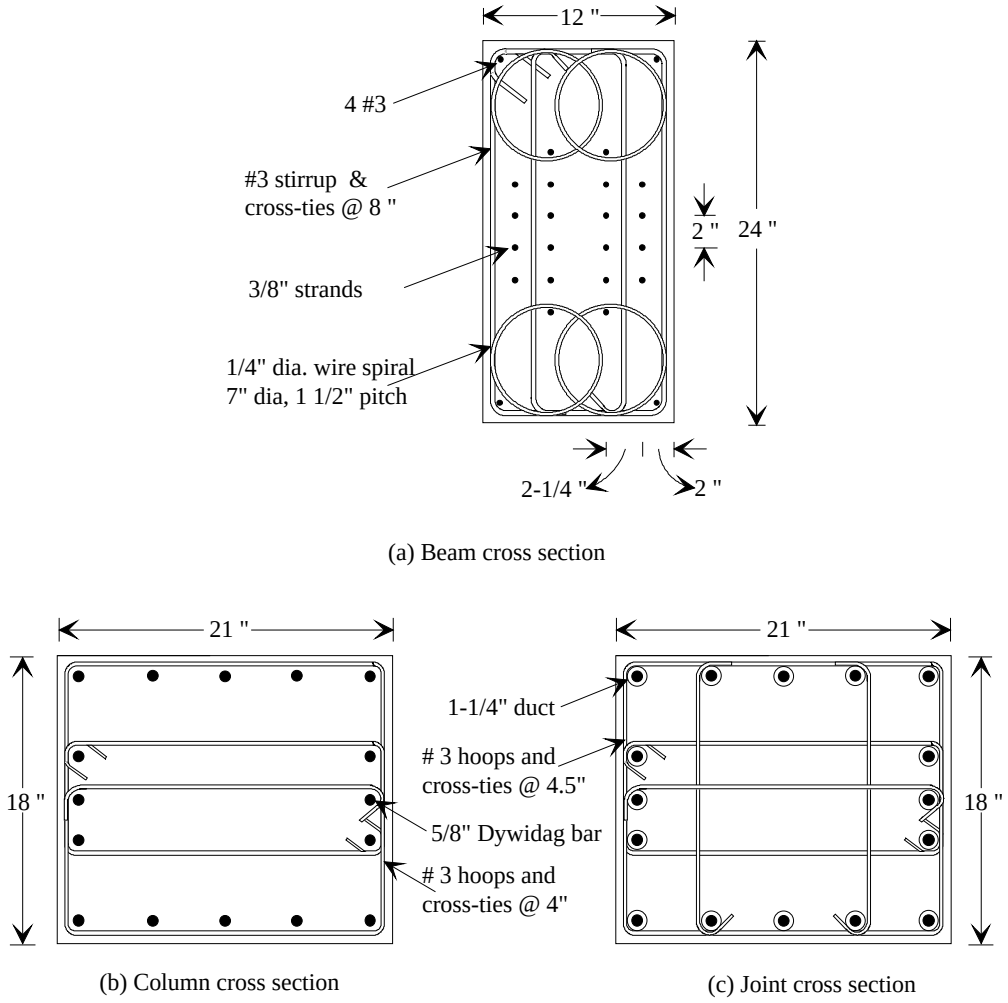

Figure 3.29 Cross Section Details for Specimen PT-NE

The shear design for the beam was carried out by treating the prestressing force as an axial force. Because this force is greater than $A_g f'_c/20$, the contribution of concrete to the shear strength of the member was utilized. The calculation of the concrete contribution to shear strength was performed according to the provisions for prestressed members in Chapter 11 of the ACI 318-89 code. This resulted in 8 in. spacing of the stirrups and cross-ties, which was much greater than the spacing of stirrups and ties in the other specimens where concrete contribution to shear strength was not utilized. The concrete contribution to the column shear strength

was ignored because no axial force was applied on the column.

The joint shear transfer mechanism for this connection was significantly different from that in the other specimens and the usual mechanism observed for monolithic joints. In general, two shear transfer mechanisms are typically identified in monolithic joints. These include a diagonal compression strut mechanism formed along the main diagonal of the joint panel resulting from the horizontal and vertical compression resultants acting at the beam and column critical sections, and a truss mechanism composed of small diagonal struts distributed over the joint panel. These struts are in equilibrium with tensile stresses in the horizontal and vertical reinforcement and bond stresses along beam bars and exterior column bars.

The latter of these two mechanisms is possible only when good bond is maintained along the beam reinforcement after beam hinging. In this specimen, beam longitudinal reinforcement, which was the prestressing strand, was completely debonded through the joint. As a result, the second mechanism was not possible, leaving only a diagonal compression strut to transfer the horizontal shear force through the joint, as shown in Fig. 3.30. Horizontal joint reinforcement was only needed to maintain the integrity of (confine) the joint after diagonal cracks formed. Somewhat arbitrarily, 66 percent of the amount of transverse reinforcement required by the ACI-ASCE 352 provisions was provided in the joint. This reduced amount was used in hope of learning something about the quantity of joint reinforcement needed for prestressed connections like this.

3.3.4.2 Material Properties

The tensile properties for the reinforcing bars and prestressing steel used in this specimen are summarized in Table 3.8.

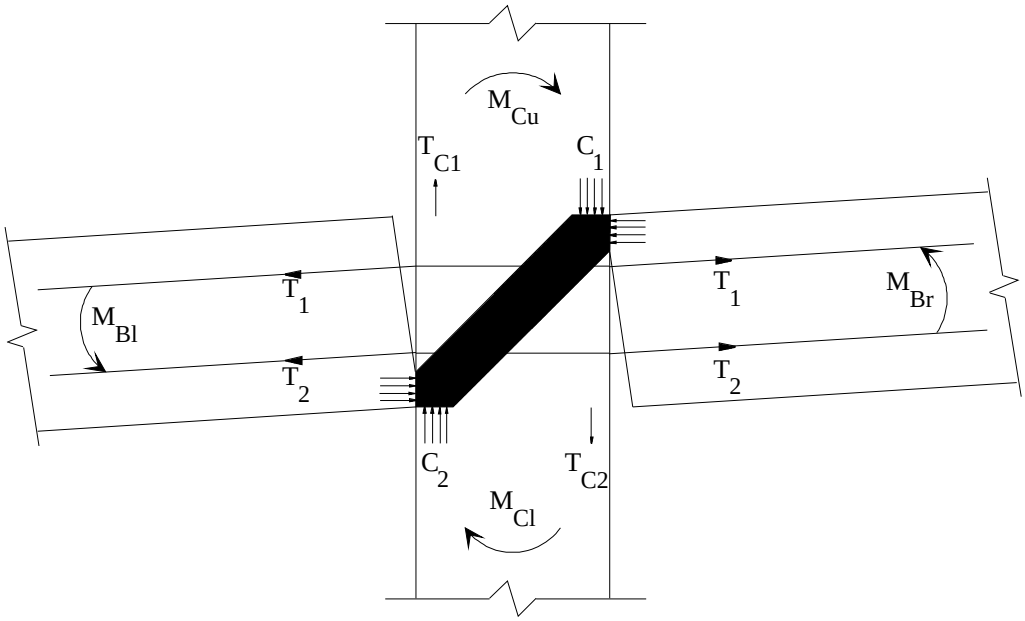

Figure 3.30 Joint Diagonal Compression Strut for Pretensioned Connection

The design compressive strength of the concrete used for the precast beams and column was assumed to have a compressive strength of 6000 psi. The actual compressive strengths for the concrete and the grout are shown in Table 3.9.

Table 3.8 Reinforcing Steel Properties for Specimen PT-NE

Bar Size	f_y (ksi)	ε_y (%)	f_u (ksi)
#3	64.5	0.223	105.2
5/8 in. Dywidag	145.3*	0.500	161.4
3/8 in. dia. Strands	242+	0.865	285

* Based on $0.9f_u$ as per PCI Design Handbook [33].

+ Limit of proportionality.

Table 3.9 Compressive Strength of Concrete and Grout for Specimen PT-NE

Concrete & Grout	28-day Strength (psi)	Strength at Last Day of Testing (psi)	Age at Last Day of Testing (days)
Beams and Column	6440	6300	35
Joints Grout	5940	5160	21

3.3.4.3 Fabrication and Erection

As mentioned previously, this specimen consists of one continuous beam and two column elements. Because the beam was pretensioned, a prestressing bed was built to facilitate the pretensioning operation. Figure 3.31 shows the prestressing bed as well as the reinforcing cage for the beam. Pretensioning force was applied using a ram and hand pump, and the force was measured using a calibrated pressure transducer. The two column elements were cast with their bars connected, as shown in Fig. 3.32, to ensure that the two pieces fit together again when the connection was assembled. This would typically not be necessary if commercial couplers are used.

Figures 3.33, 3.34, and 3.35 show the erection procedure for the specimen. After the lower column of the assembly was erected, the beam was mounted on top of the column and a 1/2 in. joint was left between the two elements. Ducts within the beam were fit over reinforcement that projected from the top of the lower column element. Reinforcement extending below the bottom of the upper column element was coupled with the lower column bars that extended through the beam. Finally, the joints between the lower column element and beam, the upper column element and beam, the ducts through the beam, and the pocket surrounding the bar couplers

Figure 3.31 Prestressing Bed and Reinforcing Cage for Beam of Specimen PT-NE

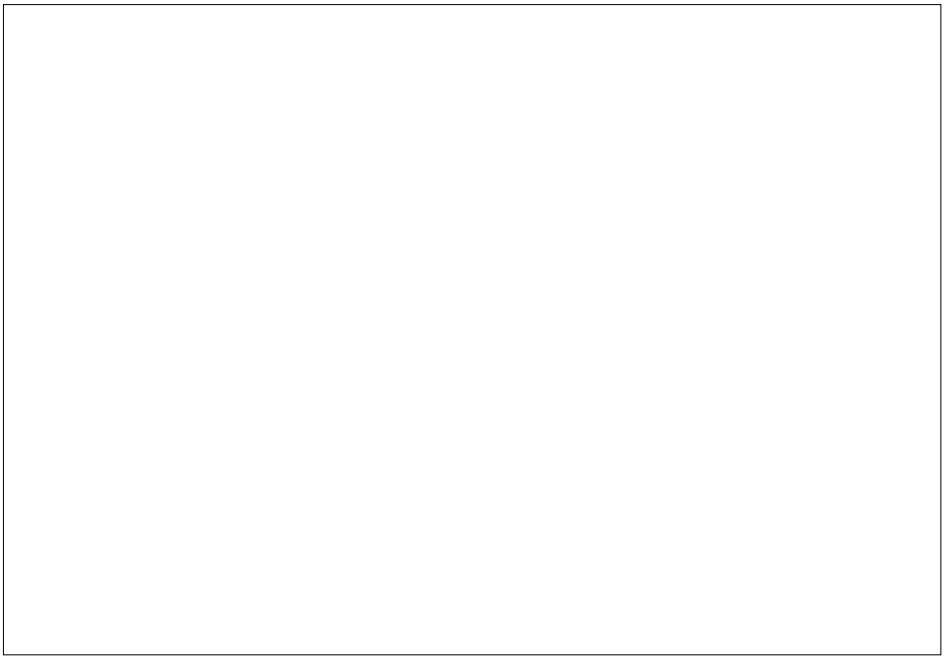

Figure 3.32 Reinforcing Cages for Columns of Specimen PT-NE

Figure 3.33 Erection of Lower Column Element of Specimen PT-NE

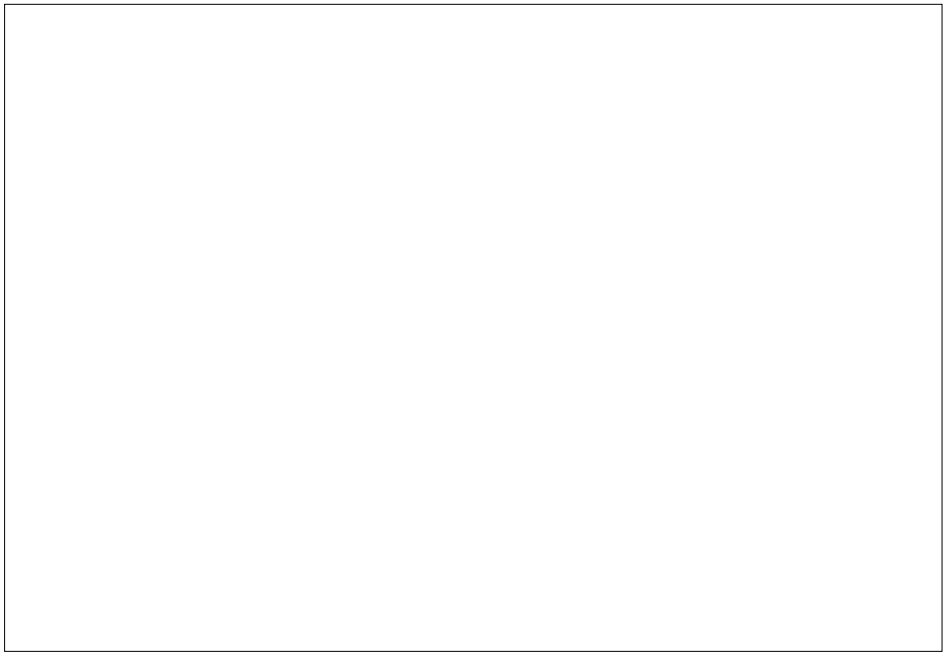

Figure 3.34 Erection of Beam of Specimen PT-NE

Figure 3.35 Erection of Upper Column Element of Specimen PT-NE

were grouted simultaneously with fiber-reinforced grout.

The specimen tested in this program had a cruciform shape. The beam in actual precast construction would likely extend two or more spans as shown schematically in Fig. 3.36.

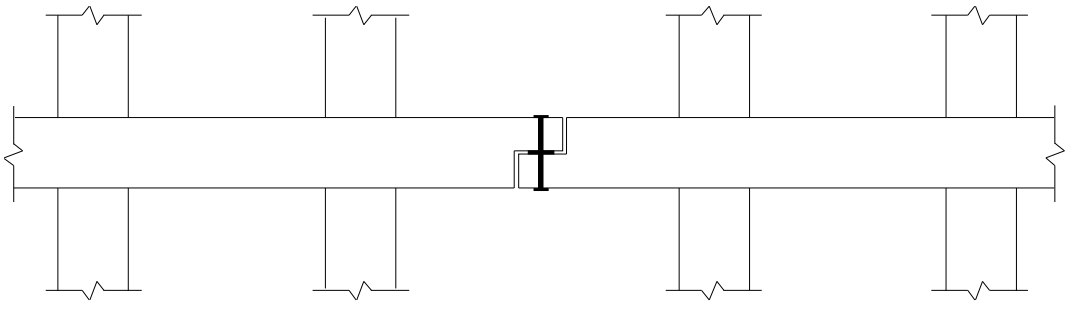

Figure 3.36 Possible Framing Using PT-NE Connections

3.4 OBSERVATIONS FROM CONSTRUCTION

The connections tested in this study were intended to evaluate different types of ductile connections (Section 2.3) designed to satisfy the objectives stated in Section 2.4. Most of the connection concepts used were selected in part because of the promise they were perceived to hold for ease and speed of construction. During construction, some problems that were not evident during design were detected. As a result, some of the connection concepts facilitated construction better then others. The objective of this section is to report problems that were encountered during construction as well as to indicate which connection details were simple to construct.

Reinforcement cages for beams in Specimen DB-TC were difficult to assemble. This specimen utilized a combination of plates and bars in the haunches to provide part of the force path between the beams and columns. In addition, ducts were cast in the haunches to facilitate placement of the high-strength threaded bars used to connect the beams to the column. As a result, the haunches were very congested and required precise placement of reinforcing steel, which made construction of the beam-column connection difficult and time consuming.

Specimen GJ-TC was much easier to construct than Specimen DB-TC. Beams of Specimen GJ-TC were more lightly reinforced, and as a result, reinforcing cages were easier to assemble. Vertical ducts provided in the beams for the dowels had relatively small tolerances. This could introduce fit problems when beams are placed. This tolerance problem can be easily overcome by using larger ducts if beam longitudinal reinforcement permits. The beam top reinforcement was easy to connect to the Lenton couplers embedded in the column, and the cast-in-place topping can be conveniently used to tie together the floor system and beams. In general, construction of Specimen GJ-TC was simple and expedient.

Reinforcing cages for beams in Specimen GJ-FR were congested and difficult to assemble, in part because reinforcement was proportioned to remain

elastic. Congestion was aggravated by plates that were part of the friction devices on the sides of the beams. Nuts were also required on the inside of the plates. The bottom connection was effective in transferring force from the beams to the column but required a pocket in each beam and sufficient tolerance to install (thread and tighten) the high-strength bolts. Tolerance in this connection was dependent upon accuracy of the hole locations in the plates, location of the beam bottom reinforcement, as well as location of the nuts in the corbel.

Each U-shaped plate assembly connected to the column was constructed by welding three plates together. The angle between connected plates was intended to be 90-degrees, but maintaining the angle between welded plates is difficult. Consequently, it may be necessary to fabricate the U-shaped plate assemblies with the brass shims in place prior to erection of the beams.

Precise tensioning of bolts in the friction devices was the key to attaining the desired connection performance. This was simple to achieve in the laboratory but would require special attention in the field.

Members of Specimen PT-NE were simple to fabricate. Pretensioning of beams has become a common procedure in the precast industry. Ducts in the joint region had sufficient tolerance to slip the beam over column reinforcement, but more tolerance is advisable in actual construction, especially if the beam is continuous over two columns as was shown in Fig. 3.36. Couplers used in the column did not facilitate coupling of longitudinal bars. Commercially available couplers would likely eliminate these problems in actual construction. Overall, this connection permitted rapid erection while using no cast-in-place concrete (dry construction). This contrasts Specimen GJ-TC which also permitted rapid erection, but utilized a significant amount of cast-in-place concrete.

In summary, Specimen PT-NE enabled the most rapid fabrication and erection. Specimen GJ-TC was only slightly less efficient to fabricate and erect. In addition, it also utilized the most cast-in-place concrete of any of the specimens constructed in this study. Specimen DB-TC was the most cumbersome to fabricate

and erect because of reinforcement congestion, complexity of connection details, and the need for temporary support during erection.

3.5 TEST SETUP

In order to simulate connection deformations representative of deformations experienced by interior beam-column connections in frame buildings subjected to seismic excitation, test specimens would ideally be loaded to deform as shown in Fig. 3.37a. To simplify the test setup used to impose predetermined story drifts (Δ in Fig. 3.37a), specimens were deformed as shown in Fig. 3.37b. The equivalence of the two deformed shapes is discussed in the next section. Deformations in the precast beam-column connections were imparted by displacing the two beam tips in opposite directions (upward and downward) while permitting no lateral displacement at the top and bottom of the column. Rotation of the column ends in the plane of the specimen was permitted.

In an effort to conserve project funds, an existing test setup used previously for testing composite frame connections [36] was modified slightly to accommodate the connections in this test program. The test setup is shown in Fig. 3.38. A 1-3/4 in. nominal inside diameter pipe was embedded in the columns 6 in. from the column ends. A 1-3/4 in. diameter pin was greased and placed through the embedded pipes and fastened to the bottom and top column fixtures. The bottom fixture consisted of two MC18x51.9 channels, 24 in. long, welded to a 1-1/4 in. thick plate and tied to the reaction floor as shown in Fig. 3.38. The top fixture, also shown in Fig. 3.38, consisted of two C12x20.7 channels tied to the reaction wall. To prevent any lateral

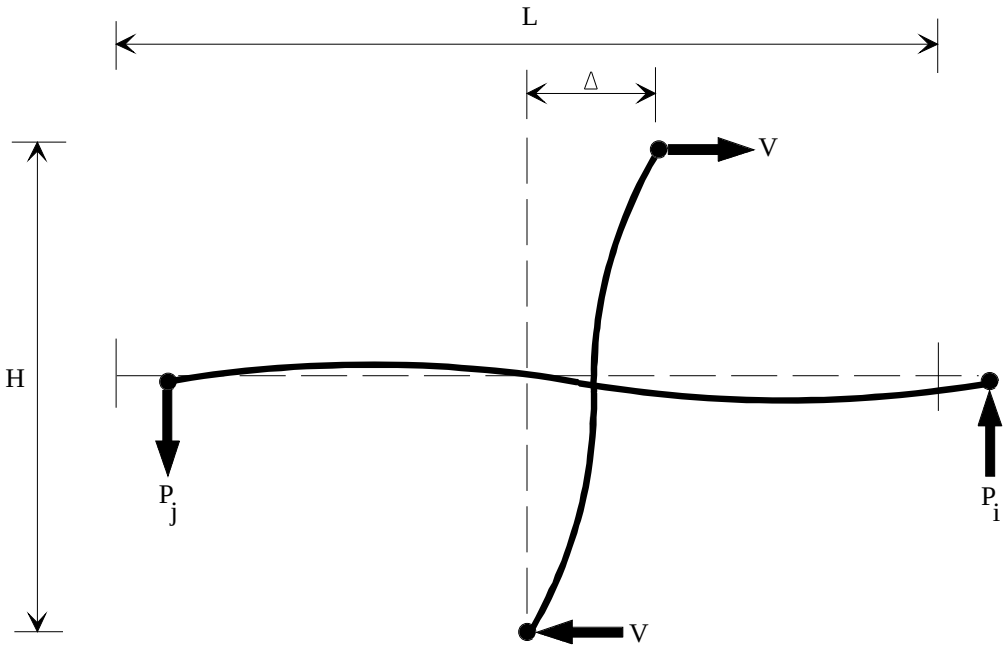

a) Ideal Deformed Shape for Connection

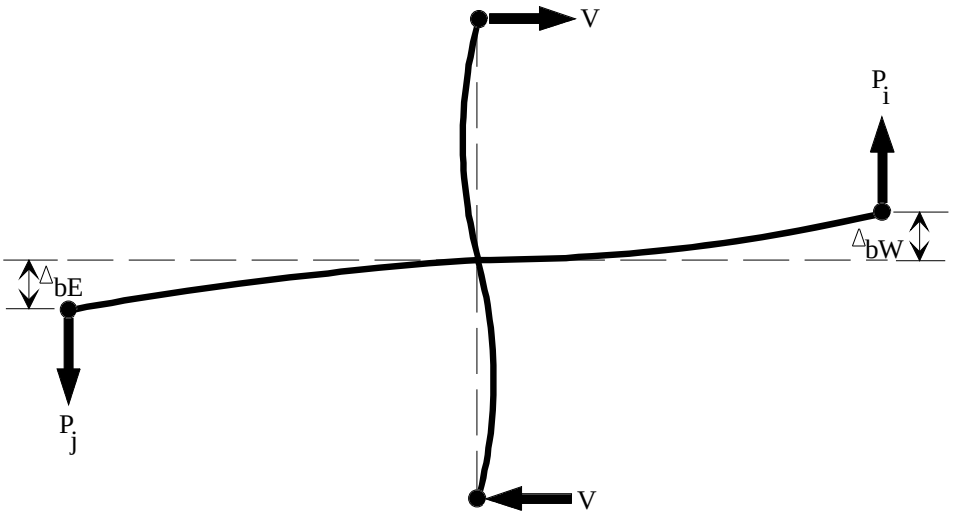

b) Deformed Shape in Test setup

Figure 3.37 Deflected Shape of Subassemblage

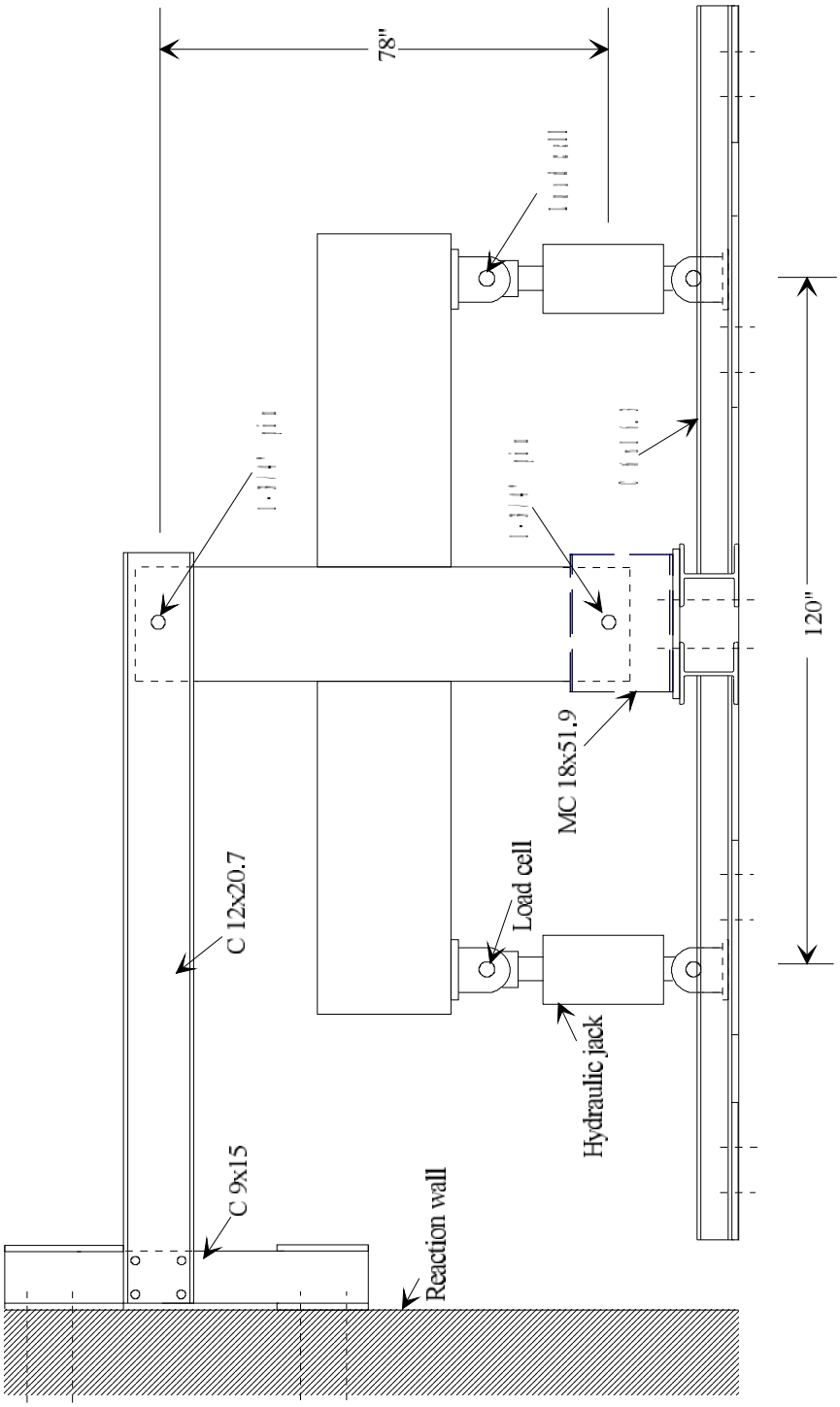

Figure 3.38 Existing Test Setup

movement and buckling of the channels, two L2-1/2x2-1/2x3/16 angle braces on each side of the frame were connected diagonally from the column top to the reaction wall and from the middle of the span of the channels to the reaction wall. Loads were applied to the beam tips by hydraulic rams bolted to the beam elements and a C6x16.3 channel that spanned between floor tie-down locations.

Because of the unanticipated capacity of the second connection (Specimen GJ-TC), the test setup approached its capacity, and as a result, became more flexible. Considerable movement at the top of the column occurred due to initiation of buckling of the channels and the angle braces. In addition, both ends of the column translated due to bending of the 1-3/4 in pins. Flexibility of the test setup was continuously measured and was taken into account as will be explained in Section 3.7. It was decided following testing of Specimen GJ-TC that a new test setup for remaining specimens had to be fabricated.

The diameter of the steel pin at the each end of the column was increased to 2-1/2 inches. The bottom column fixture consisted of two MC18x51.9 channels, 24 in. long, welded to a 1 in. thick plate tied to the reaction floor as shown in Fig. 3.39. The top fixture, consisted of two W14x38 sections connected to each other with three 3/4 in. steel plates top and bottom and tied to the reaction wall. To prevent any lateral movement, L5x5x1/2 angle brace was placed diagonally from the column top to the reaction wall. A schematic of the second test setup is shown in Fig. 3.39. Photographs showing Specimen GJ-TC in the first test setup and Specimen GJ-FR in the second test setup are shown in Fig. 3.40 and Fig. 3.41, respectively.

The specimens were loaded at the beam ends using hydraulic rams with a capacity of 192 kips in compression (upward loading) and 157 kips in tension (downward loading). Each ram was connected to a beam end with four 5/8 in. dia. Dywidag bars. The interface between the beams and clevis was filled with hydrostone to make the applied pressure uniform on the face of each beam. The test

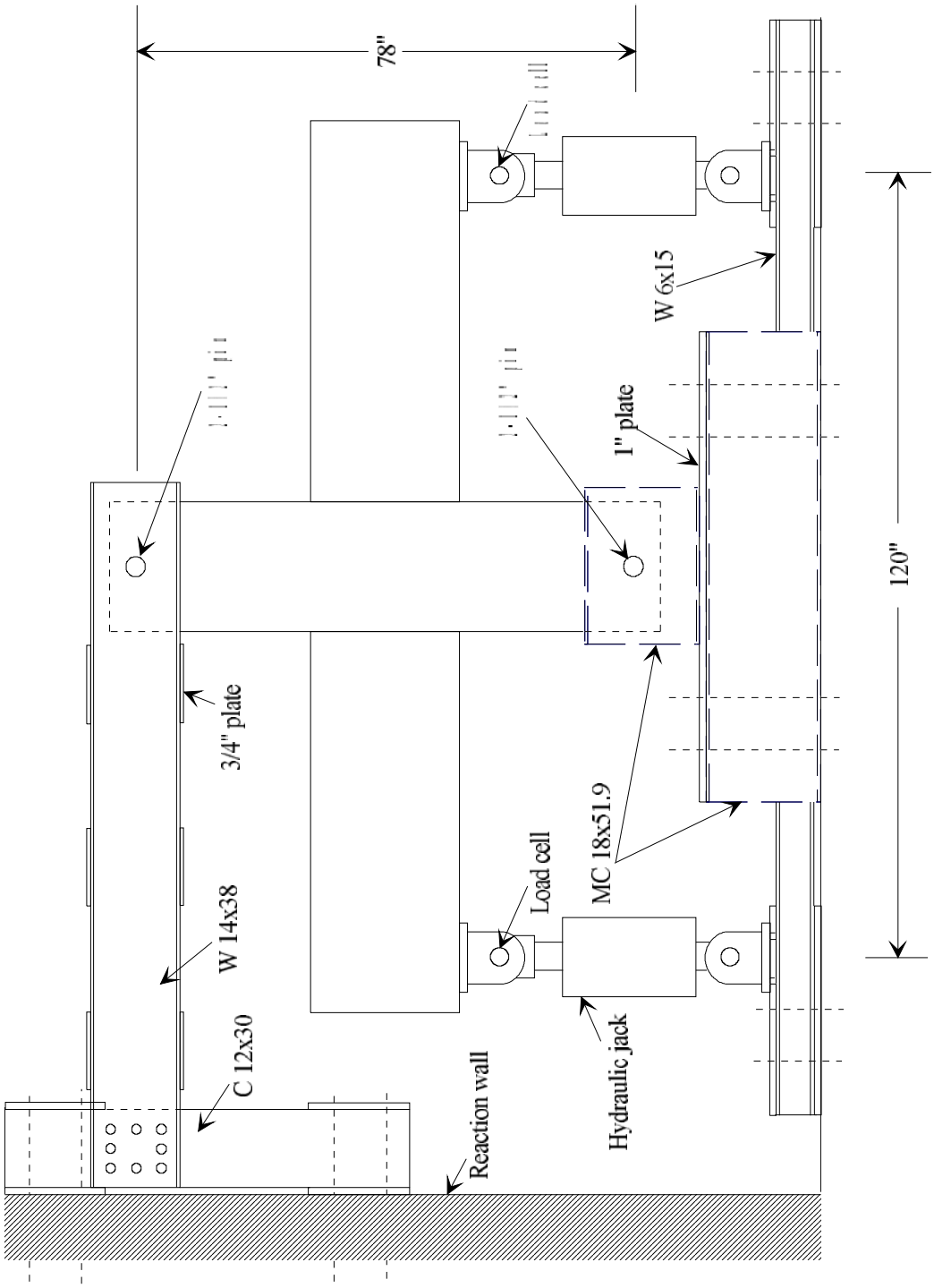

Figure 3.39 Second Test Setup

Figure 3.40 Specimen GJ-TC in First Test Setup

Figure 3.41 Specimen GJ-FR in Second Test Setup

was controlled manually using hydraulic hand pumps connected to the rams.

3.6 DISPLACEMENT/LOADING HISTORY

The same displacement/loading program was applied to all specimens and is shown in Fig. 3.42. This "loading program" was developed by PRESSS researchers during Phase I.

The "displacement history" was specified in terms of the story drift angle. For the rest of this paper, whenever the term "drift ratio" is used it means "story drift angle". For a beam-column connection deformed as in an actual structure, story drift angle is defined as:

$$R = \frac{\Delta}{H} \tag{3.1}$$

where Δ is the column relative displacement, and H is the column height (see Fig. 3.37a).

As mentioned in the previous section, it was more practical to construct a test setup that displaced the beam tips, as shown in Fig. 3.37b, than to impose deformations consistent with the deformed shape shown in Fig. 3.37a. For this case the story drift angle is defined as:

$$R = \frac{\Delta_{bE} + \Delta_{bW}}{L} \tag{3.2}$$

where Δ_{bE} and Δ_{bW} are the east and west beam tip deflections, respectively, and L is the beam length for the entire subassemblage. No axial load was applied to the column.

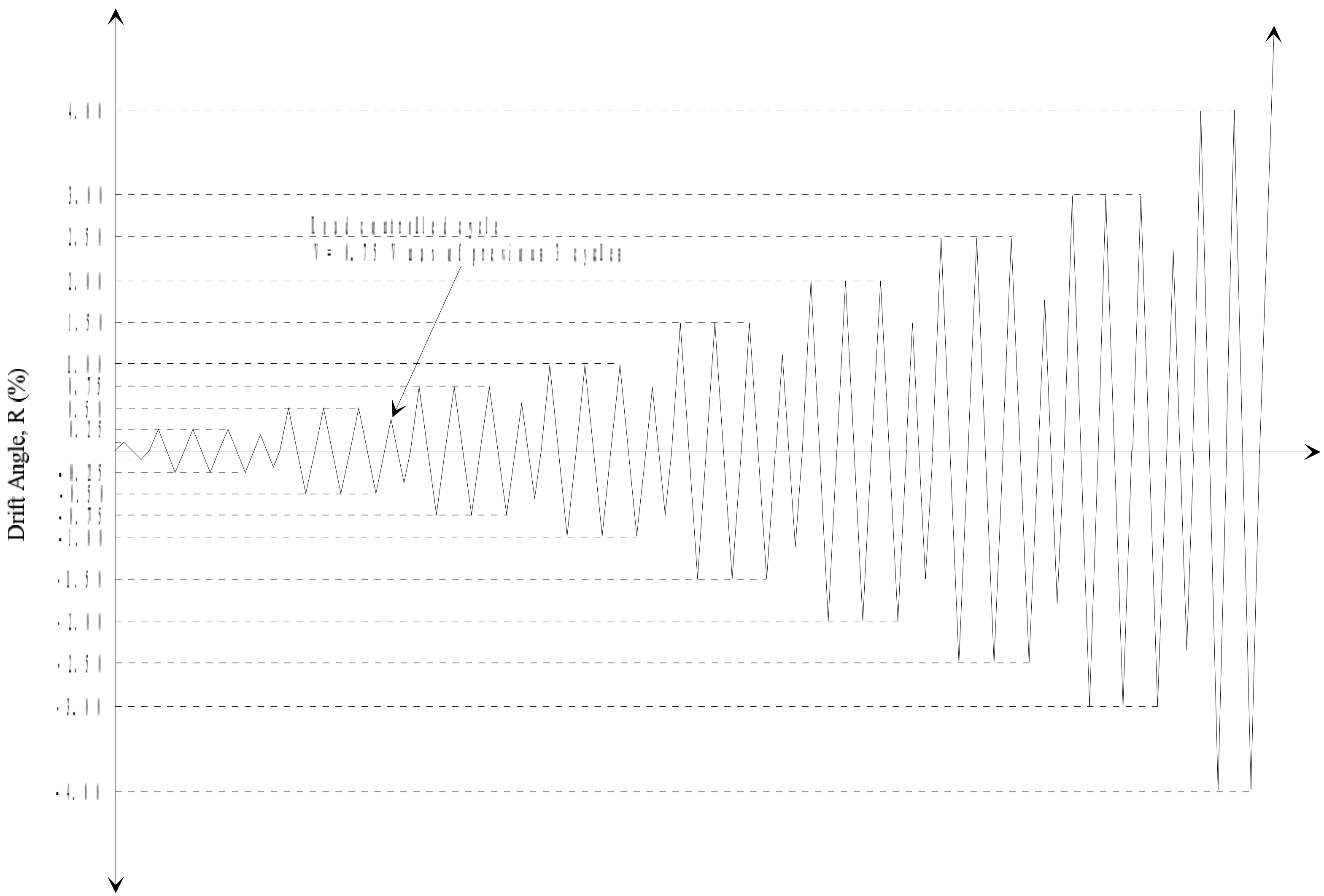

Figure 3.42 Displacement History

Each subassemblage was taken to progressively amplified drift reversals comprising the following sequence:

- One cycle at 0.1 percent drift ratio followed by three cycles each at 0.25 and 0.5 percent drift ratio. Cycles in this range were considered simulating loading in the serviceability range.
- Three cycles each at 0.75, 1, 1.5, and 2 percent drift ratio. The maximum drift ratio cycle in this range represented what is normally considered to be the maximum deformation that a structure subjected to earthquake loads should withstand without endangering life safety.
- Three cycles each at 2.5, and 3 percent drift ratio followed by two cycles at 4 percent drift ratio. Cycles in this range and beyond were considered excessive but gave insight into the potential of the structure for larger ductility demands and helped to identify the causes of eventual failure or loss of resistance of the particular subassemblage. In addition, following each set of three cycles to a prescribed drift ratio, an intermediate cycle was imposed to a peak load of 75 percent of the previously attained peak load to investigate stiffness degradation.

3.7 INSTRUMENTATION

Specimens were instrumented to obtain information about overall specimen response, and to observe the behavior of particular details. Three types of measuring devices were used: load cells, linear potentiometers, and strain gauges.

Loads applied at beam tips were measured with shear load cells that were substituted for a pin in the ram clevis. Beam tip displacements were monitored by 15 in. motion transducers fixed to the floor and connected at mid-depth of the beam above the applied load. These two measurements allowed the calculation of story shear and story drift angle. Story shear V and story drift angle R are given by:

$$V = (P_{bE} + P_{bW})\frac{L}{2H} \tag{3.3}$$

$$R = \frac{\Delta_{bE} + \Delta_{bW}}{L} \tag{3.4}$$

where P_{bE}, P_{bw} = east and west beam tip loads, respectively

L = beam length = 120 in.

H = column height = 78 in.

Δ_{bE}, Δ_{bW} = east and west beam tip displacements, respectively.

Rigid body motion was measured with linear potentiometers located at the level of the pins supporting the column. This motion was sometimes significant. The reason for this rigid body motion and the procedure to account for it is discussed in the next section.

The instrumentation used varied from specimen to specimen, depending on the connection design and expected behavior. In general, linear potentiometers were used to determine beam rotations, column rotations, and joint distortion. For some specimens more instrumentation was used to monitor the behavior of a specific element. The locations of the linear potentiometers used for the various specimens are shown in Figs. 3.43 to 3.46. Select reinforcing steel in the beams, column, and joint confinement was instrumented with strain gauges.

The locations of strain gauges in all the specimens are shown in Figs. 3.47 to 3.50. In Specimen DB-TC the high-strength threaded bars were not instrumented for two reasons. First, the bars were somewhat inaccessible in the ducts. Second, and more important, it was undesirable to alter the bond characteristics between the

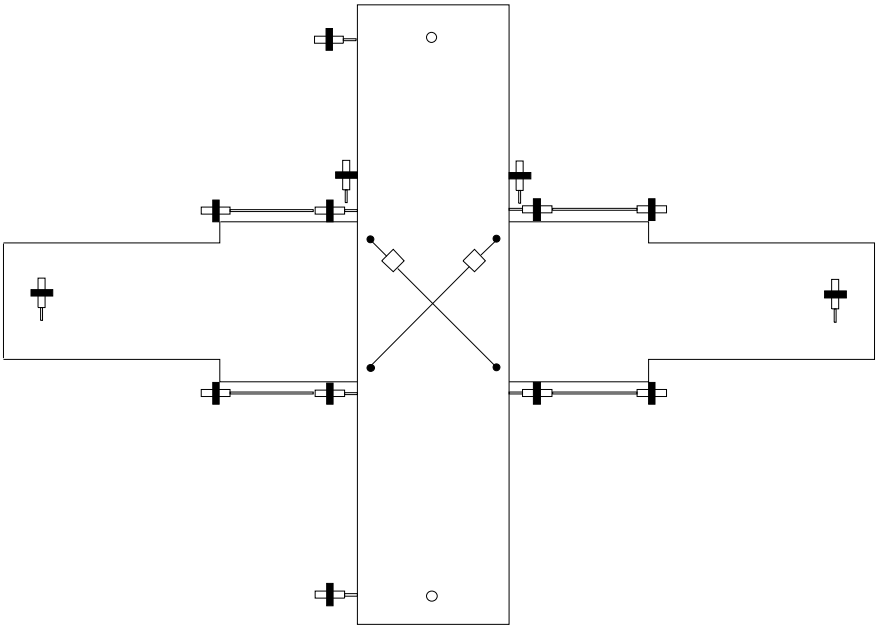

Figure 3.43 Linear Potentiometer Locations for Specimen DB-TC

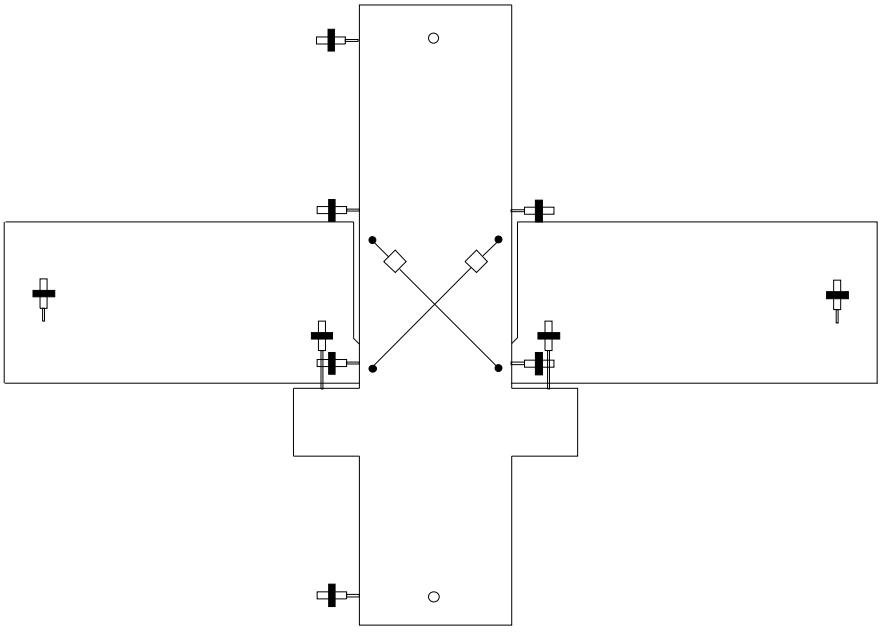

Figure 3.44 Linear Potentiometer Locations for Specimen GJ-TC

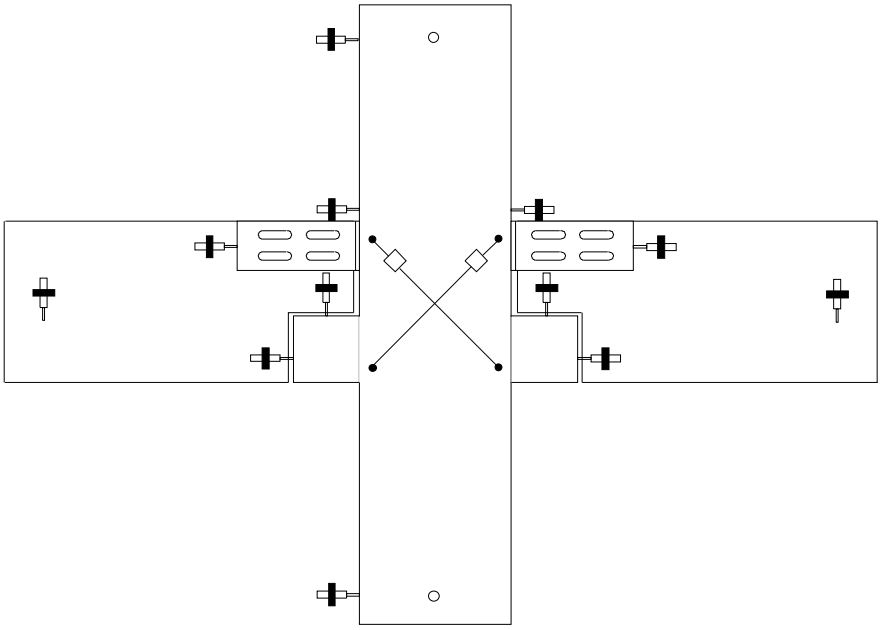

Figure 3.45 Linear Potentiometer Locations for Specimen GJ-FR

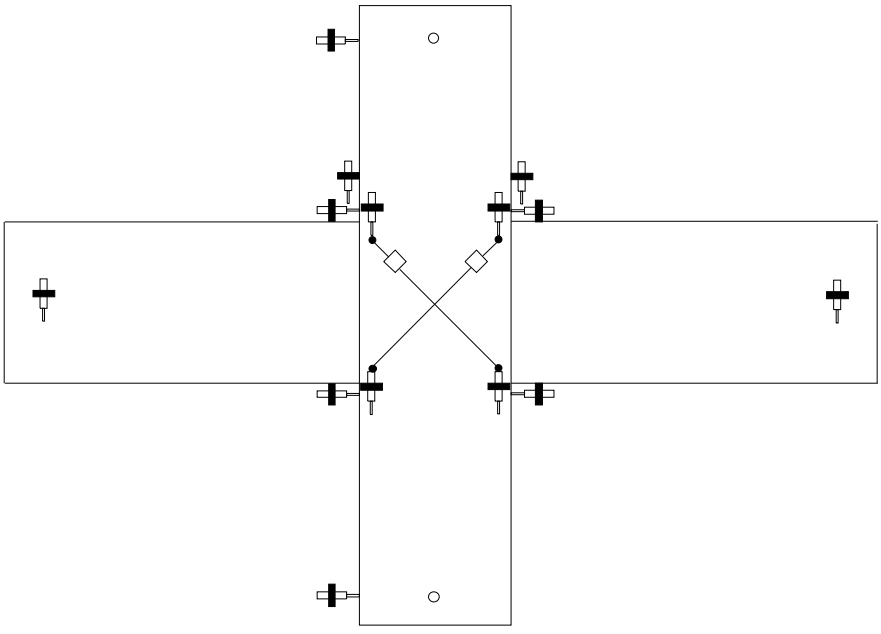

Figure 3.46 Linear Potentiometer Locations for Specimen PT-NE

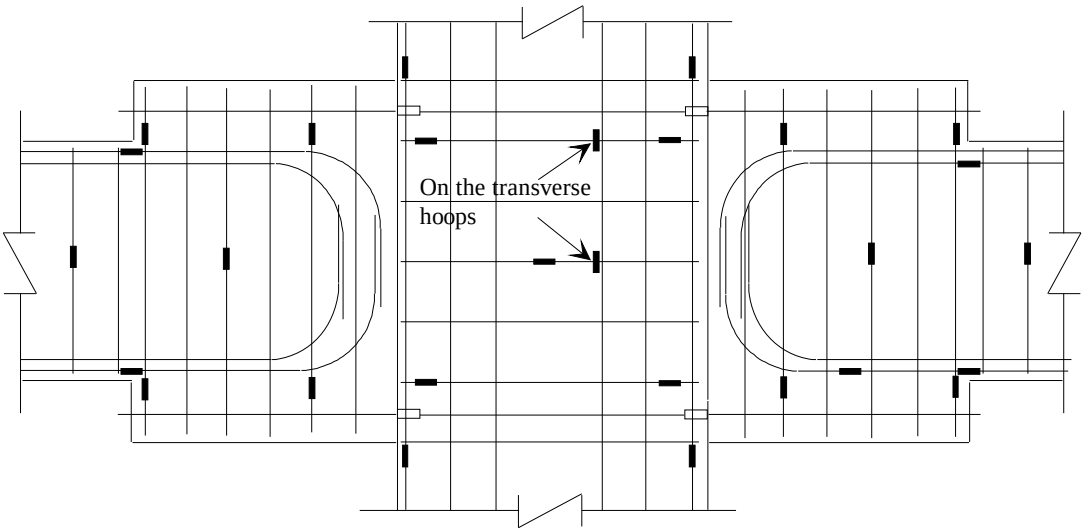

Figure 3.47 Strain Gauge Locations for Specimen DB-TC

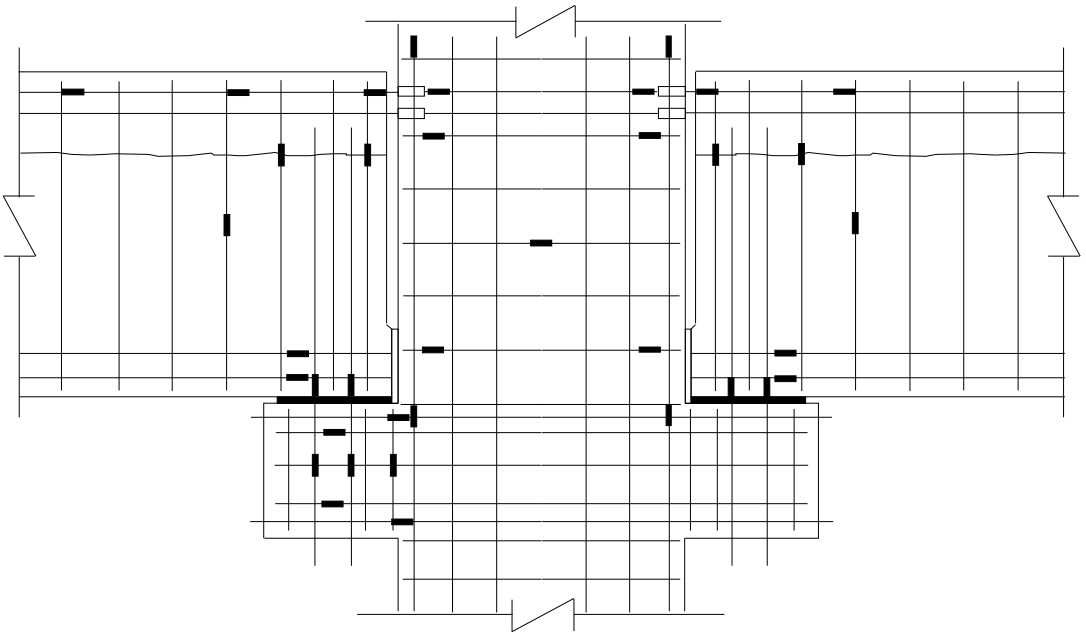

Figure 3.48 Strain Gauge Locations for Specimen GJ-TC

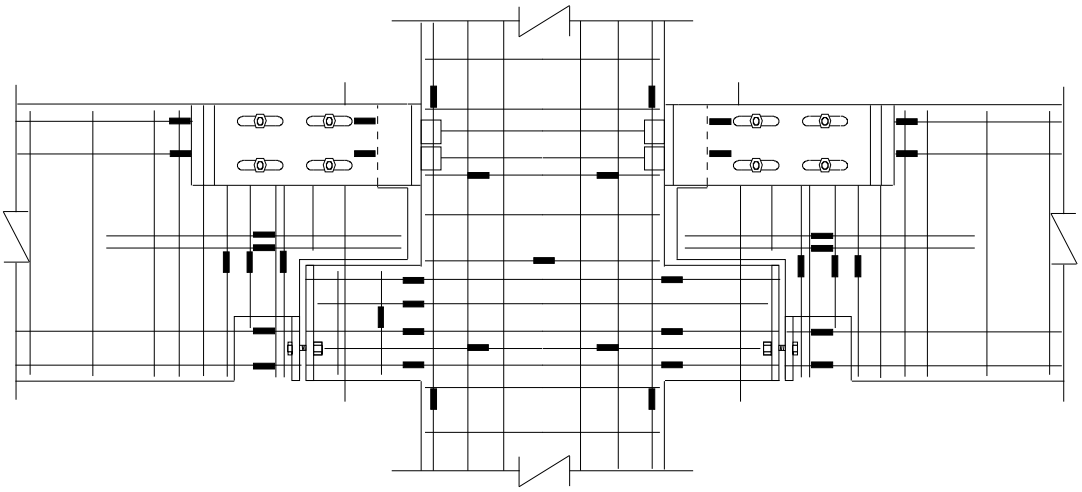

Figure 3.49 Strain Gauge Locations for Specimen GJ-FR

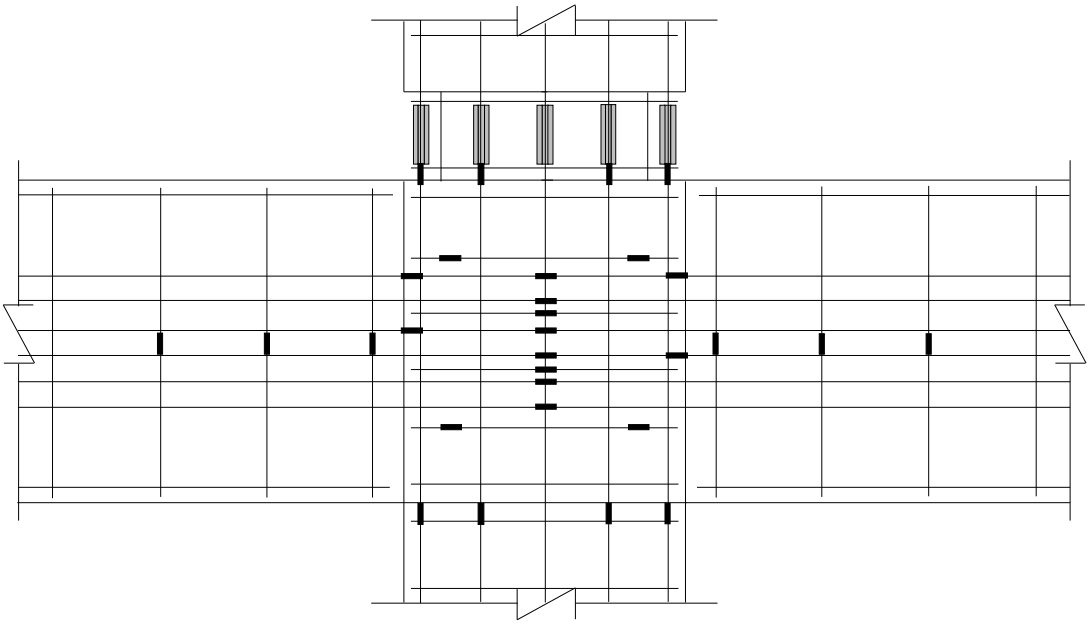

Figure 3.50 Strain Gauge Locations for Specimen PT-NE

grout and high-strength bars, especially because the length of the bars was much

shorter than the length required to develop the strength of the bars. Hoops and cross-ties that were instrumented in the joint in the direction of loading, as well as the main reinforcement in the column, were the same for all the specimens. For Specimen PT-NE, some of the prestressing strands were instrumented.

However, note that since the wires in prestressing strand are not straight, a piece of strand with strain gauges attached had to be loaded in a testing machine to quantify an "apparent" modulus of elasticity. Also note that the strain gauges shown in Figs. 3.47 to 3.50 are not the total number of strain gauges used. More strain gauges were used in the same locations shown to account for malfunction or damage to gauges while casting.

3.8 TEST PROCEDURE AND DATA ACQUISITION

The same test procedure was used for all specimens. At the beginning of each test, a couple of readings from the instruments were taken to check repeatability. As discussed in Section 3.5, most of each test was conducted under displacement control rather than load control. Equal displacements were imposed on the beam tips by using manual hand pumps and dial gauges to continuously monitor movement of the beams. In each displacement cycle, several displacement increments were made before reaching the maximum displacement in order to provide sufficient data for plotting continuous force-displacement curves.

Considerable horizontal movement in the plane of the frame was caused by flexibility in the steel loading frame, and to a lesser extent by sloppiness in the pins at the top and bottom of the column. This movement resulted in rigid body rotation for the entire subassemblage and, in turn, amplified the true beam end displacements. To subtract the component of beam end displacements due to rigid body movement from the gross measured beam displacements the following procedure was performed:

1. Displacements at the top and bottom of the column, namely Δ_{cT} and Δ_{cB} respectively, were measured.

2. Displacements at the tip of the east and west beams, namely Δ_{bE} and Δ_{bW}, respectively, were measured. Note that $\Delta_{bE} = \Delta_{bW} = \Delta_b$ at all times because the test was controlled by displacement.

3. The net beam tip displacement Δ_{bn} was determined as follows:

$$\Delta_{bn} = \left(\frac{\Delta_{bE} - \Delta_{bW}}{L} - \frac{\Delta_{cT} - \Delta_{cB}}{H} \right) \frac{L}{2} \tag{3.5}$$

where L = beam span for entire subassemblage = 120 in.

H = column height = 78 in.

Upward displacements imposed on the beam tips were taken as positive. Westward displacements at the column top and bottom pins were taken as positive.

A complete set of readings was taken at every displacement increment, and the net deflection of both beams was calculated immediately in order to determine how much adjustment the following displacement increment required.

At the peak of each displacement cycle, cracks on all faces of the specimen were marked. Different colors were used to denote the different loading directions. Photographs were taken normally at the peak of each cycle, and at other stages when interesting behavior was observed.

After the maximum displacement level had been attained, unloading of the beams was carried out by displacement control also. Equal proportions of the maximum displacement were removed until the two beam tip deflections were back at zero displacement. A new cycle was then commenced

Following the third cycle of each drift level, the specimen was loaded to 75 percent of the maximum load attained in the previous three cycles as explained in Section 3.5. Loading in this cycle was also achieved through imposing small and

equal increments of displacement at the tips of the beams. The load was monitored through an X-Y plotter until the required load was achieved.

Electronic data acquisition was performed using a high-speed scanner which was controlled by a microcomputer. A scan, which constitutes a voltage reading of every strain gauge, linear potentiometer, and load cell, was taken at every displacement increment, and a hard copy of the reading was obtained simultaneously. The software used, called HPDAS2, displays the engineering units of every scan on the screen to help in monitoring the test. The data was then saved on a floppy disk for further analysis. Due to the large surface area for marking cracks, and the use of manual hand pumps to provide hydraulic pressure, at best, four cycles were completed per day.

CHAPTER 5

EVALUATION OF EXPERIMENTAL RESULTS

5.1 INTRODUCTION

In the previous chapter the overall behavior of the specimens was presented. This was done by discussing the story shear-drift ratio response of each specimen, cracking and spalling (if any), and the mode of failure. When necessary, information about a particular specimen component was presented to better understand the specimen behavior and mode of failure. Behavior of the specimens is evaluated in this chapter. Comparisons of response envelopes, energy dissipation, residual drift, stiffness, and stiffness degradation will be made. Data gathered with the strain gauges are presented and discussed. Due to the large number of strain gauges used, only data from gauges which lead to specific conclusions are presented. Assumptions made during design of the specimens (discussed previously) are evaluated using strain gauge data.

5.2 RESPONSE ENVELOPE CURVES

In the tests presented here, the loading was cyclic, applied pseudo statically, to simulate cyclic loading during an earthquake. Often, it is desirable to know the monotonic response of a connection for insight into the strength, stiffness, and ductility. When the points corresponding to the peak response of the first cycle of each set of cycles are connected, the resulting curve is referred to as response envelope. In general, as a specimen is cyclically loaded to a new drift level, the response passes very near the peak of the first cycle of the previous set of cycles, unless significant strength degradation has occurred during the latter cycles to the previous drift level.

Figure 5.1 shows the envelope curves for all the specimens (and the retest of Specimen GJ-FR). These curves correspond with loading in the negative direction. Envelopes of the positive response are not shown since they are quite similar to the envelopes for loading in the negative direction.

A number of differences and some similarities exist in the envelope curves shown in Fig. 5.1. Not all the specimens reached the same maximum drift ratio. Specimen DB-TC, which was considered to have failed prematurely, reached a maximum drift ratio of 2 percent. Specimen PT-NE, on the other hand, reached a maximum drift ratio of 5 percent. All other specimens attained a maximum drift ratio of 3 percent.

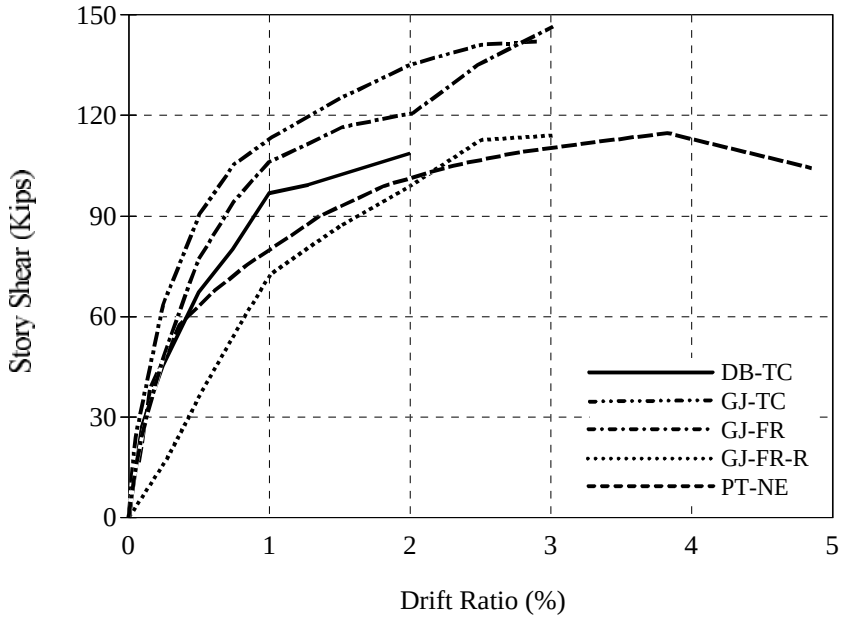

Figure 5.1 Response Envelopes

Table 5.1 Comparison of Theoretical and Experimental Story Shear Capacity

	Calc. Stry. Shear $V_{u,calc}$ (Kips)	Exprmtl. Stry. Shear $V_{u,exp}$ (Kips)	$\frac{V_{u,exp}}{V_{u,calc}}$	V_{exp} @ 2% Drift (Kips)	Drift Ratio @ $V_{u,calc}$ (%)	Drift Ratio @ $V_{u,exp}$ (%)	Max. Drift Ratio (%)
DB-TC	112.4	109.2	0.97	109.2	2.00	2.00	2.00
GJ-TC	112.9	142.5	1.26	136.8	0.87	3.00	3.00
GJ-FR	117.8	148.4	1.26	120.7	1.22	2.98	3.00
GJ-FR-R	106.7	114.0	1.07	99.1	2.14	3.00	3.00
PT-NE	108.2	114.7	1.06	98.4	2.28	3.80	5.00

Figure 5.1 also illustrates that the ultimate strength of the connections during testing was different from one specimen to another. As explained earlier, the design moment capacity of the beams was 300 k-ft. From statics the corresponding design story shear was 111 kips. The actual moment capacities varied slightly from the target moment capacity primarily due to differences in steel strength. Also, the amount of steel that can be actually used versus the calculated quantity can make some difference in the target versus design moment. Table 5.1 lists the values of the calculated story shear capacities without consideration of steel strain hardening. These values are based on measured material properties for steel obtained from monotonic tensile coupon tests, and for concrete obtained from compression tests on cylinders performed on the last day of testing. Also listed in Table 5.1 are the experimentally obtained story shear capacities.

Table 5.1 shows that all specimens, with the exception of DB-TC, reached the calculated story shear capacity. Specimen DB-TC nearly reached the calculated story shear but failed at a location outside the connection as explained earlier. Specimens GJ-TC and GJ-FR both had 25 percent more strength than was expected. The retest of Specimens GJ-FR and Specimen PT-NE had around 7 percent extra strength. Furthermore, it is interesting that all the specimens reached the calculated story shear at a different drift ratio. Specimen GJ-TC reached the theoretical story

shear at 0.87 percent drift ratio, and continued to resist additional load until 3 percent drift ratio. Specimen GJ-FR, on the other hand, reached its theoretical story shear at a slightly higher drift than Specimen GJ-TC (1.22 percent). The retest of Specimen GJ-FR and Specimen PT-NE attained their calculated story shear capacity at slightly more than 2 percent drift ratio. In general, Specimen GJ-TC was the strongest and Specimen PT-NE was the stiffest among all specimens. Further comparison of specimen stiffnesses will be presented later.

5.3 HYSTERETIC BEHAVIOR

5.3.1 Energy Dissipation

Major earthquakes release tremendous amounts of energy. In order for a building to withstand an earthquake without collapsing, the building must be capable of absorbing and dissipating a sufficient amount of energy imparted to the structure. Each structural frame system possesses viscous damping and inelastic hysteretic damping to dissipate energy during an earthquake. Because inelastic hysteretic damping in a structure is primarily responsible for the energy dissipated, the energy dissipation characteristics of the connections tested in this study are evaluated.

The total amount of energy dissipated by each specimen was obtained by calculating the area inside the story shear-interstory drift curves. Figure 5.2 illustrates the total amount of energy dissipated by each specimen. Different amounts of energy were dissipated by the various specimens. Specimen DB-TC dissipated the least energy due to its premature failure and use of high-strength thread bars for the

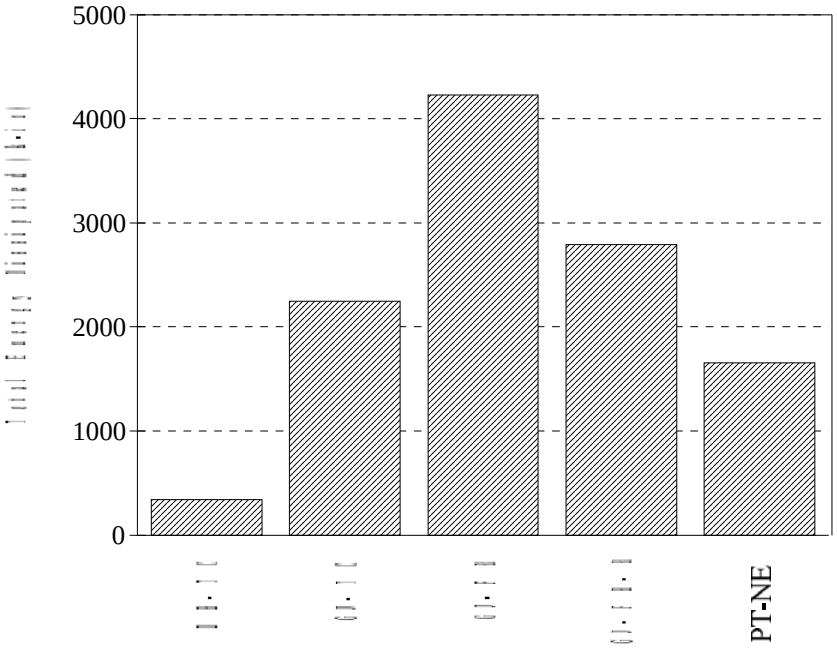

Figure 5.2 Total Energy Dissipated by Each Specimen

connecting elements. In general, most of the energy was dissipated after considerable inelastic deformations occurred in the connecting elements, which was not the case for Specimen DB-TC prior to failure. Specimen GJ-FR was superior to all other specimens in terms of total energy dissipated. This was anticipated since the main function of the friction plates was to introduce a source of energy dissipation.

The energy dissipated by Specimen GJ-TC was approximately half of that dissipated by Specimen GJ-FR. Although these two specimens attained the same drift level and story shear, pinching of the hystereses of Specimen GJ-TC greatly affected its energy dissipation. During test GJ-FR-R the total energy dissipated was also superior to the other tests but was less than the energy dissipated during the first test of Specimen GJ-FR. Two reasons accounted for this reduction in total energy dissipated. First, the loading history for this test did not contain the 0.75 percent drift ratio cycle, and the third cycle of each set of cycles was not performed.

Second, the strength of the specimen was reduced from that used in the original test.

Specimen PT-NE was not expected to dissipate energy because the story shear-drift response was anticipated to be elastic and follow the same path while loading and unloading. In reality some energy was dissipated due to cracking and crushing of concrete, and due to yielding of strands at high drift levels. The total amount of energy dissipated by Specimen PT-NE was the second lowest in the series of test specimens.

Figure 5.3 illustrates the energy dissipated during the first cycle of each set of drift cycles. Notice that the energy dissipated prior to 1 percent drift ratio was minimal for all specimens. Nonlinear response in some of the specimens initiated at approximately 1 percent drift ratio. Up to 1.5 percent drift ratio, Specimen DB-TC was comparable to most of the other specimens. As drift ratio increased, energy dissipated in each cycle increased approximately exponentially for all specimens except DB-TC. However, for Specimen GJ-FR and the retest GJ-FR-R, the energy dissipated per cycle increased at a higher rate for drift ratios of 2 percent and beyond. Remember that this is slightly larger than the drift when slip started in the beams. The energy dissipated per cycle for Specimen GJ-TC was increasing but at a lower rate because pinching was more pronounced at higher drift levels. Specimen PT-NE dissipated very little energy as expected up to 3 percent drift ratio. Most of the energy was dissipated in the 4 and 5 percent drift ratio cycles when joint deterioration was substantial. Actually, if the energy dissipated in cycles beyond 3 percent drift ratio were excluded, the total energy dissipated for Specimen PT-NE (shown in Fig. 5.2) would be reduced by approximately 50 percent. Finally, it is interesting to note that the energy dissipated by Specimen GJ-FR during the first cycle at 3 percent drift ratio was approximately 75 percent of the total energy dissipated during all the initial cycles for Specimen PT-NE.

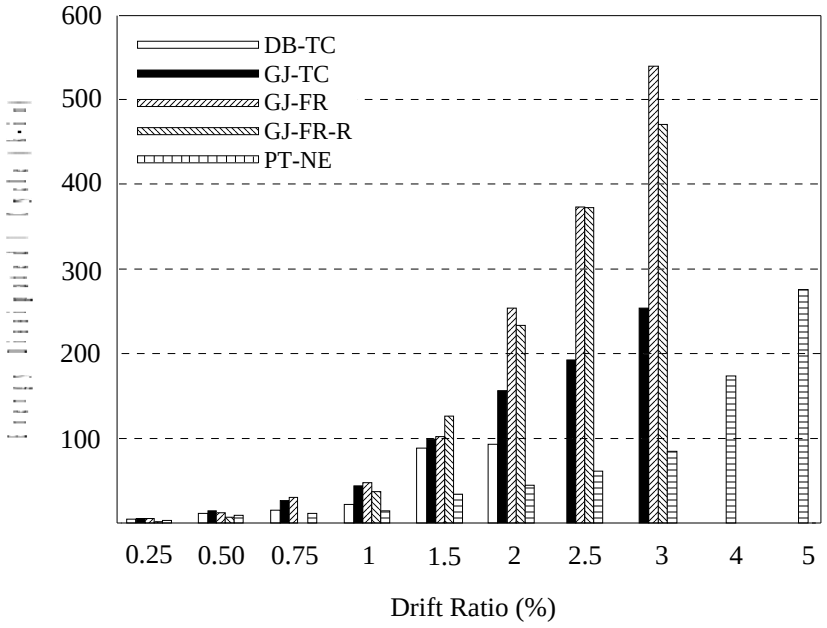

Figure 5.3 Energy Dissipated in the First Cycle of Each Set of Cycles

5.3.2 Equivalent Viscous Damping Ratio

As mentioned in the previous section, viscous damping is one of the properties of a structure that contributes to dissipating energy that is imparted to the structure. This type of damping, although not entirely realistic, is usually assumed in structures subjected to dynamic excitation because it leads to simple mathematical modeling. Hysteretic damping, associated with inelastic deformations in structural members/connections, usually accounts for most of the energy dissipation in a structure. Energy dissipation for the connections is quantified here as the equivalent viscous damping ratio. The equivalent viscous damping ratio H_{eq} is the ratio of energy dissipated in a half cycle to the strain energy of an equivalent linear system divided by the constant 2π [13]. The definition of H_{eq} is illustrated in Fig. 5.4. Values of the equivalent viscous damping ratio are used here to compare the energy

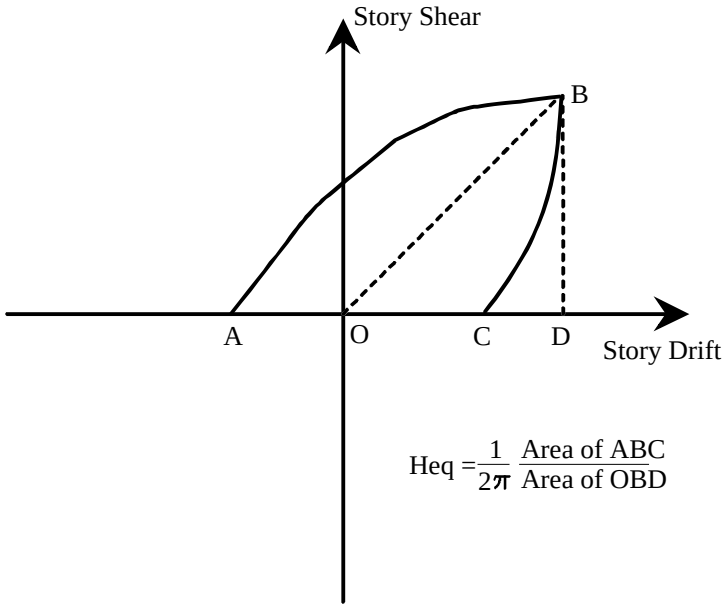

Figure 5.4 Definition of Equivalent Viscous Damping Ratio, Heq

dissipation capacity and indirectly measure the influence of pinching of hysteresis loops on energy dissipation. Because Specimen DB-TC failed before significant yielding occurred, it was not included in this discussion.

The equivalent viscous damping ratios for Specimens GJ-TC, GJ-FR, GJ-FR-R, and PT-NE for 1 percent drift ratio and higher are shown in Fig. 5.5. The ratios at 1 percent drift for Specimens GJ-TC and GJ-FR, and retest GJ-FR-R are practically the same. This is so because up to this point all specimens behaved elastically. The equivalent viscous damping ratios shown for Specimen PT-NE are both low and practically constant from 1 to 3 percent drift. However, ratios increase for drifts beyond 3 percent due to the rapid joint deterioration. The ratios for Specimen GJ-FR and retest GJ-FR-R started at approximately the same level as GJ-TC but increased at a much higher rate.

It is interesting to compare Specimens GJ-TC and GJ-FR because they both attained the same maximum drift ratio. However, Fig. 5.5 suggests that the

behavior

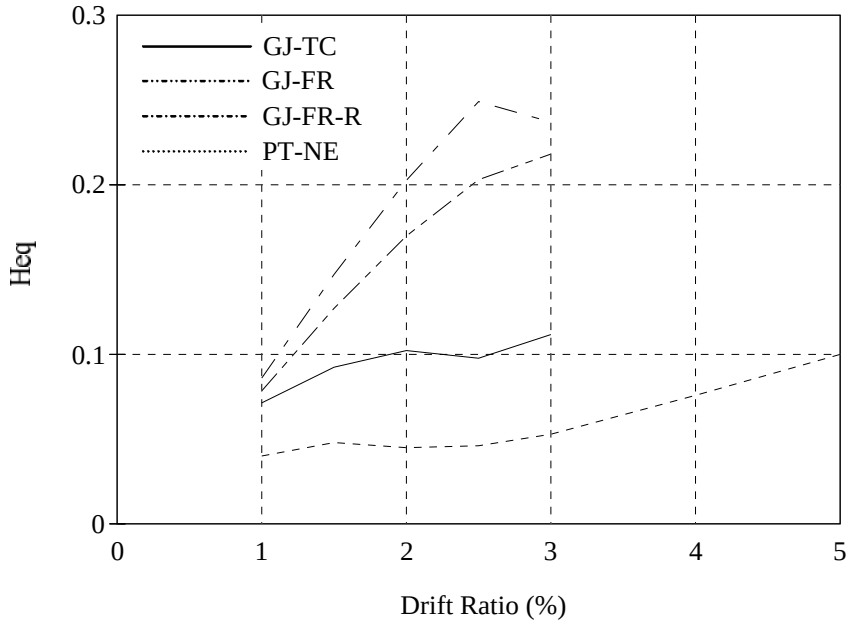

Figure 5.5 Equivalent Viscous Damping Ratio

was quite different. Low equivalent viscous damping ratio indicated that energy dissipation was low. The increase in the equivalent viscous damping ratio for Specimen GJ-FR and retest GJ-FR-R is an indication that energy dissipation increased as drift ratio increased. The relatively constant trend of the equivalent viscous damping ratio of Specimen GJ-TC indicates that although the drift ratio increased to the same drift ratio as Specimen GJ-FR and retest GJ-FR-R, energy dissipated did not increase significantly. This indirectly indicates that pinching of the story shear-drift ratio response for Specimen GJ-TC increased enough to offset the increase in drift ratio that resulted in increased energy dissipation for Specimen GJ-FR and GJ-FR-R. It is interesting that the equivalent viscous damping ratio for retest GJ-FR-R was slightly higher at the drifts shown than for the original specimen GJ-FR. This demonstrates that the structural members did not suffer significant damage in the original test specimen despite the high drift ratio attained and the

amount of energy dissipated.

5.4 COMPARISON OF RESIDUAL DEFORMATIONS

Because residual deformations in a structure following an earthquake may increase the cost of repairing structural as well as nonstructural elements, it is important to assess the ability of the structure to return to its original position after an earthquake. In an effort to study the ability of the connections tested in this program to return to their undeformed position, the residual drift for each specimen following each set of cycles is shown in Fig. 5.6.

The plot shown in Fig. 5.6 can be divided into two regions. The first region, from the start of the test through a drift ratio of 1 percent, shows that all the specimens behaved similarly. At 1 percent drift the residual drift was approximately 1/6 of the drift ratio for Specimens DB-TC, GJ-TC, and PT-NE. Specimen GJ-FR and retest GJ-FR-R had a residual drift of approximately 1/4 the drift ratio. In the second region, beyond 1 percent drift ratio, the residual drift history for each specimen is different. The sudden jump in residual drift for Specimen DB-TC was due to crushing of concrete and failure of the specimen. The rapid increase in residual drifts for Specimens GJ-TC, GJ-FR, and retest GJ-FR-R were due to yielding of reinforcement in Specimen GJ-TC and slip of the connecting elements/friction devices in Specimen GJ-FR (and retest GJ-FR-R). Residual drift for Specimen GJ-FR following a 3 percent drift cycle was approximately 1.8 percent, while residual drift following the same drift cycle was only 1.45 percent for Specimen GJ-TC. Specimen GJ-TC attained the lower residual drift because of the pinching associated with the hysteresis loops.

Specimen PT-NE performed quite differently from the other specimens. This specimen was designed so that the prestressing strands remained elastic even at high drift levels. As a result, the connection tended to return to its original undeformed shape when unloaded. Because of cracking in the column and spalling of concrete at

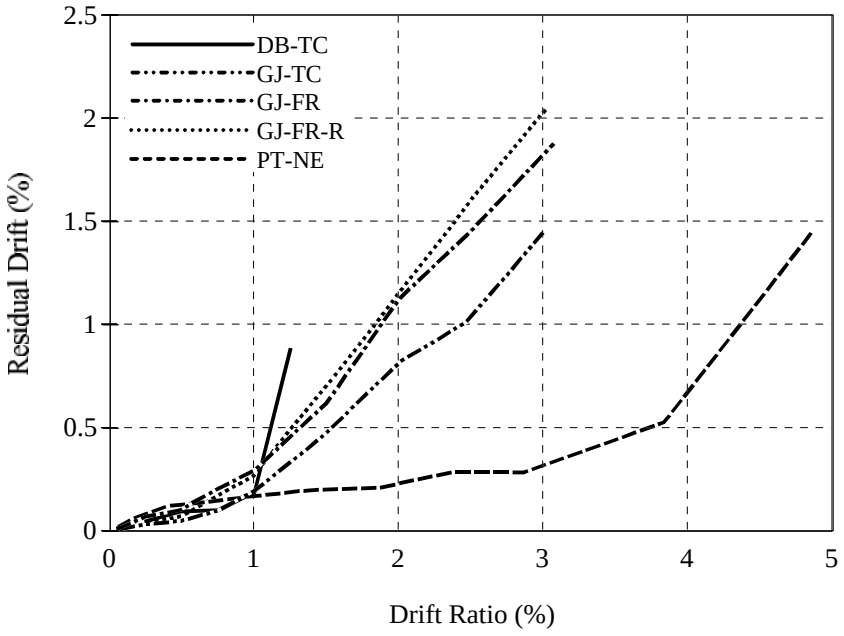

Figure 5.6 Residual Drifts in Test Specimens

the beam-column interfaces, some residual deformations were expected. Only 10 percent of the drift attained at 3 percent drift ratio remained as residual drift for Specimen PT-NE (compared to 60 percent for Specimen GJ-FR and approximately 50 percent for Specimen GJ-TC). A sudden increase in residual drift for Specimen PT-NE was observed for drifts exceeding 3 percent. This was not due to yielding of the strands (strain gauges did not indicate yielding), but rather due to rapid deterioration of the joint. The residual drift for Specimen PT-NE at completion of the test was 30 percent of the maximum drift ratio attained. The self-righting nature of Specimen PT-NE is very advantageous, especially in the drift range of interest (approximately a 2 percent drift ratio). However, the nature of this response is the result of hysteresis loops that are extremely pinched and which dissipated little energy.

5.5 COMPARISON OF STIFFNESS AND DUCTILITY

5.5.1 General

Elastic and secant stiffnesses are tabulated and compared in this section for the test specimens. Estimates of ductility are presented, and stiffness degradation is discussed.

Methods for estimating the elastic stiffness of connections are somewhat arbitrary (as is estimating the deformation associated with first yield of a connection). The approach which was adopted for use by the PRESSS researchers is described below.

Using the response envelope curve for a connection as shown in Fig. 5.7, the following procedure is performed to estimate the elastic stiffness of a connection:

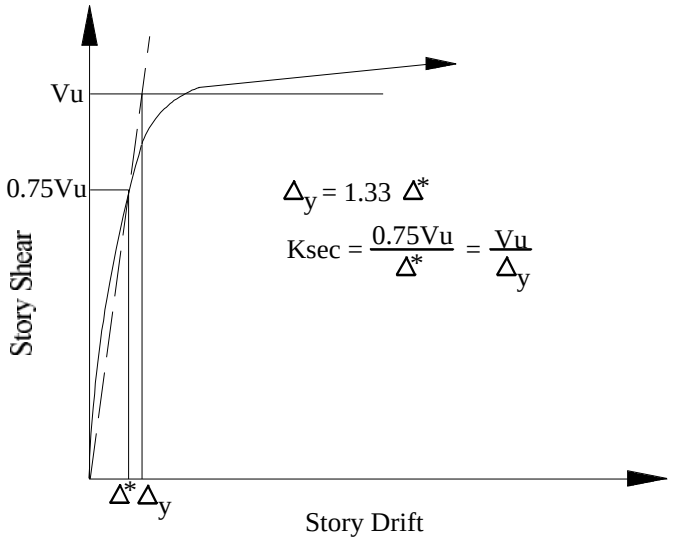

Figure 5.7 Definition of Secant Stiffness and Yield Displacement

1. Calculate the story shear capacity V_u, using actual material properties and geometry of the subassemblage.

2. Obtain the drift ratio corresponding to three-quarters of the calculated story shear capacity V_u. Call this drift Δ^*.

3. Draw a line between the origin and point (Δ^*,0.75V_u), and extend this line to intersect with the horizontal line corresponding with the calculated story shear capacity V_u. From this point then draw a vertical line that crosses the horizontal axis. The corresponding drift is referred to as the yield displacement, Δ_y. Note that according to this procedure the yield displacement Δ_y is 1.33 Δ^*. This definition of the yield displacement will enable the calculation of connection ductilities, especially for connections displaying nonlinear behavior but lacking inelastic material response.

4. The elastic stiffness of a connection, which is actually a secant stiffness, is then defined as:

$$K_{\text{sec}} = \frac{0.75V_u}{\Delta^*} = \frac{V_u}{\Delta_y} \tag{5.1}$$

Using the definitions presented above, the elastic stiffness of each subassemblage was calculated. Table 5.3 presents the elastic secant stiffness of the connections. Also shown in Table 5.3 are the estimated displacements at first yield, and the ductility, μ, of the connections. Ductility, μ, is defined as:

$$\mu = \frac{\Delta_u}{\Delta_y} \tag{5.2}$$

where Δ_u is the maximum displacement experienced by the connection.

Due to a basic difference in behavior of Specimen PT-NE relative to the other specimens, stiffness of the connection was calculated in a different fashion.

This difference is primarily in the definition of the yield displacement. As explained earlier, Specimen PT-NE was not intended to yield up to deformations exceeding the design drift. The calculated story shear capacity of 54.6 kips (shown in Table 5.3) is actually the story shear that corresponds with opening of the interface between the beams and column. When this interface opens the stiffness dramatically changes. Although it does not correspond to yielding of prestressing strands or reinforcing bars, for convenience and comparison with the other specimens it is referred to as the yield point. Calculations performed for this connection are presented in Appendix A.

Table 5.2 Stiffness and Ductility of Subassemblages

Specimen	Calc. Stry. Shear Cap. $V_{u,calc}$ (k)	Secant Stiffness K (k/in)	Yield Displacement Δ_y (in)	Ductility μ
DB-TC	112.4	148.4	0.748	2.09
GJ-TC	112.9	254.0	0.443	5.28
GJ-FR	117.8	169.2	0.697	3.36
GJ-FR-R	106.7	112.3	0.949	2.47
PT-NE	54.6*	288.0	0.190	15.8

* Explained in text.

Stiffnesses of the connections varied over a wide range. Specimen PT-NE was the stiffest connection followed by Specimen GJ-TC. The stiffnesses of Specimens GJ-FR and DB-TC were relatively similar, and were approximately 60 percent of the stiffnesses of Specimens GJ-TC and PT-NE. As expected, retest GJ-FR-R displayed the lowest stiffness because it was cracked during previous loading. To understand whether the stiffnesses, in relative terms, were satisfactory, the yield displacement was compared with a reasonable ultimate drift. Because an interstory drift ratio of 2 percent was deemed acceptable during design, it was also used here

to evaluate the yield displacements. This drift corresponds with a column displacement of 1.56 in. (for a specimen story height of 78 in.). Excluding retest GJ-FR-R, the yield displacements listed in Table 5.3 varied from 0.19 in. to 0.75 in. All of the yield displacements were reasonably far-removed from the 2 percent design value, and the two most flexible connections could be stiffened with modifications to the connection hardware. The wide range in yield displacements does indicate, however, that due to the jointed nature of precast concrete construction, design of such structures might be controlled by stiffness rather than strength.

Although the ultimate displacements achieved in the laboratory for Specimens GJ-TC and GJ-FR were identical, their ductility ratios differed considerably. Specimen GJ-TC had a ductility ratio approximately 60 percent higher than Specimen GJ-FR. Once again, this was primarily related to the flexibility associated with the connecting elements between the beams and column. The very high ductility ratio obtained for Specimen PT-NE is mainly attributed to the definition of yield displacement that was adopted for use with the nonlinear-elastic system.

5.5.2 Stiffness Degradation

In the previous section, an attempt was made to calculate the secant stiffness associated with elastic behavior of each subassemblage. This information was used to estimate ductility of each connection. Ideally, stiffness of a connection does not degrade when it is cyclically loaded. However, all reinforced concrete members experience some stiffness degradation during cyclic loading. Stiffness degradation has the effect of reducing hysteretic damping because the area under the load-displacement curve tends to decrease. As a result, the response of the structure can become larger. Stiffness degradation is attributable to opening and closing of cracks, sliding along concrete crack surfaces, concrete crushing or spalling, and

bond degradation.

In this section stiffness degradation of the connections is studied. Two types of stiffness are computed and presented: the equivalent stiffness and the peak-to-peak stiffness. Both types of stiffness are presented below.

5.5.2.1 Equivalent Stiffness

The definition of "equivalent stiffness" is illustrated in Fig. 5.8. A line is drawn from the point of zero story shear, at the beginning of a half-cycle in a loop, to the peak story shear in that half-cycle. The equivalent stiffness is defined as the slope of that line. This stiffness calculation is often used to evaluate stiffness degradation.

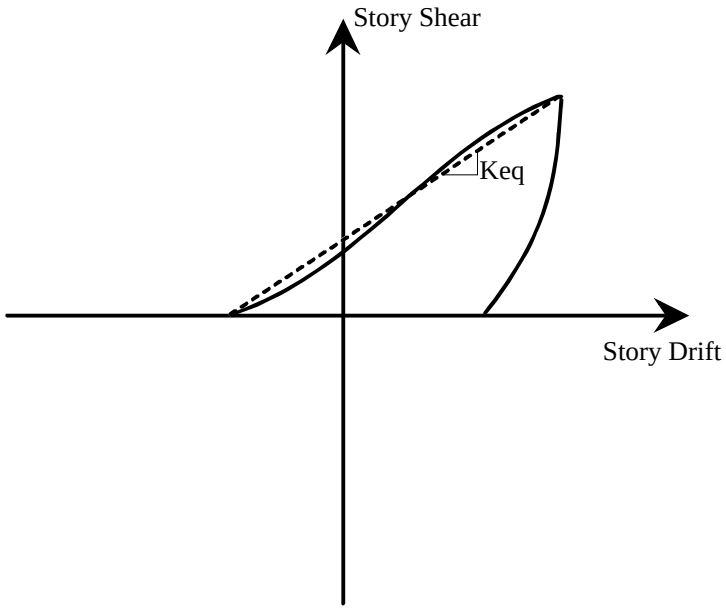

Figure 5.8 Definition of Equivalent Stiffness

Notice that, according to this definition, a hysteresis loop having an elasto-plastic shape and another with severe pinching will have the same equivalent stiffness as long as the initial and peak values are the same. The equivalent viscous damping

described in Section 5.3.2 indirectly assesses pinching of the hysteresis loops.

It was described in Section 3.5 that following each set of three cycles to a particular drift level, a fourth cycle was performed to 75 percent of the peak load attained in the three previous cycles. The main reason for performing these cycles was to assess the stiffness degradation of the connection. Notice that this procedure is consistent with the procedure described earlier for estimating the secant stiffness associated with elastic behavior of a connection.

The equivalent stiffness of the various connections is shown in Fig. 5.9. The stiffness presented is based on the first cycle of each set of cycles. The equivalent stiffness based on the 75 percent-of-maximum-story-shear cycle is shown in Fig. 5.10. These load cycles were not performed for drift levels beyond 3 percent. They

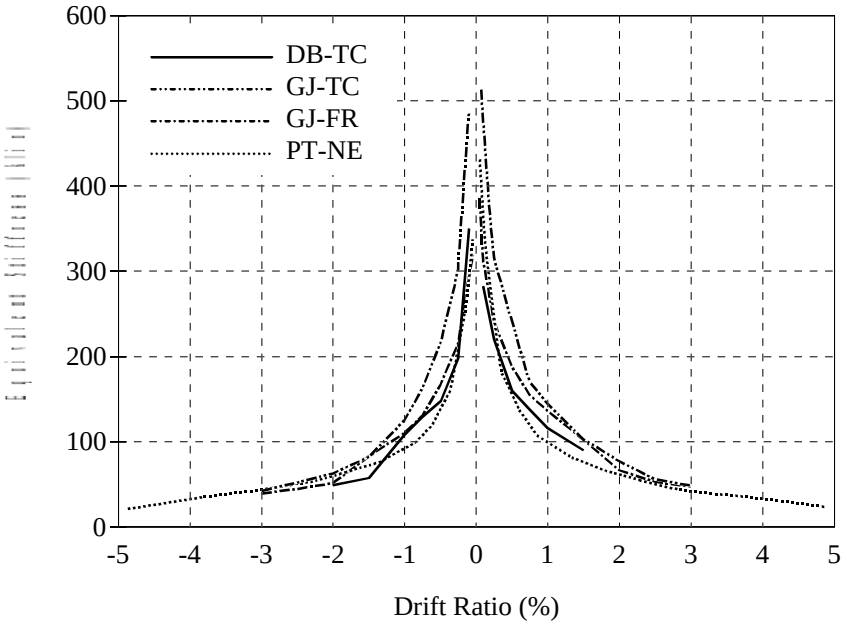

Figure 5.9 Equivalent Stiffness for the First Cycle of Each Set of Cycles

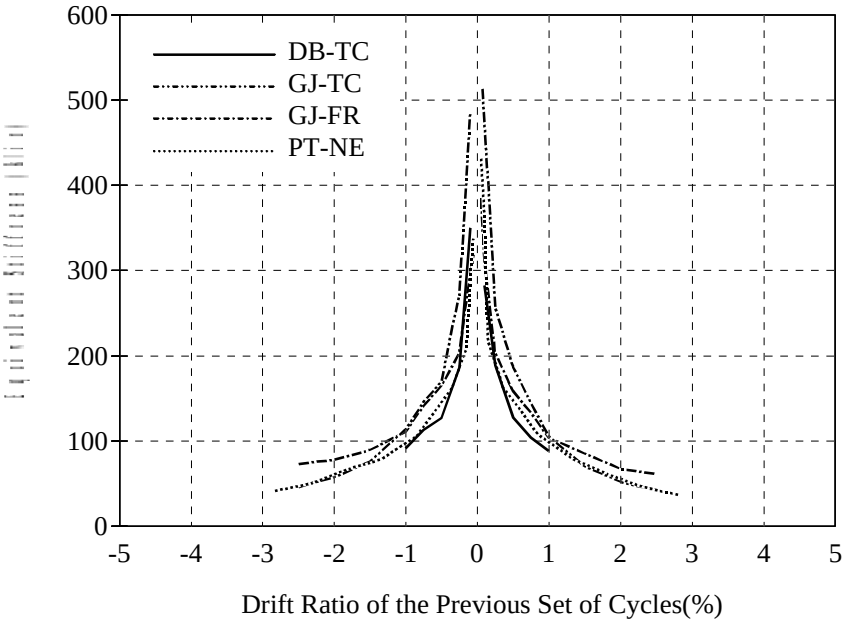

Figure 5.10 Equivalent Stiffness for 75 Percent-of-Maximum-Story-Shear Cycle of Each Set of Cycles

also were not performed at 3 percent drift ratio for Specimens GJ-TC and GJ-FR because both failed during the second cycle at 3 percent drift ratio. Figure 5.11 shows the equivalent stiffness of each connection as a percentage of the initial stiffness of the connection (i.e. the stiffness at 0.1 percent drift ratio). Figures illustrating the stiffness of the connections are useful for comparing stiffness degradation among the connections, while the figure showing normalized stiffness is useful for understanding the rate of stiffness degradation for each specimen. The following observations are made from Figures 5.9, 5.10, and 5.11:

- All connections demonstrated rapid deterioration of stiffness. Most of the stiffness degradation occurred during the cycles below 1 percent drift ratio. In subsequent cycles further stiffness deterioration occurred primarily due to increased plastic deformations and concrete spalling in some specimens.
- Positive half-cycles demonstrated slightly higher stiffness than negative

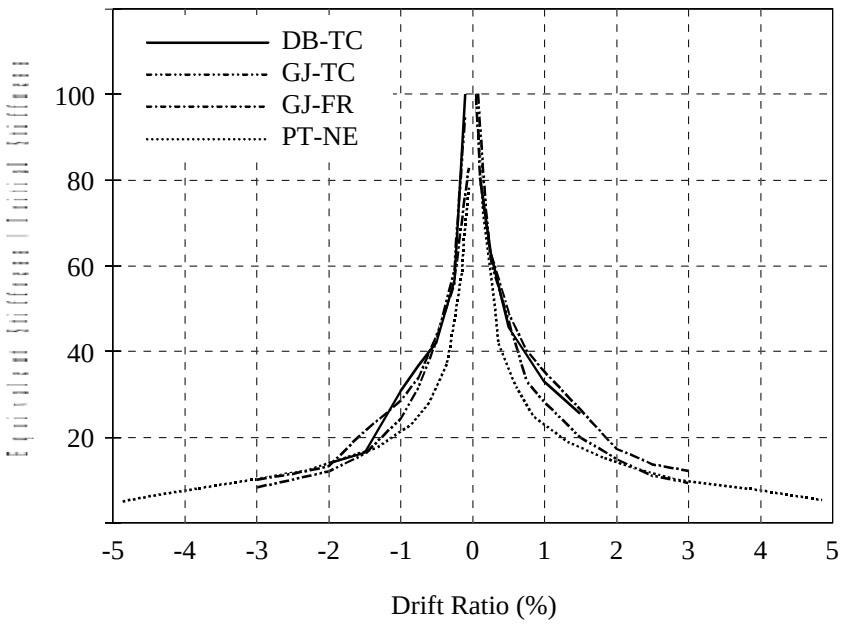

Figure 5.11 Normalized Equivalent Stiffness

cycles for all the specimens. Damage incurred during a positive half-cycle affected the strength in the subsequent negative half-cycle.

- Specimen GJ-TC generally had the highest equivalent stiffness. Specimens GJ-FR, DB-TC, and PT-NE had comparable stiffnesses at low drift levels (not greater than 0.5 percent). All specimens (except DB-TC which failed prematurely) approached the same stiffness at a drift ratio of 3 percent.

- The stiffnesses shown in Fig. 5.9 based on the first cycle of each set of cycles, was typically slightly higher than those based on the 75 percent maximum load cycle shown in Fig. 5.10. This was anticipated because loading to a new drift level typically results in additional damage to the connection, resulting in a loss of stiffness. It was mentioned before that using the definition of equivalent stiffness, a connection displaying elasto-plastic response and another with severe pinching will yield the same equivalent stiffness as long as the initial point (at zero story shear) and the peak load are the same. This suggests that this form of stiffness comparison

does not recognize pinching of the hysteresis loops. However, when equivalent stiffness is based on the 75 percent maximum load cycle rather than the first cycle, pinching can be recognized. Initially, Specimen GJ-TC had a higher effective stiffness than Specimen GJ-FR. However, at a drift ratio of 1 percent and beyond, as pinching of Specimen GJ-TC became more pronounced, the stiffness of Specimen GJ-FR was higher than for Specimen GJ-TC.

- The normalized equivalent stiffness shown in Fig. 5.11 was intended to give insight into the rate of stiffness deterioration of each specimen. Specimens GJ-TC and PT-NE, which had the highest initial stiffness, demonstrated more rapid deterioration of stiffness than the other specimens. Specimen PT-NE had the highest rate of stiffness deterioration of all the connections. Crushing and spalling of concrete was more pronounced in this specimen than in any other specimen.

5.5.2.2 Peak-to-Peak Stiffness

The definition of a "peak-to-peak stiffness" is shown in Fig. 5.12. This secant stiffness calculation was used to compare stiffness degradation that occurred during a full cycle. The peak-to-peak stiffness is defined as the slope of the line that connects the peak positive and negative response during a load cycle.

The histories of peak-to-peak stiffness degradation for the connections are shown in Fig. 5.13. The normalized peak-to-peak stiffness degradation histories are shown in Fig. 5.14. The peak-to-peak stiffness was based on the first cycle of each set of cycles. As for equivalent stiffness, the degradation appeared to be approximately logarithmic. Due to the nature of the hysteresis loops and the definition of the two types of secant stiffness, the peak-to-peak stiffness values were always slightly higher than the equivalent stiffness values. For the same reason as

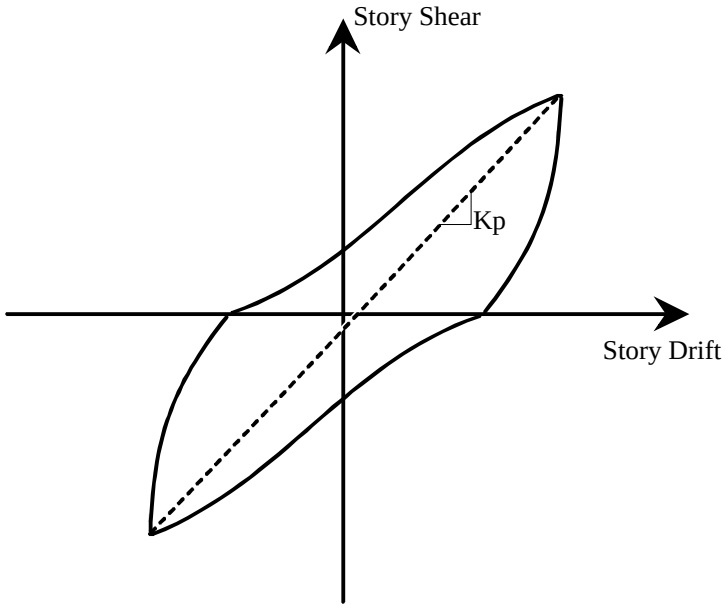

Figure 5.12 Definition of Peak-to-Peak Stiffness

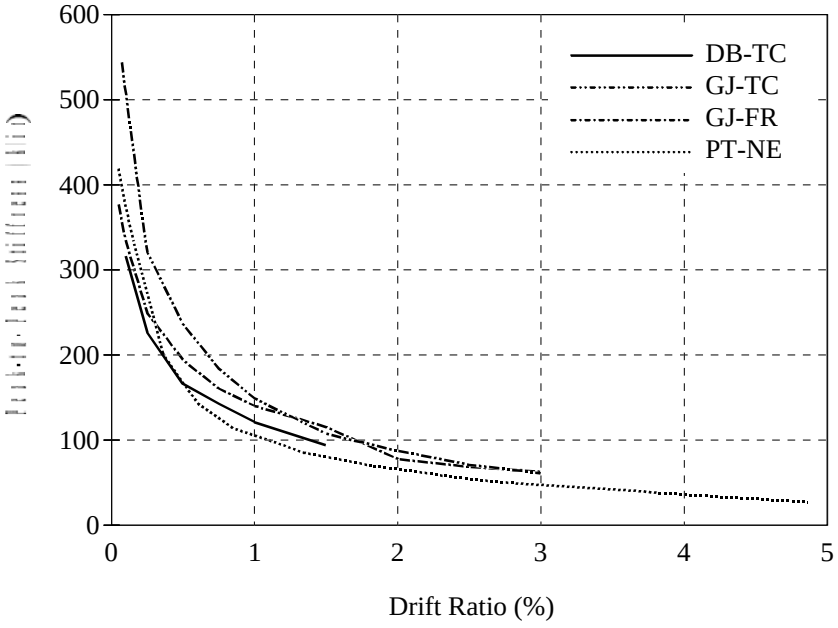

Figure 5.13 Peak-to-Peak Stiffness for First Cycle of Each Set of Cycles

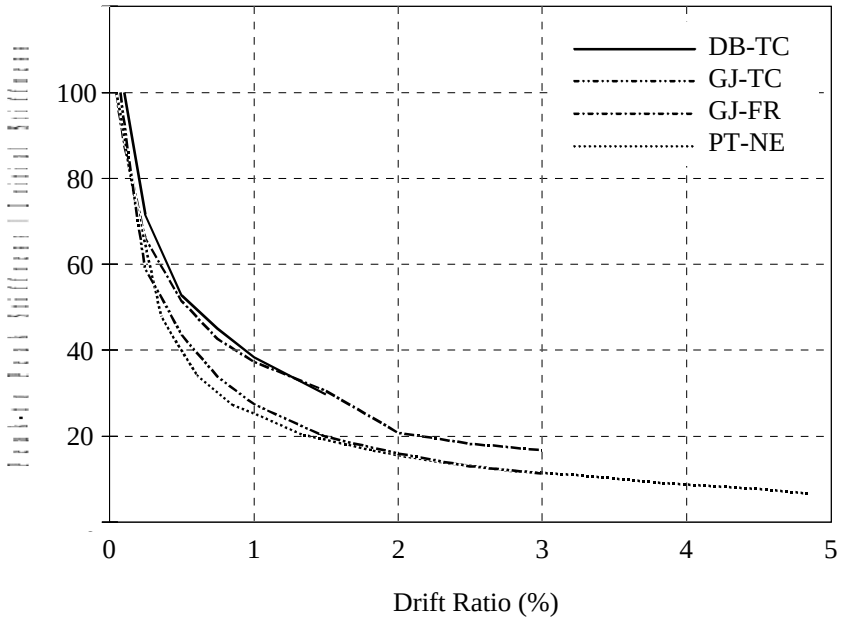

Figure 5.14 Normalized Peak-to-Peak Stiffness

explained earlier, the peak-to-peak stiffness based on the 75 percent maximum load cycle (not shown here) was lower than that based on the first cycle. However, this was not true for Specimen GJ-FR after slip in the friction connections occurred. Because very little pinching of the hysteresis loops was observed for this specimen, the peak-to-peak stiffness based on the 75 percent maximum load cycle was higher than based on the first cycle. Figure 5.13 indicates that most of the stiffness degradation occurred during the initial load cycles. Specimen GJ-TC had the highest peak-to-peak stiffness followed by Specimen PT-NE. Figure 5.14 indicates that Specimen PT-NE and GJ-TC had the highest rate of stiffness degradation.

Most of the observations made using the equivalent stiffness could also be made using the peak-to-peak stiffness. Figure 5.15 supports this statement by demonstrating that the relationship between the equivalent stiffness and peak-to-peak stiffness is best described by a line with a slope approximately equal to unity.

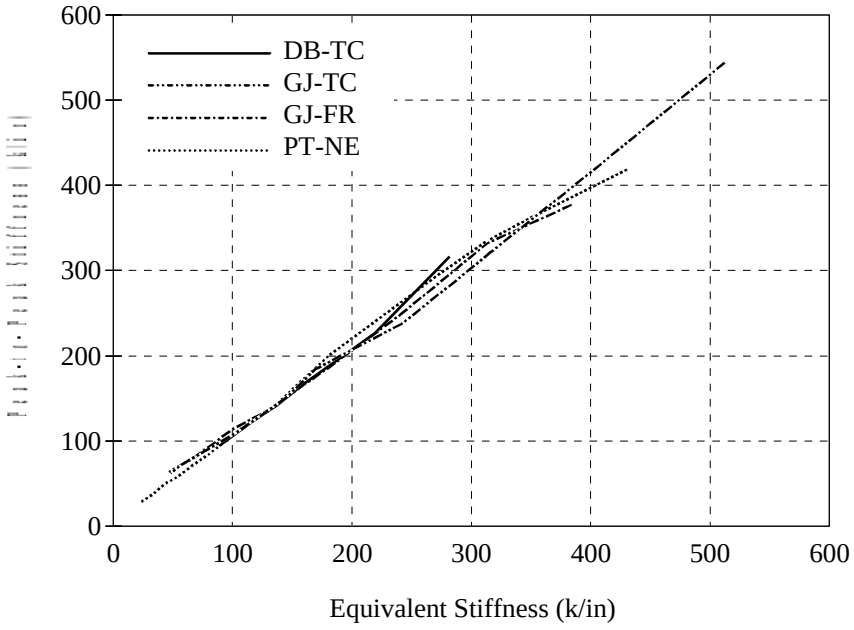

Figure 5.15 Relationship Between Equivalent and Peak-to-Peak Stiffness

5.6 INTERNAL BEHAVIOR OF THE SPECIMENS

The internal behavior of the specimens is evaluated using data collected from strain gauges. Approximately forty to sixty 5mm strain gauges were mounted on reinforcing bars in each specimen. Strain gauges were used on beam longitudinal reinforcement, stirrups, and strands in the case of Specimen PT-NE, on column longitudinal reinforcement, on joint hoops, and on corbel reinforcement. Some of the strain gauges malfunctioned early during tests, while others remained effective until large strains were imposed on them. Due to the large number of gauges used, only data that leads to specific conclusions are presented here. When necessary, strains were converted to stresses. Stress analysis was difficult above the yield strain due to the complex strain reversals. The stress-strain model used for conversion from strain to stress takes into account the yield plateau, strain hardening, and Bauschinger effect on the steel during cyclic loading.

5.6.1 Column Bars

Strain in column longitudinal bars was measured by gauges located at sections just above and below the joint. Columns were designed to remain elastic in order to avoid hinging and undesirable strong beam-weak column behavior. The ratio of the column-to-beam strengths was kept to a value of at least 1.4 for all specimens. Figure 5.16 shows strain in column longitudinal bars for Specimen GJ-TC during the entire test. To avoid repetition, strain at the same location for other specimens is not shown because it qualitatively resembles that shown in Fig. 5.16.

The column longitudinal reinforcing bars did not yield in any of the specimens. Figure 5.17 shows envelopes of strain in column longitudinal bars as a function of the applied story shear. Columns of Specimens GJ-TC and GJ-FR nearly reached yield at a drift ratio of 3 percent. At this drift, the beams were well beyond yield (or slip of the friction connection), and the beam moments were higher than that calculated based on nominal properties. Specimen PT-NE used high-strength steel for the column reinforcement. As a result, strain in these bars was consistently higher. The vertical lines in Fig. 5.17 represent the calculated story shear capacity for each specimen. Strain in the column bars at the calculated story shear capacity was approximately 70 percent of the yield strain for Specimen PT-NE and approximately 80 percent for all other specimens.

5.6.2 Beam Bars and Stirrups

Because the beams in the specimens were different, beam bars in each specimen were intended to have a different function. Therefore, for clarity each

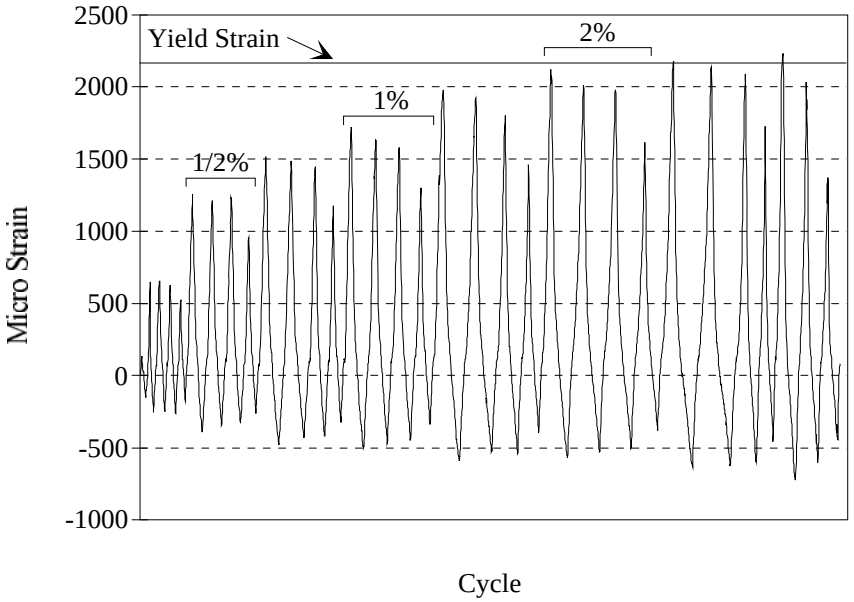

Figure 5.16 Strain History of Column Longitudinal Reinforcement for Specimen GJ-TC

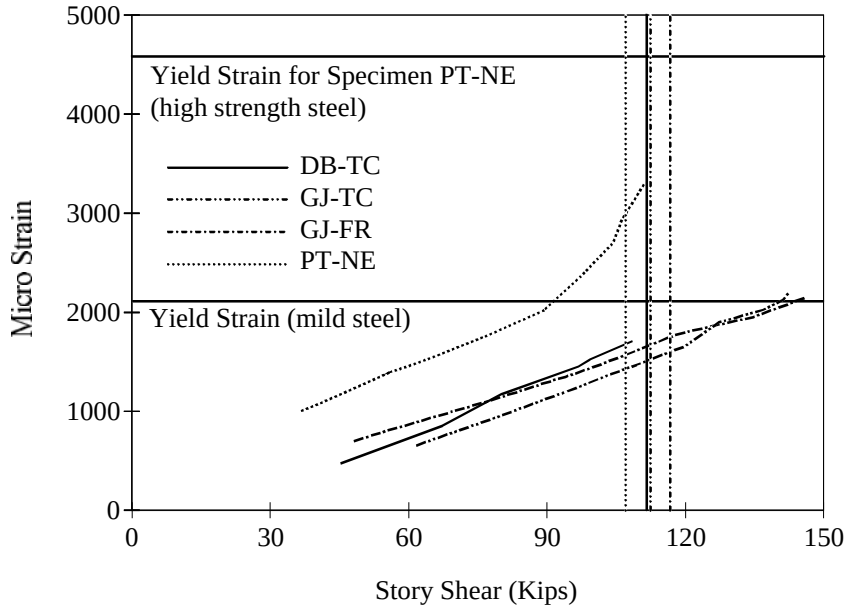

Figure 5.17 Longitudinal Column Reinforcement Strain Envelopes vs. Story Shear

specimen is presented separately to identify the main function of the beam

longitudinal reinforcement and then to evaluate the actual behavior through strain gauge data. In addition, some strain gauge data from beams stirrups is presented.

5.6.2.1 Specimen DB-TC

Beams were connected to the column by high-strength threaded bars that were embedded and grouted inside ducts in the dogbone region of the beams. These bars were intended to yield in tension and in compression. The bars, however, were not instrumented for reasons mentioned earlier in Section 3.6. Therefore, no strain data were collected from these particular bars.

Ductile connections, as defined before, were intended to concentrate most of the nonlinear response in the connecting elements of the beams while keeping the precast members virtually undamaged. Therefore, the beams were designed so the section at the dogbone interface would not yield and consequently develop a flexural hinge. Strain gauges were mounted on the #6 bars at the interface of the dogbones. Typical strains for these bars are shown in Fig. 5.18. Each group represents a particular drift level. As can be seen, the longitudinal reinforcement strains were increasing but never reached yield up to the failure of the specimen. Even though the specimen was considered to have failed prematurely, it should be noted that the load achieved at failure was 97 percent of the design load.

Transverse reinforcement in the beams was also instrumented. The beams were designed for a higher shear than that produced by the design moment in order to avoid shear strength deterioration and hinging in the beams. Strain gauges were mounted on the stirrups adjacent to the dogbone interface. Figure 5.19 indicates that these stirrups yielded at a very early stage in the test. It was explained earlier that this specimen failed prematurely due to crushing of concrete near the dogbone

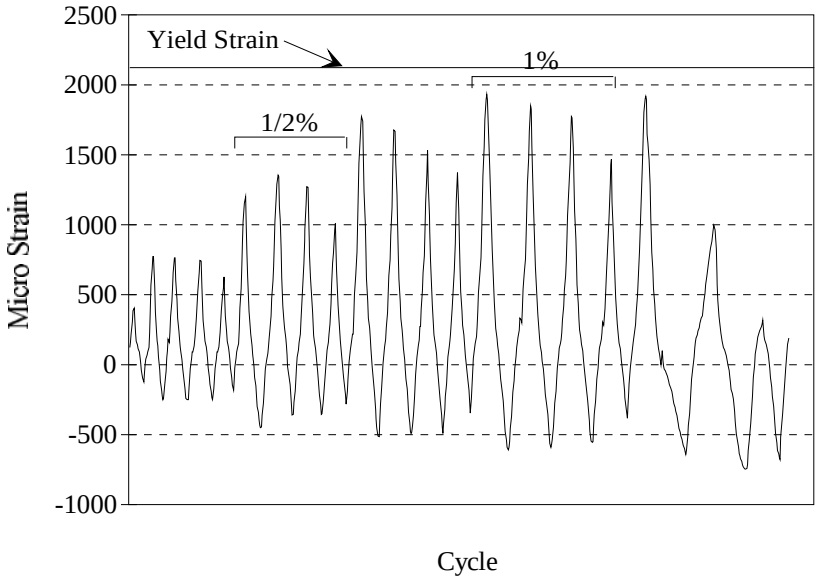

Figure 5.18 Strain History of Beam Longitudinal Reinforcement for Specimen DB-TC

region. To better understand the early yielding of these stirrups and premature failure of the specimen, a sketch of the force path from the main portion of the beam into the dogbone is presented in Fig. 5.20a. To resist large forces in the #6 bars in the beams, the bars were anchored by 90-deg hooks. When the beam is loaded as shown, tensile force is developed in the #6 bars and in the threaded bars connecting the beam to the column. A path must be provided to permit transfer of force between these two sets of bars. The path that developed in the test specimen was a compression strut between the hook and node A.

Because the angle, α, between this strut and the tension ties was large, a large force had to be developed in the compression strut to maintain equilibrium. When stress in the compression strut reached the limiting strength of the concrete, crushing occurred. From observations of the specimen after failure, the angle of the compression strut was approximately 45 degrees, and the width of the compression strut was approximately 4 in. From equilibrium of forces, the ratio of the stress in

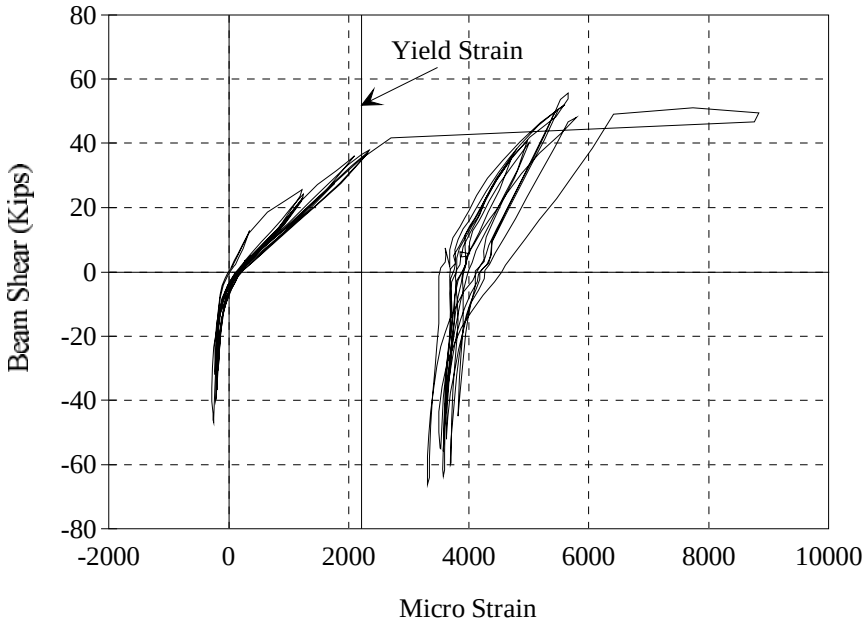

Figure 5.19 Beam Shear vs. Stirrup Strain at End of Dogbone for Specimen DB-TC

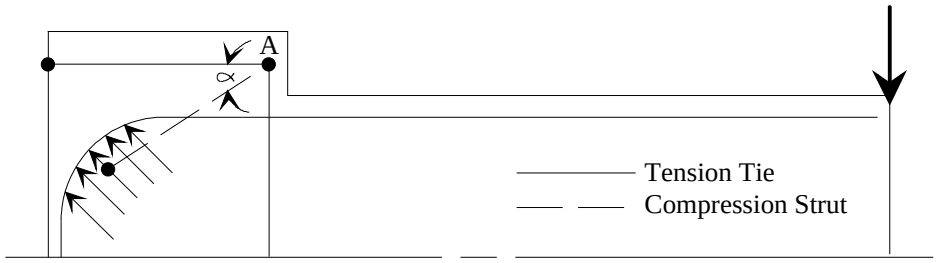

(a)

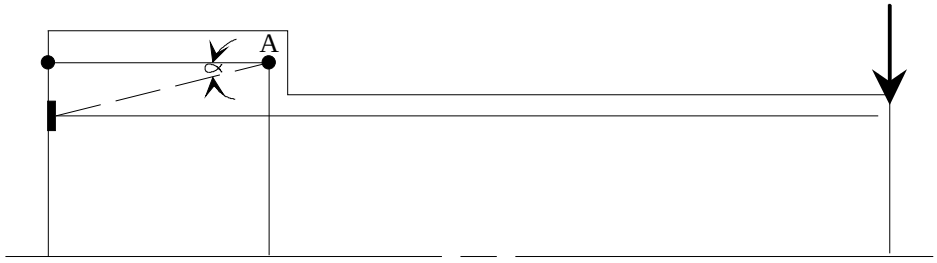

(b)

Figure 5.20 Different Force Paths for Specimen DB-TC

the compression strut to the strength of concrete on the last day of testing was approximately 60 percent. In addition, in order for equilibrium to be satisfied in the vertical direction, large forces were imposed on the stirrups at the end of the dogbone, which led to early yielding of that reinforcement. In order to delay or prevent this type of behavior, the #6 bars could have been anchored using a plate as shown in Fig. 5.20b. In this case the angle α is much smaller which leads to a more efficient force path and lower stresses in the compression strut and stirrups.

5.6.2.2 Specimen GJ-TC

Beam top bars in this specimen were intended to yield in both tension and compression while the bottom bars remained elastic. As a result, all nonlinear behavior was intended to be concentrated in the top connecting elements. Strain gauges were mounted on the beam top bars at the interface of the beam and column, and at 12 in. and 24 in. from the face of the column. This was done to investigate the length over which yielding occurred. Strain gauges were also mounted on the bottom longitudinal bars at the location of the vertical dowel bars.

Strain in the top bars at the beam-column interface was converted to stress in order to investigate the extent of yielding of these bars. The stress-strain history is shown in Fig. 5.21. Although most of the nonlinear response was in tension, the bars did yield a significant amount in both tension and compression. The yield stress of these bars, as obtained from tensile coupon tests, was 67.7 ksi, and the ultimate strength was 107.6 ksi. Figure 5.21 indicates that stress in the bars reached more than 90 ksi both in tension and compression. This is considerably higher than the design nominal stress of 60 ksi. This increase in stress imposed substantial demands on the bottom connection that was intended to behave as a pin, and eventually led to its failure. Figure 5.22 shows the strain history of the beam top bars at 24 in. from

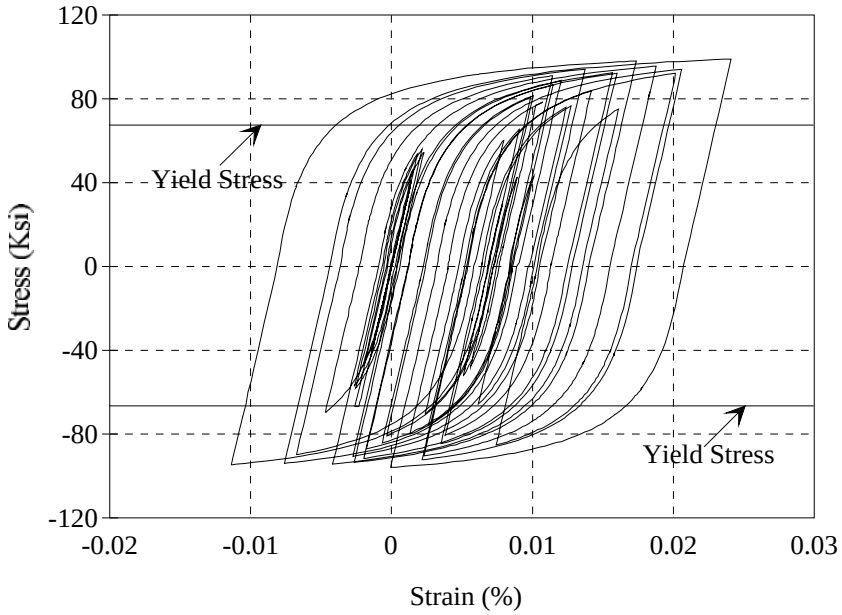

Figure 5.21 Stress-Strain History of Beam Top Bars at Beam-Column Interface for Specimen GJ-TC

the face of the column. Yielding started at this location during the 2.0 percent drift ratio cycles, and considerable yielding occurred after that.

Figure 5.23 shows the strain history in the beams bottom bars at the vertical dowel location. No appreciable yielding took place in these bars and they remained essentially elastic as intended. The deterioration of the grout around the dowels and the yielding of the dowels in shear due to strain hardening of the top bars was the main cause of poor performance of the pin that led to the severe pinching of the hysteresis loops. Measured strains in the beam transverse reinforcement (not shown here) were considerably less than yield.

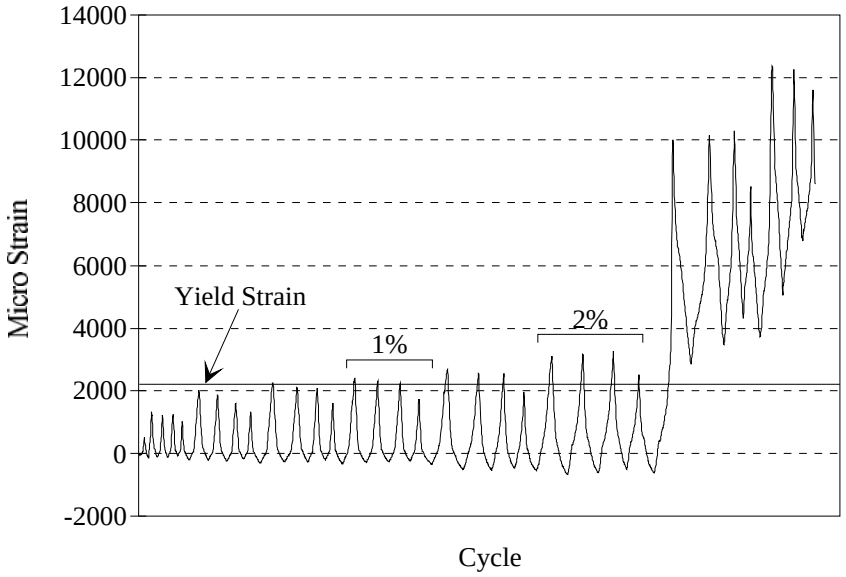

Figure 5.22 Strain History of Beam Top Bars at 24 in. from Beam-Column Interface for Specimen GJ-TC

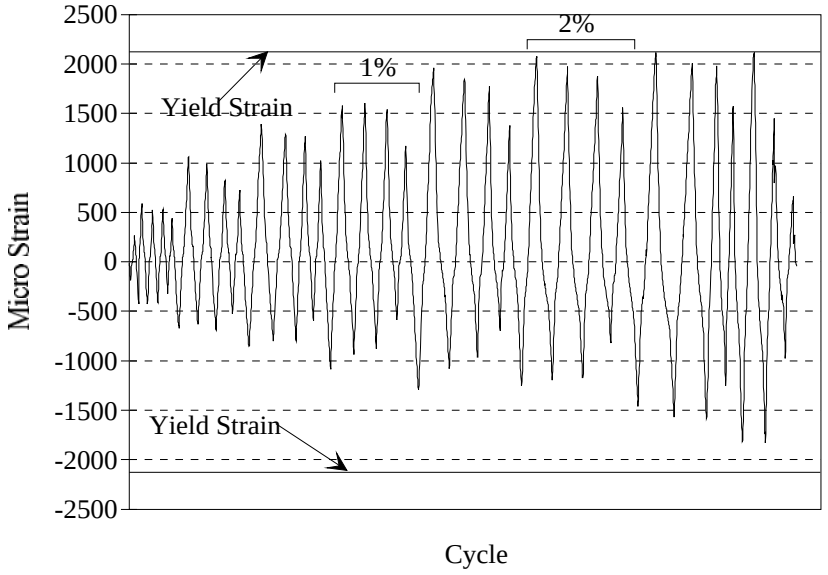

Figure 5.23 Strain History of Beam Bottom Bars for Specimen GJ-TC

5.6.2.3 Specimen GJ-FR

The design objective for this specimen was to proportion all members so they remained elastic while energy was dissipated through slip of friction between beams and the column. Beams top and bottom reinforcement was proportioned with 30 percent extra strength relative to the force needed to create slip in the friction devices. The beams were reinforced symmetrically with 8-#7 bars top and bottom. Strain gauges were mounted on both sets of steel to monitor the variation of strain during the test. The strain history for the top bars just outside the steel box (see Fig. 3.16) is shown in Fig. 5.24, and the history for the bottom bars at the location of the grout pocket is shown in Fig. 5.25. Strain remained below yield as intended throughout most of the test (through 2 percent drift). Strain in the bottom bars was typically higher than in the top bars. This can be attributed to the fact that the strain gauges in the bottom bars were located closer to the column face (where moments are larger) than were gauges on the top bars.

The strut-and-tie procedure used in Section 3.3.3.1 described proportioning of beams in this specimen. Special detailing in the dapped end of the beams required steel to be provided in the horizontal direction and some extra stirrups provided just outside the dap. Figure 5.26 shows the beam shear versus strain response for the horizontal steel, and Fig. 5.27 presents the beam shear versus strain response for the extra stirrups. Positive shear corresponds with load applied upward on the tip of the beam. The highest strain plotted in Fig. 5.26 corresponds with downward loading which was the condition that required this horizontal steel, as explained in Section 3.3.3.1. Figures 5.26 and 5.27 demonstrate that the steel remained elastic for most of the test and that the amount of steel provided was both necessary and sufficient. Aside from the failed welds in the friction devices, this specimen remained virtually undamaged through cycles of 3 percent drift ratio.

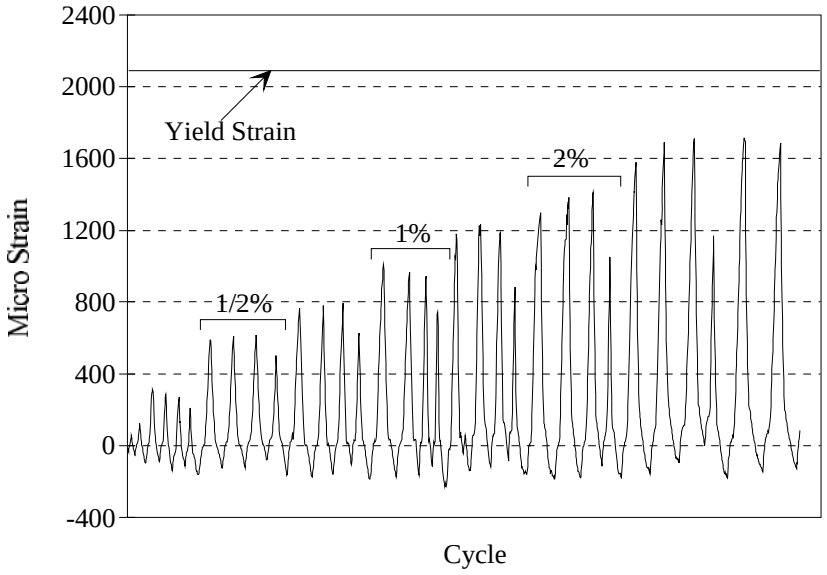

Figure 5.24 Strain History of Beam Top Bars for Specimen GJ-FR

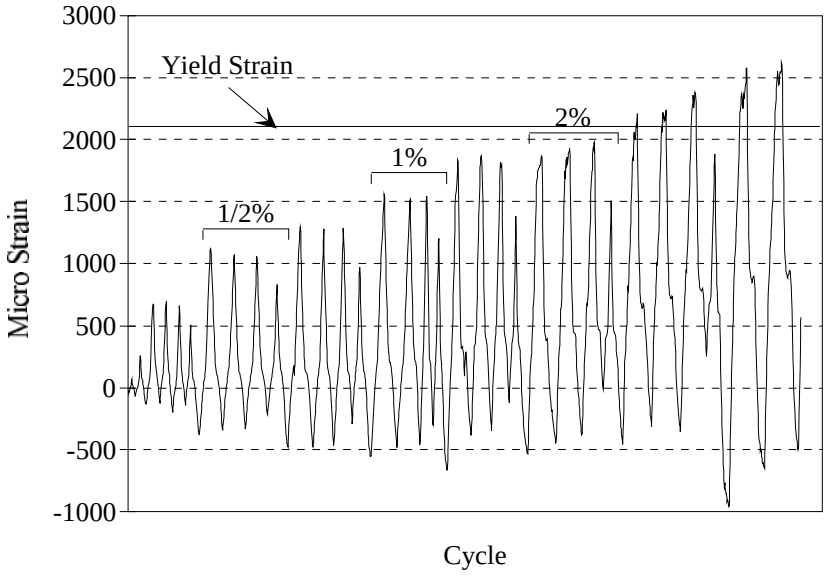

Figure 5.25 Strain History of Beam Bottom Bars for Specimen GJ-FR

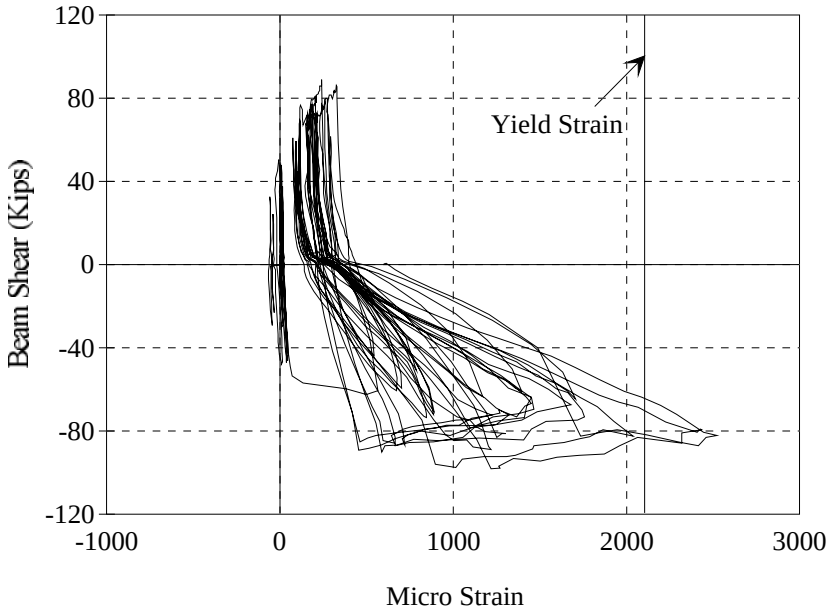

Figure 5.26 Shear vs. Strain of Horizontal Steel of Beam Dapped End for Specimen GJ-FR

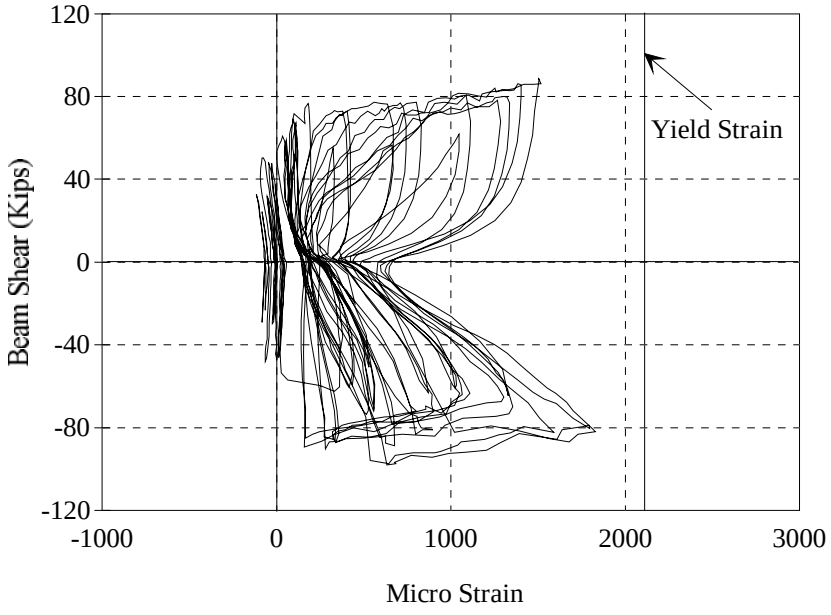

Figure 5.27 Shear vs. Strain of Vertical Steel of Beam Dapped End for Specimen GJ-FR

5.6.2.4 Specimen PT-NE

The beam in this specimen was designed so the prestressing strands remained elastic at least until achieving the design drift ratio of approximately 2 percent. To achieve that, the strands were debonded in the joint and 24 in. on each side of the joint using plastic sheathing. Strain gauges were mounted on all six levels of the strands. Most of the strain gauges were placed in the middle of the joint, while the remaining gauges were placed closer to the beam-column interface. Because the strands were debonded, the strains measured at any location along the debonded length should be the same. Also, the strain at all levels of the strands must be approximately the same. This can be explained using Fig. 3.30 and is supported by strain data presented in Fig. 5.28. Due to the reversed loading, when the crack opens on each side of the column, the amount of elongation, Δ, that each strand experiences must be the same and equal to:

$$\Delta = 2\theta\left(\frac{h}{2} - c\right) \tag{5.3}$$

where θ = beam rotation

h = depth of the beam

c = depth of the compression block

Because prestressing strands consist of six wires twisted about a central wire, strain gauges were not mounted parallel to the longitudinal axis of each strand but rather inclined at an angle parallel to an outer wire. To investigate the effect of the inclination of the gauge on the strain readings, a gauged strand was tested in a universal test machine. The load was read from a calibrated load cell, while the strain was read using a strain indicator device. Using this information, an apparent modulus of elasticity, E_a, for the strands was calculated as follows:

$$E_a = \frac{P}{A\varepsilon} \tag{5.4}$$

where P = load as measured by the load cell

A = area of the strand

ε = strain as measured by the strain indicator

The apparent modulus of elasticity obtained was 34,500 ksi. This is considerably higher than the true modulus of elasticity which is approximately 28,000 ksi.

Although many strain gauges were mounted on the strands, only a few functioned well, and only three strain gauges performed well throughout the entire test. These three strain gauges were located, fortunately, on the first , second, and fourth layers. A plot of the strain histories is shown in Fig. 5.28. Strains from the three different layers are nearly identical, which confirms that the amount of elongation in all layers must be the same, as explained above. Also notice that the strands remained perfectly elastic until 2.5 percent drift ratio as was intended in the design. Some yielding took place in subsequent cycles but was not extensive enough to cause considerable permanent deformations.

Although there is no supporting data, it is believed that the high stress level in the strands can lead to further debonding of the strands beyond the 24 in. length in each beam. Consequently, yielding of the strands can be delayed further by using a longer debonded length. Beam shear versus strain in the second strand layer is plotted in Fig. 5.29. As anticipated, strand strain is always positive (indicating tension). The shape of the plot, which is symmetric, further supports the hypothesis that stress in all strands will always be the same regardless of the loading direction. The beams remained uncracked throughout the test.

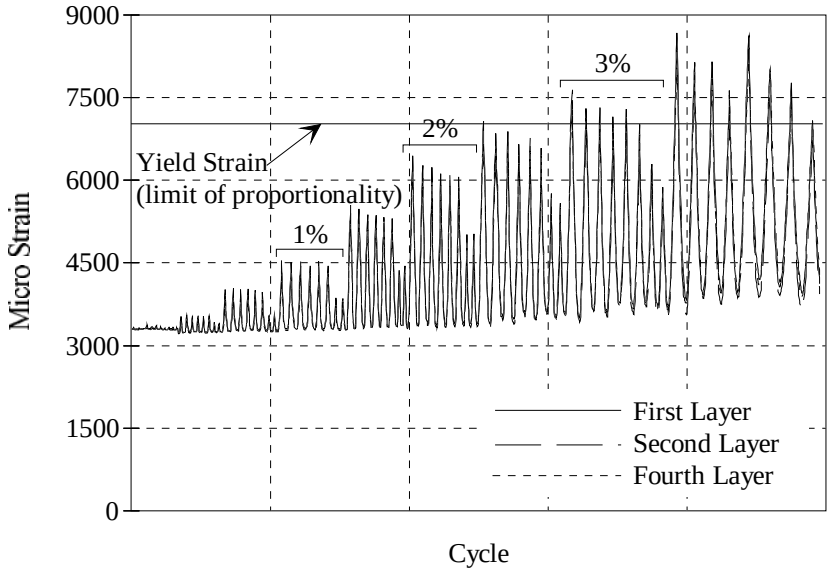

Figure 5.28 Strain Histories for Different Layers of Strands in Specimen PT-NE

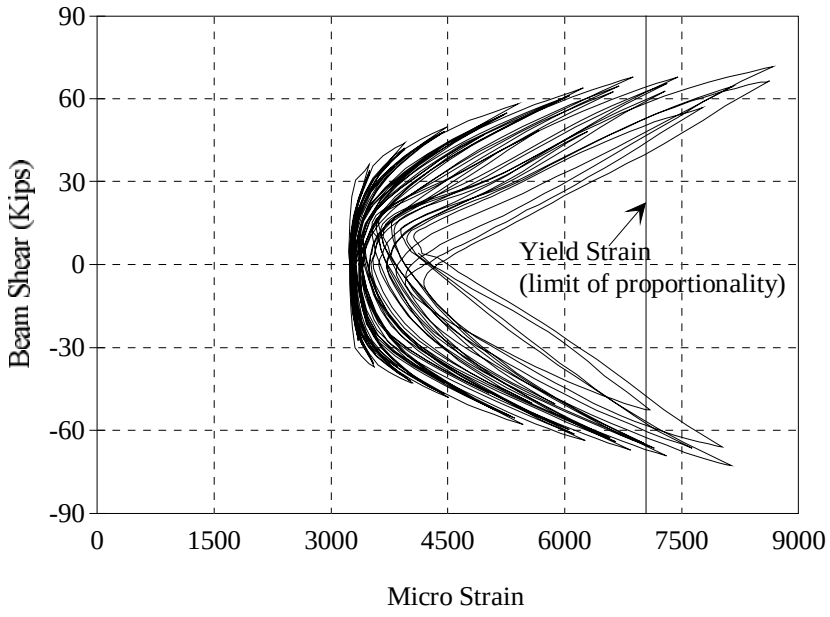

Figure 5.29 Beam Shear vs. Strain for Second Strand Layer in Specimen PT-NE

5.6.3 Corbel Reinforcement

Only Specimens GJ-TC and GJ-FR contained corbels. Loads applied on the corbels were not typical of loads applied on corbels in simply supported structures. For such corbels, design procedures are outlined in design codes, such as ACI 318-89 [1]. For the corbels used in this study, no suitable design recommendations exist. As a result, the corbels were designed using strut-and-tie models, and were proportioned to ensure no failure would occur during testing.

The critical loading case for the corbels in Specimen GJ-TC correspond with loading the beams upward. The loading conditions and detailing of reinforcement were explained in detail in Section 3.3.2.1. Strain gauges were mounted on the top bars, bottom bars, and intermediate steel mesh. In general, the strain gauges indicated low levels of strain in most of the steel provided in the corbels, indicating the design was quite conservative. Horizontal reinforcement near mid-depth of the corbel experienced slightly higher strains than the top and bottom reinforcement. An additional factor that contributed to the low strains in the corbel reinforcement (besides a conservative design model), was the flexibility of the vertical dowel bars connecting the beams and the corbels. Compliance of the dowel bars resulted in lower loads than were expected when the beams were loaded upward. As a result, the corbel reinforcement was not fully utilized.

The beam shear versus strain histories for the top and bottom steel are shown in Fig. 5.30 and Fig. 5.31, respectively. As mentioned earlier, the ultimate strain attained in both cases was considerably lower than the yield strain. Positive shear corresponds with upward loading on the beam tip. Notice that when the applied load on the beam was downward, strain was minimal. However, when the applied loading was upward, strain not only increased but was positive (indicating tension) in both the top and bottom bars. This indicates that the entire corbel was actually under

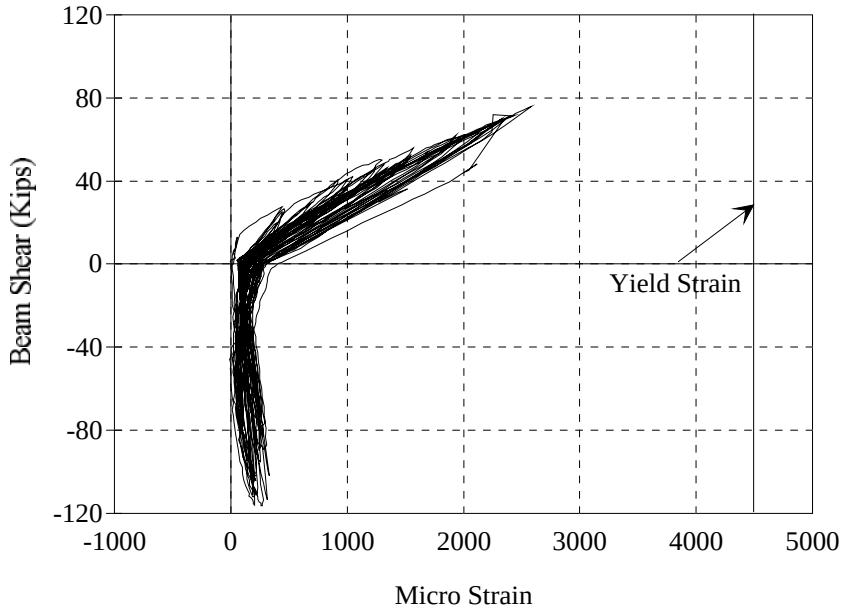

Figure 5.30 Beam Shear vs. Strain Response of Corbel Top Reinforcement in Specimen GJ-TC

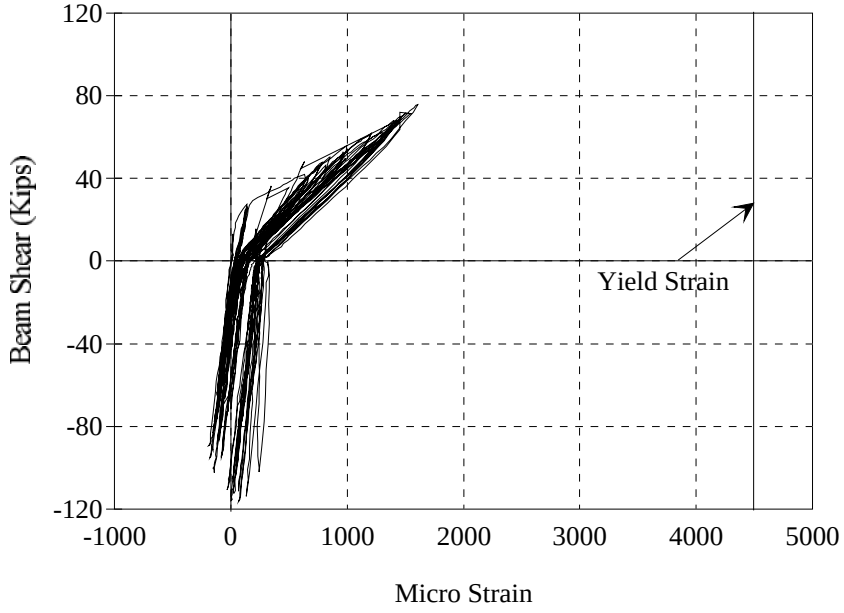

Figure 5.31 Beam Shear vs. Strain Response of Corbel Bottom Reinforcement in Specimen GJ-TC

tension as was shown earlier in Chapter 3 using the strut-and-tie model, and that

horizontal force was the dominant force in the corbels, unlike more typical corbels where horizontal force is a secondary concern.

Like Specimen GJ-TC the critical loading case for corbels in Specimen GJ-FR corresponded with upward loading on the beams. However, unlike Specimen GJ-TC, the flow of forces through the corbels was more easily predicted. The loading conditions and detailing of reinforcement were explained in Section 3.3.3.1. The bottom steel consisted of three layers, while the top steel consisted of one layer (see Fig. 3.20). Strain gauges were mounted on the first and third layers of the bottom group of bars, and on the top bars.

Figure 5.32 shows the beam shear versus strain histories for the bottom layer of the bottom group of bars. Steel remained elastic through 2 percent drift ratio. Some yielding occurred following that in both tension and compression. Yielding was mainly attributed to the continued increase in strength of the connection after slip occurred. In addition, bars demonstrated more yielding in compression than in tension. This is explained by the fact that the third layer of bottom bars was actually outside the compression zone leaving only six bars to resist compression forces instead of ten. This was verified by the strain data measured in the third layer (not shown here), which showed only positive strains for both upward and downward loading on the beams. The beam shear versus strain history for the top reinforcement is shown in Fig. 5.33. Some yielding occurred during cycles to 2.5 percent drift ratio and beyond. The shape of the curve in Fig. 5.33 demonstrates that this steel was utilized only during downward loading on the beams. Minimal compressive strain was measured when load was reversed.

In general, the corbels in both specimens behaved satisfactorily. The design of corbels for Specimen GJ-TC was more conservative than those in Specimen GJ-FR due to the uncertainty associated with the force path between each beam and

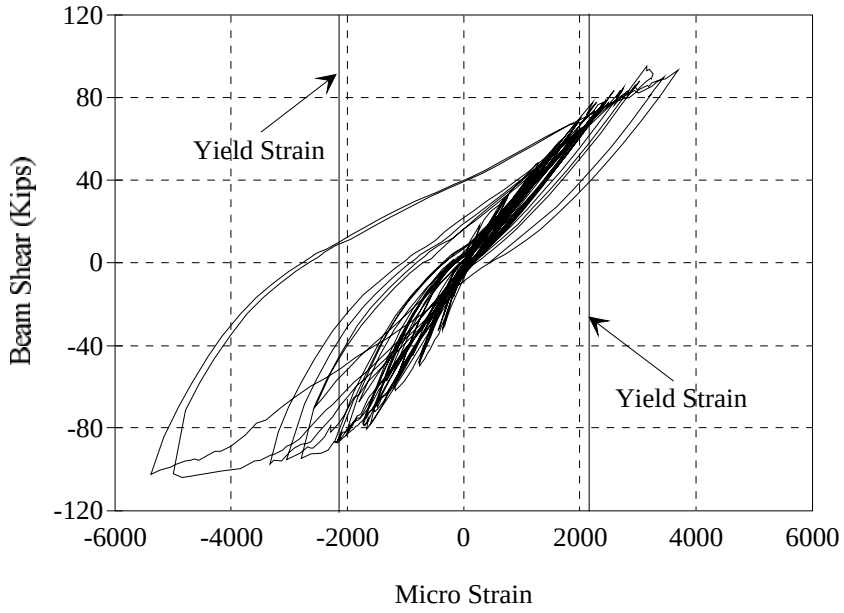

Figure 5.32 Beam Shear vs. Strain Response of Corbel Bottom Reinforcement in Specimen GJ-FR

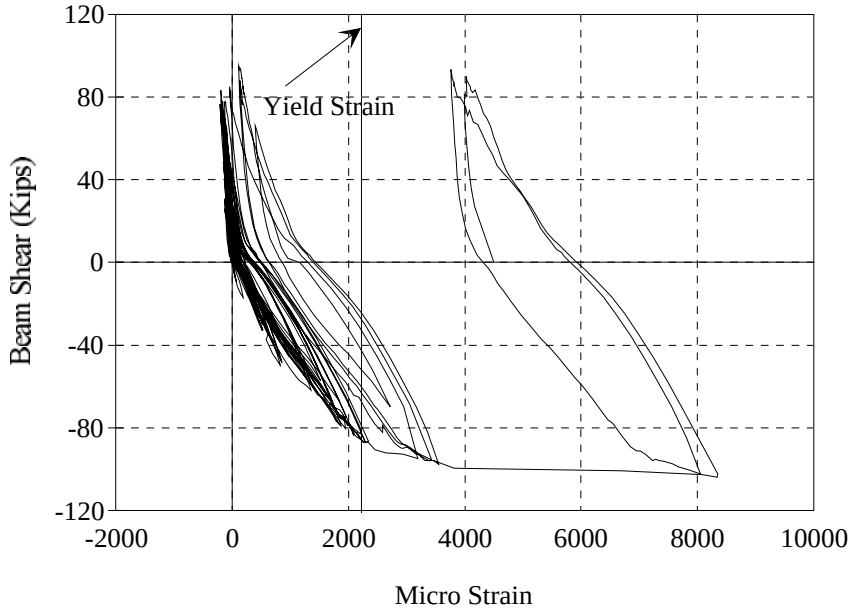

Figure 5.33 Beam Shear vs. Strain Response of Corbel Top Reinforcement in Specimen GJ-FR

corbel. Some yielding of reinforcement occurred in the corbels of Specimen GJ-FR

which led to more visible cracking than in Specimen GJ-TC. The strut-and-tie approach was useful for proportioning such corbels with unusual loading conditions.

5.6.4 Joint Shear Strength

The design and reinforcement details for the joint region were discussed in Chapter 3 without showing the details of the calculations. In this section, joint design for each of the specimens is evaluated using strain data collected from gauges attached to joint transverse reinforcement. The joint design for the first two specimens (DB-TC and GJ-TC) was performed according to the ACI 318-89 recommendations (which are very similar to the recommendations of ACI-ASCE Committee 352). These design provisions were based on tests conducted on monolithic connections. However, similarities exist between the monolithic connections and the first two connections investigated in this study. The joint reinforcement provided for the remaining specimens (GJ-FR and PT-NE) was less than that required by ACI 318-89. The influence/participation of the joint reinforcement on the joint behavior will be discussed in this section.

The forces applied on the joint of a moment-resisting frame connection are shown in Fig. 5.34. Summing the horizontal forces acting above the center line of the joint yields:

$$V_j = T + C - V_{col} \tag{5.5}$$

where V_j = horizontal shear acting on the joint

T = tensile force in the beam reinforcement

C = compressive force in the beam concrete

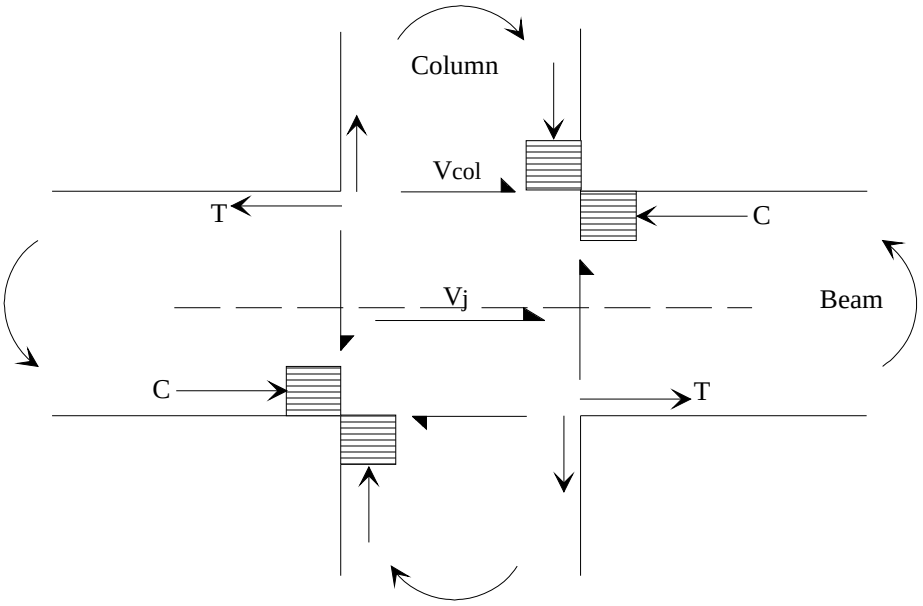

Figure 5.34 Forces Acting on the Joint of a Moment-Resisting Frame Connection

V_{col} = shear in the column

ACI 318-89 requires that these forces be calculated using a 1.25 factor applied to the steel yield stress in order to obtain an upper limit on the shear applied on the joint.

A nominal joint shear strength is specified to compare with the calculated shear , V_j. The specified nominal shear strength is a function of the concrete strength and not the joint transverse reinforcement. However, the nominal shear strength does depend on the degree of confinement to the joint provided by the beams and by a minimum amount of transverse reinforcement. The worst case corresponded with the joint being confined by beams on only two faces with a width of the beam less than 75 percent of the column width. For such a case the nominal shear strength of the joint, V_{jn}, is:

$$V_{jn} = 12\sqrt{f_c'}A_j \tag{5.6}$$

To achieve the specified nominal joint shear strength, a minimum amount of transverse reinforcement in the joint is required for confinement of the concrete. This quantity is given by the larger of the following two equations:

$$A_{sh} = 0.3(sh_c \frac{f_c^{'}}{f_{yh}})[\frac{A_g}{A_{ch}} - 1] \tag{5.7}$$

$$A_{sh} = 0.09 sh_c \frac{f_c^{'}}{f_{yh}} \tag{5.8}$$

where A_{sh} = total cross-sectional area of transverse reinforcement in one layer

s = spacing of transverse reinforcement equal to one-quarter the column minimum dimension, or 4 in.

h_c = cross-sectional dimension of column core measured center-to-center of confining reinforcement

A_g = gross area of column

A_{ch} = cross-sectional area of column measured out-to-out of transverse steel.

Because the basic dimensions for all the specimens were the same, maximum spacing allowed by the above equations was 4 in. The amount of transverse reinforcement required in one set of hoops was A_{sh} = 0.66 in^2, as governed by the second equation. Therefore, the total area of reinforcement required in the joint was the number of sets in the joint based on a 4 in. spacing multiplied by the area of each set (5x0.66 = 3.3 in^2).

This amount of reinforcement with a 4 in. spacing was provided in Specimen DB-TC. The location of the strain gauges are shown in Fig. 3.47. Evaluation of strain gauge data up to specimen failure indicated that strain was always below yield strain (approximately 80 percent at failure). Figure 5.35 shows the story shear

versus strain history from a strain gauge in the middle of the joint. Also, visual inspection of the joint following the test revealed no signs of joint distress and closing of most joint cracks following unloading.

The joint reinforcement in Specimen GJ-TC was identical to that in Specimen DB-TC. The location of the strain gauges are shown in Fig. 3.48. Figure 5.36 shows the story shear versus strain history for a gauge at the middle of the joint. The strain shown is the highest detected by any strain gauge in the joint. Some yielding occurred in these hoops near the end of the test. The story shear at that stage was approximately 20 percent higher than the calculated design story shear. Strain in the lower hoops of the joint, shown in Fig. 5.37, experienced the least strain during the test. Also, strain readings were not nearly as symmetrical as in Fig. 5.36. This was

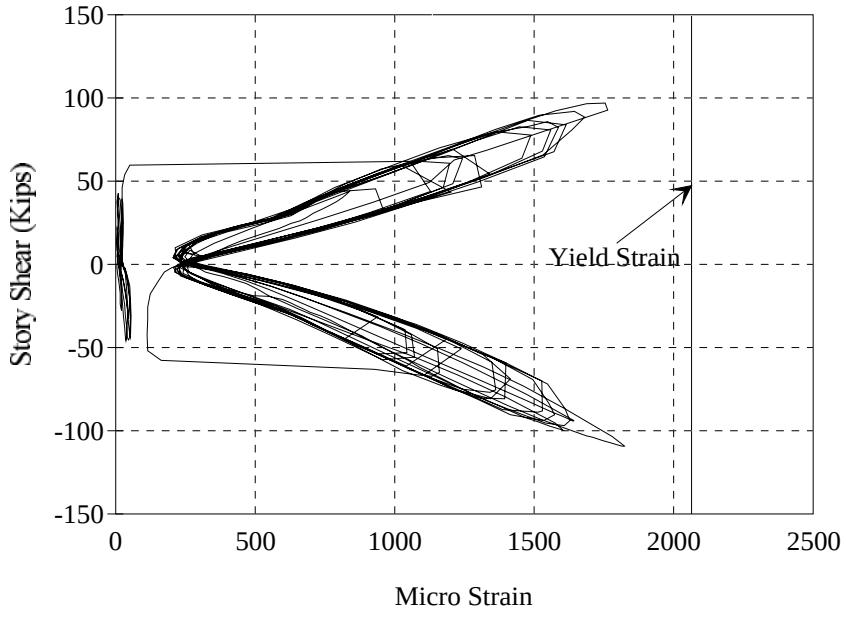

Figure 5.35 Story Shear vs. Strain Response for Joint Reinforcement in Specimen DB-TC

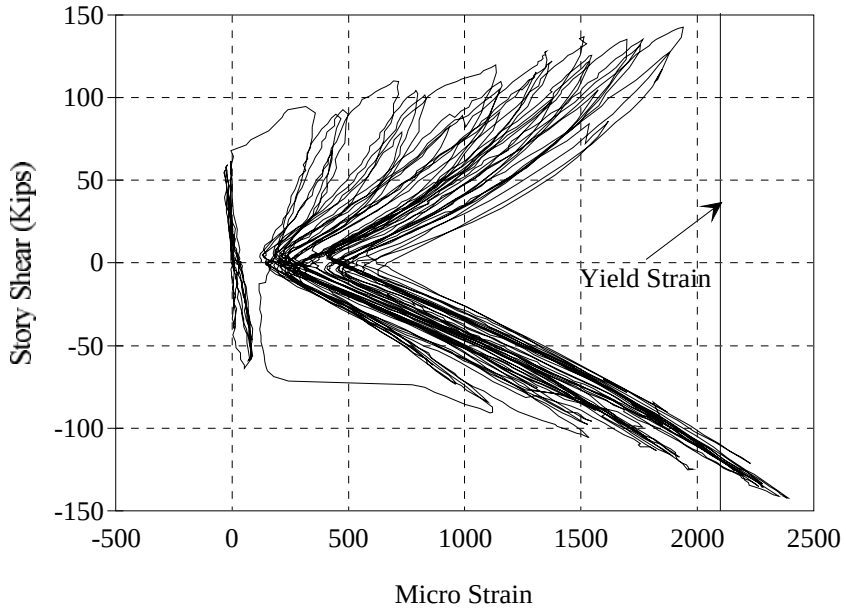

Figure 5.36 Story Shear vs. Strain Response for Central Joint Reinforcement in Specimen GJ-TC

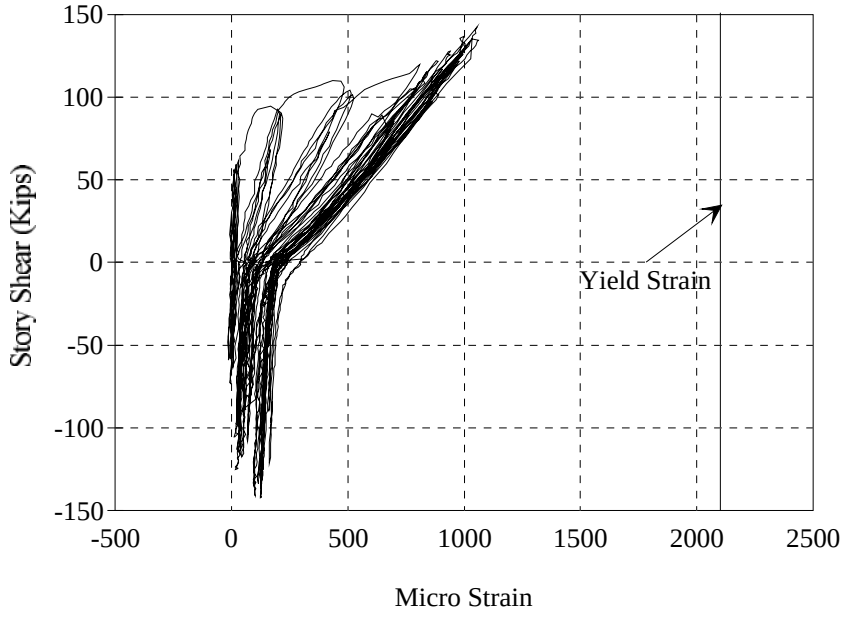

Figure 5.37 Story Shear vs. Strain Response for Lower Joint Reinforcement in Specimen GJ-TC

anticipated because force in the bottom of the beam during positive bending was not

transmitted directly to the joint through tension as shown in Fig. 5.34. Instead, tensile force in the bottom of a beam was transmitted to the corbel, then into the column below the joint region. The joint behaved quite well throughout the test. The ultimate story shear was approximately 1.25 times the nominal story shear. All joint cracks remained small throughout the test and closed after removal of load.

For the previous two specimens, the amount of joint reinforcement provided was obtained using the ACI 318-89 / ACI-ASCE Committee 352 recommendations for monolithic connections. In both cases joint reinforcement remained essentially elastic. In Specimen GJ-FR the joint shear mechanism was similar to that shown in Fig. 5.34. Like Specimen GJ-TC, a gap existed between the beams and column over most (60 percent) of the beam depth. The amount of joint reinforcement provided in Specimen GJ-FR was 5 sets of hoops with 5 legs of #3 bars, which is 16 percent less than was provided in Specimens DB-TC and GJ-TC. The primary reason for the reduction in quantity of joint reinforcement was congestion of steel. In light of the satisfactory behavior of joints in the previous two specimens, a reduction in joint reinforcement seemed warranted.

Strain gauges were mounted on the joint hoops at locations shown in Fig. 3.49. Figure 5.38 shows the story shear versus strain history for a middle set of hoops. The plot indicates that the joint reinforcement remained essentially elastic for most of the test. Some yielding occurred at the end of the test, but the amount was not substantially more than for Specimen GJ-TC. Figure 5.39 presents the story shear versus strain history for a lower set of hoops. Strain in these hoops was minimal. This is attributed to the corbels acting as part of the joint. The joint showed no signs of distress in both tests of this specimen (GJ-FR and GJ-FR-R), and most joint shear cracks closed after loads were removed from the specimen at conclusion of testing.

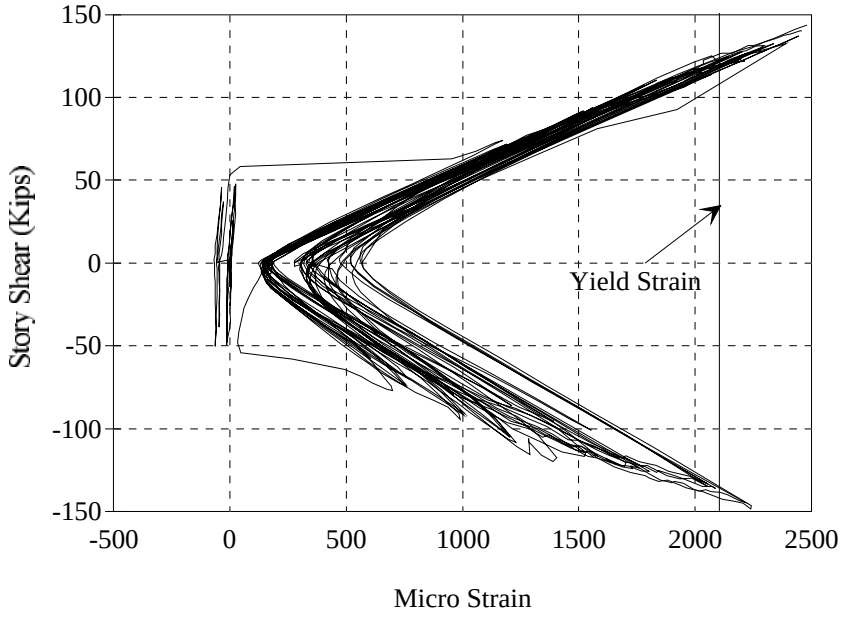

Figure 5.38 Story Shear vs. Strain Response for Central Joint Reinforcement in Specimen GJ-FR

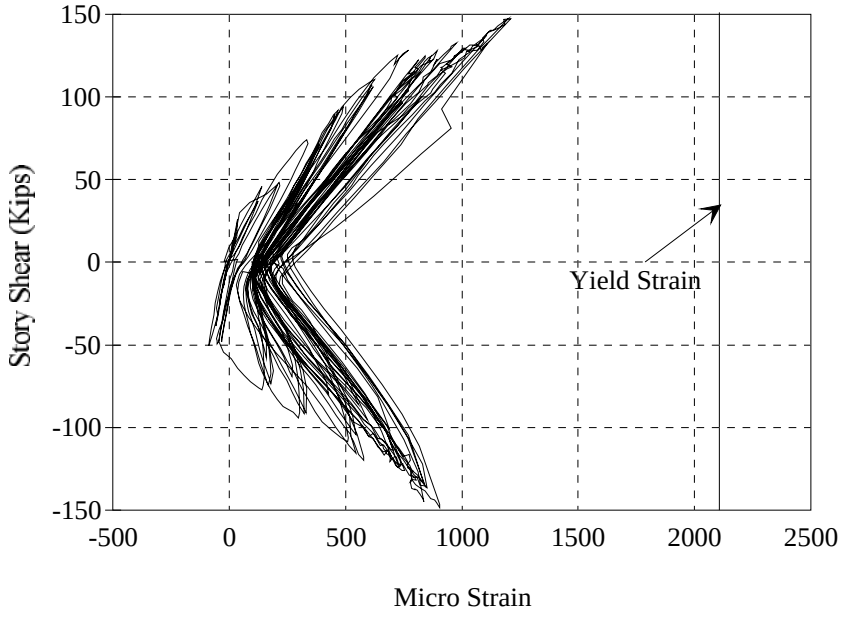

Figure 5.39 Story Shear vs. Strain Response for Lower Joint Reinforcement in Specimen GJ-FR

The joint shear mechanism for a debonded pretensioned joint, similar to

Specimen PT-NE, is different from that for the other specimens. Figure 5.40 shows the forces acting on the joint of a debonded pretensioned system. The main difference is that tensile reinforcement is unbonded and does not contribute to the shear transfer in the joint. Summing the forces acting on the top half of the joint in the horizontal direction yields the joint shear, V_j, :

$$V_j = C - V_{col} \tag{5.9}$$

where the parameters in the above equation are as defined for Eq. 5.5. Note that the joint shear in Eq. 5.9 is approximately the same as that in Eq. 5.5 even though the term T does not exist in Eq. 5.9. Because of the steel location, the resultant tensile force T is located at mid-depth of the beam. In order to achieve the same beam moment as for other specimens, the force C must be larger to overcome the

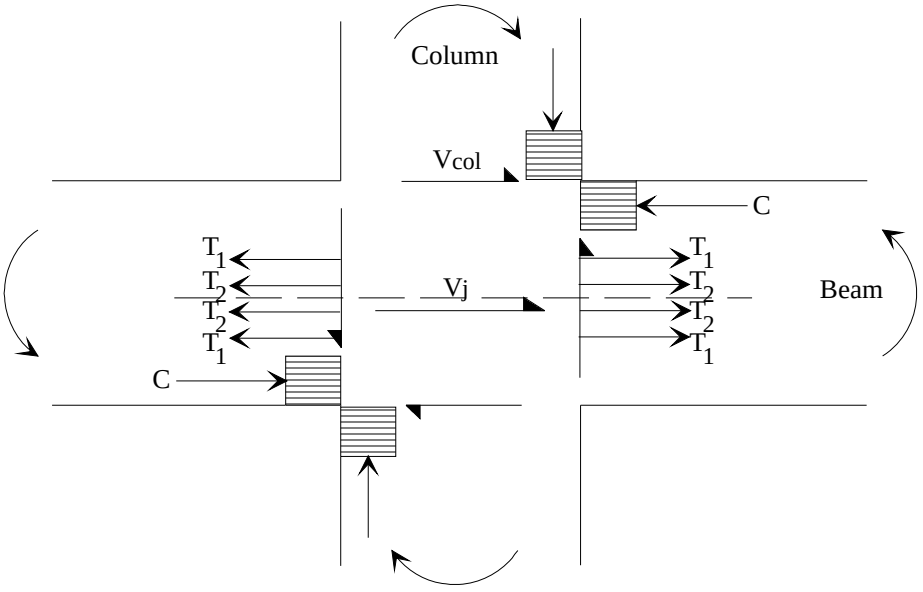

Figure 5.40 Forces Acting on the Joint of a Debonded Prestressed Moment-Resisting Frame

difference in the internal lever arm. The joint shear mechanism is simpler because it consists of only a compression strut. The column and beam compression force

resultants combine to form a diagonal joint compression strut.

Because the joint shear mechanism was obviously different from that for a monolithic joint, a reduced amount of transverse reinforcement was used in Specimen PT-NE with the hope of mobilizing the strength of the joint. (Recall that the strength of the joint in the previous three precast specimens was not severely tested.) However, sufficient steel had to be used to permit development of the design flexural strength of the beams before the joint failed. The quantity of transverse reinforcement in the joint was dictated somewhat by congestion of prestressing strands and column longitudinal reinforcement. Four sets of hoops, rather than five used in the other specimens, were used in the joint of Specimen PT-NE. The total area of hoop reinforcement provided was $4x0.55 = 2.2$ in^2. This was 16 percent less than the amount provided in Specimen GJ-FR and 33 percent less than provided in Specimens DB-TC and GJ-TC (as required by ACI 318-89).

Strain gauges were mounted on the four sets of hoops at the locations shown in Fig. 3.50. Figure 5.41 shows the story shear versus strain response for the top set of hoops. The strain data indicate that the outer-most layers of transverse reinforcement remained elastic throughout most of the test. Some yielding occurred but only during the 4 and 5 percent drift ratio cycles. Figure 5.42 shows the story shear versus strain response for hoops in the central part of the joint. Yielding of these hoops occurred during cycles to 1.5 percent drift ratio. Considerable inelastic response occurred in subsequent cycles. It was discussed earlier that joint deterioration was the primary cause of failure. Behavior through cycles to 3 percent drift ratio was generally satisfactory. However, joint crack widths during these cycles were somewhat larger than for the other specimens (0.005 in. versus 0.015 to 0.02). During the 4 and especially 5 percent drift ratio cycles joint cracks became

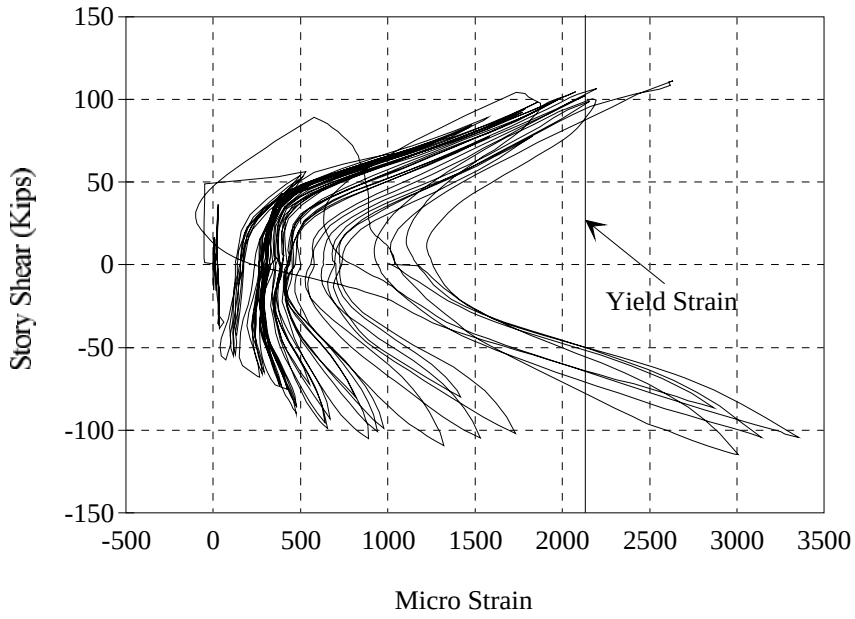

Figure 5.41 Story Shear vs. Strain Response for Upper Joint Reinforcement in Specimen PT-NE

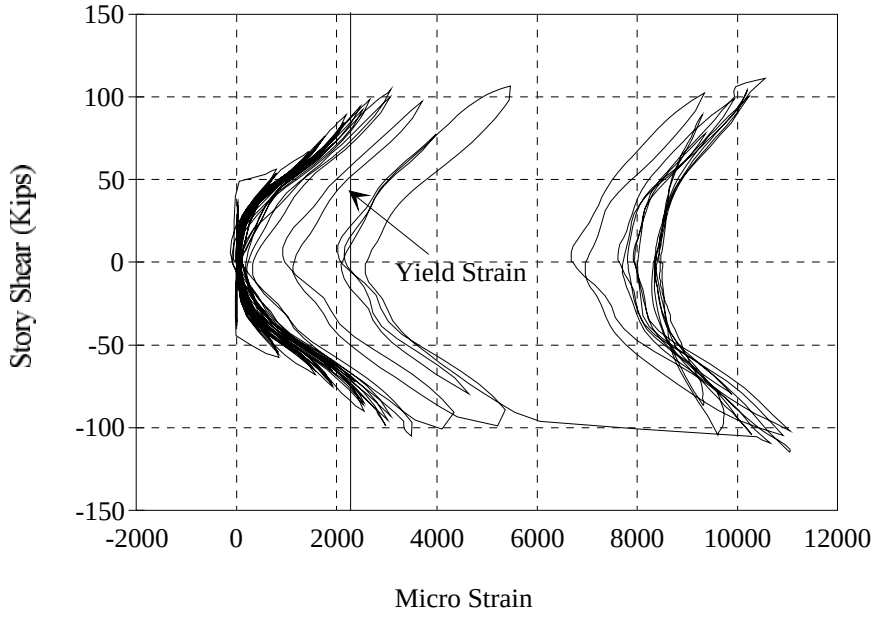

Figure 5.42 Story Shear vs. Strain Response for Central Joint Reinforcement in Specimen PT-NE

much larger and spalling of joint concrete occurred. Joint reinforcement provided

was sufficient to drift levels beyond the design drift (approximately 2 percent). Failure of the joint occurred at large drifts when forces concentrated at the joint corners were more concentrated and slightly larger than during 2 and 3 percent drift ratio cycles.

MacRae and Priestley [26] proposed a rational procedure to calculate the amount of joint reinforcement needed for similar connections. The procedure is based on a strut-and-tie approach. Hoop tensile forces are equilibrated at the core boundary by diagonal struts directed toward the center of compression of the beam and column compression resultants, and by vertical forces in column bars as shown in Fig. 5.43. The forces shown in the column bars correspond with the beams reaching flexural capacity. In this model it is assumed that a portion of the force differential in the outer layer of column bars is transferred by bond within the diagonal compression strut and the remainder by strut-and-tie action involving the joint transverse reinforcement. The force differential in the other column bars is assumed to be transferred by bond through the diagonal compression strut. The force that can be

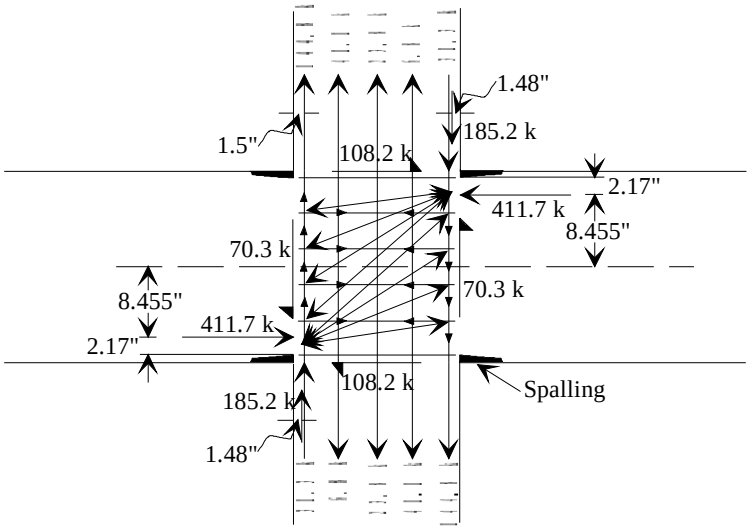

Figure 5.43 Possible Strut-and-Tie Model for the Joint of Specimen PT-NE

transferred by bond through the beam compression zone is given by:

$$\Delta T_1 = n\varepsilon_0 u_u c \tag{5.10}$$

where n = number of bars

ε_0 = surface area per unit length of bar

u_u = ultimate bond stress = $k\sqrt{f_c'}$

c = beam compression zone depth

A value of k = 24 was suggested by MacRae and Priestley. Therefore, using Eq. 5.10 ΔT_1 is:

$$\Delta T_1 = 5(\pi)(0.625)\frac{24\sqrt{6300}}{1000}(5.1) = 95.4 \ kips$$

The force in the outer layers of the column bars, from Fig. 5.43, are:

$$T_1 = 144.8 \ kips$$
$$C_1 = 31.3 \ kips$$

The amount of column bar force to be carried by the strut-and-tie mechanism, ΔT_2, is:

$$\Delta T_2 = T_1 + C_1 - \Delta T_1$$
$$\Delta T_2 = 144.8 + 31.3 - 95.4 = 80.7 \ kips \tag{5.11}$$

Finally, the amount of joint transverse reinforcement is calculated by:

$$A_{jh} = \frac{\Delta T_2}{f_{yh} \tan\theta} \tag{5.12}$$

where f_{yh} = yield stress of joint reinforcement

θ = the angle between the horizontal axis and the line from the center of compression of the beam and column compression resultants to the intersection of the extreme column bar at joint midheight, which, from Fig. 5.43 is equal to 25.1^0.

$$A_{jh} = \frac{80.7}{64.5 \tan 25.1^0} = 2.67 \ in^2$$

The amount of joint reinforcement, according to this approach is approximately 20 percent more than what was provided, and is approximately 20 percent less than what is required by ACI 318-89 for monolithic joints.

CHAPTER 6

ANALYTICAL MODELING OF PRECAST FRAME SYSTEMS

6.1 INTRODUCTION

In the previous chapters the experimental program was presented and discussed in detail. To this point, the focus has been on the behavior of isolated subassemblages representing a small portion of a precast frame system. The subassemblage tests were necessary to investigate the behavior of particular connection details and provide information, such as hystereses, about individual connections. In this chapter the focus is shifted to the behavior of entire precast frames. Using the data gathered in the laboratory from the subassemblages, 5- and 15-story frames were evaluated using nonlinear dynamic time history analyses. Frames incorporating behavioral characteristics of connections tested in the laboratory were subjected to various earthquake records. The objective of the analyses was to evaluate the suitability of the different frame systems for use in earthquake resistant buildings. This was accomplished through consideration of gross measures of response, such as story drifts and shears, residual drifts, and local ductility demands.

6.2 DESIGN OF THE FRAMES

Elevations of the frames used in this analytical study are shown in Fig. 6.1. Each frame is intended to represent one of the two perimeter lateral-force-resisting frames aligned in the short direction of the building plan shown in Fig. 2.7. Symmetry in both orthogonal directions was taken into consideration to reduce calculation time and the amount of data storage required. Each frame is divided into

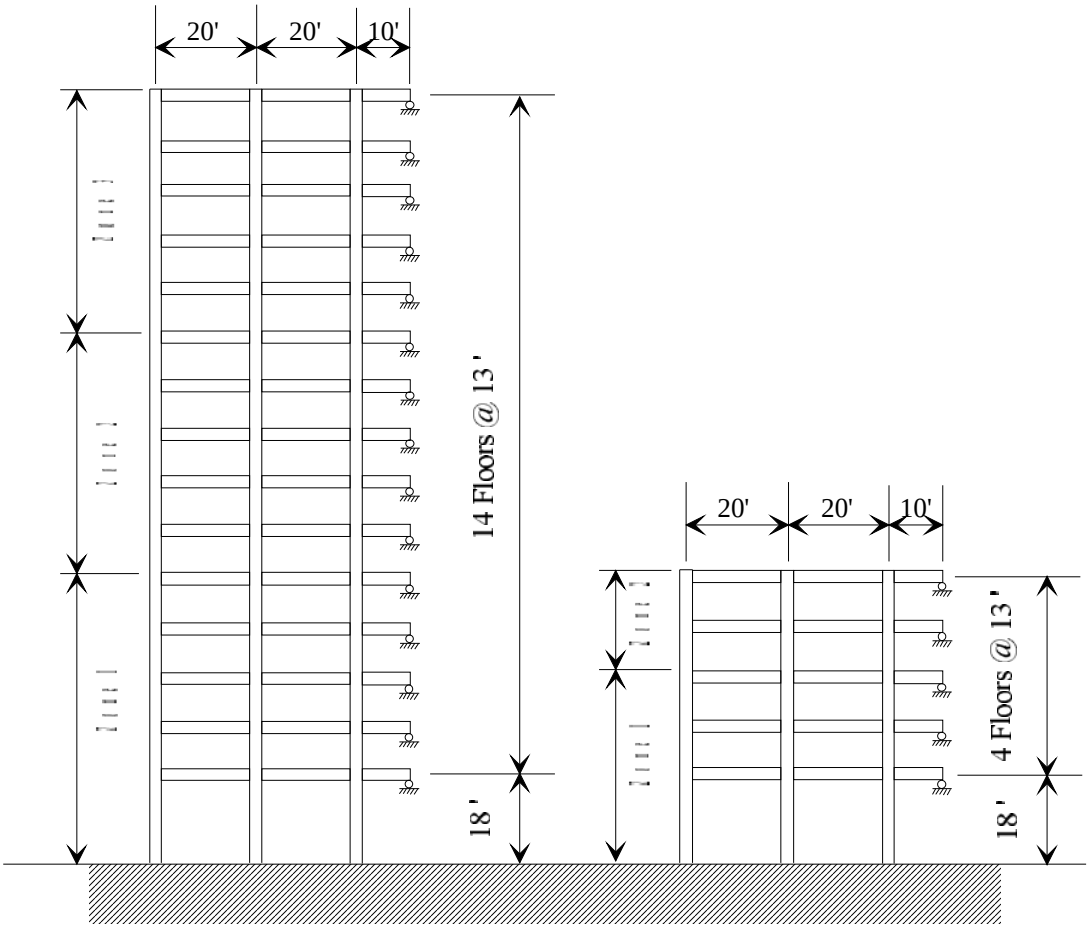

a) 15-Story Frame b) 5-Story Frame

Figure 6.1 Elevations of Frames Used in the Analytical Study

different strength zones along its height. It was assumed in this study that beam and column sizes remained the same over the entire height of the building. Only reinforcement quantities changed in the different zones. In a more-refined design and analysis process, dimensions of columns and beams may also change along the height of the building, especially for the 15-story building.

The frames were proportioned using the equivalent-lateral-force procedure in the UBC-91 [22] for Seismic Zone 4, an R_w of 12, and soil factor S equal to 1.2. The beam sizes were 24x48 in. and 24x42 in., and column sizes were 42x36 in. and

36x36 in., for the 15- and 5-story frames, respectively. These sizes were primarily chosen to satisfy drift limitations and limitations on joint shear stresses. The floors were assumed to be 8 in. thick hollow core units with a 2.5 in. topping, resulting in a uniform load of 87 psf. An additional 16 psf of equivalent load for exterior cladding, 10 psf for partitions, and 10 psf of miscellaneous load were added to each floor level. The weight of each building was estimated to be 57133 kips for the 15-story building and 17913 kips for the 5-story building.

Using the lateral-static-force procedure of UBC-91 [22], the distribution of lateral forces for both buildings was calculated and is shown in Table 6.1. The forces shown in Table 6.1 are the forces applied on the entire building, i.e. on both lateral-force-resisting frames. To estimate the required strengths of beams and columns in the various zones, static analyses was performed on the 15- and 5-story frames. In addition to the lateral forces shown in Table 6.1, dead and live loads were included in the analysis. The dead load consisted of the weight of the frame itself; the weight of the exterior cladding of 16 psf converted to load applied on the perimeter frames only; the weight of the planks, topping, and 20 psf uniform load applied over an area equal to the length of the frame times half the span perpendicular to the frame, i.e. 100'x14.25' (see Fig. 2.7). The live load was taken as 50 psf on the same floor area.

The controlling design forces were obtained by checking the following load combinations:

$$U = 0.75(1.4D + 1.7L + 1.87E) \tag{6.1}$$

$$U = 0.9D + 1.43E \tag{6.2}$$

where *D*, *L*, and *E* are the dead, live, and earthquake loads respectively. Table 6.2 lists the maximum design forces determined by elastic analysis for the beams and

columns in all zones for both buildings. Columns were designed so that the summation of column flexural strengths at any joint was at least 40 percent greater than the summation of beam flexural strengths.

Table 6.1 Distribution of Equivalent-Lateral-Static Forces

Level	15-Story Frame			5-Story Frame		
	Height (ft)	Weight (kips)	Force (kips)	Height (ft)	Weight (kips)	Force (kips)
15	200	3308	433.2			
14	187	3833	216.2			
13	174	3833	201.1			
12	161	3833	186.1			
11	148	3833	171.1			
10	135	3833	156.1			
9	122	3833	141.0			
8	109	3833	126.0			
7	96	3833	111.0			
6	83	3833	95.9			
5	70	3833	80.9	70	3164	358.5
4	57	3833	65.9	57	3650	283.8
3	44	3833	50.9	44	3650	219.1
2	31	3833	35.9	31	3650	154.3
1	18	3996	21.7	18	3799	93.3
Total		57133	2093.0		17913	1109.0

Table 6.2 Maximum Member Design Forces as Obtained by Elastic Analysis

Zone	15-Story Frame			5-Story Frame		
	Beam Moment (k-ft)	Column Moment (k-ft)	Column Force (kips)	Beam Moment (k-ft)	Column Moment (k-ft)	Column Force (kips)
1	2098	3108	1170	1133	1596	353
2	1881	1835	780	605	694	133
3	1323	1339	388	-	-	-

6.3 ANALYTICAL MODELING OF SUBASSEMBLAGES

A nonlinear dynamic analysis program named IDARC [24] was used to perform time-history analyses of the structures described above. The objective of the analyses was to study the global and local behavior of precast frame systems incorporating connection behavior based on results of subassemblage tests conducted in the laboratory. The laboratory subassemblage tests were first modeled using quasi-static cyclic analysis performed with IDARC, and using the same displacement history applied in the laboratory as input for the computer program. The experimental data gathered in this study were used to calibrate the models, especially initial stiffness and stiffness degradation.

Three different hysteretic models were used to study the overall behavior of the frames. The first model corresponds with Specimen GJ-TC. This specimen experienced severe pinching of the story shear-drift ratio response due to the flexibility of the vertical dowels in the beam-corbel connections as was described earlier in Section 4.2.1.2. The second model corresponds with Specimen GJ-FR. This specimen experienced minimal pinching of the story shear-drift ratio response and dissipated the most energy. If the beam-corbel connection used in Specimen GJ-FR had been used in Specimen GJ-TC, it is anticipated that behavior of the two specimens would have been similar. Although beam-corbel connections in

Specimen GJ-TC proved to be largely ineffective, the model to resemble behavior of that specimen, which was characterized by severe pinching, is used here to study the effect of severe pinching of the hysteresis loops on behavior of the structures. The third model corresponds with the nonlinear elastic behavior demonstrated by Specimen PT-NE. Details of each hysteretic model and any additional assumptions are explained in the following subsections.

6.3.1 Hysteretic Model for Pinched Behavior

The hysteretic model used to represent significant pinching in the load-deformation response of beam-column connections is shown in Fig. 6.2. The rules governing this model are based on a backbone curve that includes a yield point and a slight increase in resistance after yield. The strength increase following yield of the connection is mainly attributed to strain hardening of the steel. The post yield slope depends on the stress-strain characteristics of the reinforcing steel used. For this study, the post-yield slope is approximated based on observations from the testing of Specimen GJ-TC. During unloading, stiffness of the connection is the same as the initial stiffness. For loading in the opposite direction (reversal of load), pinching or reduction in stiffness at low load levels occurs.

Pinching in Specimen GJ-TC was mainly attributed to flexibility in the beam-corbel connections. The increase in stiffness outside the pinching region corresponds with reaching the load required to close the gap that forms at the beam-corbel connection when the beam is subjected to positive moment. When stiffness increases, the load-deformation response follows a direct path to the maximum displacement achieved during the previous cycle. The slope of this portion of the

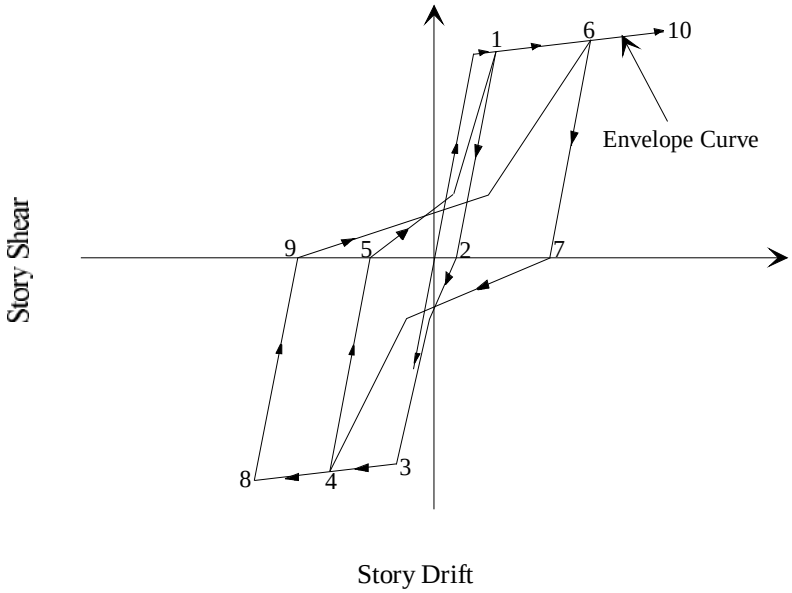

Figure 6.2 Hysteresis Model for Pinched Behavior

load-deformation response is the new elastic stiffness. The loading and unloading path for an arbitrary load history can be followed in Fig. 6.2.

The initial stiffness of the connection is also an important parameter in the analytical model. In general, for the specimens tested in this program, the calculated initial stiffness was typically higher than the measured stiffness. This was anticipated, to some degree, for the precast connections. For Specimen GJ-TC for instance, in addition to the gap that already existed between each beam and the column, there was significant flexibility introduced in the beam-column connection because of the detail between the beams and corbels.

IDARC requires as input the moment-curvature envelope curves for the columns and beams. The columns, which were treated as monolithic, were represented by trilinear moment-curvature relationships. The initial response was based on uncracked section properties up to the cracking moment. The second segment was based on cracked-section properties up to the yield moment. The third segment extends from the yield moment to the flexural capacity computed using a

rectangular stress distribution in the concrete with an ultimate concrete strain of 0.003 in/in.

The moment-curvature relationship for the beams was based primarily on the behavior of the yielding connecting elements at the top of the beams. The moment-curvature envelope for the beams was bilinear. The first segment, which relates to the initial stiffness of the connection, was based on cracked-section properties. The limiting moment for the first segment (yield moment) corresponds with the initiation of yielding of the connecting elements. The corresponding curvature was calculated based on cracked section properties and steel yield strain. This approach yielded an initial stiffness for a beam-column connection that was approximately 25 percent higher than the measured stiffness. This difference was attributed to the initial flexibility in the beam-to-corbel connections. Because a different, less-flexible detail could be used, the computed initial stiffness was not downgraded. The second segment was initially based on the calculated moment capacity and corresponding curvature of the beam section adjacent to the column. However, because this calculation yielded a slope lower than what was observed in the laboratory, the slope of the second line was based on the stiffness observed in the laboratory and was taken as 2 percent of the initial slope. The hysteresis loops from tests on Specimen GJ-TC and those from IDARC, based on the calculations stated above, are shown in Figs. 6.3 and 6.4, respectively.

6.3.2 Modeling of Connections with Friction Devices

The hysteretic model for this connection is shown in Fig. 6.5. As explained earlier, connections between the beams and column in this connection type were designed to slip at a prescribed load level. The beam sections outside the connection

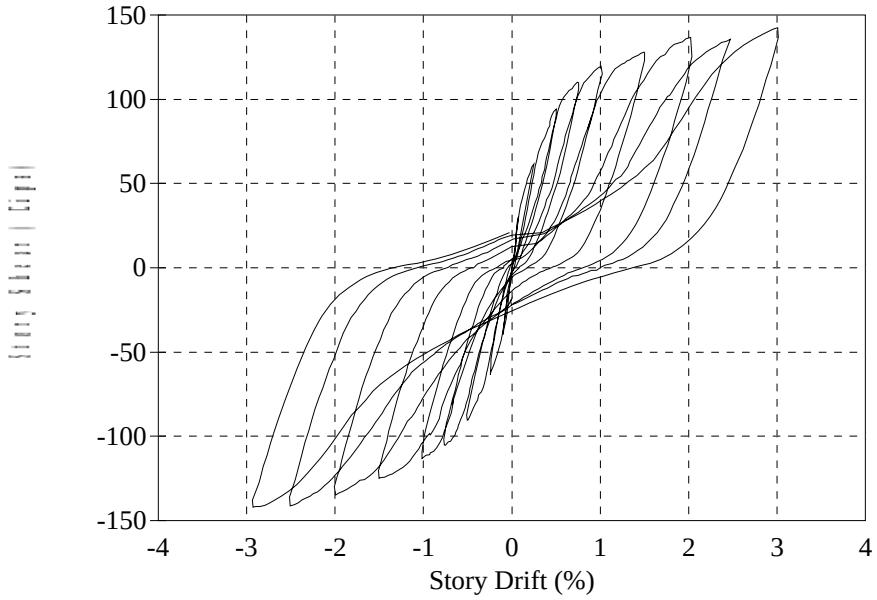

Figure 6.3 Experimental Hysteresis Loops for Specimen GJ-TC

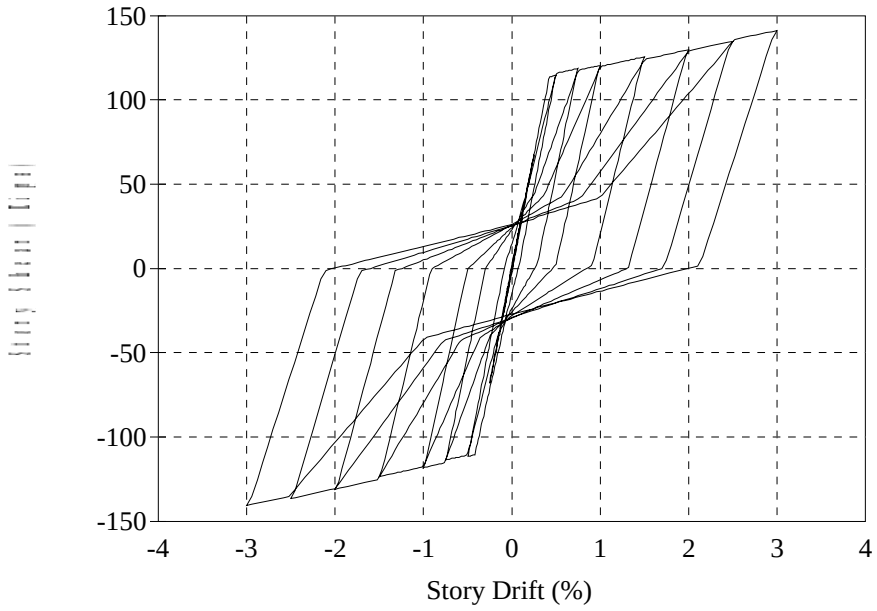

Figure 6.4 Analytical Hysteresis Loops for Pinched Connection Response

region and the columns were expected to remain elastic. It is assumed in this

hysteretic model that the connection behaves elastically up to the slip load. When slip occurs in the friction connections, moment resistance of the connection is maintained and increases slightly with additional slip. During unloading, the stiffness is the same as the initial elastic stiffness. Contrary to the hysteretic model used to describe behavior similar to that observed for Specimen GJ-TC, no pinching is assumed to occur in this model. During loading in the opposite direction, the load-deformation path is directed slightly below a point corresponding with initial slip of the friction device. The loading and unloading path for an arbitrary load history is illustrated in Fig. 6.5.

Theoretically, the level of load corresponding with slip is supposed to remain constant. The slip load is a function of the friction coefficient and clamping force. However, the friction coefficient, which is usually assumed to be constant between two surfaces, can vary. Clamping force, temperature, scale on the surfaces, and the

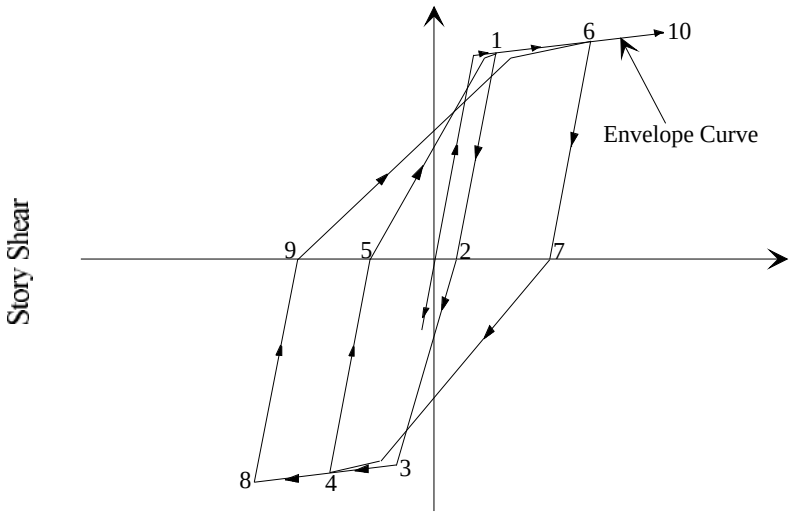

Figure 6.5 Hysteresis Model for Connection with Friction Devices

rate of loading can affect the coefficient of friction. None of the above factors

varied significantly enough to be considered in the design of the connection; a constant coefficient of friction between steel and brass of 0.2 was used. This coefficient was based on results of experiments by Grigorian et al. [20] at the University of California at Berkeley (described in section 3.3.3). The slip force of the beam can be calculated using the following equation:

$$F_s = N_s N_b F_b \mu \tag{6.3}$$
$$F_s = 2*8*64*0.2 = 204.8\ kips$$

where N_s = number of sliding surfaces = 2.

N_b = number of bolts on both faces of the beam = 8.

F_b = tension force in each bolt = 64 kips.

μ = coefficient of friction = 0.2.

The beam moment corresponding with the slip force is calculated as:

$$M_s = F_s d \tag{6.4}$$
$$M_s = 204.8*17.75 = 3635\ k-in$$

where d is the distance from the center of the plates to the pin at the bottom of the beams (which in this case consists of three 1-1/8 in. A490 bolts). The pin was intended to act as a pivot point for the beams to rotate about.

The same moment-curvature relationship for the columns, as described in the previous section, was used in this model. The moment-curvature envelope for the friction connections is bilinear. The first segment is related to the initial stiffness of the connection. The moment defining the end of the elastic segment corresponds with the slip moment given by Eq. 6.4. Curvature corresponding with this moment is calculated based on the following assumptions:

- For the slip load given by Eq. 6.3, the strain in the friction plates is

calculated. Similarly, the strain in the connecting bolts at the bottom of the beams is calculated.

- A linear strain variation is assumed over the depth *d* as (defined above) and the curvature is calculated.

As for the previous model, these calculations yielded approximately 33 percent more stiffness than measured.

Specimen GJ-FR demonstrated more flexibility than the other specimens for the following reasons:

- The use of high-strength bolts in the beam-corbel connection resulted in additional flexibility at the section between each beam and corbel.
- Bending of the plates that made up part of each friction device, and elongation of the bolts connecting the friction device hardware to the couplers in the column also contributed to connection flexibility.

These factors can be minimized by pretensioning the connecting bolts (both top and bottom) and by increasing the stiffness of the plate assemblies used in the friction devices. As a result, the calculated initial stiffness was not reduced.

Ideally, as the beams slip, the moment resisted should remain constant and the second segment of the moment-curvature envelope should remain flat. However, the experimental data indicated that moment increased with increasing displacements. This behavior is due to the bolts used to clamp the plates in the friction device coming into bearing with the sides of the slotted holes as a result of the concentrated rotations that occurred at the beam ends. Based on the experimental data, the slope of the second segment was taken as 2 percent of the initial stiffness. The hysteresis loops from testing Specimen GJ-FR and those produced by IDARC are shown in Figs. 6.6 and 6.7, respectively.

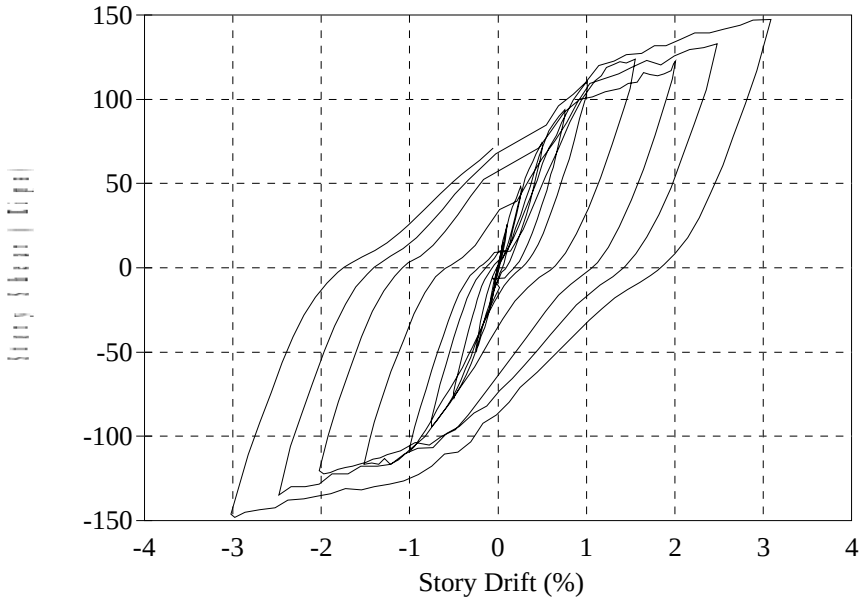

Figure 6.6 Experimental Hysteresis Loops for Specimen GJ-FR

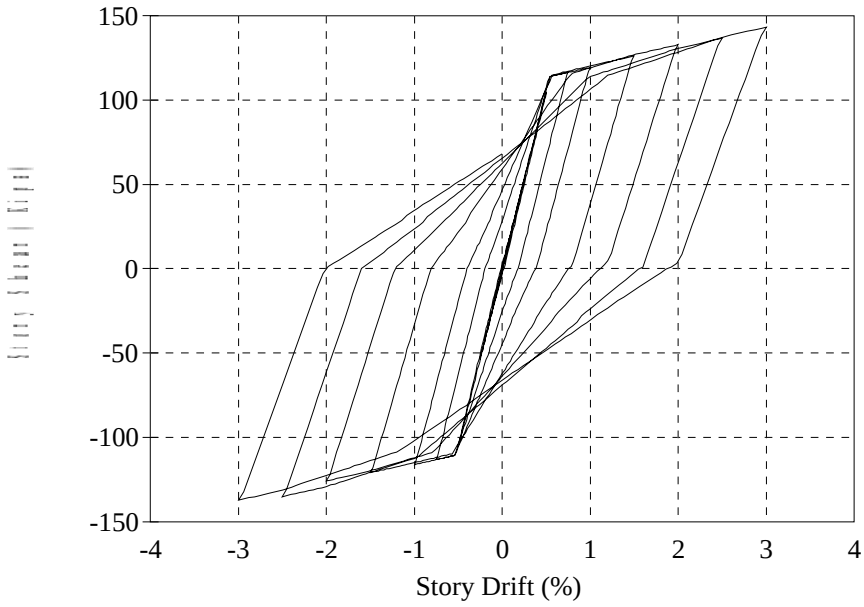

Figure 6.7 Analytical Hysteresis Loops for Connection with Friction Devices

6.3.3 Modeling of Prestressed Connections

The model used to describe the load-drift ratio response of a prestressed connection is shown in Fig. 6.8. For this model it is assumed that the connection behaves linear-elastic until the joint (or crack) opens at the beam-column interface. The moment required to fully open the joint is twice the moment that results in decompression of one side of the beam (for more explanation see Appendix A). Following joint opening, the stiffness changes dramatically. In subsequent cycles, the load-deformation response during loading is directed toward the maximum displacement achieved in the previous cycle. The hysteretic model also assumes that the connection does not return to zero drift following unloading. A small residual drift that is a percentage of the maximum drift achieved in the previous cycle represents crushing and spalling of concrete in the connection region. This model slightly overestimated the energy dissipated by the connections especially at low

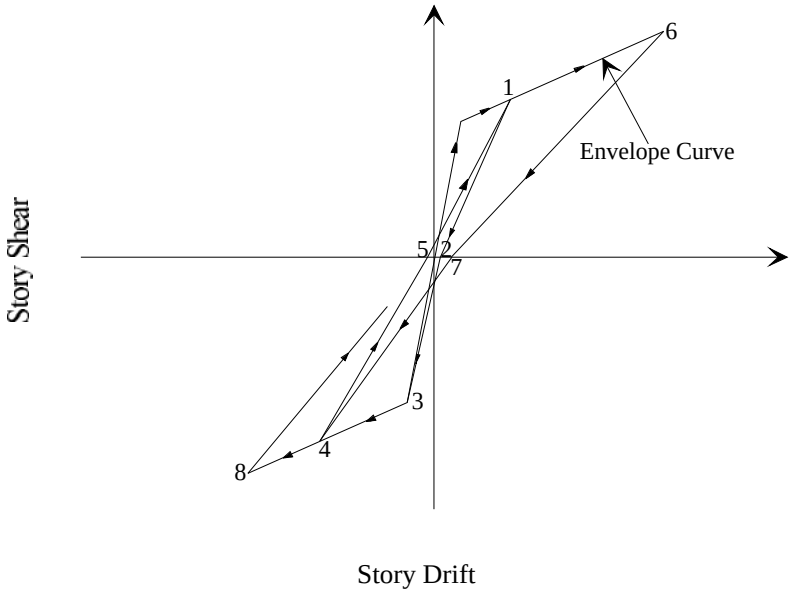

Figure 6.8 Hysteresis Model for Pretensioned Connection

displacement levels. Observed behavior illustrated in Fig. 4.12, demonstrated that

the unloading path is not a straight line as assumed in the model, but actually tends to be more curved. However, as more cycles were imposed on the connection, the load-deformation response became less like nonlinear elastic behavior due to crack opening and closing and due to spalling of concrete cover. The loading and unloading path for an arbitrary load history is illustrated in Fig. 6.8.

Comparison of the experimental hysteresis with the hysteresis obtained analytically using IDARC is shown in Figs. 6.9 and 6.10, respectively. The analytical model predicts very well the strength of the connection, and predicts the stiffness and residual drift reasonably well. The model described by Fig. 6.8 indicates the envelope curve is bilinear. However, as soon as the curvature corresponding with the prestressing steel reaching the limit of proportionality is achieved, the envelope curve flattens. The calculations for determining the beam moment-curvature up to the limit of proportionality are included in Appendix A.

6.3.4 IDARC Hysteresis Parameters

In order to achieve the force-deformation characteristics for each of the models described in the previous subsections, IDARC utilizes four parameters to modify the hysteretic rules. These parameters affect:

- Stiffness degradation
- Strength degradation (ductility-based)
- Strength degradation (energy-controlled)
- Pinching of hysteresis loops.

Each parameter has a different range of values. Values can be changed to reflect the severity of degradation associated with each parameter. Two sets of values (one for beams and another for columns) were used in this study to describe each of the

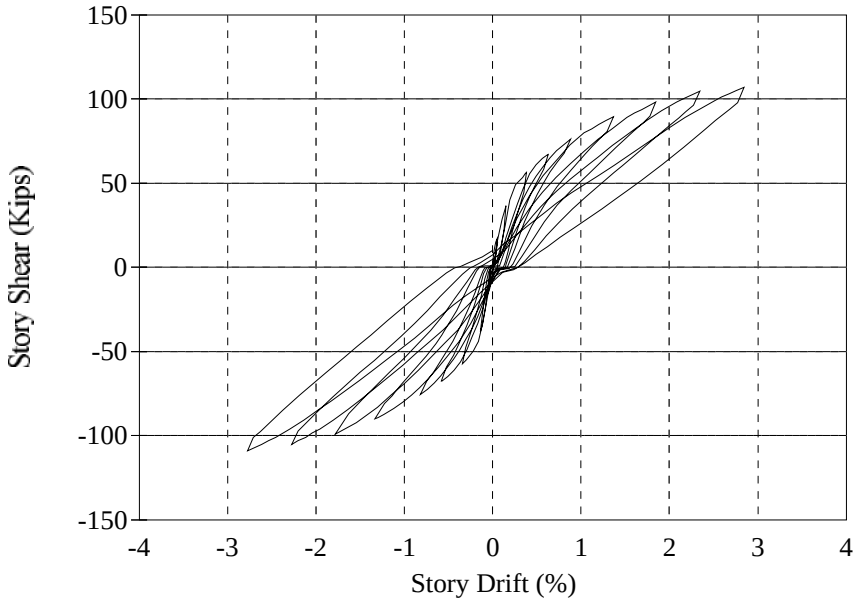

Figure 6.9 Experimental Hysteresis Loops for Specimen PT-NE

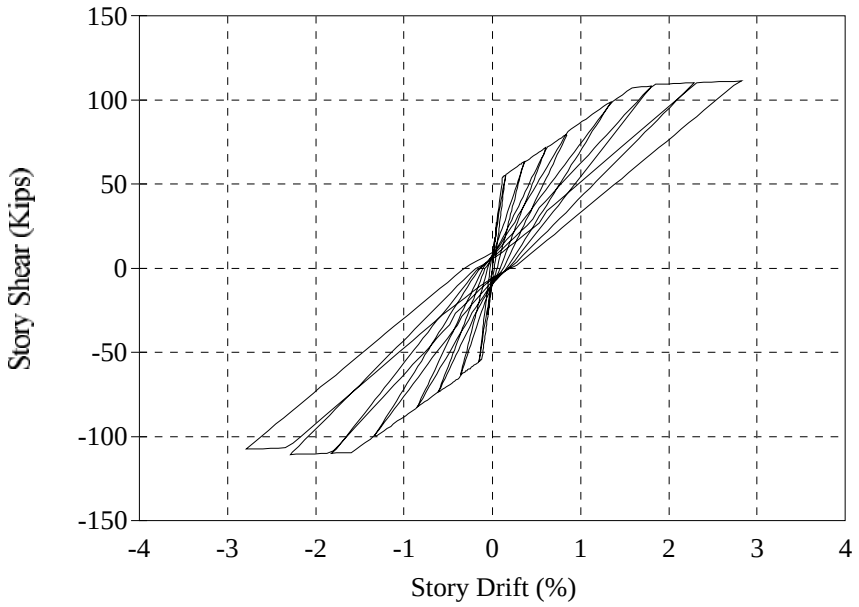

Figure 6.10 Analytical Hysteresis Loops for Pretensioned Connection

hysteretic models described previously. The parameter values used are listed in

Table 6.3.

Table 6.3 IDARC Hysteresis Parameters

		Stiffness Degradation Parameter	Strength Degradation Parameter (ductility-based)	Strength Degradation Parameter (energy-controlled)	Pinching Parameter
Connection with Pinched Behavior	Beams	6.0	0.0	0.0	0.2
	Columns	9.0	0.0	0.0	1.0
Connection with Friction Devices	Beams	6.0	0.0	0.0	0.8
	Columns	9.0	0.0	0.0	1.0
Prestressed Connections	Beams	0.1	0.0	0.0	0.1
	Columns	9.0	0.0	0.0	1.0

6.4 EARTHQUAKE GROUND MOTIONS

Four different ground motions were selected for incorporation in this study: the N-S component of El Centro, California, 1940; the S-W component of Vina del Mar, Chile, 1985; the N-S component of Hachinohe, Japan, 1968; the N-S Corralitos component of Loma Prieta, California, 1989. The acceleration records for the four ground motions are shown in Figs. 6.11 through 6.14. The peak ground acceleration (PGA) for each of these records is different. In an effort to normalize and scale the records to allow easier comparison of the analytical results, the spectral intensity for each of the records was made equal. The procedure is explained below.

The El Centro 1940 record was chosen as the baseline. This record is widely used because it has a wide-band spectrum and because it is considered representative of earthquakes typical in the western United States. The El Centro 1940 record was scaled to a PGA of 0.4g in order to introduce a significant amount of damage in

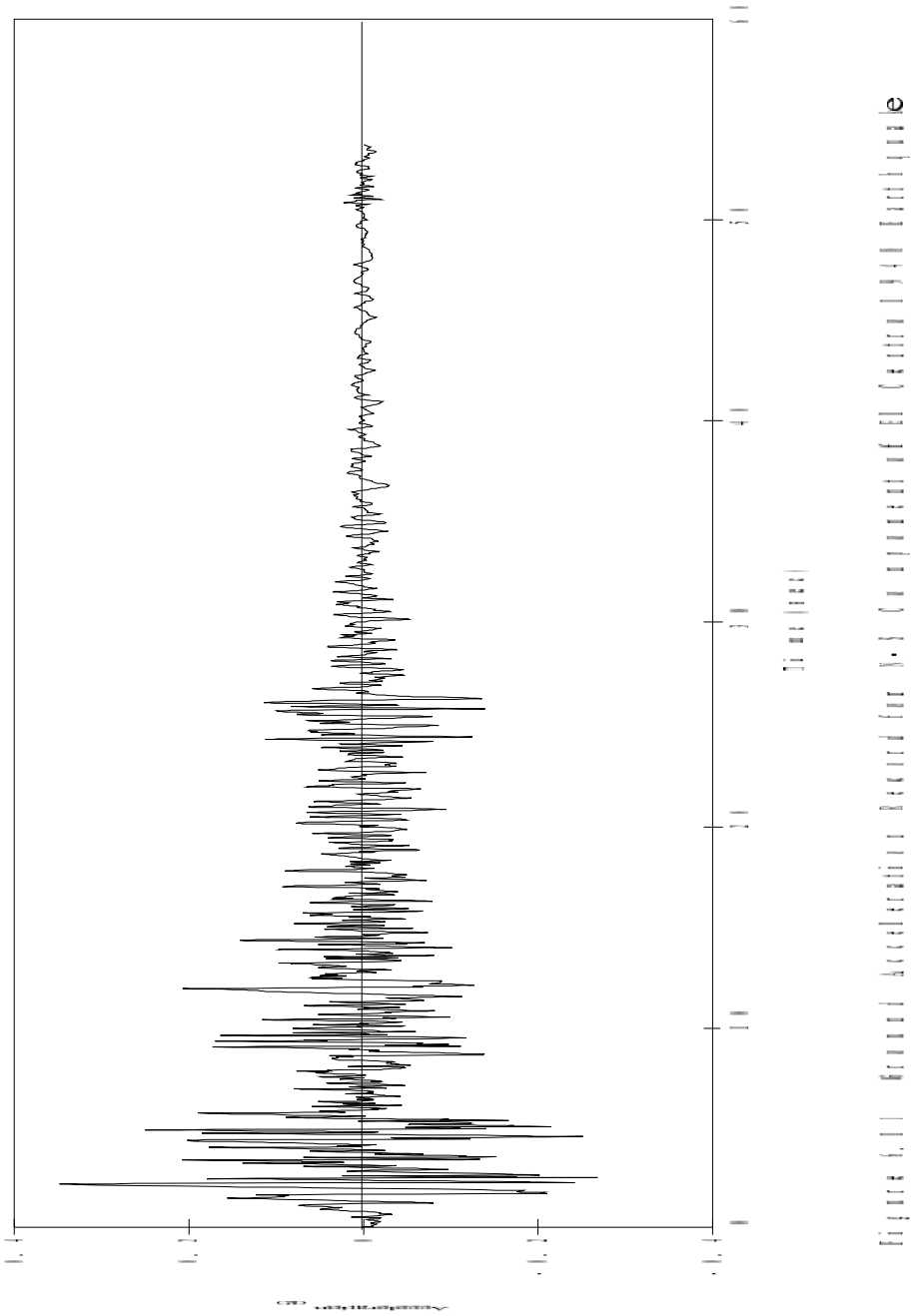

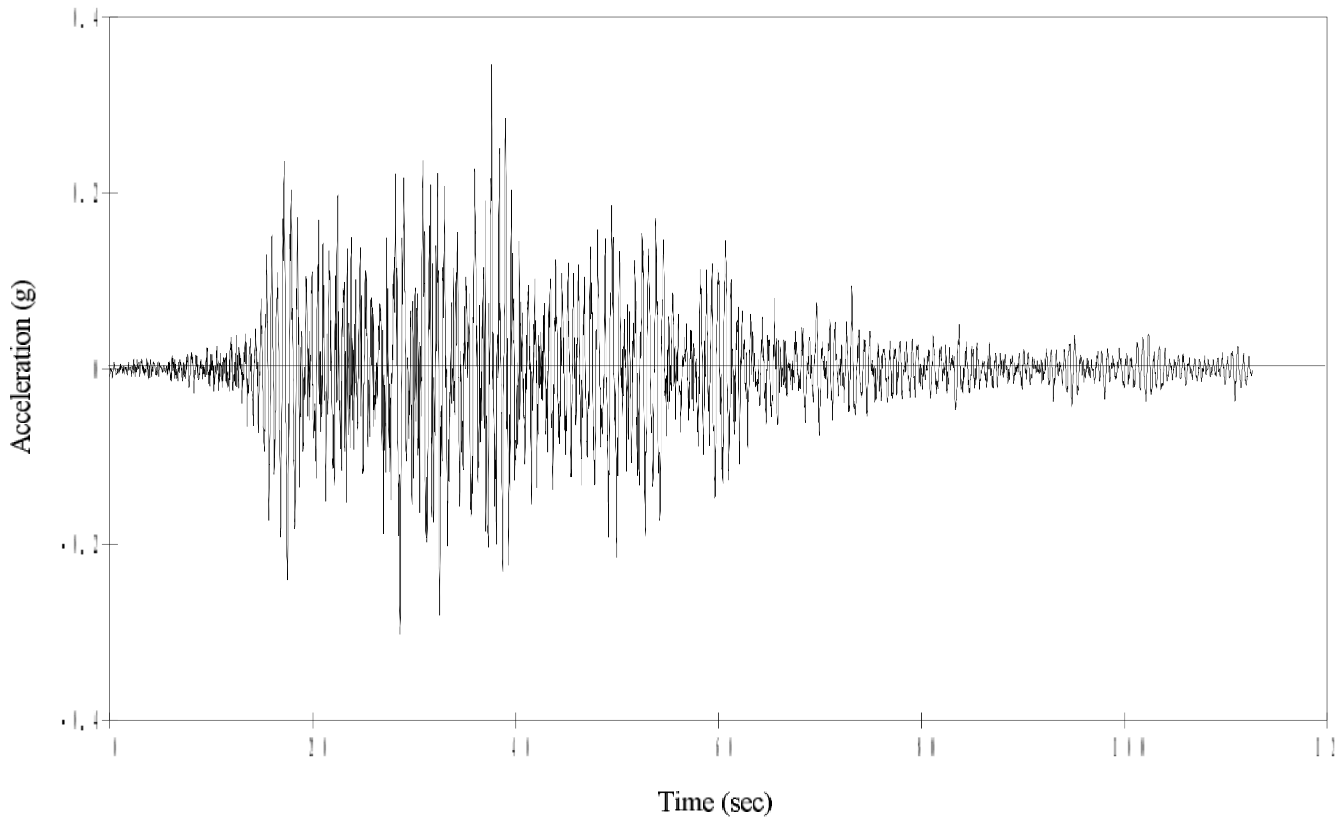

Figure 6.12 Ground acceleration Record for S-W Component of Vina Del Mar 1985 Earthquake

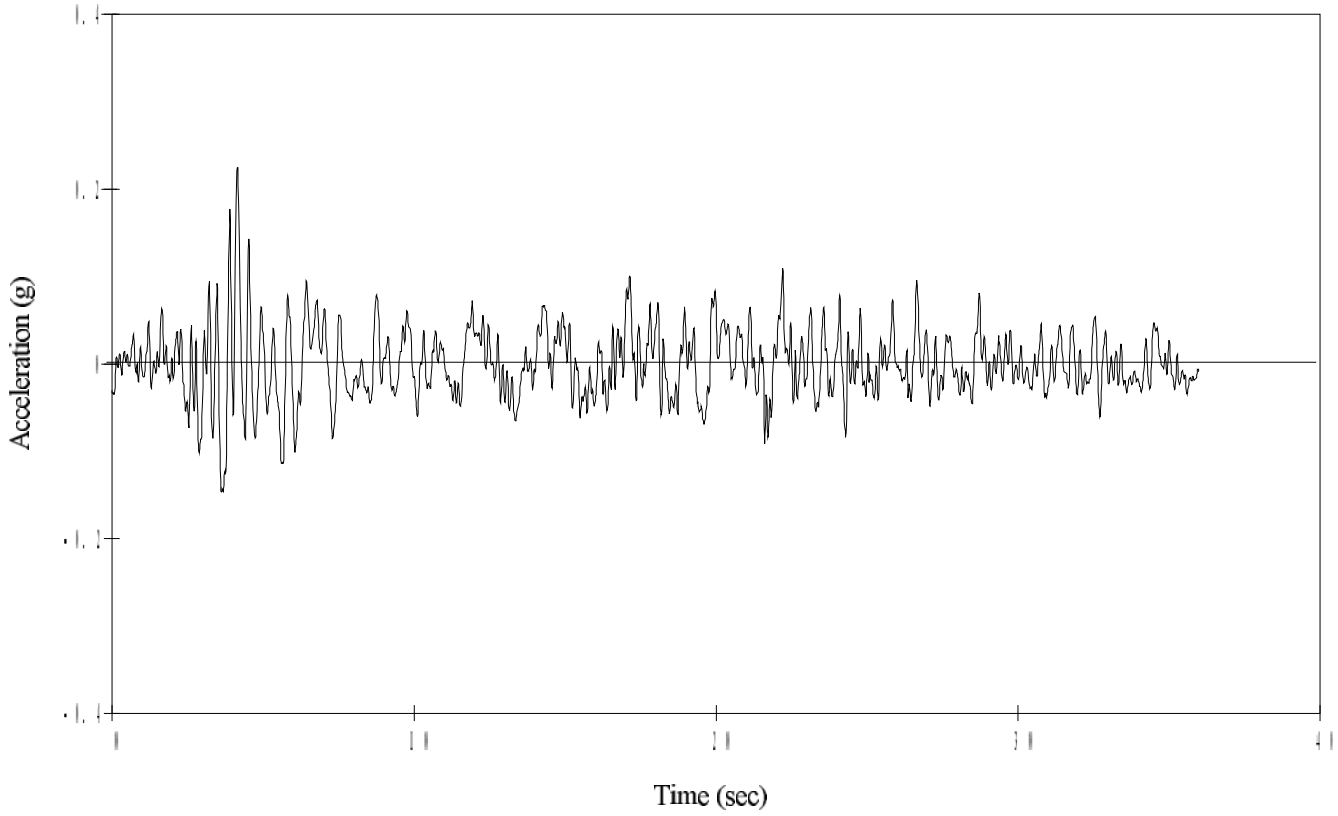

Figure 6.13 Ground Acceleration Record for N-S Component of Hachinohe 1968 Earthquake

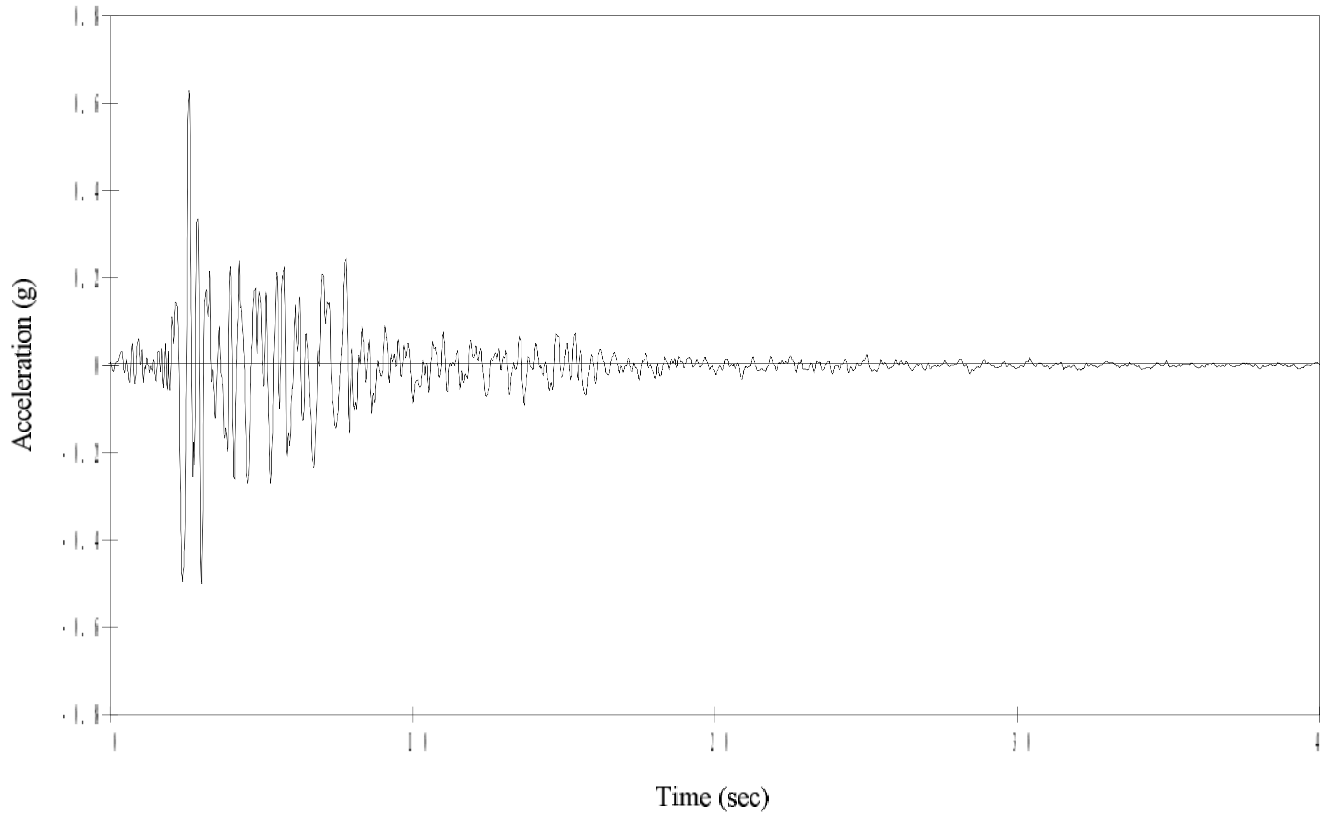

Figure 6.14 Ground Acceleration Record for N-S Component of Loma Prieta-Corralitos 1989 Earthquake

some of the configurations examined. Spectral intensity is defined as the area under the velocity spectrum curve with 2% critical damping as follows:

$$SI = \int_{T_1=0.1}^{T_2=2.5} S_v(T,2\%) \tag{6.5}$$

The spectral intensity for each of the records was calculated, then the ratio of the spectral intensity for El Centro (with 0.4g PGA) and the spectral intensity for each of the unscaled records was used to scale each record up or down. Information about each of the earthquakes and their PGA before and after scaling is shown in Table 6.4.

Table 6.4 Earthquake Ground Records

Earthquake Record	Direction	Maximum Acceleration	Maximum Scaled Acceleration
El Centro 1940	N-S	0.348g	0.400g
Vina del Mar 1985	S-W	0.348g	0.367g
Hachinohe 1968	N-S	0.225g	0.333g
Corralitos 1989	N-S	0.629g	0.611g

The resulting earthquake records were all scaled to different PGA. The elastic acceleration, velocity, and displacement spectra for 2% damping and the scaled earthquake records are shown in Figs. 6.15, 6.16, and 6.17, respectively. The acceleration spectra indicate that response to Vina del Mar and Corralitos are generally higher than for El Centro and Hachinohe for structures with periods between 0.5 and 1 second. However, for periods larger than approximately 1 second, acceleration response for El Centro and Hachinohe is typically higher than for Vina del Mar and Corralitos. This is especially clear for the Hachinohe record which exhibits high spectral accelerations for periods between 2 to 3 seconds.

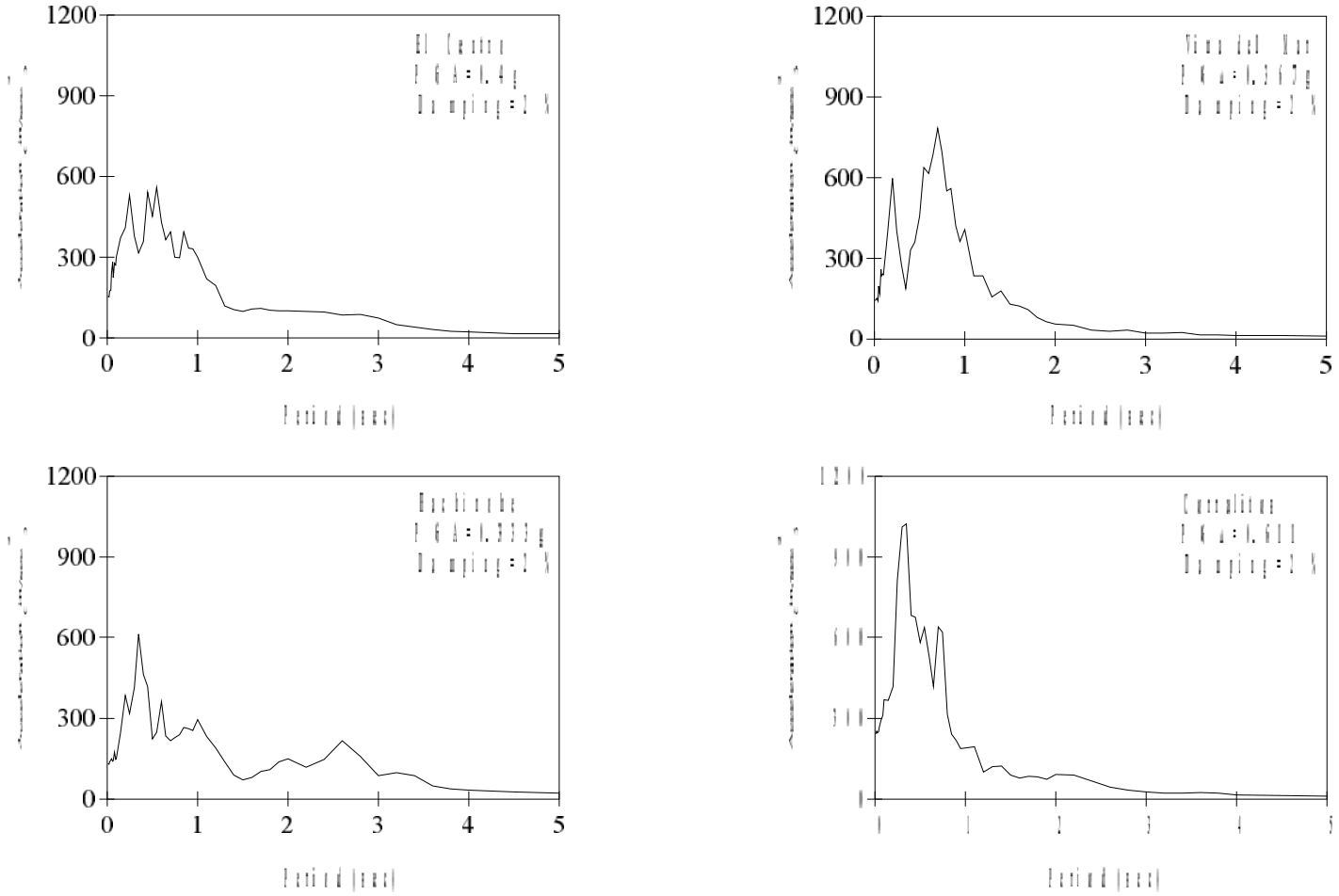

Figure 6.15 Acceleration Spectra for the Scaled Earthquake Records

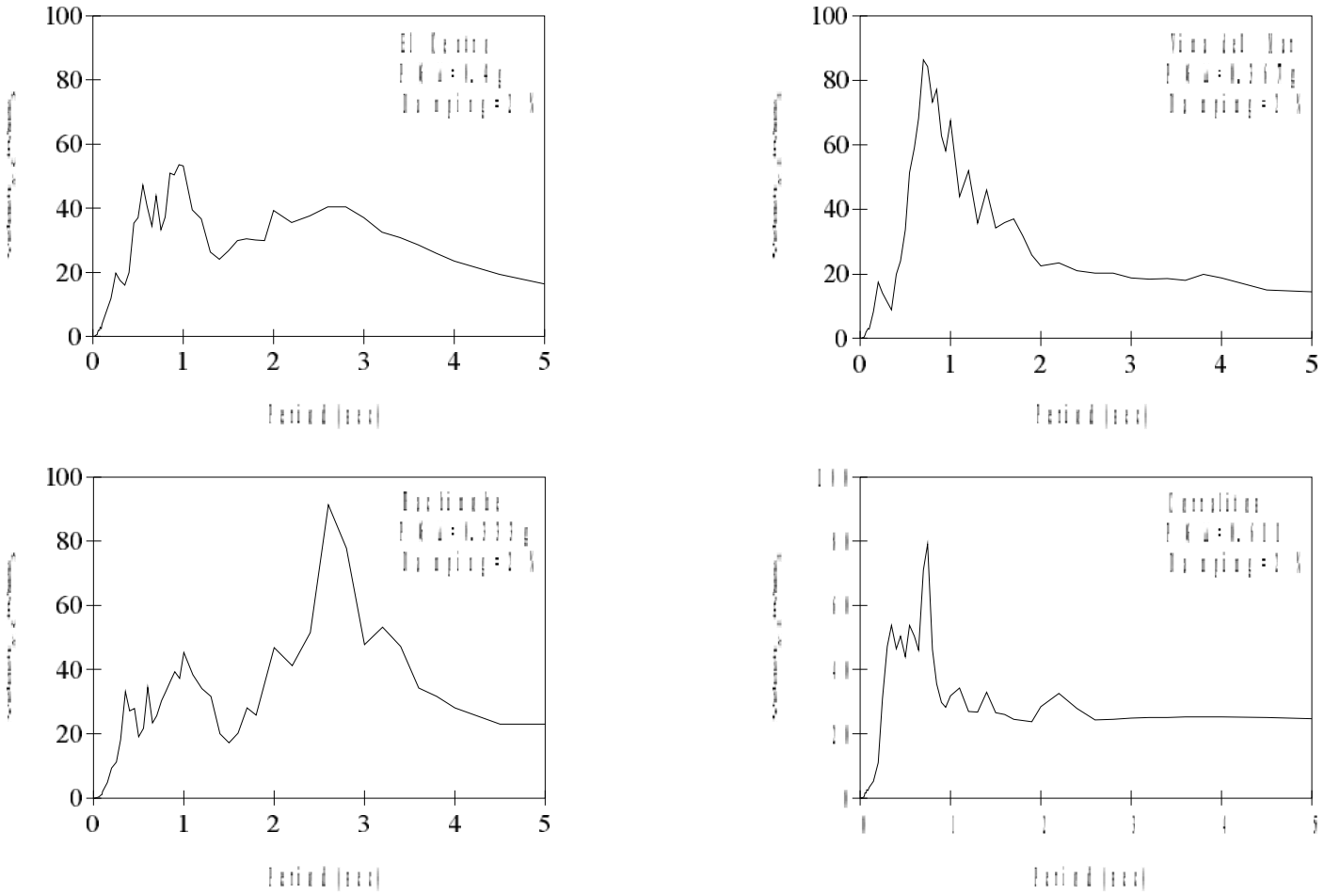

Figure 6.16 Velocity Spectra for the Scaled Earthquake Records

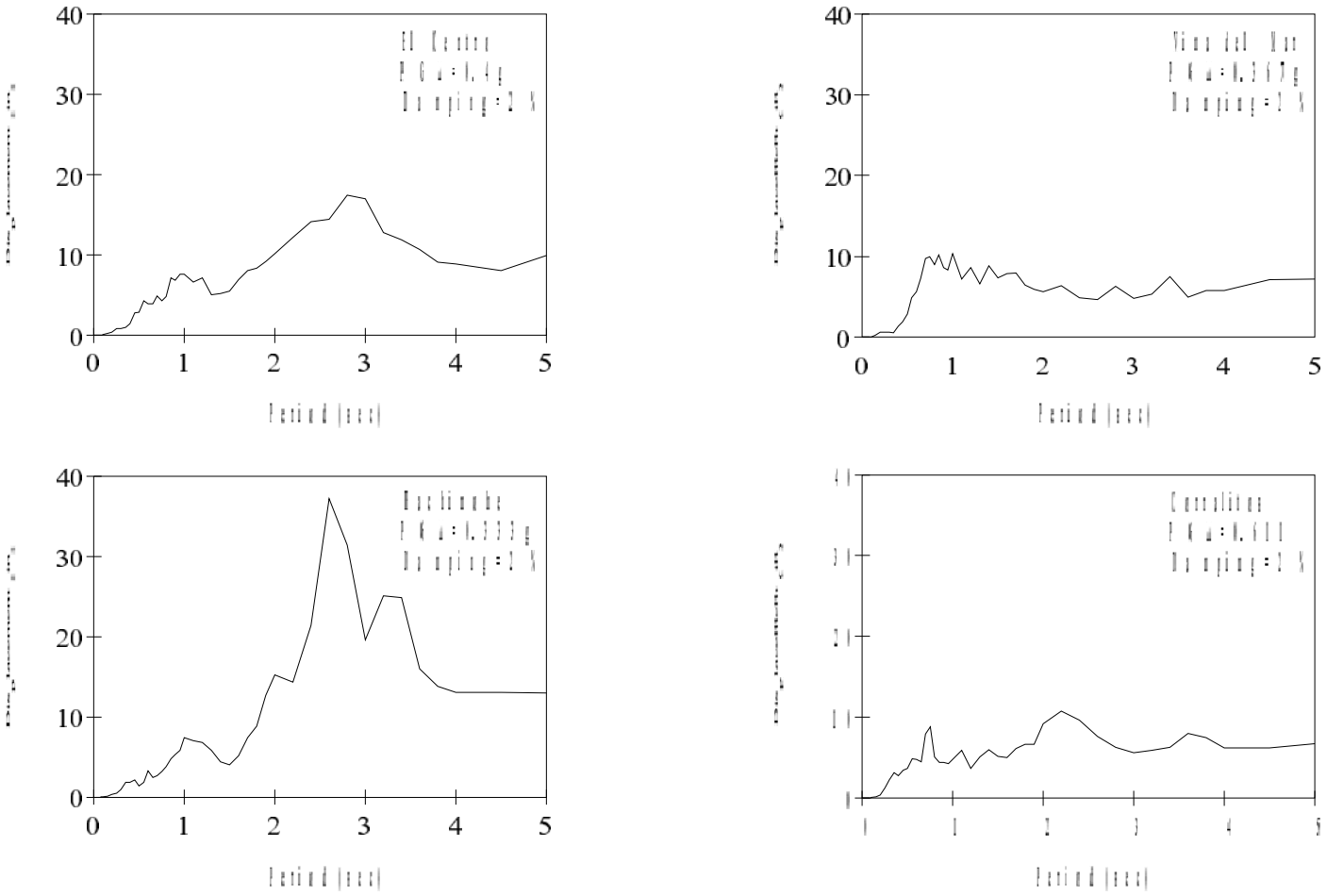

Figure 6.17 Displacement Spectra for the Scaled Earthquake Records

Spectral displacements , on the other hand, are substantially higher for the El Centro and Hachinohe records for periods higher than 1.5 seconds. The relevance of these observations will be evident in later discussion.

6.5 DYNAMIC RESPONSE ANALYSES

The two building frames described earlier were analyzed with a nonlinear time-history analysis program named IDARC. Each frame was subjected to the four records described in the previous section after being scaled to the corresponding PGA shown in Table 6.4. The nonlinear behavior of the connections was represented by the three different connection models described previously. Connection strengths for all cases were identical, and 2 percent damping was included in the analysis.

In the sections that follow, the computed responses for the different combinations of frame size, connection behavior, and ground motion are compared. In particular, story drifts, story shears, residual drifts, and ductility demands are compared.

6.6 RESULTS OF ANALYSES

Results from the analyses were prepared in tabular and graphical forms. For the latter case, plots of displacement and story shear versus time; and displacement, story drift, and story shear envelopes over the height of the building are presented. Results of each building are presented separately, and conclusions will be drawn later.

6.6.1 5-Story Frame

6.6.1.1 Period of Vibration

The initial fundamental periods of vibration for the different connection models are 0.89, 0.93, and 0.76 seconds for the frame with pinched, friction, and pretensioned connection models, respectively. These periods may be considered relatively high in comparison to a similar 5-story monolithic frame where uncracked section properties are typically used. The high period of vibration, especially for the pinched and friction models, is mainly attributed to the flexibility of the connection hardware and the existence of an open joint between the beams and column.

6.6.1.2 Floor Displacements

The displacement histories at the roof level for the various hysteretic models and earthquake records are shown in Figs. 6.18 through 6.21. The pretensioned connection hysteretic model consistently produced the maximum displacements for all earthquake records. Maximum displacements for the pinched and friction hysteretic models were very similar. The maximum displacement of all cases was calculated for the Hachinohe ground motion. The acceleration response spectrum for the Hachinohe ground motion (Fig. 6.15) indicated the record contains more longer-period components than the other ground motions. The roof displacement for the pretensioned connection case when subjected to the Hachinohe ground motion was 14.91 in., which corresponds with an average 1.78 percent drift ratio over the entire structure. Even though the initial period of the structure was 0.76 second, as soon as significant yielding occurred in the structure, the period was elongated. The period of vibration of the structure during the Hachinohe ground motion can be

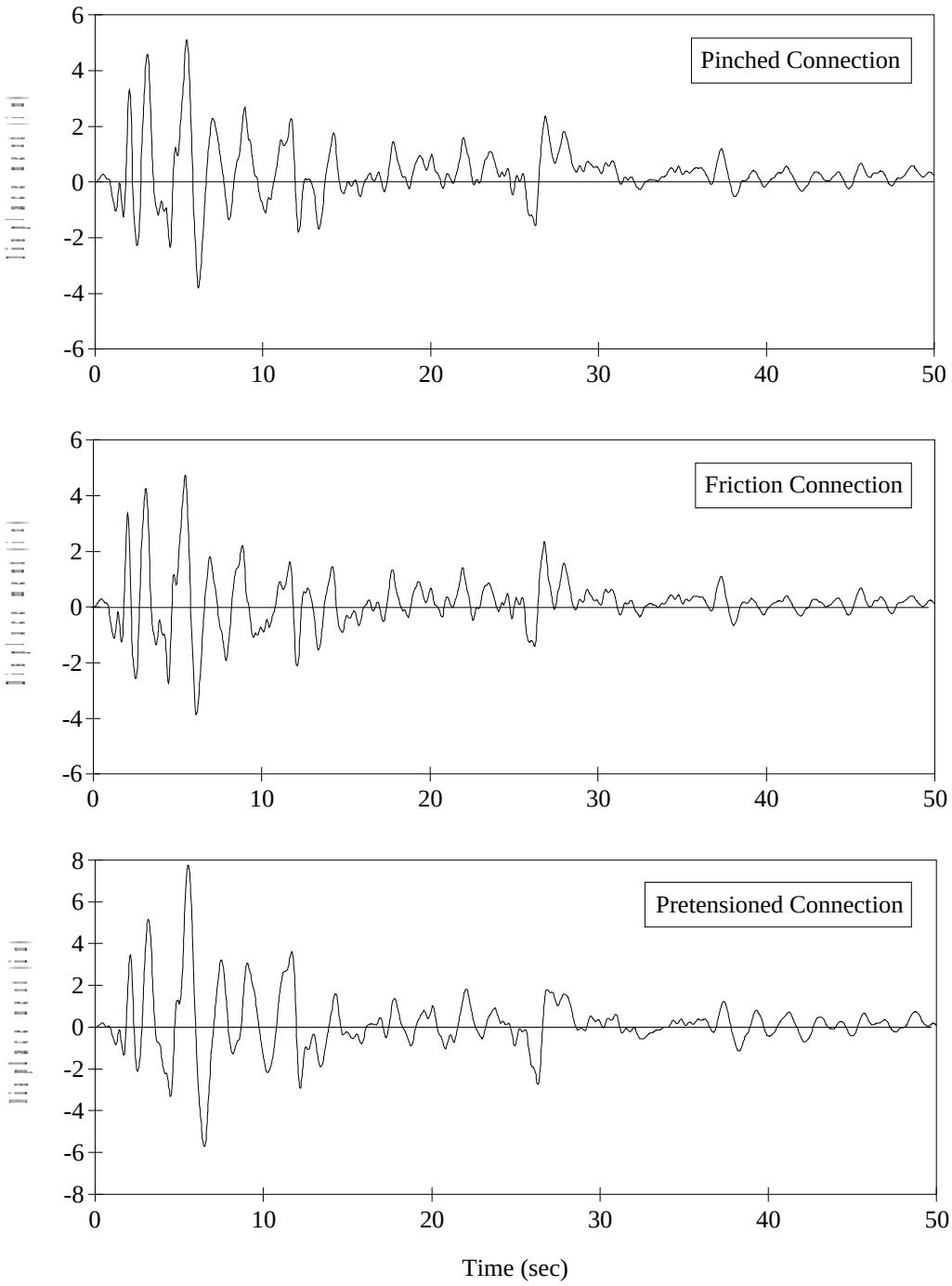

Figure 6.18 Displacement Histories for the Roof of the 5-Story Frame with Different Connection Models Subjected to the El Centro Ground Motion

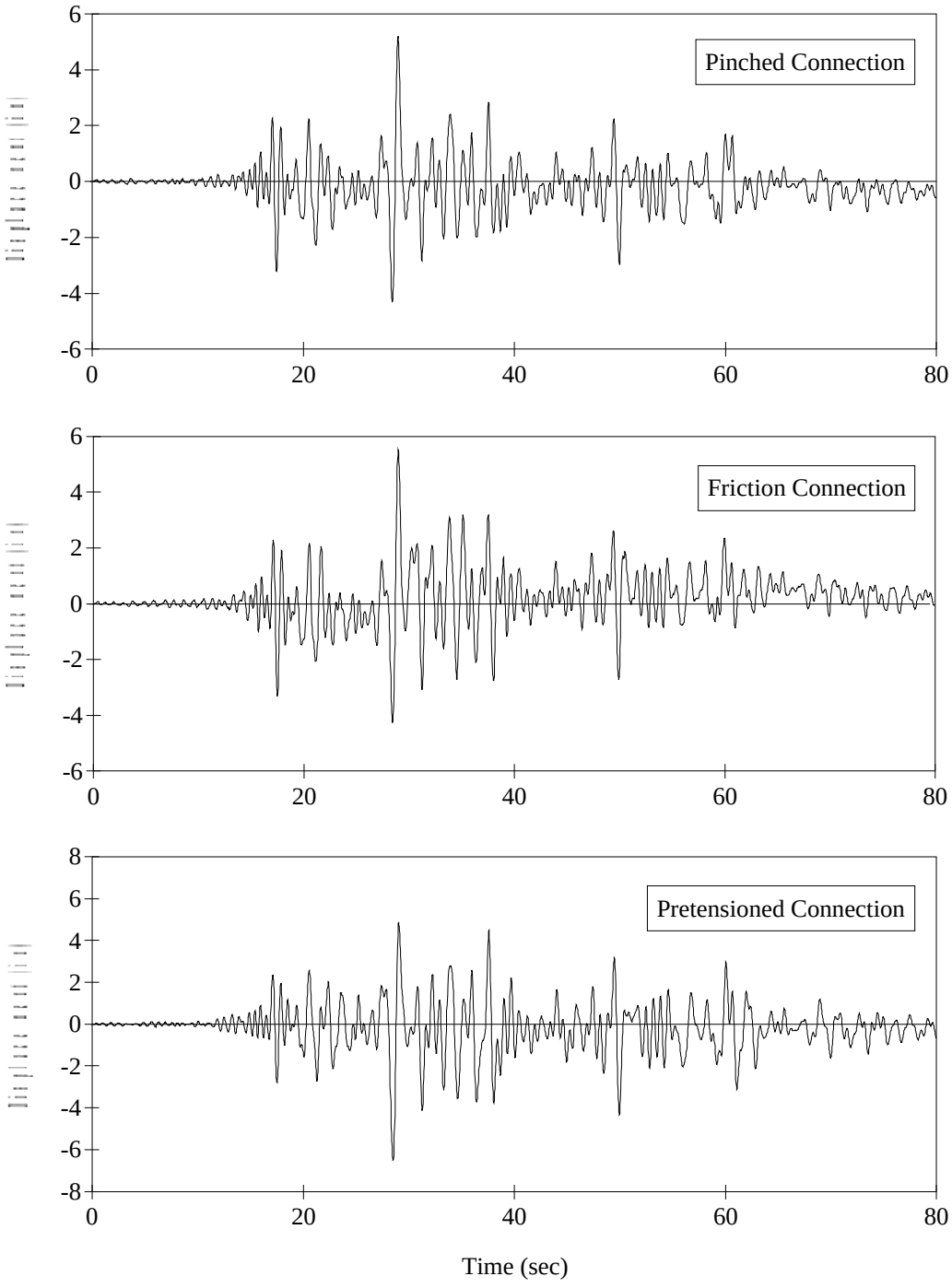

Figure 6.19 Displacement Histories for the Roof of the 5-Story Frame with Different Connection Models Subjected to the Vina del Mar Ground Motion

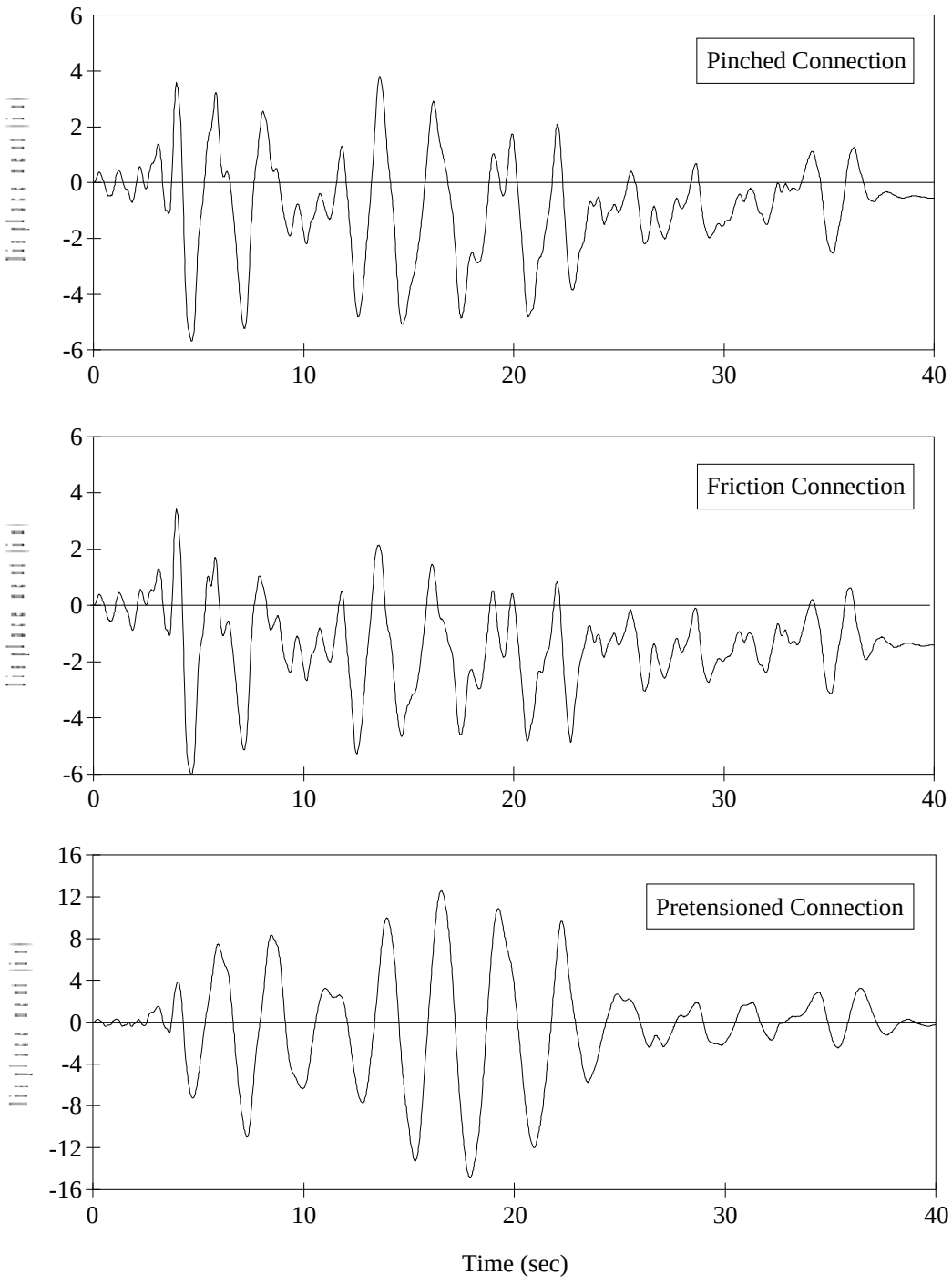

Figure 6.20 Displacement Histories for the Roof of the 5-Story Frame with Different Connection Models Subjected to the Hachinohe Ground Motion

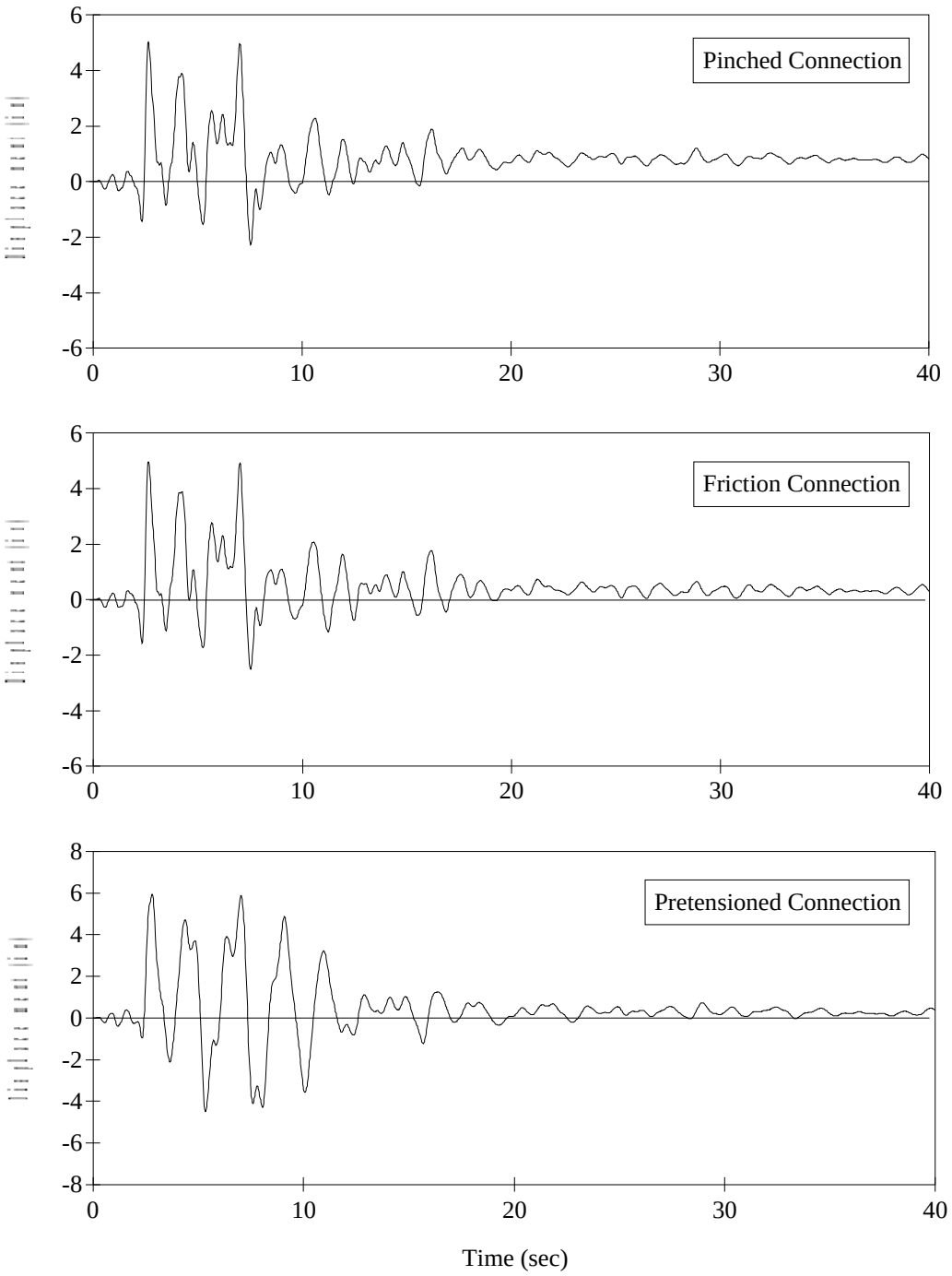

Figure 6.21 Displacement Histories for the Roof of the 5-Story Frame with Different Connection Models Subjected to the Corralitos Ground Motion

approximated from Fig. 6.20 to be 2.5 to 3 seconds. Using the period

approximation and the displacement response spectrum for the Hachinohe ground motion (Fig. 6.17), the structure is expected to experience large displacements. Unlike the response for the other hysteretic models where the maximum response occurred at approximately 5 seconds into the record, the maximum response for the pretensioned hysteretic model occurred much later at approximately 18 seconds. This may be due in part to the minimal amount of energy dissipation in the system. Once the structure yielded at approximately 5 seconds, the response continued to build as the period lengthened toward the high-displacement response region.

Residual displacements were computed for all connection models. However, the residual displacements were typically small, and in no case exceeded 0.2 percent for the overall building height. The Corralitos record is a good example of a base motion that might lead to significant residual displacements. The maximum acceleration occurred very early in this record and was substantially greater than the accelerations that followed. This single, large acceleration pulse was large enough to impart inelastic deformations early in the record. There did not appear to be a significant peak acceleration in the opposite direction that was capable of yielding the structure and returning it close to its original position. This was a major concern in developing the friction connection, because once the connections slip significantly in one direction, they may remain in that position. The maximum residual drift (0.35 percent) occurred in the first story of the frame incorporating friction connections when subjected to the Hachinohe record. Although the largest residual displacements occurred for the frame with friction connections, these displacements were still relatively small and could probably be removed by loosening the friction connections, righting/aligning the structure, and retensioning the bolts in the friction connections.

The displacement envelopes for the three hysteretic models and four ground motions are shown in Fig. 6.22. The pretensioned connection model yielded the

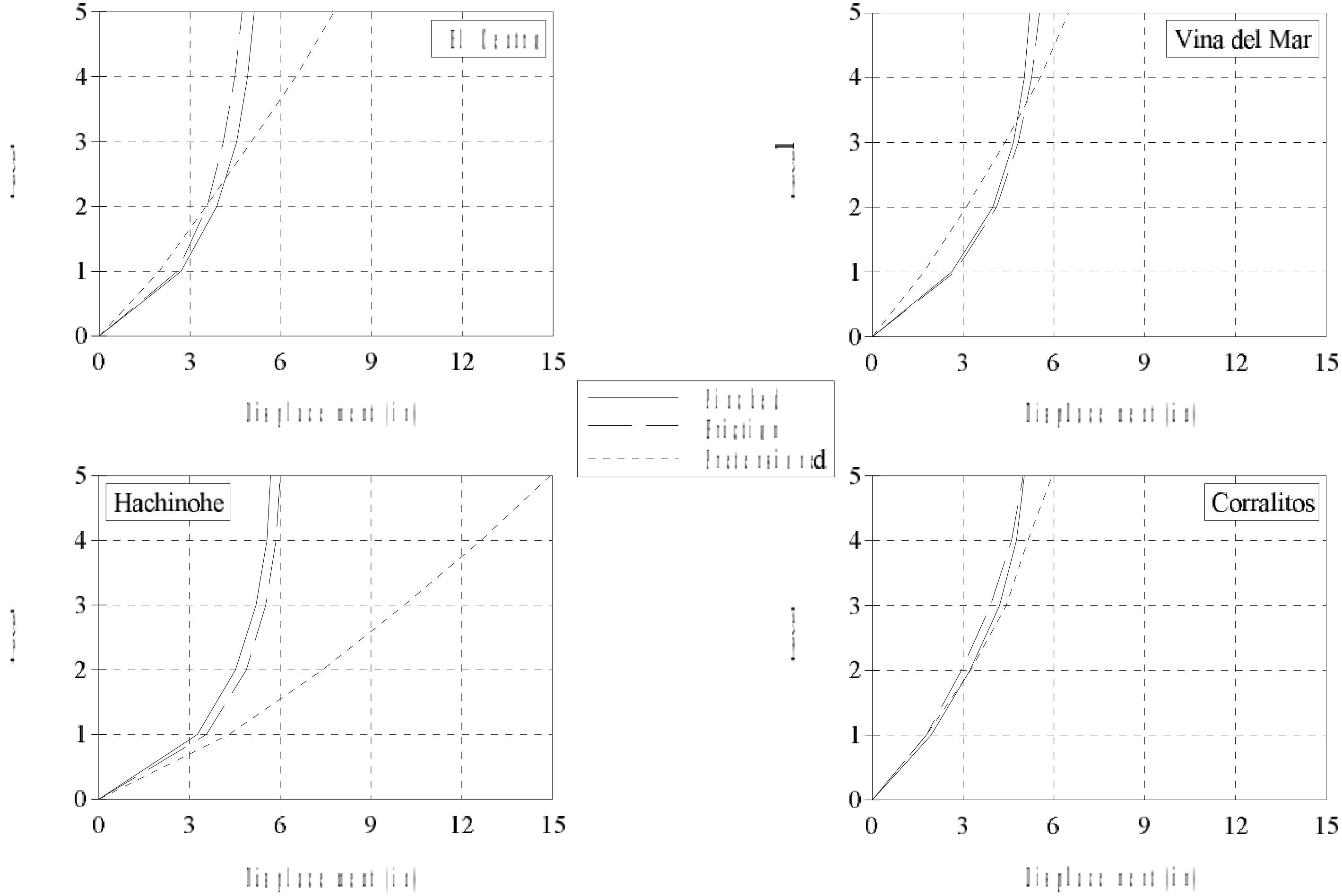

Figure 6.22 Floor Displacement Envelopes for the 5-Story Frame

largest displacements in the upper stories of the structure. The pinched and friction connection models produced lateral displacement profiles that were very similar. The pretensioned connection model, unlike the other two models, yielded displacement envelopes that nearly resembled straight lines. This resulted in higher as well as lower interstory drift ratios at certain levels as will be explained in the next section.

Table 6.5 Maximum Roof Displacements and Building Drifts for 5-Story Building

	Pinched Connection		Friction Connection		Pretensioned Connection	
	Displ. (in)	Drift (%)	Displ. (in)	Drift (%)	Displ. (in)	Drift (%)
El Centro	5.12	0.61	4.73	0.56	7.76	0.92
Vina del Mar	5.20	0.62	5.52	0.66	6.49	0.77
Hachinohe	5.68	0.68	6.00	0.71	14.91	1.78
Corralitos	5.01	0.60	4.99	0.59	5.95	0.71

The maximum roof displacements and building drifts are shown in Table 6.5. As mentioned previously, the maximum building drifts for the pinched and friction connection models are consistent for all earthquake records. The maximum building drift for all three hysteretic models occurred for Hachinohe ground motion. However, in the case of the pretensioned connection model, the maximum building drift was 1.78 percent. This drift is considered excessive and could lead to moment magnification and perhaps frame instability. The UBC [22] implies a maximum inelastic drift of $3R_w/8 = 4.5$ times the elastic drift of 0.25 percent for structures with a fundamental period of vibration greater than 0.7 seconds. This leads to a maximum drift of 1.125 percent, and suggests that the 1.78 percent drift is unacceptable from a code perspective.

6.6.1.3 Interstory Drifts

Interstory drift is defined as the ratio of the difference in the horizontal displacement between two consecutive floors to the story height, which was 18 feet for the first story and 13 feet for all other stories. This ratio is often presented as a percentage of the story height. The interstory drift envelopes for the three hysteretic models and four earthquake records are shown in Fig. 6.23.

The interstory drift envelopes for the frames with pinched and friction hysteresis models are very similar. The highest interstory drift for these models is in the first story. Interstory drifts decrease with increasing height. The largest interstory drift for these two models is approximately 1.5 percent for the Hachinohe ground motion.

Interstory drifts for the frame incorporating the pretensioned hysteretic model are quite different from the drifts calculated for the other two hysteretic models. In general the interstory drift for the first story is less than those for the other two models, except for the Hachinohe ground motion. Above the ground story, interstory drifts for the pretensioned hysteretic model decrease or remain relatively constant with increasing height. The approximately constant interstory drifts for all but the Hachinohe record indicate that the inelastic rotations and ductility demands on the members is almost constant over the entire height of the building. Ductility demands will be examined more closely later in this chapter.

The interstory drifts encountered here must be compared with some acceptable interstory drift. As mentioned earlier, the UBC implies a maximum inelastic interstory drift of 1.125 percent for structures classified as special moment-resisting frames and with a fundamental vibration period greater than 0.7 second. In general, the interstory drifts were less than this implied interstory drift limit, except for the Hachinohe ground motion where frames with hysteresis for pinched behavior

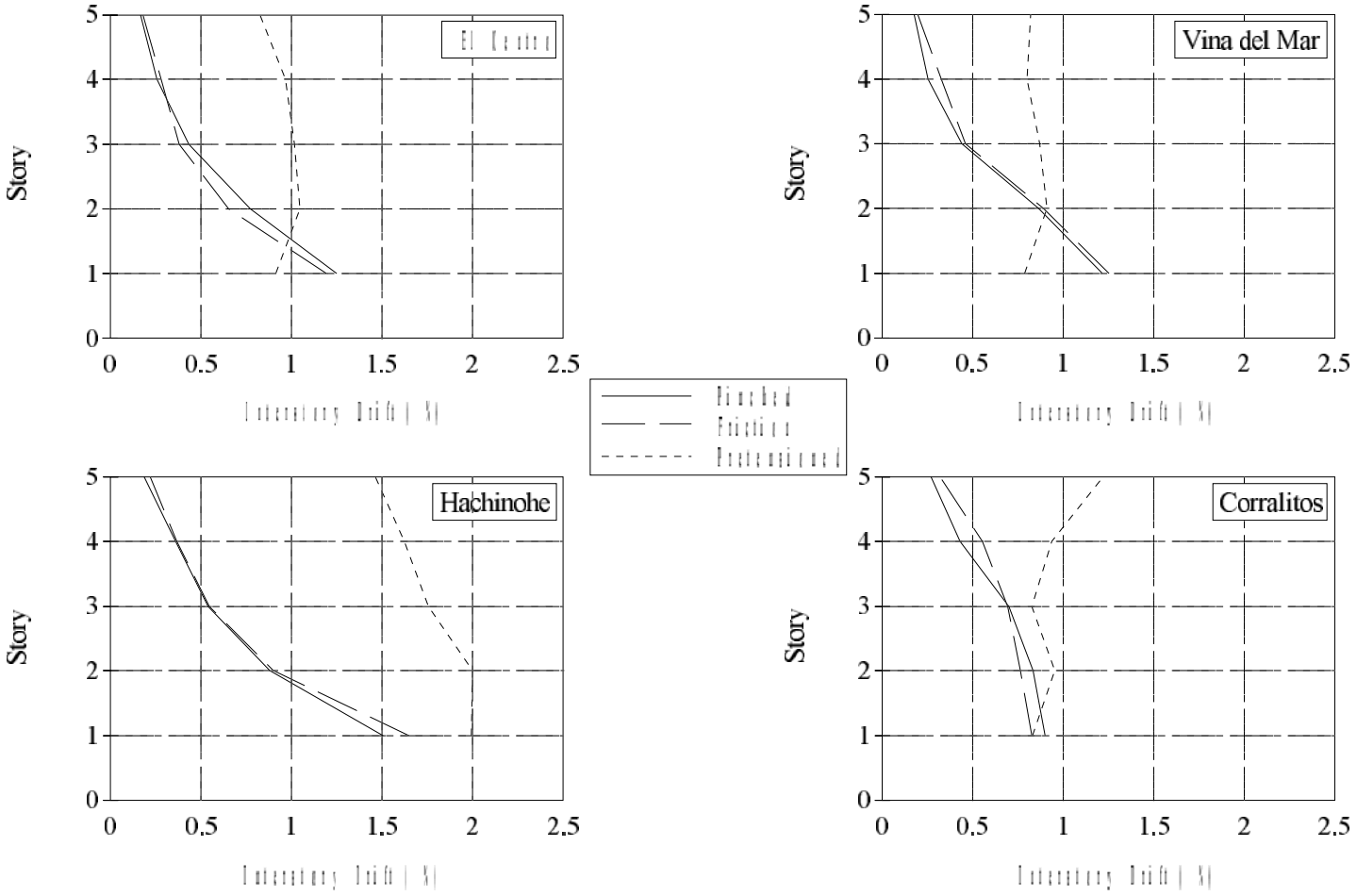

Figure 6.23 Interstory Drift Envelopes for the 5-Story Frame

and friction connections attained approximately 1.5 percent interstory drift in the first story, and the frame incorporating the pretensioned hysteretic model reached 1.5 percent or more interstory drift in all stories. The interstory drifts for the frame incorporating the pretensioned hysteretic model suggests that such a structural system with similar initial stiffness characteristics should be designed using a reduced R_w value (lower than the R_w = 12 used to design the structures studied here).

6.6.1.4 Story Shears

The base shear histories for the different connection models and ground motions are shown in Figs. 6.24 through 6.27. The base shear waveforms for pinched and friction connection behavior reach approximately the same maximum values at the same time. In addition, the overall shape of the waveforms is quite similar. The waveforms for the frame with pretensioned connections had a significantly lower maximum base shear (approximately 20 percent of the maximum base shear for the other systems). In addition, most of the local maxima observed in the waveforms for pinched and friction connection behavior are quite subdued for all but the Hachinohe ground motion.

The story shear envelopes for all combinations of hysteretic models and base motions are shown in Fig. 6.28. Story shear envelopes are approximately the same (within 10 percent) for pinched and friction connection behavior for all base motions. The story shear envelopes for the pretensioned connection model were unlike envelopes for the frames with pinched and friction connections. Story shears were typically less than values for the pinched and friction connection systems, in some cases by as much as 35 percent.

The maximum story shears generally occurred at the base for all three hysteretic models. For the Corralitos ground motion, the maximum story shear

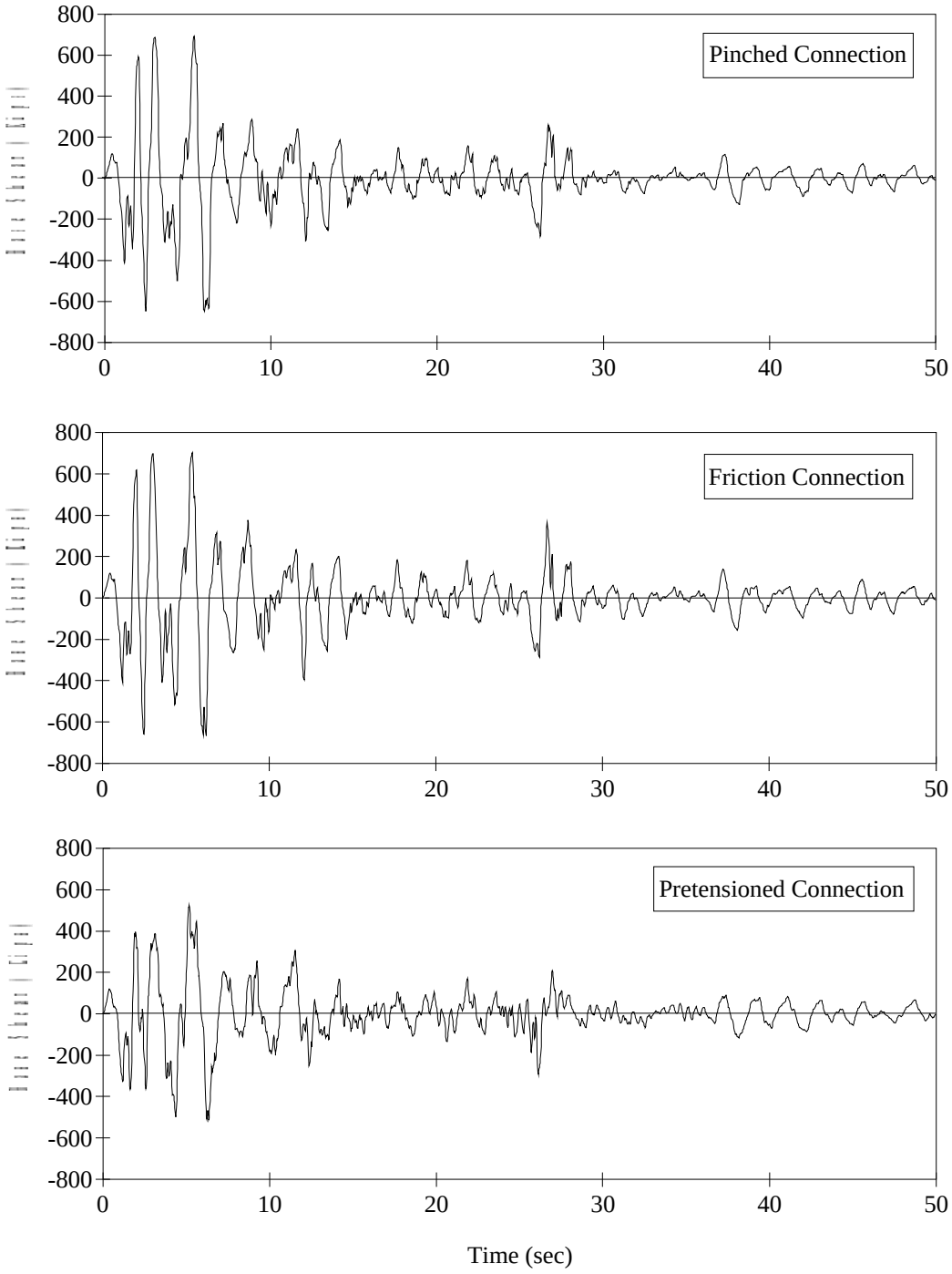

Fig. 6.24 Base Shear Histories for the 5-Story Frame with Different Connection Models Subjected to the El Centro Ground Motion

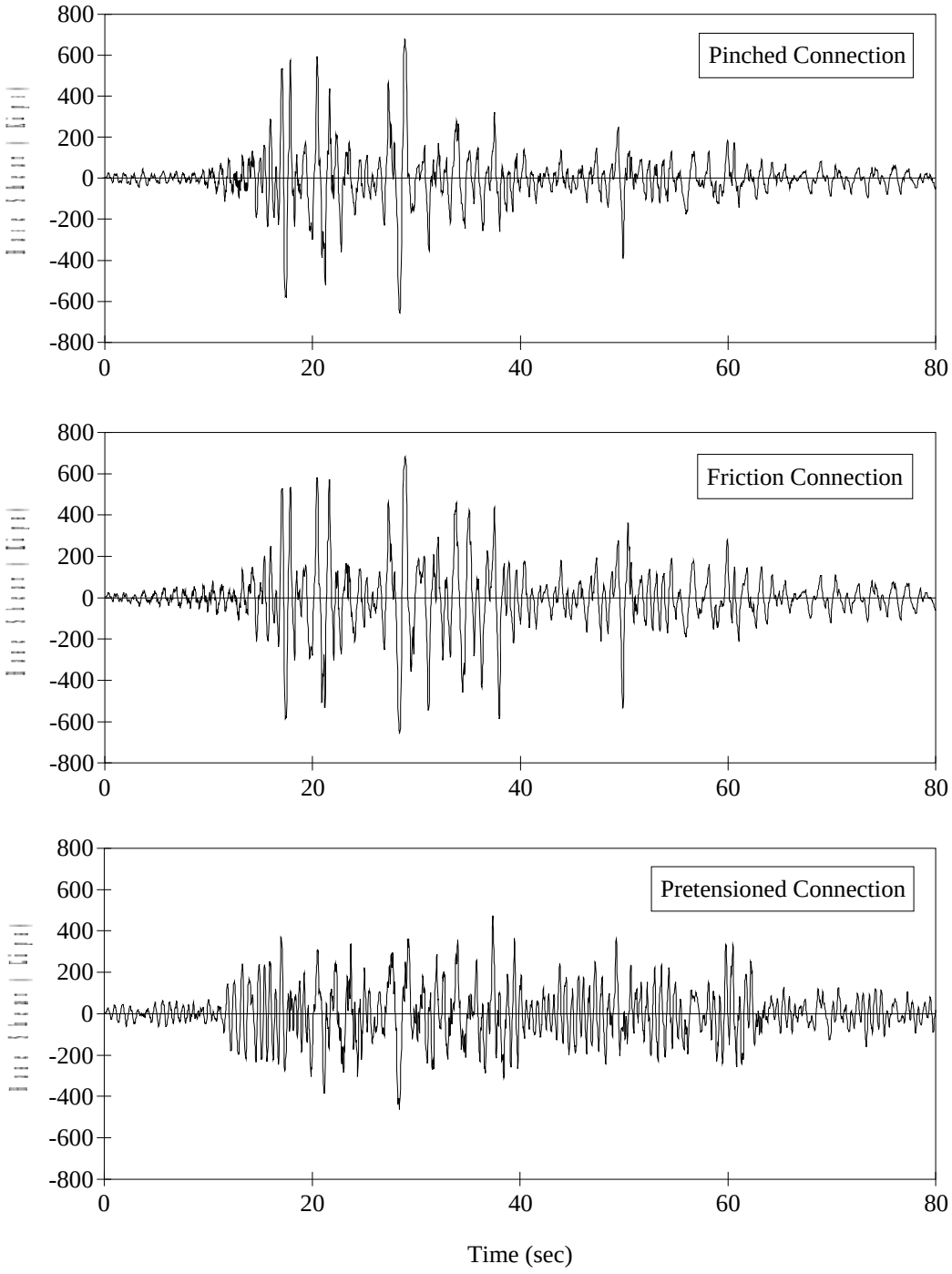

Fig. 6.25 Base Shear Histories for the 5-Story Frame with Different Connection Models Subjected to the Vina del Mar Ground Motion

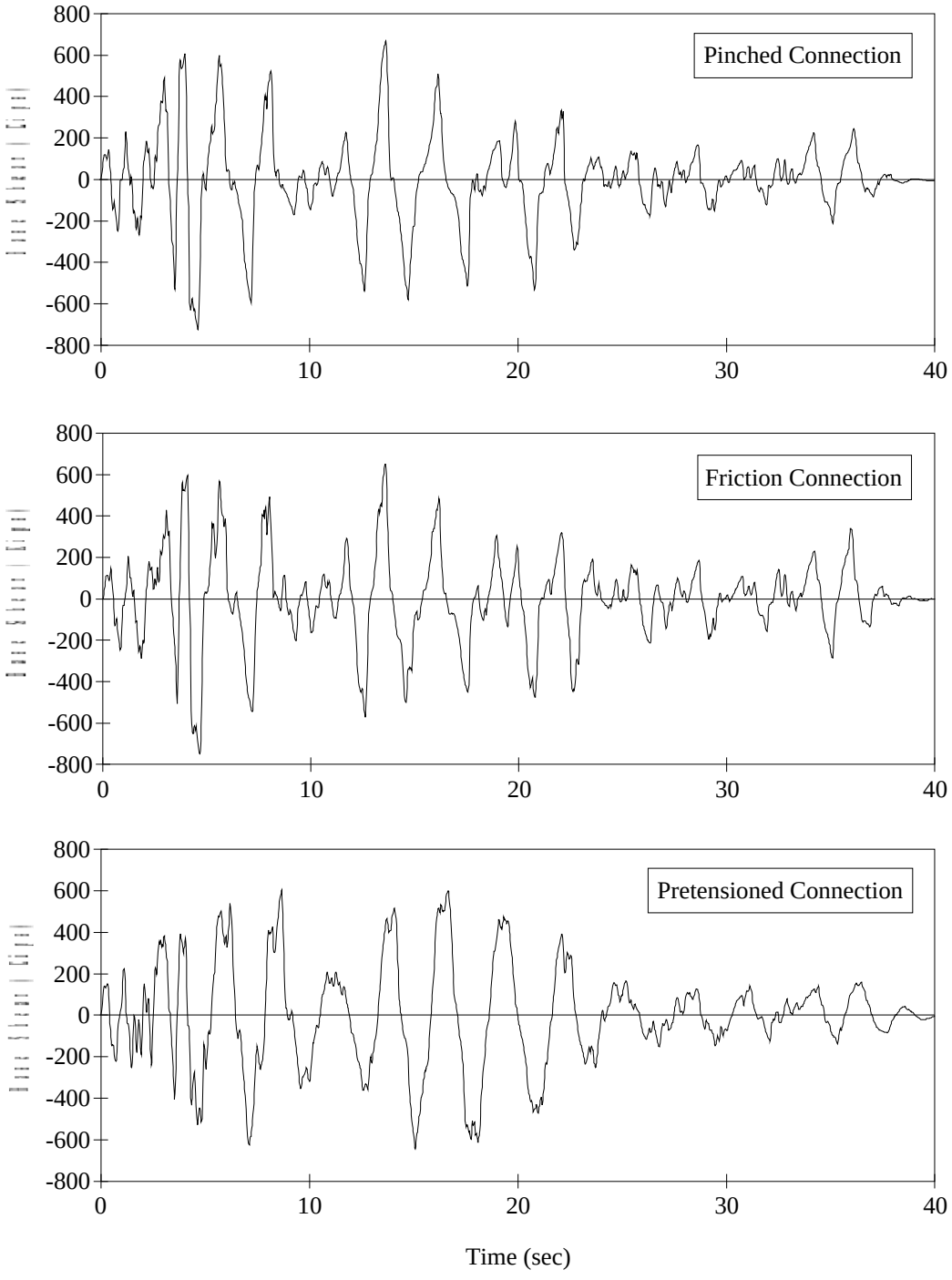

Fig. 6.26 Base Shear Histories for the 5-Story Frame with Different Connection Models Subjected to the Hachinohe Ground Motion

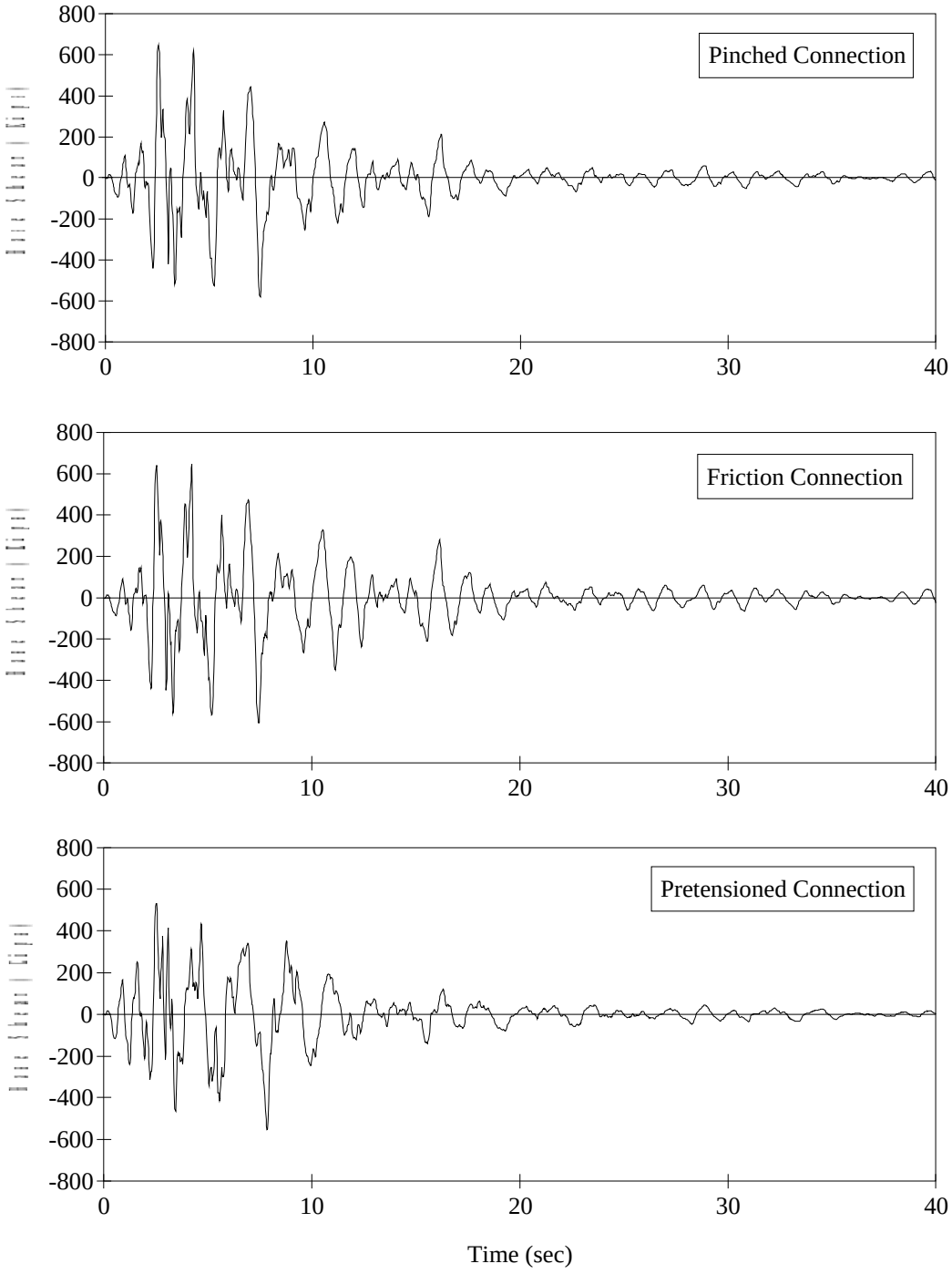

Fig. 6.27 Base Shear Histories for the 5-Story Frame with Different Connection Models Subjected to the Corralitos Ground Motion

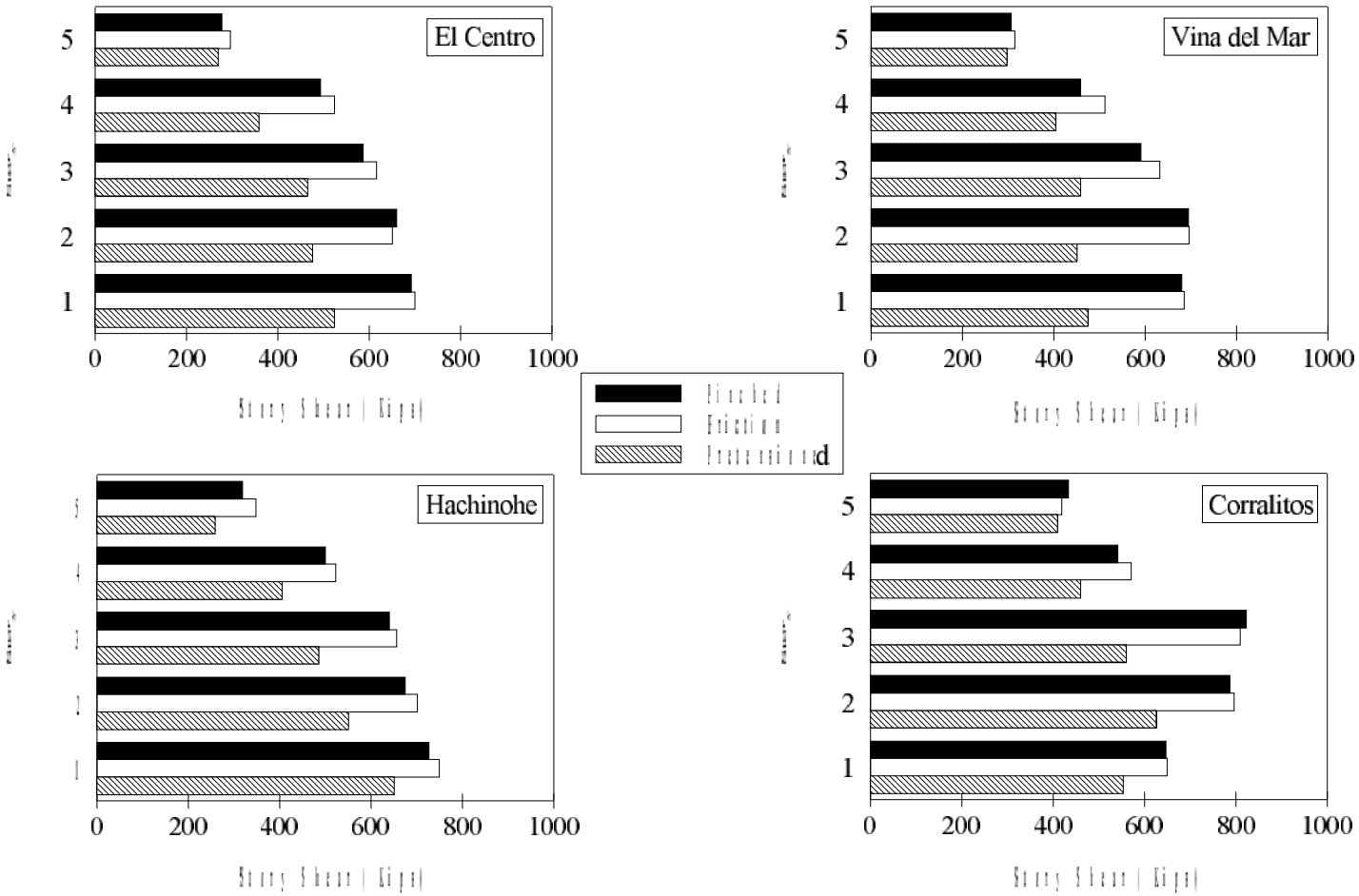

Figure 6.28 Story Shear Envelopes for the 5-Story Frame

occurred at the second story for the pretensioned connection model, and at the third story for the other two models. Story shear envelopes for the other base motions more closely resemble story shear distributions for systems dominated by first-mode behavior; maximum story shears typically decrease only slightly from the base shear value to the second or third story shear. The acceleration response spectrum for the Corralitos record (presented in Fig. 6.15) indicates high response for short periods. The irregular shape of the story shear envelopes (which were not very different from story shears at the instant of maximum story shear) suggest that higher modes of response were excited by the Corralitos record.

6.6.1.5 Inelastic Action

To examine the extent of damage experienced by each of the frames, the nonlinear response locations are noted in Figs. 6.29 through 6.32. The term "nonlinear response" is used instead of "plastic hinge" because the term plastic hinge implies inelastic material behavior occurs at particular member sections. This is not the case for most of the systems examined here. For the frame system with pinched behavior in the connections, the symbol at the end of the beams simply means that yielding was initiated. For systems with friction connections, the symbol means that slip occurred at this connection location. For the system with pretensioned connections, the symbol means that the crack at the beam-column interface is completely open. The symbol at the end of a column indicates that yielding of reinforcement was initiated. For the frames studied, the moment-axial load combinations were always less than the balanced point, so yielding of column reinforcement was possible. To determine the extent of nonlinear response and determine which system suffered more damage, moment-curvature relationships must be studied. This is done in the next section.

CHAPTER 7

SUMMARY AND CONCLUSIONS

7.1 INTRODUCTION

Precast concrete moment-resisting frames are rarely used in seismic regions of the US because of a lack of explicit design recommendations in codes of standard practice, such as the UBC [22]. The UBC classifies a precast frame system as an "undefined structural system". Such a system cannot be used unless it is shown through tests and/or calculation that its lateral force resistance and energy absorption are equivalent to one of the structural systems defined in the code. As a result, the US-PRESSS program was initiated to address this need. The ultimate objective of the program is the development of design recommendations for precast concrete frame systems for use in seismic regions.

As part of the US-PRESSS program, a study was undertaken at the University of Texas at Austin to experimentally and analytically investigate different types of precast frame connections/systems for use in seismic-resistant buildings.

7.2 SUMMARY OF EXPERIMENTAL PROGRAM

The US-PRESSS program concentrated on "ductile connection" concepts. A ductile connection concentrates inelastic or nonlinear action in connecting elements while the precast members remain virtually elastic. This is in sharp contrast to "rigid connections" where the connecting elements are proportioned to have more strength than the precast beams. There has been substantial research conducted on this type of connection, especially in Japan and New Zealand [7,25,31]. Four types of ductile connections were considered in this study: tension/compression yielding,

where energy is dissipated through tension and compression yielding of connecting elements; friction, where energy is dissipated through slip between connecting elements; nonlinear elastic, where nonlinear behavior is achieved through crack opening and closing at the interface between each prestressed beam and column; and shear yielding, where energy is dissipated when yielding occurs in steel elements similar to shear links used in an eccentrically-braced steel frame. Only the first three connection types were tested in this study.

Four half-scale beam-column subassemblages representing interior connections in the lower stories of a 15-story frame were tested. Two connections represented the tension/compression yielding concept (DB-TC and GJ-TC). One connection represented the friction concept (GJ-FR). One connection represented the nonlinear elastic concept (PT-NE).

Specimen DB-TC utilized vertical haunches at the end of the beams, that contained ducts, to connect the beams to the columns. High-strength threadbars were inserted through the ducts and threaded into Lenton couplers that were embedded in the column, then the ducts were grouted.

Specimen GJ-TC utilized corbels and vertical high-strength dowels to connect the bottom of each beam to the column. The vertical dowels were intended to prevent uplift of the beam ends and permit rotation of the beams about the beam-corbel connection. Beams contained ducts with sufficient tolerance to slip the beams over the dowels. The voids around the dowels were then grouted and nuts were threaded onto the dowels to prevent beam uplift. Conventional reinforcing bars in the top of the beams were threaded into Lenton couplers that were embedded in the column, then the top 6 inches of the beams was cast in place. A 1 in. gap over the top 75 percent of the beam depth was left between the beams and column to allow the beam top reinforcement to yield in both tension and compression.

Specimen GJ-FR utilized special connection hardware to enhance the energy dissipation capacity of the connection. The top of each beam was connected to the column by a steel plate assembly that was embedded in the beam and bolted onto

the side of the column. The plate assemblies contained 4 in. slotted holes that permitted sliding along vertical plate surfaces on the sides of the beams. Brass plates, 1/8 in. thick, were placed between all sliding surfaces to provide consistency in the level of force required to produce slip. The slip force was controlled by the clamping force applied to the plates and the friction coefficient. Corbels were also used in this specimen as part of the bottom connection. The bottom connection, which was intended to prevent uplift of the beam and to act as a pivot point for beam rotation, was considerably different from that used in Specimen GJ-TC. The major difference was the direct force path used in Specimen GJ-FR to transfer force from the beams to the column, which was unlike Specimen GJ-TC where force was transmitted through a complex path involving shearing of the vertical dowels.

Specimen PT-NE differed from other specimens in that the beam was continuous through the connection region. The beam was pretensioned using 20 centrally-located 3/8 in. strands pretensioned to 40 percent of f_{pu}. In order for the strands to remain elastic through 2 percent drift ratios, the strands were debonded through the joint and for 2 feet on each side of the joint.

Connection subassemblages were subjected to reversed cyclic deformation histories.

7.3 SUMMARY OF EXPERIMENTAL RESULTS

The most important information gathered from the tests was the story shear-drift ratio responses which provided insight into connection stiffness, stiffness degradation, energy dissipation, and residual drift.

Specimen DB-TC behaved well through cycles to 1 percent drift ratio. However, the use of high-strength bars resulted in less energy dissipation than would be anticipated for monolithic beam-column connections. During loading to 1.5 percent drift ratio the specimen failed as a result of concrete crushing in the beams.

The behavior of Specimen GJ-TC was reasonable through displacement cycles to a 2.5 percent drift ratio. However, pinching of hysteresis loops was very evident. Most of the pinching was attributed to shear and flexural deformations that occurred in the vertical dowels at the interface between the corbels and beams. Stiffness of the beam-corbel connection was generally less for loading in the positive direction as a result of gap opening at the bottom of the beam. Failure of Specimen GJ-TC resulted from fracture of the vertical dowels during displacement cycles to 3 percent drift ratio.

Specimen GJ-FR behaved well through the first two cycles to 3 percent drift ratio. Energy dissipation was enhanced by the friction connections as was intended. Testing was terminated during the third cycle to 3 percent drift ratio because a weld between plates in one of the friction connections failed as a result of larger-than-anticipated force being developed in the connection.

Specimen PT-NE yielded story shear-drift response through 2 percent drift ratios that can be characterized as bilinear-elastic. As a result, energy dissipation was minimal. Some pinching of the hysteresis loops occurred at low drift levels as a result of slip in the column bar couplers once the column cracked. Pinching would have been substantially less if commercial couplers intended for coupling conventional bars had been used. The strands remained essentially elastic throughout the test. Energy dissipation increased during cycles to 4 percent drift ratio due to deterioration of the joint. Strength degradation was observed during cycles to 5 percent drift ratio due to failure of the joint.

In general, energy dissipated by Specimen GJ-FR was the highest followed by Specimen GJ-TC, and then Specimen PT-NE. Flexibility in the beam-corbel connections in Specimen GJ-TC was the primary cause for the pinched hysteresis and lower energy dissipation, and failure of the joint in Specimen PT-NE was the primary cause for higher-than-anticipated energy dissipation.

Stiffness of Specimen PT-NE was the highest followed by Specimen GJ-TC and then Specimens DB-TC and GJ-FR. The assemblage of plates used in the top

connections and the high-strength bolts used in the bottom connections were the primary source of flexibility resulting in the low stiffness observed for Specimen GJ-FR.

7.4 SUMMARY OF ANALYTICAL PROGRAM

In the experimental program, the behavior of isolated subassemblages was investigated. The subassemblage tests provided detailed information about the load-deformation behavior of connections. In order to determine whether a frame built with similar connection details will perform well during an earthquake, the behavior of 5- and 15-story frames was evaluated using a program named IDARC which performs nonlinear dynamic time-history analysis. The 15-story frame was the same frame used as the prototype for the experimental program. The 5-story frame had the same footprint as the 15-story frame and was proportioned in a manner consistent with the larger prototype; using the equivalent lateral force procedure of the UBC for seismic zone 4, an R_w of 12, and S equal to 1.2. The primary reason for using two frames was to study the difference in behavior of frames characterized by two very different fundamental periods of vibration.

Three different hysteretic models were investigated. The first model represented pinched behavior similar to that observed for Specimen GJ-TC. The second model represented the behavior observed for Specimen GJ-FR. This model had very slight pinching of the load-deformation response. The third model represented the behavior observed for Specimen PT-NE. The hysteretic model was bilinear-elastic with limited energy dissipation and residual drift as observed during testing of Specimen PT-NE.

Each frame representing the three different connection models was subjected to four different earthquake records: N-S component of El Centro 1940, S-W component of Vina del Mar 1985, N-S component of Hachinohe 1968, and N-S component of Corralitos-Loma Prieta 1989. The earthquakes were scaled to give

equal spectral intensity. A hybrid configuration for the 5-story frame was studied to evaluate the behavior of a frame with a combination of pretensioned and friction connections.

7.5 SUMMARY OF ANALYTICAL RESULTS

The response quantities investigated in the analytical study were floor displacements, interstory drifts, residual drifts, story shears, and ductility demands. The pretensioned hysteretic model consistently yielded the largest displacements and interstory drifts for the top floors of the 5-story frame (the maximum roof displacement was 150 percent larger during the Hachinohe record), and for nearly all floors for the 15-story frame (25 percent larger at the roof level also during the Hachinohe record). The pinched and friction hysteretic models produced similar displacements and interstory drifts over the height of both structures for all ground motions. The interstory drifts were higher than for the pretensioned model for the first story of the 5-story frame except for the Hachinohe record (the maximum was approximately 55 percent during the Vina del Mar record). In general, interstory drifts were high for the first and second stories of the 5-story frame cases, approaching or exceeding the 1.125 percent maximum interstory drift implied by the UBC. Interstory drifts for the pinched and friction hysteretic models decreased rapidly for the upper stories, but decreased only slightly or increased for the pretensioned model for all but the Hachinohe record. Although interstory drifts for the pretensioned hysteretic model were slightly larger than for the other two models for the 15-story frame, interstory drifts (the maximum was approximately 0.67 percent) were significantly lower than for the 5-story frame. Residual drifts were more pronounced for the friction hysteretic model and 5-story frame. However, the maximum residual drifts occurred in the first story and were only 0.35 percent.

The pinched and friction hysteretic models produced very similar story shears, and the pretensioned connection model produced the lowest story shears.

The difference was in some cases as much as 25 to 35 percent lower than for the pinched and friction hysteretic models.

Column ductility demands for the 5-story frame were high, often exceeding the 4.5 value implied by the UBC. The demands were consistently high for the pinched and friction models, and varied considerably for the pretensioned model depending on the earthquake record. Ductility demands decreased with increasing height above the base. For the 15-story frame, ductility demands for all hysteretic models were low (only exceeding 1.75 at two locations).

Beam average ductility demands were also high for the 5-story frame for all hysteretic models (6.0 for the model with pinched behavior, 5.1 for the friction connection model, and 28.3 for the pretensioned connection model). Due to differences in the definition of ductility (actually, the definition of yield curvature) for the pinched, friction, and pretensioned hysteretic models, absolute comparisons of ductility demands are somewhat meaningless. However, computed interstory drifts for all hysteretic models were lower than interstory drifts obtained in laboratory tests. Therefore, the large computed ductility demands are not of great concern. Ductility demands on beams in the 15-story frame were considerably lower than for the 5-story frame.

A hybrid case for the 5-story frame was studied in which the middle bay of the frame had friction connections while the remainder of the frame utilized pretensioned connections. Displacements and interstory drifts were substantially reduced (up to 50 percent in some cases) compared to the frame with only pretensioned connections.

7.6 RECOMMENDATIONS AND CONCLUSIONS

Design and construction recommendations based on results of both the experimental and analytical studies are presented here.

- The experimental study demonstrated that it is possible to design and construct precast beam-column connections, where beams and columns are joined with ductile connecting elements, to withstand severe inelastic deformations resulting from earthquake forces.

- The use of only perimeter frames for lateral-force-resistance, which was a premise in the development of connection dimensions and strengths for the experimental program, revealed some potential problems during design of connections and during testing. It was concluded from the experimental program that the large forces required to be resisted by the perimeter lateral-force-resisting frames resulted in large beam and column sizes and large amounts of reinforcement that made detailing of the members extremely difficult. Consequently, high-strength steel was used in some specimens to reduce the amount of steel needed, typically in the connecting elements. The use of high-strength steel had an adverse effect on stiffness of Specimens DB-TC and GJ-FR. In addition, the use of high-strength steel in Specimen DB-TC resulted in very low energy dissipation even though the specimen reached 1.5 percent drift in one direction and 2 percent drift in the other direction.

The analyses performed on the 5-story frame indicated that interstory drifts tended to be quite large. The interior gravity-load-resisting frames would be expected to withstand these large deformations while maintaining gravity-load-carrying capacity. If gravity-load-carrying frames must be designed and detailed to accommodate these deformations, it may be more sensible to distribute the lateral-force-resisting system to all frames.

Furthermore, concentration of the lateral-force-resisting system on the perimeter of the structure will also place a substantial demand on the floor diaphragms and connections between the perimeter frames and floor diaphragms. The large distances between perimeter frames will necessitate that the floor diaphragms possess sufficient strength and stiffness to effectively transfer inertia

forces from the interior of the structure to the perimeter frames.

- Some of the connection details were substantially easier to fabricate and assemble than others. Specimens PT-NE and GJ-TC utilized reinforcing cages and connecting elements that were the simplest to assemble. Both specimens were efficient to erect; neither required temporary support of the beam element(s). However, Specimen GJ-TC required cast-in-place concrete on the top of the beams to complete the connection between the beam and column elements. Complex connection hardware and the shallow beam in Specimen DB-TC led to severe congestion of reinforcement in the beam elements, making this specimen the most difficult to fabricate. In addition, temporary support for the beams was required during erection.

- Due to the jointed nature of precast frames, special attention must be paid to the stiffness of the structure. Designers of such systems must be aware that overall flexibility of precast beam-column connections is very sensitive to the stiffness of the connecting elements. As a result, proportions of connections between precast elements may be controlled by stiffness rather than strength. For example, the use of high-strength steel to substitute for the strength of larger amounts of conventional steel will likely lead to insufficient stiffness.

- A clear path for transfer of forces between beams and columns is essential to achieve good behavior. Use of connecting elements that provided an indirect path for force transfer between precast elements was the common thread that precipitated the premature failure of Specimens DB-TC and GJ-TC. Improved behavior of the beam-corbel connection was demonstrated by Specimen GJ-FR when that connection was designed to provide a direct path for force transfer from the beam, through the corbel, to the column.

- Most specimens contained at least one connection detail that demonstrated good performance throughout testing. For example, the top connection of Specimen GJ-TC, which consisted of threaded bars coupled with Lenton couplers, and the

bottom connection of Specimen GJ-FR, which was the corbel/dapped beam combination that provided a direct path for force transfer from the beam to the column, behaved quite well in the two tests. Therefore, it is suggested that the behavior of Specimen GJ-TC would be improved substantially if a bottom connection similar to that used in Specimen GJ-FR were used. In addition, this bottom connection would result in a more aesthetically appealing connection.

- All but Specimen PT-NE contained joint reinforcement similar to that recommended by ACI-ASCE Committee 352. In all three specimens the joint behaved well without any sign of distress, suggesting these recommendations, although somewhat inappropriate for some of the connections, will produce suitable designs for most precast beam-column joints. The amount of joint reinforcement provided in Specimen PT-NE was 66 percent of that required by ACI-ASCE 352. The joint shear mechanism for this specimen was different from other specimens, and consisted primarily of a diagonal compression strut. The joint in this connection behaved satisfactorily through 3 percent drift cycles. Stiffness of the joint did not appear to deteriorate until 4 percent drift cycles, and strength did not deteriorate until 5 percent drift cycles. A strut-and-tie method was demonstrated to calculate the amount of reinforcement needed to provide a force-path for the joint shear forces. More research is needed to further rationalize the design of joints for prestressed connections.

- Results of the analytical study indicated that ductility demand decreased with increase in building height (and period of vibration) for all three hysteretic models. In general, ductility demands were more than $3R_w/8$ implied by the UBC for the 5-story frame, and less for the 15-story frame.

- The 5-story frame incorporating the pretensioned hysteretic model demonstrated excessive drifts for all earthquake records. The behavior was enhanced considerably when additional energy dissipation was introduced by using friction connections in the middle bay of the frame. Drifts were reduced by

approximately 50 percent for some of the earthquake records. All hysteretic models, including the pretensioned model, yielded reasonable response for the 15-story frame.

7.7 RESEARCH NEEDS

- None of the connections tested in this study incorporated precast floor panels. Additional work needs to be performed to develop connections between floor elements and precast frame elements to enable the necessary transfer of floor diaphragm forces to the lateral-force-resisting frame systems.

- The top connection of Specimen GJ-FR, and to a lesser extent, Specimen GJ-TC, may cause distortion and damage in the floor diaphragm due to opening or closing of the gap. It may be possible to invert these connections so that the gap opening occurs at the bottom of the beams. Details for "inverted" connections should be developed and tested in future studies.

- All beam-column subassemblages tested in this study were planar specimens. In order to test the feasibility of space-frame assemblages that would likely be used in a distributed lateral-force-resisting frame system, design and behavior of three-dimensional beam-column subassemblages should be investigated. Furthermore, connections should incorporate slabs to further investigate the effect of slabs on connection behavior.

- For the structures analyzed in this study, it is evident that pretensioned connections are more suitable for structures with longer periods of vibration. However, more research is needed to identify a safe lower bound for the period of the structure.

- Both the 5- and 15-story structures were designed using the static-lateral-force procedure of the UBC with an R_w factor of 12. If the pretensioned connections were to be used for a structure similar to the 5-story structure used in

this study, it appears a smaller R_w factor should be used. However, more research is needed to establish an appropriate R_w factor or a displacement-based design procedure for short-period structures.

APPENDIX A

DESIGN CONSIDERATIONS FOR SPECIMEN PT-NE

A.1 INTRODUCTION

The design of specimen PT-NE was different from the other specimens due to the expected nonlinear elastic behavior. In general, the other specimens were designed and proportioned using existing guidelines for design of reinforced concrete members. No guidelines exist for design of members expected to behave in a nonlinear elastic fashion. The aim of this appendix is to explain the nonlinear elastic behavior and to shed some light on the steps involved in design of such connections.

A.2 THE NONLINEAR ELASTIC SYSTEM

An idealized force-displacement curve for a nonlinear elastic connection is shown in Fig. A.1. The nonlinear behavior of this connection is introduced not through yielding of materials but through a change in stiffness of the system when a joint or crack opens at the beam-column interface. As a result, the theoretical energy dissipated by this system is zero since the loading and unloading curves follow the same path. Connections with this type of behavior will have minimal residual deformations after an earthquake.

The force V_1 in Fig. A.1 represents the story shear at which a joint/crack starts to open at the beam-column interface. The force V_2 is the story shear at which strands reach their limit of proportionality. The design procedure to estimate these two forces is explained in the next section.

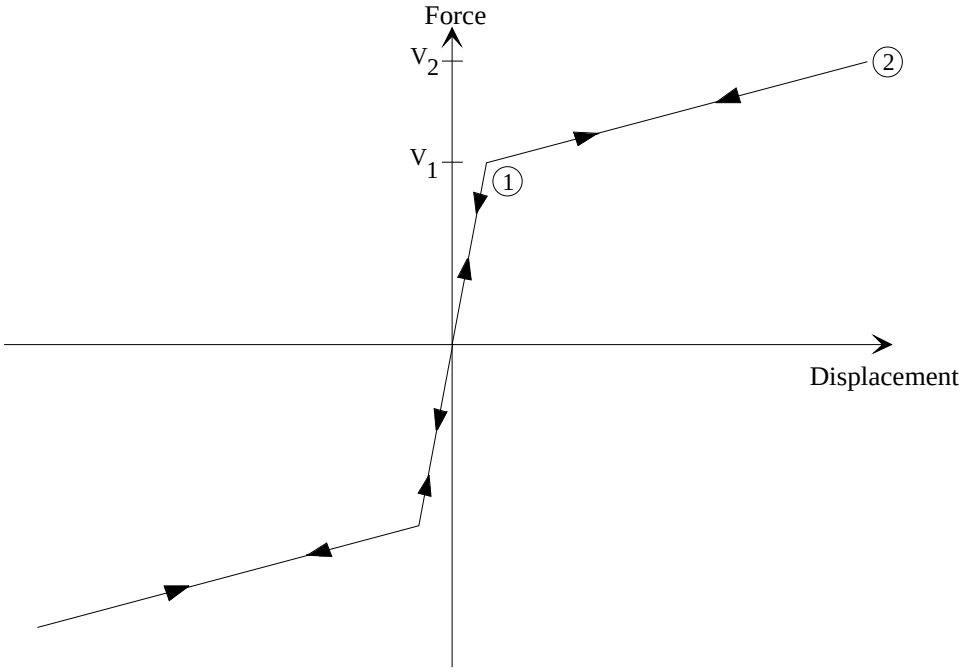

Figure A.1 Nonlinear Elastic Force-Displacement Curve

A.3 DESIGN CONSIDERATIONS

The following calculations are based on the actual material properties for the steel and concrete, and on the actual prestressing force as determined from measurements taken during stressing and force releasing operations. These properties are:

$f_{pu} = 285\ ksi$

$E = 28000\ ksi$

$f_c^{'} = 6.30\ ksi$

$F_{ps} = 219.4\ kips$

A.3.1 Estimating Beam Flexural Capacity

A.3.1.1 Beam Cracking Strength

The flexural strength at cracking is given in Eq. A.1:

$$M_{b,cr} = \left(\frac{F_{ps}}{A_b} - f_t \right) Z_b \qquad \text{(A.1)}$$

It is assumed that the beam cracks when the tensile stress, f_t, is $7.5\sqrt{f_c'}$. Solving Eq. A.1, the cracking moment of the beam is obtained:

$$\begin{aligned} M_{b,cr} &= \left(\frac{219.4}{12*24} - \frac{-7.5\sqrt{6300}}{1000} \right) \frac{12(24)^2}{6} \\ &= (0.762 + 0.596)1152 \\ &= 1564\ k-in \end{aligned}$$

The beam force to cause cracking, $P_{b,cr}$, is:

$$P_{b,cr} = \frac{M_{b,cr}}{L_b} = \frac{1564}{49.5} = 31.6\ kips \qquad \text{(A.2)}$$

The corresponding story shear, V_{cr}, is:

$$V_{cr} = P_{b,cr} \frac{L}{H} = 31.6 \frac{120}{78} = 48.6\ kips \qquad \text{(A.3)}$$

Since the loading is cyclic in nature, the beam will reach a tensile stress of $7.5\sqrt{f_c'}$ only once before the crack is initiated. In subsequent cycles, the beam behaves as uncracked, due to the prestressing force, but only until stress at the extreme tensile fiber reaches zero. After that, the beam behavior deviates from linear due to continued opening of the crack. To calculate the moment that results in zero stress at the extreme fiber, f_t will be taken as zero in Eq. A.1.

$$\begin{aligned} M_{b,o} &= \left(\frac{219.4}{12*24} - 0 \right) \frac{12(24)^2}{6} \\ &= (0.762 - 0)1152 \\ &= 878\ k-in \end{aligned}$$

The behavior will not deviate significantly from linear behavior until the crack has propagated to the centroidal axis of the beam. This is because prestressing steel strains will change very little until this stage of crack opening is reached. At this stage the moment, M_1, is twice M_o. This is also supported by the experimental results.

The beam force, $P_{b,1}$, is:

$$P_{b,1} = \frac{M_{b,1}}{L_b} = \frac{2*878}{49.5} = 35.5 \ kips \tag{A.4}$$

The corresponding story shear, V_1, is:

$$V_1 = P_{b,1}\frac{L}{H} = 35.5\frac{120}{78} = 54.6 \ kips \tag{A.5}$$

A.3.1.2 Beam Maximum Flexural Strength

The beam capacity is assumed to be reached when the stress in the strands reaches the limit of proportionality. The stress at the limit of proportionality is taken as 85 percent of the ultimate strength of the strands. Consequently, the strain at the limit of proportionality is:

$$\varepsilon_{lp} = \frac{0.85 f_{pu}}{E} \tag{A.6}$$

$$\varepsilon_{lp} = \frac{0.85*285}{28000} = 0.00865$$

The total force in the strands at the limit of proportionality is:

$$F_{lp} = nA_{ps}E\varepsilon_{lp} \tag{A.7}$$

where n = number of strands

A_{ps} = area of each strand

Substituting into Eq. A.7:

$$F_{lp} = 20*0.085*28000*0.00865 = 411.7 \ kips$$

In order to calculate the beam flexural strength, the strength of the confined

concrete in the plastic hinge region must be calculated first. Spirals were placed in the beams at the top and bottom to ensure a high effective compression strain. The volumetric ratio of the confining steel provided, which should be approximately 2 percent with a spiral pitch not exceeding $D_s/4$, where D_s is the spiral diameter, is:

$$\rho_s = \frac{A_{sp}\pi D_s}{\frac{\pi}{4}D_s^2 s} = \frac{4A_{sp}}{D_s s} \tag{A.8}$$

$$\rho_s = \frac{4*0.05}{6*1.5} = 0.022 = 2.2\%$$

The lateral confining stress, f_l, provided by the spiral steel is given by:

$$f_l = \frac{2A_{sp}f_{yh}}{D_s s} = 0.5\left(\frac{4A_{sp}}{D_s s}\right)f_{yh} = 0.5\rho_s f_{yh} \tag{A.9}$$

$$f_l = 0.5*0.022*60 = 0.66 \text{ ksi}$$

Mander et al. [27] suggested an equation for the strength of confined concrete based on the consideration of triaxial compression with equal effective lateral confining stresses given by the following:

$$f_{cc}^{'} = f_c^{'}\left(-1.254 + 2.254\sqrt{1+\frac{7.94f_l}{f_c^{'}}} - \frac{2f_l}{f_c^{'}}\right) \tag{A.10}$$

$$f_{cc}^{'} = 6.30\left(-1.254 + 2.254\sqrt{1+\frac{7.94*0.66}{6.30}} - \frac{2*0.66}{6.30}\right) = 10.0 \text{ ksi}$$

The strain of the confined concrete at peak stress, ε_{cc}, can be calculated from the following formula [27] :

$$\varepsilon_{cc} = 0.002(1+5(K-1)) \tag{A.11}$$

$$\varepsilon_{cc} = 0.002(1+5(\frac{10.0}{6.307}-1)) = 0.00786$$

A typical stress-strain curve for unconfined and confined concrete is shown in Fig. A.2. In general, the initial portion of the two curves coincide because at small strains the confining steel is not effective. As more strain is imposed on the concrete, the confining steel starts to exert pressure on the concrete, thus enhancing

its compressive strength.

In the calculation of the maximum moment capacity of the section, it is assumed that the concrete cover of 0.5 in. has spalled. Also, based on the experimental observations, more concrete spalled at the top and bottom of the beam than the cover. It is assumed that twice the concrete cover is ineffective for the purpose of calculating the moment capacity. The consequence of not taking into consideration cover spalling will give a higher estimate of the moment capacity due to the larger internal lever arm. To calculate the beam flexural strength, it is assumed that the maximum strain reached is ε_{cc}. The laboratory test showed no signs of concrete crushing inside the spirals nor any sign of spiral fracture that would suggest the concrete was at a strain higher than that corresponding with ultimate concrete stress. Based on all of the above, the confined concrete was assumed to follow a stress-strain relationship up to the ultimate concrete stress shown in Fig. A.2 as described by the following equation:

$$f_{cc} = f_{cc}^{'}\left\{4.9\left(\frac{\varepsilon}{\varepsilon_{cc}}\right) - 10.7\left(\frac{\varepsilon}{\varepsilon_{cc}}\right)^{2} + 10.6\left(\frac{\varepsilon}{\varepsilon_{cc}}\right)^{3} - 3.8\left(\frac{\varepsilon}{\varepsilon_{cc}}\right)^{4}\right\} \quad \text{(A.12)}$$

By integrating Eq. A.12:

$$A = 0.7855 f_{cc}^{'} \varepsilon_{cc} \quad \text{(A.13)}$$

Also, the centroid of the resultant of the area under the curve is:

$$x = 0.575 \varepsilon_{cc} \quad \text{(A.14)}$$

The depth of the neutral axis, *c*, can now be calculated by:

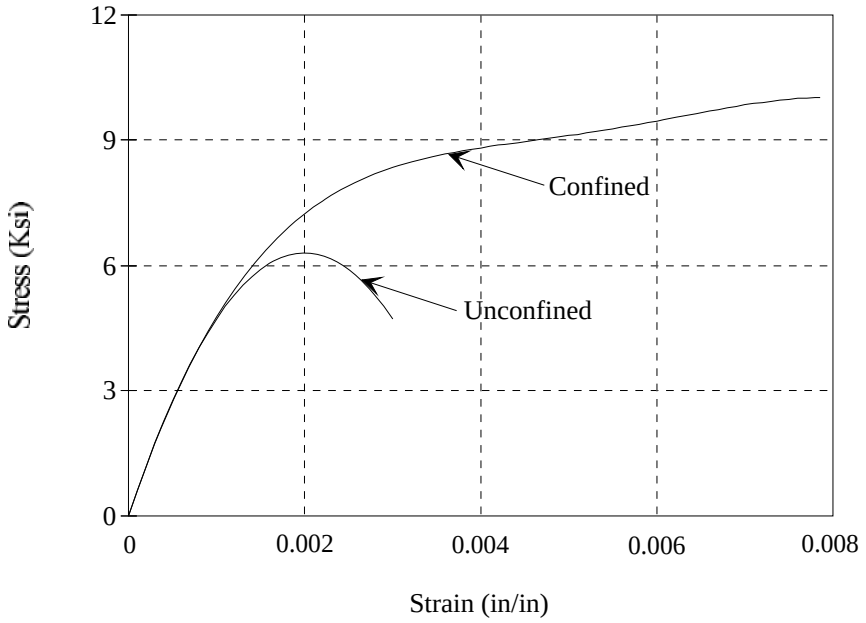

Figure A.2 Stress-Strain Relationships for Unconfined and Confined Concrete

$$c = \frac{F_{lp}}{0.7855\, f_{cc}^{'}\, b_c} \tag{A.15}$$

$$c = \frac{4117}{0.7855 * 10.0 * (12 - 2(0.5 + 0.375))} = 5.1 \text{ in}$$

The maximum beam moment is:

$$M_{b,2} = F_{lp}\left(\frac{h_c}{2} - (1 - 0.575)c\right) \tag{A.16}$$

$$M_{b,2} = 4117\left\{\frac{(24 - 2(1.0 + 0.375))}{2} - 0.425 * 5.1\right\} = 3482 \text{ k} - \text{in}$$

The maximum beam force, $P_{b,2}$, is:

$$P_{b,2} = \frac{M_{b,2}}{L_b} = \frac{3482}{49.5} = 70.3 \text{ kips} \tag{A.17}$$

The corresponding story shear, V_2, is:

$$V_2 = P_{b,2}\frac{L}{H} = 70.3\frac{120}{78} = 108.2 \text{ kips} \tag{A.18}$$

A.3.2 Idealization of Moment-Curvature Relationship

As was shown in Fig. A.1, the behavior of this connection can be idealized by two straight lines. The first line represents the behavior of the connection up to the point where the joint/crack starts opening at the beam-column interface. The second line represents the behavior after the gap has opened, up to the point when the prestressing steel reaches its limit of proportionality.

To approximate the initial line, it is important to investigate the behavior of the beam after the moment reaches M_o. The gap does not open instantaneously as the moment reaches M_o; it opens gradually as the crack continues propagating into the section. Therefore, it is assumed at this stage that no appreciable elongation occurs in the strands due to their long unbonded length, and as a result, the tensile force remains the same as the initial prestressing force. It can be observed from Fig. A.2 that the stress-strain relationship at small strains (up to 0.001) can be approximated by a straight line of the form:

$$f_c^{'} = E_c \varepsilon_c \tag{A.19}$$

where $E_c = 57\sqrt{f_c^{'}}$ (A.20)

By assuming different concrete strains, section analyses can be performed to calculate the moment-curvature relationship as follows:

- Assume a concrete strain ε_c.
- Calculate the depth of the neutral axis by assuming a triangular stress distribution.

$$c = \frac{F_{ps}}{0.5(E_c \varepsilon_c)b} \tag{A.21}$$

where b is the total width of the beam.

- Calculate the moment.

$$M = F_{ps}(b - \frac{c}{3}) \tag{A.22}$$

- Calculate the curvature.

$$\phi = \frac{\varepsilon_c}{c} \tag{A.23}$$

Figure A.3 shows the moment-curvature relationship up to a concrete strain of 0.001. It must be noted that the calculations presented are based on the assumption that the prestressing force is unchanged at this level. This assumption is not far from the truth because up to a moment of $2M_o$, the crack will open only to the centroidal axis of the beam. Therefore, taking into consideration the long unbonded length of the strands, the change in strain will be negligible. Consequently, and based on the results of the laboratory test, it is assumed that the beam behaves linearly up to a moment of twice M_o. Therefore, the point at which the joint/crack starts opening is taken to be:

$$M_1 = 2M_o = 1756k - in \tag{A.24}$$

The corresponding curvature is:

$$\phi_1 = 0.0000556rad$$

Notice that the slope of the line between the origin and (M_1,ϕ_1) is lower than the slope if ϕ_1 was simply taken as twice the curvature of M_o, as shown in Fig. A.3. Therefore, the initial stiffness of the beam was taken lower than the theoretical uncracked beam stiffness. This is based totally on the experimental results in order to better approximate the stiffness of subassemblage in the nonlinear dynamic analyses presented in Chapter 6.

The moment at which the prestressing steel reaches the limit of proportionality was calculated before and found to be equal to:

$$M_2 = 3482\ k - in$$

The section curvature at ultimate can be calculated as:

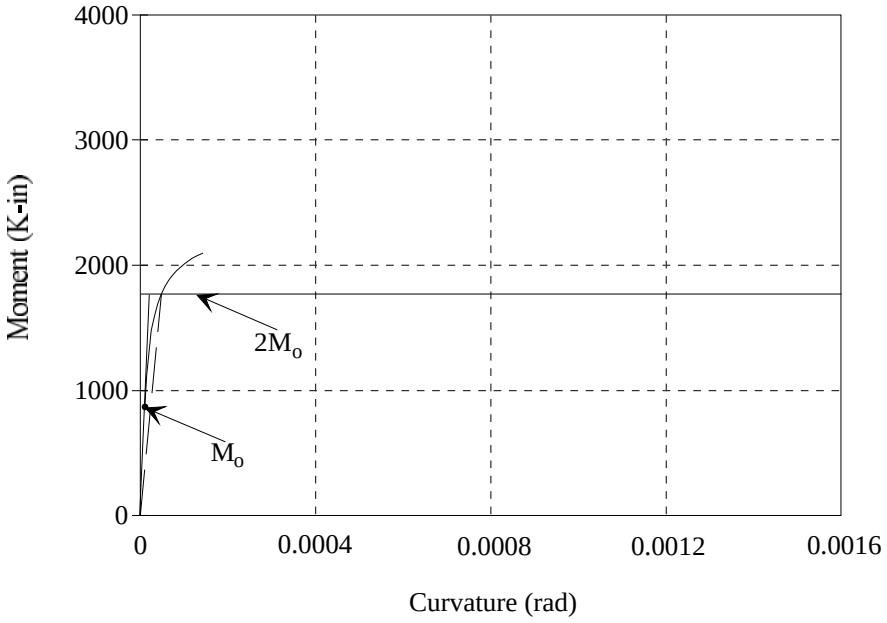

Figure A.3 Post Crack Initiation Moment-Curvature Relationship

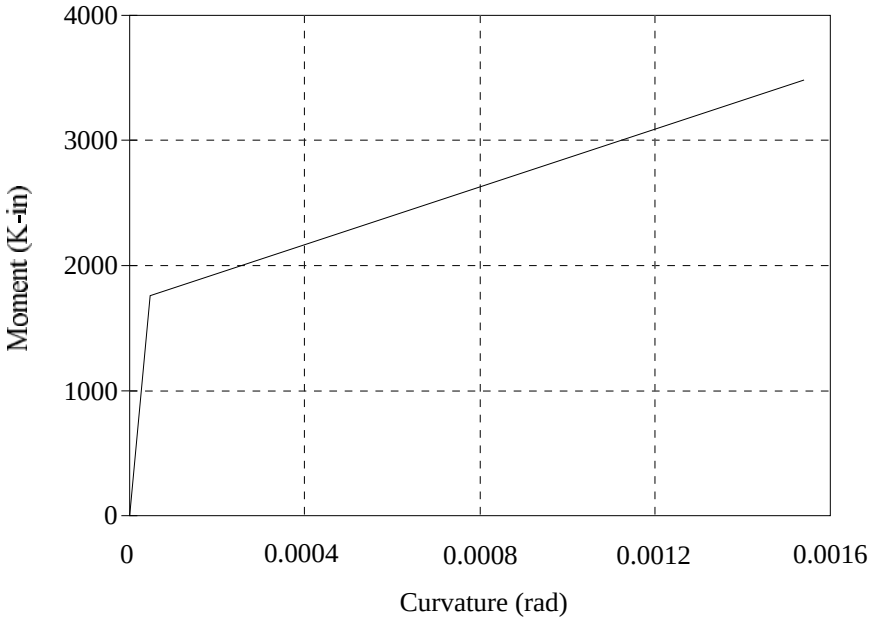

Figure A.4 Idealized Moment-Curvature Relationship

$$\phi_2 = \frac{\varepsilon_{cc}}{c} \tag{A.25}$$

$$\phi_2 = \frac{0.00786}{5.1} = 0.00154\ rad$$

The corresponding idealized moment-curvature relationship is shown in Fig. A.4. The section ductility is defined as:

$$\mu = \frac{\phi_2}{\phi_1} \tag{A.26}$$

$$\mu = \frac{0.00154}{0.0000556} = 27.7$$

Note that this definition of ductility is not the conventional definition for typical reinforced concrete members, but it represents the ratio of two limit states. The section ductility, μ, can be larger than 27.7 depending on the initial stress level in the beam. In general, the ductility increases as the initial stress level decreases and the length of the unbonded strands increases.

A.3.3 Estimating Beam Nonlinear Rotation Capacity

In the above section the depth of the neutral axis at the limit of proportionality was found to be:

$$c = 5.1\ in$$

The increase in the strand strain , $\Delta\varepsilon$, can be calculated as the difference between the initial strain and the strain at the limit of proportionality.

$$\Delta\varepsilon = \frac{(F_{lp} - F_{ps})}{A_{ps} E} \tag{A.27}$$

$$\Delta\varepsilon = \frac{(411.7 - 219.4)}{20 * 0.085 * 28000} = 0.00404$$

The debonded length of the strands consisted of the depth of the column plus two feet on each side of the column to yield a total length of 69 in. Therefore, the increase in the length of the strands is:

$$\Delta L = L_i \Delta\varepsilon \tag{A.28}$$

$$\Delta L = 69 * 0.00404 = 0.279 \ in$$

It is important to realize that this increase in length of the strands is the same at any level throughout the depth of the beam. Some of this increase occurs on the right side of the column and the other on the left side. The result is that each layer of strand extends by the same amount ΔL. At mid-depth of the beam the elongation on each side of the column will be ΔL /2. Therefore, the inelastic rotation of the beam relative to the column face can be calculated as:

$$\theta_{pb} = \frac{\frac{\Delta L}{2}}{\frac{h_c}{2} - c} \tag{A.29}$$

$$\theta_{pb} = \frac{\frac{0.279}{2}}{\frac{24 - 2(0.5 + 0.375)}{2} - 5.1} = 0.0232 \ rad$$

This rotation is the nonlinear rotation of the beam due to the crack opening at the beam-column interface. The corresponding drift ratio due only to beam nonlinear rotation is:

$$R = \frac{(\theta_{pb} L_b)_i + (\theta_{pb} L_b)_j}{L} \tag{A.30}$$

where the subscripts *i* and *j* refer to the beams on each side of the column.

$$R = \frac{0.0232 * 49.5 + 0.0232 * 49.5}{120} = 0.0192 = 1.92\%$$

Two points are worth mentioning here. First, the above calculated drift ratio is the contribution of beam nonlinear rotation only. The expected ultimate drift ratio will also include the elastic deformations of the beams and column. Debonding of the strands beyond 2 feet on each side of the column may also occur due to the repeated loading and unloading which will lead to a slightly higher estimate of *R*. Second, the choice of the debonded length of strands depends on the desired drift

ratio when the strands reach their limit of proportionality. The 69 in. debonded length was based on a target design drift ratio of 2 percent.

REFERENCES

1. ACI Committee 318, "Building Code Requirements for Reinforced Concrete (ACI 318-89)," American Concrete Institute, Detroit, Michigan, 1989.
2. ACI-ASCE Committee 352, "Recommendations for Design of Beam-Column Joints in Monolithic Reinforced Concrete Structures," Journal of the American Concrete Institute, Vol. 82, No. 3, May-June, 1985, pp. 266-283.
3. Aiken, I. D., and Kelly, J. M., "Earthquake Simulator Testing and Analytical Studies of Two Energy Absorbing Systems for Multistory Structures," Report No. UCB/EERC - 90/03, University of California, Berkeley, California, October, 1990.
4. Applied Technology Council, "Design of Prefabricated Concrete Buildings for Earthquake Loads," Berkeley, California, 1981.
5. Blakeley, R. W. G., and Park, R., "Prestressed Concrete Sections with Cyclic Flexure," American Society of Civil Engineers, Journal of Structural Engineering, Vol. 99, No. ST8, August, 1973, pp. 1717-1742.
6. Blakeley, R. W. G., and Park, R., "Seismic Resistance of Prestressed Concrete Beam-Column Assemblies," Journal of the American Concrete Institute, Detroit, Michigan, September, 1971, pp. 677-692.
7. Bull, D. K., and Park, R., "Seismic Resistance of Frame Incorporating Precast Prestressed Concrete Beam Shells," Precast Concrete Institute Journal, July-August, 1986, pp. 54-93.
8. Cheok, G. S., and Lew, H. S., "Performance of 1/3-Scale Model Precast Concrete Beam-Column Connections Subjected to Cyclic Inelastic Loads - Report No. 1," NISTIR 4433, National Institute of Standards and Technology, Gaithersburg, Maryland, October, 1990.
9. Cheok, G. S., and Lew, H. S., "Performance of 1/3-Scale Model Precast Concrete Beam-Column Connections Subjected to Cyclic Inelastic Loads -

Report No. 2," NISTIR 4589, National Institute of Standards and Technology, Gaithersburg, Maryland, June, 1991.

10. Cheok, G. S., and Stone, W. C., "Performance of 1/3-Scale Model Precast Concrete Beam-Column Connections Subjected to Cyclic Inelastic Loads - Report No. 3," NISTIR 5246, National Institute of Standards and Technology, Gaithersburg, Maryland, August, 1993.
11. Cheok, G. S., and Lew, H. S., "Performance of Precast Concrete Beam-to-Column Connections Subject to Cyclic Loading," Precast Concrete Institute Journal, Vol. 36, No. 3, May-June, 1991, pp. 56-67.
12. Cheok, G. S., and Lew, H. S., "Model Precast Concrete Beam-to-Column Connections Subject to Cyclic Loading," Precast Concrete Institute Journal, Vol. 38, No. 4, July-August, 1993, pp. 80-92.
13. Clough, R., and Penzien, J., "Dynamics of Structures," J. Wiley & Sons, New York, 1975.
14. Constantino, M. C., Reinhorn, A. M., Mokha, A., and Watson, R., "Displacement Control Devices for Base Isolated Bridges," Earthquake Spectra, Vol. 7, No. 2, 1991.
15. Englekirk, R. E., "An Analytical Approach to Establishing the Seismic Resistance Available in Precast Concrete Frame Structures," Precast Concrete Institute Journal, Vol. 34, No. 1, January-February, 1989, pp. 92-101.
16. Englekirk, R. E., "Development and Testing of a Ductile Connector for Assembling Precast Concrete Beams and Columns," Precast Concrete Institute Journal, March-April, 1995, pp. 36-51.
17. Englekirk, R. E., "Seismic Design Considerations for Precast Concrete Multistory Buildings," Precast Concrete Institute Journal, May-June, 1990, pp. 40-51.
18. French. C. W., Amu, L., and Tarzikhan, C., "Connections Between Precast Elements - Failure Within Connection Region," American Society of Civil

Engineers, Journal of Structural Engineering, New York, New York, December, 1989, pp. 3171-3192.

19. French. C. W., Olanrewaju, A., and Charbel, T., "Connections Between Precast Elements - Failure Outside Connection Region," American Society of Civil Engineers, Journal of Structural Engineering, New York, New York, February, 1989, pp. 316-340.
20. Grigorian, C. E., Yang, T. S., and Popov, E. P., "Slotted Bolted Connection Energy Dissipators," Report No. UCB/EERC - 92/10, University of California, Berkeley, California, July, 1992.
21. Hawkins, N. M., "US-Japan Seminar on Precast Concrete Construction in Seismic Zones," Precast Concrete Institute Journal, Vol. 32, No. 2, March-April, 1987, pp. 75-85.
22. International Conference of Building Officials, "Uniform Building Code (UBC-91)," Whittier, California, 1991.
23. Kanoh, Y., "Review of Japanese Precast Concrete Frame Structures Used as Building Structures," Seminar on Precast Concrete Construction in Seismic Zones," Japan Concrete Institute, Japan, 1986, pp. 35-54.
24. Kunnath, S. K., Reinhorn, A. M., and Lobo, R. F., "IDARC - Version 3.0, Inelastic Damage Analysis of RC Structures," Technical Report NCEER-92-0022, State University of New York at Buffalo, 1992.
25. Kurose, Y., Nagami, K., and Saito, Y., "Beam-Column Joints in Precast Concrete Construction in Japan," American Concrete Institute Special Publication, Specimen-123, 1991, pp. 493-514.
26. MacRae, G. A., and Priestley, M. J. N., "Precast Post-Tensioned Ungrouted Concrete Beam-Column Subassemblage Tests," Report No. PRESSS-94/01, University of California, San Diego, La Jolla, California, March, 1994.

27. Mander, J. B., Priestley, M. J. N., and Park, R., "Theoretical Stress-Strain Model for Confined Concrete," American Society of Civil Engineers, Journal of Structural Engineering, Vol. 114, No. 8, pp. 1804-1826.
28. Mast, R. F., "A Precast Concrete Frame System for Seismic Zone Four," Precast Concrete Institute Journal, Vol. 37, No. 1, January-February, 1992, pp. 50-64.
29. Pall, A. S., Verganalakis, V., and Marsh, C., "Response of Friction Damped Braced Frames," American Society of Civil Engineers, Journal of Structural Engineering, 108(6), 1987, pp. 1313-1323.
30. Palmieri, L., French, C. W., Saqan, E. I., and Kreger, M. E., "Ductile Connections for Precast Concrete Frame Systems," American Concrete Institute Special Publication, Mete Sozen Symposium, October, 1994.
31. Park, R., "A Perspective on the Seismic Design of Precast Concrete Structures in New Zealand," Precast Concrete Institute Journal, May-June, 1995, pp. 40-60.
32. Popov, E. P., and Engelhardt, M. D., "Seismic Eccentrically Braced Frames," Journal of Constructional Steel Research, Vol. 10, 1988, pp. 321-354.
33. Precast/Prestressed Concrete Institute,"PCI Design Handbook - Precast/Prestressed Concrete," Chicago, Illinois, 1992.
34. Priestley, M. J. N., and Tao, J. R., "Seismic Response of Precast Prestressed Concrete Frames with Partially Debonded Tendons," Precast Concrete Institute Journal, Vol. 38, No. 1, January-February, 1993, pp. 58-69.
35. Schlaich, J., Schafer, K., and Jennewein, M., "Toward a Consistent Design of Structural Concrete," Precast Concrete Institute Journal, Vol. 32, No. 3, May-June, 1987, pp. 74-150.
36. Sheikh, T. M., "Moment Connections Between Steel Beams and Concrete Columns," Ph.D. Dissertation, The University of Texas at Austin, December, 1987.
37. Stanton, J., "Connections in Precast Concrete Structures," Concrete International, Vol. 9, No. 11, November, 1987, pp. 49-53.